ADVANCES IN MULTI-SCALE ANALYSIS OF BRAIN COMPLEXITY

EDITED BY: Danny J. J. Wang, Kay Jann, Albert Yang and Christoph M. Michel

PUBLISHED IN: Frontiers in Neuroscience

frontiers Research Topics

frontiers

ISSN 1664-8714
ISBN 978-2-88963-770-6
DOI 10.3389/978-2-88963-770-6

About Frontiers

Frontiers is more than just an open-access publisher of scholarly articles: it is a pioneering approach to the world of academia, radically improving the way scholarly research is managed. The grand vision of Frontiers is a world where all people have an equal opportunity to seek, share and generate knowledge. Frontiers provides immediate and permanent online open access to all its publications, but this alone is not enough to realize our grand goals.

Frontiers Journal Series

The Frontiers Journal Series is a multi-tier and interdisciplinary set of open-access, online journals, promising a paradigm shift from the current review, selection and dissemination processes in academic publishing. All Frontiers journals are driven by researchers for researchers; therefore, they constitute a service to the scholarly community. At the same time, the Frontiers Journal Series operates on a revolutionary invention, the tiered publishing system, initially addressing specific communities of scholars, and gradually climbing up to broader public understanding, thus serving the interests of the lay society, too.

Dedication to Quality

Each Frontiers article is a landmark of the highest quality, thanks to genuinely collaborative interactions between authors and review editors, who include some of the world's best academicians. Research must be certified by peers before entering a stream of knowledge that may eventually reach the public - and shape society; therefore, Frontiers only applies the most rigorous and unbiased reviews.
Frontiers revolutionizes research publishing by freely delivering the most outstanding research, evaluated with no bias from both the academic and social point of view. By applying the most advanced information technologies, Frontiers is catapulting scholarly publishing into a new generation.

What are Frontiers Research Topics?

Frontiers Research Topics are very popular trademarks of the Frontiers Journals Series: they are collections of at least ten articles, all centered on a particular subject. With their unique mix of varied contributions from Original Research to Review Articles, Frontiers Research Topics unify the most influential researchers, the latest key findings and historical advances in a hot research area! Find out more on how to host your own Frontiers Research Topic or contribute to one as an author by contacting the Frontiers Editorial Office: researchtopics@frontiersin.org

ADVANCES IN MULTI-SCALE ANALYSIS OF BRAIN COMPLEXITY

Topic Editors:
Danny J. J. Wang, University of Southern California, Los Angeles, United States
Kay Jann, University of Southern California, Los Angeles, United States
Albert Yang, National Yang-Ming University, Taiwan
Christoph M. Michel, Université de Genève, Switzerland

Citation: Wang, D. J. J., Jann, K., Yang, A., Michel, C. M., eds. (2020). Advances in Multi-Scale Analysis of Brain Complexity. Lausanne: Frontiers Media SA.
doi: 10.3389/978-2-88963-770-6

Table of Contents

frontiers in Neuroscience

EDITORIAL
published: 15 April 2020
doi: 10.3389/fnins.2020.00337

Editorial: Advances in Multi-Scale Analysis of Brain Complexity

Albert C. Yang[1,2]*, *Kay Jann*[3], *Christoph M. Michel*[4] *and Danny J. J. Wang*[3]

[1] *Division of Interdisciplinary Medicine and Biotechnology, Beth Israel Deaconess Medical Center, Harvard Medical School, Boston, MA, United States,* [2] *Digital Medicine Center, Institute of Brain Science, National Yang-Ming University, Taipei, Taiwan,* [3] *Laboratory of Functional MRI Technology, Keck School of Medicine, Stevens Neuroimaging and Informatics Institute, University of Southern California, Los Angeles, CA, United States,* [4] *Functional Brain Mapping Lab, Department of Fundamental Neurosciences, University of Geneva, Geneva, Switzerland*

Keywords: brain, complexity, EEG, fMRI — functional magnetic resonance imaging, multiscale (MS) modeling

Editorial on the Research Topic

Advances in Multi-Scale Analysis of Brain Complexity

In neuroscience, a defining but elusive question regarding the human brain is its astonishingly structural and functional complexity. This complexity arises from the interaction of numerous neuronal circuits that operate over a wide range of temporal and spatial scales, enabling the brain to adapt to the constantly changing environment and to perform various high-level mental functions. Such dynamical and functional adaptability is often reduced during the aging process and considerably impaired in patients with neuropsychiatric diseases, leading to rigid, fixed, or on the opposite, unpredictable behaviors. Recently, attempts have been made to apply concepts adopted from complexity science to more fully understand complex brain functions as indicated by the signals from the brain and their implications on human behavior. Therefore, this Research Topic, "Advances in Multi-Scale Analysis of Brain Complexity," is devoted to the research of brain complexity at multiple spatial and temporal scales and its role in neuropsychiatric diseases.

In this Research Topic, a significant portion of focus was on the multi-scale analyses of brain complexity in Alzheimer's disease (AD), which is a progressive brain disorder with gradual memory loss that correlates to cognitive deficits in the elderly population. Importantly, the complexity analysis of brain signal, such as an electroencephalography (EEG), could be a marker for disease severity. Fan et al. applied machine learning algorithms to classify the different stages of AD using the complexity analysis of scalp EEG signals with an accuracy of 80% in differentiating normal and mild cognitive impairment (MCI). The study further found that temporal and occipitoparietal brain regions were more discriminative with regard to classifying severe AD cohort vs. normal controls, which could be a marker for evaluating the severity of AD (Fan et al.). Niu et al. applied multiscale entropy analysis in resting-state fMRI data from the Alzheimer's disease neuroimaging initiative database. They found that both MCI and AD patients had significant reductions in the complexity of resting-state fMRI signals compared to healthy controls, and AD patients also demonstrated lower complexity than that of the MCI subjects (Niu et al.). Grieder et al. investigated alterations of functional connectivity and brain signal complexity within the default mode network (DMN) in 15 mild Alzheimer's disease patients as compared to 14 controls. Their findings suggested that cognitive decline in Alzheimer's disease is reflected by decreased brain signal complexity in DMN nodes, which might further lead to disrupted DMN functional connectivity (Grieder et al.). These findings support the notion that the multi-scale analysis of brain signal complexity may provide a functional or imaging marker of cognitive impairments in the neurodegenerative disease. Interestingly, Eagleman et al. applied brain signal complexity using 1/f power law scaling as well as measures of complexity from non-linear dynamics in geriatric patients that carry increased

OPEN ACCESS

Edited and reviewed by:
Vince D. Calhoun, Georgia State University, United States

***Correspondence:**
Albert C. Yang
cyang1@bidmc.harvard.edu

Specialty section:
This article was submitted to Brain Imaging Methods, a section of the journal Frontiers in Neuroscience

Received: *05 November 2019*
Accepted: *20 March 2020*
Published: *15 April 2020*

Citation:
Yang AC, Jann K, Michel CM and Wang DJJ (2020) Editorial: Advances in Multi-Scale Analysis of Brain Complexity. Front. Neurosci. 14:337. doi: 10.3389/fnins.2020.00337

risk for adverse cognitive outcomes after anesthesia. This study found that both spectral and complexity measures are capable of capturing subtle differences in EEG activity with anesthesia administration—differences which future work may reveal to improve geriatric patient monitoring (Eagleman et al.).

Another focus of this Research Topic was in the developing brain. Hasegawa et al. used magnetoencephalography (MEG) to study special populations, the infant. Their analyses revealed time scale-dependent developmental trajectories based on MEG signal complexity. Specifically, MEG signal complexity predominantly increased from 5 to 15 months of age at higher temporal scales, whereas the complexity at lower temporal scales was constant across age, except in one infant who showed decreased complexity. The results of this pilot study may serve to further our understanding of the longitudinal changes in the neural dynamics of the developing infant brain (Hasegawa et al.). On the other hand, Smith et al. examined the relationship between the resting-state networks entropy and integrity in patients with autism spectrum disorder (ASD) and typically developing (TD) individuals from the Autism Brain Imaging Data Exchange (ABIDE) cohort. They found that complexity of resting-state fMRI signal within resting-state networks significantly distinguished ASD from TD, and the level of brain signal complexity was associated with ASD symptom severity. Importantly, they found that imbalanced brain connectivity and dynamics at the network level coincides with their decoupling in ASD, suggesting a link between changes in brain signal dynamics and network decoupling in the pathologic conditions (Smith et al.). Furthermore, Hager et al. explored how non-linear brain dynamics change during motor resonance, which is often used to study social interaction deficiencies in ASD. This paper performed an elegant experiment in an adult population and found that the desynchronization of the mu wave during motor resonance results in a local increase of mu entropy in sensorimotor areas, potentially reflecting a release from alpha inhibition. This release from inhibition may be mediated by the baseline complexity in the mu band. These findings suggest that dynamical complexity and network analysis of EEG may provide a useful addition for future studies of motor resonance by incorporating measures of non-linearity (Hager et al.).

Brain signal complexity is also implicated in sleep physiology. Hou et al. investigated whether lower complexity of brain waves at the pre-sleep state can facilitate sleep initiation and further improve sleep quality. The study based on polysomnographic recordings from Sleep Heart Health Study identified that lower complexity before sleep onset is associated with decreased sleep latency, indicating a potential facilitating role of reduced pre-sleep complexity in the wake-sleep transition (Hou et al.).

Additionally, there are increasing interests in studying brain signal complexity and its relationship with genetic polymorphisms. For example, brain-derived neurotrophic factor (BDNF) is a widely expressed neurotrophin in the brain and is crucial to neural plasticity. The BDNF Val66Met single-nucleotide polymorphism is associated with mood, stress, and pain conditions. In this Research Topic, Low et al. found that brain complexity alterations were associated with the interactions of BDNF Val66Met polymorphism and menstrual pain experience, suggesting that pain experience preponderantly affects the effect of BDNF Val66Met polymorphism on brain complexity.

An important, yet overlooked issue in non-linear analysis of brain signal dynamics is the choice of parameters in these non-linear methods. For example, there are several parameters that need to be determined when estimating the entropy of brain signal, and the choice of parameter may affect the reliability of entropy estimates. Yang et al. illustrate a general strategy for selecting entropy parameters to reduce the bias of entropy estimates in resting-state fMRI signals. In this paper, they present a minimizing error approach to reduce the bias of entropy estimates in resting-state fMRI data. The strategy explored a range of parameters that minimized the relative error of entropy of resting-state fMRI signals in cerebrospinal fluids where minimal physiologic information was present, and applied these parameters to calculate entropy of resting signals in gray matter regions. This strategy may help minimize the error of entropy estimates for future studies on the non-linear analysis of relatively short resting-state fMRI signals (Yang et al.).

Finally, an important question is: what are the physiologic mechanisms of brain signal complexity? Billings et al. proposes to represent resting-state fMRI signal as multiple processes occurring over multiple time scales, which could potentially implicate in the physiological mechanisms of brain signal complexity. Importantly, Wang et al. investigated the neurophysiological underpinnings of the complexity of electrophysiology and resting-state fMRI signals and their relations to functional connectivity. They found that regional neural complexity and network functional connectivity may be two related aspects of the brain's information processing—the more complex the regional neural activity, the higher functional connectivity this region has with other brain regions. Wang et al. propose that the complexity of regional neural signals may serve as an index of the brain's capacity of information processing—increased complexity may indicate greater transition or exploration between different states of brain networks, thereby indicating a greater propensity for information processing.

Overall, this Research Topic focuses on the theoretic and quantitative analysis of brain complexity in normal mental functions, as well as how it changes with neuropsychiatric diseases by using electrophysiological recordings or functional brain imaging data. These studies can provide a novel computational approach for extracting the fundamental features of the human brain. We anticipate that these approaches will provide better characterization of the heterogeneity of neuropsychiatric diseases and will highlight a subset of dynamical brain markers that will lead to translational research utilizing these complexity methods for understanding complex brain functions.

AUTHOR CONTRIBUTIONS

AY, KJ, CM, and DW read and approved the editorial.

Conflict of Interest: The authors declare that the research was conducted in the absence of any commercial or financial relationships that could be construed as a potential conflict of interest.

frontiers in Neuroscience

HYPOTHESIS AND THEORY
published: 29 May 2018
doi: 10.3389/fnins.2018.00352

Neurophysiological Basis of Multi-Scale Entropy of Brain Complexity and Its Relationship With Functional Connectivity

Danny J. J. Wang[1]*, *Kay Jann*[1], *Chang Fan*[1], *Yang Qiao*[2,3], *Yu-Feng Zang*[2], *Hanbing Lu*[3] *and Yihong Yang*[3]

[1] *Laboratory of FMRI Technology, Stevens Neuroimaging and Informatics Institute, Keck School of Medicine, University of Southern California, Los Angeles, CA, United States,* [2] *Department of Psychology, Center for Cognition and Brain Disorders, Hangzhou Normal University, Hangzhou, China,* [3] *Neuroimaging Research Branch, National Institute on Drug Abuse, National Institutes of Health, Baltimore, MD, United States*

OPEN ACCESS

Edited by:
Amir Shmuel,
McGill University, Canada

Reviewed by:
Adeel Razi,
Wellcome Trust Centre for Neuroimaging (WT), University College London, United Kingdom
Xin Di,
New Jersey Institute of Technology, United States

***Correspondence:**
Danny J. J. Wang
jwang71@gmail.com

Specialty section:
This article was submitted to Brain Imaging Methods, a section of the journal Frontiers in Neuroscience

Received: *29 January 2018*
Accepted: *07 May 2018*
Published: *29 May 2018*

Citation:
Wang DJJ, Jann K, Fan C, Qiao Y, Zang Y-F, Lu H and Yang Y (2018) Neurophysiological Basis of Multi-Scale Entropy of Brain Complexity and Its Relationship With Functional Connectivity. Front. Neurosci. 12:352. doi: 10.3389/fnins.2018.00352

Recently, non-linear statistical measures such as multi-scale entropy (MSE) have been introduced as indices of the complexity of electrophysiology and fMRI time-series across multiple time scales. In this work, we investigated the neurophysiological underpinnings of complexity (MSE) of electrophysiology and fMRI signals and their relations to functional connectivity (FC). MSE and FC analyses were performed on simulated data using neural mass model based brain network model with the Brain Dynamics Toolbox, on animal models with concurrent recording of fMRI and electrophysiology in conjunction with pharmacological manipulations, and on resting-state fMRI data from the Human Connectome Project. Our results show that the complexity of regional electrophysiology and fMRI signals is positively correlated with network FC. The associations between MSE and FC are dependent on the temporal scales or frequencies, with higher associations between MSE and FC at lower temporal frequencies. Our results from theoretical modeling, animal experiment and human fMRI indicate that (1) Regional neural complexity and network FC may be two related aspects of brain's information processing: the more complex regional neural activity, the higher FC this region has with other brain regions; (2) MSE at high and low frequencies may represent local and distributed information processing across brain regions. Based on literature and our data, we propose that the complexity of regional neural signals may serve as an index of the brain's capacity of information processing—increased complexity may indicate greater transition or exploration between different states of brain networks, thereby a greater propensity for information processing.

Keywords: multiscale entropy (MSE), complexity, BOLD fMRI, electrophysiology, functional connectivity (FC)

BACKGROUND

Neural Complexity

Complexity is a key feature characterizing the behavior of physiological systems of a living organism (Lipsitz, 2004). The brain, an information processing system with 10–100 billion neurons and $\sim 10^{14}$ synapses, exhibits the highest degree of complexity among all organs in the human body. In recent years, interest in understanding the dynamics of neural signals and their relation to information processing has increased steadily (Garrett et al., 2013). Neural complexity can be framed as the range, or capacity, of the brain to explore alternative states (Honey et al., 2007; Ghosh et al., 2008; Shew et al., 2009; Friston et al., 2012). Regions of the human brain, indeed systems of neurons, are known to organize transiently into functionally-connected networks for brief periods—from tenths of a second to seconds—only to become reorganized moments later as elements of networks with different functions. These dynamics are readily made visible using EEG (Tucker et al., 1986; Bullmore and Sporns, 2009; Betzel et al., 2012), fMRI (Allen et al., 2014; Barttfeld et al., 2015), among other measurement tools, when coupled with time series analytic methods such as independent components analysis (ICA) (Bell and Sejnowski, 1995; Beckmann and Smith, 2004; Smith et al., 2012). This flexibility of rapid transition implies not only a low energy barrier between states, but also a relatively wide repertoire of quasi-stable states that can self-organize rapidly. The brain's fluid movement among different states has been conceptualized by Friston et al. (2012), who argue that a characteristic feature of the brain is its tendency to wander, or not settle into any particular state. It is posited that systems engaging in greater transition or exploration between different states (i.e., a higher level of complexity) have greater potential and propensity for information processing (McDonough and Nashiro, 2014).

An important parameter defining complex or chaotic systems is the self-similar or "fractal" behavior across multiple measurement scales, and the tendency of the frequency spectra showing an inverse power-law ($1/f^n$–like) scaling pattern. Scale-free activity is present at almost every temporal and spatial scale in the brain (He et al., 2010); it has been observed in neuronal spike trains (Gisiger, 2001; Takahashi et al., 2004), neurotransmitter release (Lowen et al., 1997), spontaneous local field potential (LFP) (Leopold et al., 2003; Milstein et al., 2009), electrocorticography (ECoG), resting state fMRI (rs-fMRI) (Zarahn et al., 1997; Wang et al., 2003; Bullmore et al., 2004), and in fluctuations of human cognitive and behavioral performance (Gilden, 2001). For instance, neuronal populations exhibit a type of activity termed *neuronal avalanches*, characterized by the occurrence of bursts of activity that, despite their wide variation in sizes and durations, still follow precise statistical properties according to a power law (Plenz and Thiagarajan, 2007; Petermann et al., 2009; Ribeiro et al., 2010).

Figure 1 shows data from our lab using wavelet based entropy analysis (Smith et al., 2015) of rs-fMRI data from the globus pallidus internus (GPi), GPi LFP, and primary motor ECoG signals recorded during surgical implementation of deep brain stimulation (DBS) in a patient with Parkinson's disease (PD).

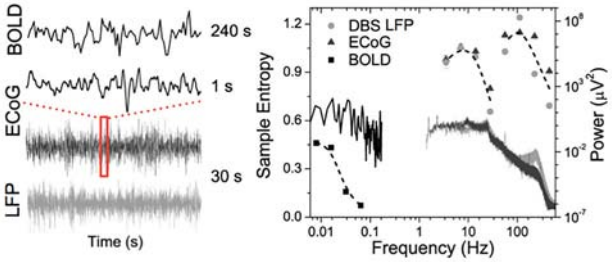

FIGURE 1 | Time courses (left) and corresponding power spectra (solid lines) and entropy (symbols) results of BOLD fMRI from GPi and GPi LFP and primary motor ECoG signals in a PD patient.

All modalities exhibit a general power-law behavior in their power spectrum. Entropy across all modalities shows similar behavior with increasing trends toward low frequencies. In addition, similar "small world" topological structure of brain networks has been observed from micro- and meso-scopic circuits to large scale brain networks (Bassett and Bullmore, 2006; Valverde et al., 2015) as well as in EEG microstate sequences (Van De Ville et al., 2010). The nearly ubiquitous power-law behavior suggests that the brain operates near states of self-organizing criticality (SOC), providing many desirable features in optimizing the brain's computational capabilities including sensory input processing, information transfer, and storage (Bak et al., 1987; Plenz and Thiagarajan, 2007; Ribeiro et al., 2010). The fact that such scale-free spatial and temporal pattern "replicates" itself across different modalities and measurement scales also offers a unique opportunity to bridge cellular and circuit level recordings with systems level brain imaging—a major goal of the BRAIN initiative (Alivisatos et al., 2012).

Quantification of Neural Complexity

People have been interested in understanding and characterizing self-organizing systems since the 1950s, and have developed basic principles like center manifold theorem (Carr, 1981) and synergistic treatment of high-dimensional self-organizing systems, such as the brain (Ginzburg and Landau, 1950), as well as the slaving principle (Haken, 1983) to highlight the role of endogenous fluctuations. These fluctuations model the dynamics attributable to fast (stable) modes that become enslaved by the slow (unstable) modes, which determine the macroscopic behavior. The time constants of these macroscopic dynamics are necessarily greater (or slower) than those of the underlying microscopic dynamics. Importantly, these endogenous fluctuations follow the scale free (power-law) distribution (Friston et al., 2011).

During the past few decades, a variety of measures derived from the fields of nonlinear statistics and information theory have been developed to describe the dynamics of physiological systems (Goldberger, 1996). Nonlinear dynamic analysis using fractal dimension (*FD*) and Hurst exponent (*H*) can be used to quantify the complexity of biological signals (Natarajan et al., 2004; Di Ieva et al., 2015). The complexity of real-world time series of finite length, however, cannot usually be estimated with

reasonable precision. For the analysis of such typically short, and noisy, time series Pincus introduced approximate entropy (ApEn) as a family of non-linear statistics to quantify regularity in physiological finite length time series (Pincus, 1991). ApEn, and its variants (e.g., sample entropy or SampEn) (Richman and Moorman, 2000), measure the conditional probability that runs of patterns that are similar for m contiguous observations remain close on subsequent incremental comparisons ($m+1$). Higher ApEn values indicate generally that the process is less predictable (or more complex). Subsequently, multi-scale entropy (MSE) analysis (Costa et al., 2002) was developed to more accurately differentiate complex processes from random fluctuations, by calculating the entropy of a signal at multiple time scales. In MSE analyses, a series of entropy values are calculated on coarse-grained time series that are constructed by averaging the original time series over a range of scales. Systems with $1/f$ power spectra exhibit constant entropy over various time scales (due to their fractal properties), whereas random noise shows a marked decrease in entropy at longer time scales (as random fluctuations are smoothed out). To date, ApEn, SampEn, and MSE have been applied successfully to biological signals such as cardiac electric activity (ECG), blood pressure, respiratory patterns, hormonal release, electromyogram (EMG), and brain electric activity (EEG), to distinguish healthy function from disease, and to predict the onset of adverse health-related events (Kaplan et al., 1991; Pincus and Keefe, 1992; Ryan et al., 1994; Schuckers and Raphisak, 1999; Abásolo et al., 2005; Pincus, 2006; Szaflarski et al., 2012; Takahashi, 2013).

Functional MRI based on the blood oxygen level-dependent (BOLD) contrast (Ogawa et al., 1990; Kwong et al., 1992) is one of the most widely used methods for noninvasive monitoring of the temporal dynamics of brain physiology (e.g., cerebral blood flow) and neuronal activity (see review Cohen and Bookheimer, 1994). Functional connectivity (FC) analysis has revealed that multiple regions of the brain, even structurally distant, are employed in parallel during both task and rest conditions (Biswal et al., 1995; Raichle et al., 2001; Damoiseaux et al., 2006). Recent fMRI and electrophysiological studies suggest that FC may exhibit dynamic changes within time scales of seconds to minutes (i.e., non-stationary processes; Chang and Glover, 2010). These non-stationary properties may not be captured fully by linear statistical methods such as cross-correlation analysis. We (Liu et al., 2013; Smith et al., 2014, 2015) and others (Yang et al., 2013; Wang et al., 2014) have recently explored the use of entropy measures as indices of the complexity and regularity of BOLD fMRI time-series in healthy young and elderly populations (see **Figure 2**) as well as in subjects associated with genetic risks of dementia, subjects with ADHD (Sokunbi et al., 2013) and schizophrenia (Takahashi et al., 2010). Significant correlations between complexity measures and functional connectivity across brain networks have also been reported (McDonough and Nashiro, 2014). These emerging studies support the validity of using entropy measures of rs-fMRI to characterize the spontaneous fluctuations of brain physiology and neuronal activities non-invasively at systems level.

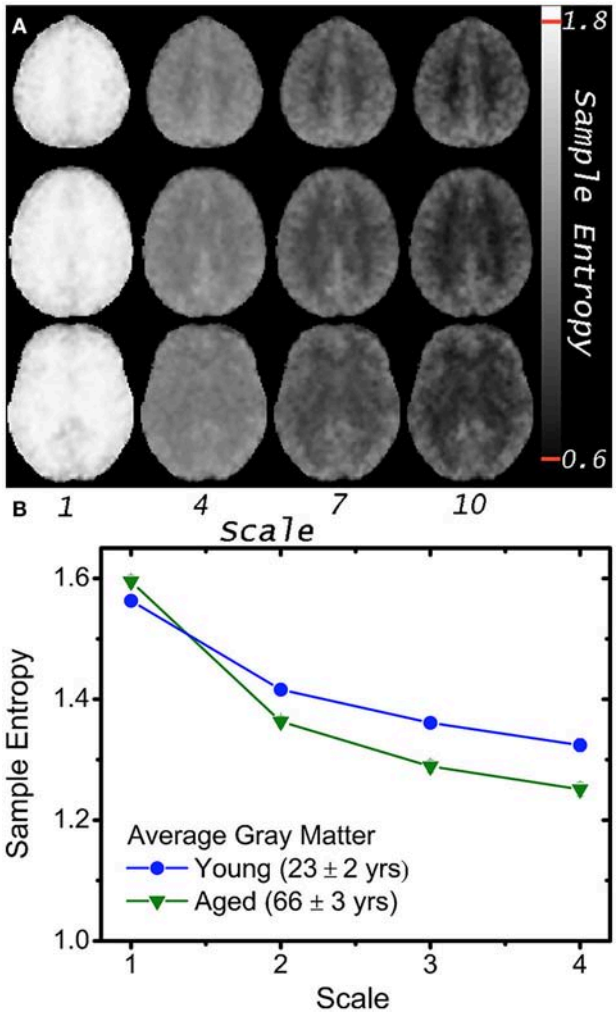

FIGURE 2 | (A) Mean MSE images of 5 volunteers at scales 1, 4, 7, and 10; note greater gray and white matter contrast in higher MSE scales (i.e., lower temporal frequencies). **(B)** Average gray matter MSE for 8 young and 8 aged volunteers at 4 scales with greater age differences at higher scales ($p < 10^{-4}$). Plotted error bars are four standard errors of the respective means, and approximately the size of the symbols (With permission from Smith et al., 2014).

Relationship Between Neural Complexity and FC

Although initial data showed promising results, the neurophysiological basis of complexity (MSE) of electrophysiology and fMRI signals as well as their relations to functional connectivity (FC) remain unclear. The complexity of fluctuating neural activity has been linked to the probability of neuronal firing, and to the likelihood of synchrony between brain regions. It has been postulated that more predictable signals (less neural complexity) facilitate phase relationships between brain regions, thus increasing the probability of synchrony, and information exchange across distributed brain regions. In contrast, the opposite is expected with more irregular signals (greater neural complexity; Ghanbari et al., 2015).

The degree of synchrony across brain regions may also differ between the fine and coarse time scales that are associated with different levels of neural complexity (McDonough and Nashiro, 2014). Coarse time scales may reflect long-range interactions across distributed neural populations, while fine time scales may reflect interconnectivity among local neural populations (Vakorin et al., 2011; McIntosh et al., 2014). The purpose of this conceptual analysis paper is to investigate neurophysiological basis of complexity (MSE) of electrophysiology and fMRI signals, and to test the hypotheses on the relations between complexity and FC through the following perspectives: (1) theoretical simulations of network dynamics with the neural mass model (NMM) based brain network modeling, (2) animal models with concurrent recordings of fMRI and electrophysiology data in conjunction with pharmacological manipulations, and (3) MSE and FC analyses of rs-fMRI data with high spatiotemporal resolutions acquired with multiband echo-planar imaging (EPI) sequences of the Human Connectome Project (Feinberg et al., 2010; Moeller et al., 2010).

THEORETICAL MODELING

Large-Scale Brain Network Models

Theoretical modeling has unique strength for understanding and potentially predicting the complex behavior of brain networks under different experimental or behavioral conditions. Since the Hodgkin–Huxley model developed in the 1950s to explain the causes of single neuron spikes, biophysical models for large-scale brain activity have been developed to understand perception and behavior, as well as the determinants of large-scale neuroimaging data. As summarized by a recent review (Breakspear, 2017), there are primarily two types of models to describe collective dynamics of neuronal ensemble (e.g., a cortical column), including the Fokker–Planck equation (FPE) that assumes uncorrelated neuronal activities within an ensemble; and NMM that assumes strong coherence of neuronal activities within an ensemble which is biologically more meaningful (Breakspear, 2017).

As description of a local population of interacting neurons, NMMs can be integrated into mesoscopic circuits, and macroscopic systems to form so called "ensemble of ensembles"—large-scale brain network models (BNMs). BNMs integrate NMMs with research findings of complex brain networks (Jirsa et al., 2010; Mejias et al., 2016), since dynamics within each NMM results from both local population activity and influences of other NMMs, and here the coupling of NMMs is informed by anatomical connectivity such as the primate CoCoMac and diffusion MRI-based data (i.e., structure-functional model). This feature makes BNMs a favorable tool in simulation studies aimed to understand and interpret resting-state fMRI data. Indeed, existing modeling work in primates combined a static skeleton of structural connectivity with regional neural dynamics, signal transmission delays, and noise to understand the emerging properties of large-scale brain networks (Honey et al., 2007, 2009; Ghosh et al., 2008; Deco et al., 2009).

Simulation of Neural Complexity and FC

In this work, the Brain Dynamics Toolbox (https://github.com/breakspear/bdtoolkit) was used for simulation that includes NMM based BNMs (Heitmann and Breakspear, 2017). The NMM describes local populations of densely interconnected inhibitory and excitatory neurons whose behaviors are determined by voltage- and ligand-gated membrane channels. Sodium and calcium channels display a nonlinear sigmoid-shaped graph of voltage-dependent conductance. Potassium channel conductance is modeled in a more complex manner, exponentially relaxing toward its voltage-dependent state. A medium-scale (mesoscopic) array (BNM) is then constructed from these local nonlinear populations by introducing long-range pyramidal connections, mimicking glutamate-induced synaptic currents. Spatiotemporal patterns arise through reentrant excitatory–excitatory feedback (Breakspear et al., 2003). Activity in the system arises purely from nonlinear instabilities (and noise can also be added). Oscillations are hence spontaneous and self-organizing.

We used CoCoMac (Honey et al., 2007) as structural connectivity matrix and set all physiologically measurable parameters within their accepted ranges to generate dynamically plausible behavior (Breakspear et al., 2003), while ensuring different nodes wouldn't stay synchronized because of too strong coupling. For each node, a simulated spike train with 10,000 data points was generated, and coarse-grained time series were constructed by averaging the original time series over scales of 2–400, respectively. MSE at each scale was calculated as the Sample Entropy (SampEn) of the corresponding time series, defined as the log likelihood of $m+1$-length patterns matching within a tolerance threshold r, provided they were matching for the first m points (Richman and Moorman, 2000; Smith et al., 2014). We used pattern length $m = 3$ and pattern matching threshold $r = 0.2$ for simulated data with a length of 10,000 data points and low noise. The mean MSE was then generated across the full scale as well as across 5 frequency bands (delta, theta, alpha, beta, and gamma), respectively.

Functional connectivity (FC) was computed by Pearson correlations between spike train time series of all pairs of network nodes. The relationship between MSE and FC of nodal spike trains was investigated by repeated simulations (total 50) while randomly varying excitatory-to-excitatory connectivity (Aee) which represents the strength of long-range FC. For each simulation we randomly picked an Aee value between 0 and 0.55 to generate spike trains using the BNM. A random noise with additive volatility of 0.001 was included in the spike train time course. Cross-correlations between the mean MSE and FC measures were calculated to estimate their associations across the whole CoCoMac and its 5 modules, respectively (see below). **Figure 3** shows our modeling parameters and simulated neural spike trains and FC matrix based on the CoCoMac (Honey et al., 2007). The simulated neural spike train of one node (solid curve) exhibits a pattern of synchronization—desynchronization with the rest nodes (gray curves). The FC matrix clearly demonstrates 5 modules of functionally connected networks, which is highly consistent with the partition of CoCoMac into 5 structural modules (corresponding to frontal/orbitofrontal, inferior temporal,

frontal/superior temporal, prefrontal/motor/somatosensory, and occipital/visual/prefrontal regions; Harriger et al., 2012).

Both MSE and FC increase with larger Aee in the whole CoCoMac as well as its 5 modules ($r \geq 0.78$, $p \leq 0.001$, Figures S1, S2). As a result, significant positive correlations ($r \geq 0.56$, $p \leq 0.001$) between FC and MSE were observed in the whole CoCoMac as well as its 5 modules by randomly varying Aee (**Figure 4A**). In the above analyses assuming a sampling rate of 200 Hz, MSE was averaged across the time scale of 1–400 corresponding to temporal frequency of 0.5–200 Hz. We also calculated averaged MSE of different frequency bands (delta, theta, alpha, beta, gamma) and the results are displayed in **Figure 4B**. There is a trend of decreasing associations between MSE and FC from the theta (4–7 Hz), alpha (8–15 Hz), beta (16–31 Hz), to gamma (32–200 Hz) band. In fact, for alpha, beta and gamma bands there is an inverted U-shaped relationship between MSE and FC, which is best fit by a quadratic function (see **Figure 4B**). For the delta band, we calculated MSE over the full (0.5–4 Hz) and a narrower range (2.7–4 Hz) to match the time points for averaging of the rest frequency bands, and the narrower band of high delta frequencies showed the highest correlation between MSE and FC ($r = 0.79$) among all frequency bands.

In addition, we performed simulations without added random noise. As expected, the MSE values became smaller and the FC larger. Nevertheless, the increasing trend of MSE and FC with larger Aee as well as their positive correlations remain unchanged.

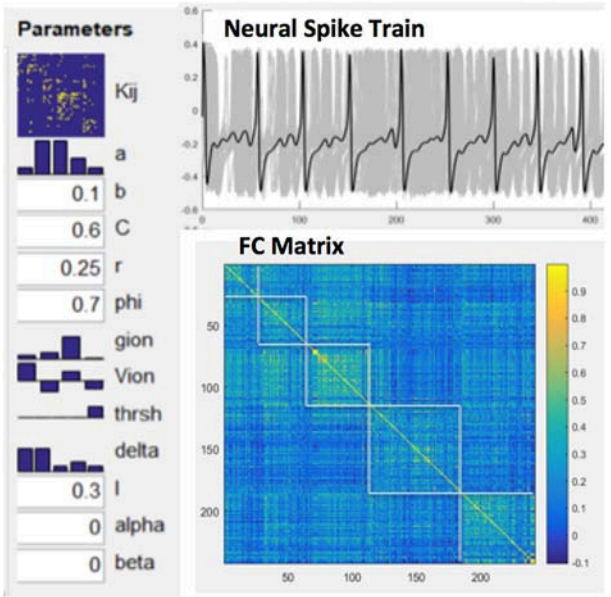

FIGURE 3 | Model parameters for NMM based brain network modeling, simulated neural spike train of one node (solid curve) and rest nodes (gray curves) and resultant FC matrix with 5 modules.

ANIMAL EXPERIMENT WITH CONCURRENT ELECTROPHYSIOLOGY AND MRI

For this section, we reanalyzed concurrent electrophysiology and MRI data acquired in rats at 9.4T (Jaime et al., 2017). The purpose of the original study was to understand the neurophysiological basis of spontaneous rs-fMRI fluctuations and FC through cross-frequency phase-amplitude coupling (PAC) between concurrently recorded local field potential (LFP) and BOLD signals in the striatum at resting state and by agonizing the AMPA (α-amino-3-hydroxy-5-methyl-4-isoxazolepropionic acid) receptors within the ventral tegmental area (VTA). All experimental procedures were approved by the NIDA-IRP Animal Care and Use Committee. Silicon-based MRI-compatible microelectrode arrays (NeuroNexus) were implanted into the left striatum in rats ($N = 8$), and a microinjection cannula was implanted above the VTA for AMPA microinjections to modulate VTA neuronal activity and connected striatum areas. After 1-week recovery from surgery, rats underwent repeated concurrent fMRI and electrophysiological recording experiments on a Bruker 9.4T scanner. A single shot GE-EPI sequence ($TR = 1{,}500$ ms, $TE = 15$ ms, matrix $= 64 \times 64$, FOV $= 1.92 \times 1.92$ cm^2, 5×0.3 mm slices) was used to acquire BOLD data for ∼60 min (7.5 min per epoch). MR gradient and RF induced artifacts on LFP were corrected as described in Jaime et al. (2017). The timing of each artifact segment was identified based on concurrently acquired slice trigger signal from the scanner. Each 60 ms LFP segment immediately following the trigger signal had high-amplitude (up to ±5 V) fast changing signals. These segments were replaced by linear interpolation. The linearly interpolated segments were then replaced by cubic-spline interpolation of the data from 35 ms before and 35 ms after the artifact segments. Finally, LFP data were low-pass filtered to 100 Hz and down-sampled to 50 Hz for final MSE analysis. Repeated fMRI/LFP data were recorded pre and post microinjection of AMPA (1 μl, 100 μM) in VTA. MSE was calculated for both LFP and fMRI data (pattern length $m = 2$, matching threshold $r = 0.5$, scale = 1–40 for LFP and 1–10 for BOLD time series). FC of fMRI data was calculated using ventral striatum as the seed area. ANOVA was then applied to detect brain regions with significant mean MSE and/or FC changes by AMPA injection. Cross-correlations were calculated between mean MSE of LFP and fMRI in ventral striatum as well as FC of fMRI within the ventral striatum cluster showing significant FC changes following AMPA injection.

Figures 5A,B show MRI of electrode positions and clusters with significant mean MSE and FC changes due to AMPA injection in animal experiment. As shown in **Figures 6A,B**, both mean MSE of LFP (recorded at electrode tip) and FC of BOLD fMRI (within ventral striatum cluster) decrease following AMPA injection, with a significant correlation ($r = 0.505$, $p < 0.001$) between the two measures (calculated with partial correlation controlling effect of animals). All metrics return to baseline at 37.5 min post AMPA with overshoot afterwards. We also

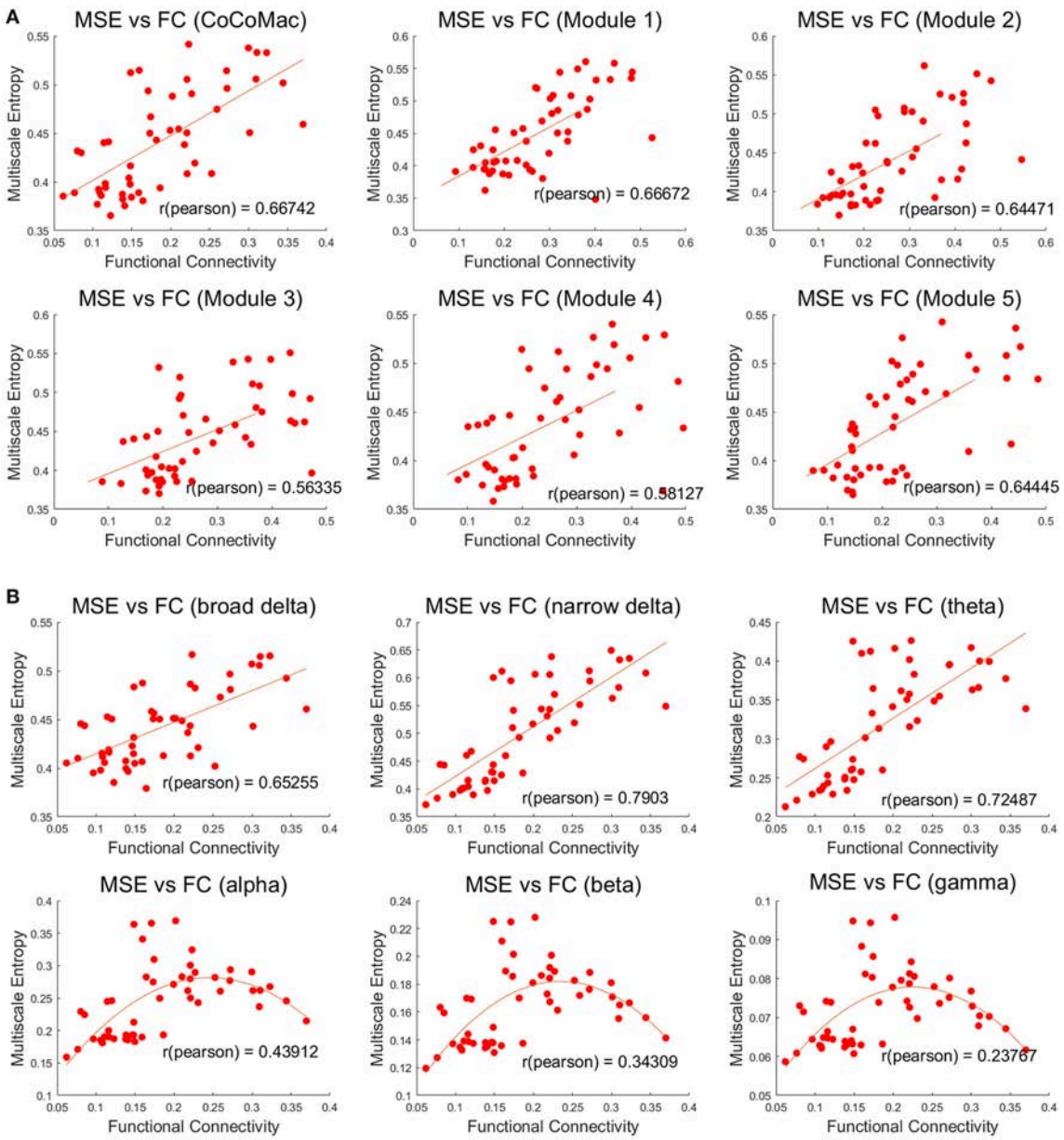

FIGURE 4 | (A) Positive correlations between mean MSE and FC of whole CoCoMac and 5 modules ($p < 0.001$). MSE was averaged across the time scale of 1 to 400 corresponding to temporal frequency of 0.5–200 Hz. **(B)** Associations between frequency band dependent MSE and FC of the whole CoCoMac. MSE was averaged within the delta (broad 0.5–4 Hz and narrow 2.7–4 Hz), theta (4–7 Hz), alpha (8–15 Hz), beta (16–31 Hz), gamma (32–200 Hz). Each data point (total 50) was generated with mean MSE and FC values simulated with a random excitatory-to-excitatory connectivity (Aee) value (0–0.55) as well as adding random noise. Fitted linear and quadratic functions are also plotted in each sub-figure.

calculated MSE of different frequency band of LFP and the results are listed in **Table 1**. Consistent with simulation results shown in **Figure 4B**, there is a trend of decreasing associations between MSE and FC from the theta, alpha, beta, to gamma band. In addition, MSE of BOLD fMRI (0.04–0.07 Hz) in ventral striatum shows a trend of decreasing followed by signal recovery in response to AMPA injection (**Figure 6C**), which is significantly correlated with that of fMRI FC ($r = 0.43$, $p = 0.0005$).

HUMAN FMRI WITH HCP SMS EPI SEQUENCES

We analyzed resting state fMRI (rs-fMRI) data of 20 subjects from the HCP database (Van Essen et al., 2013). These participants were unrelated to each other, relatively healthy individuals that were free of a prior history of significant psychiatric or neurological illnesses, but could have a history of

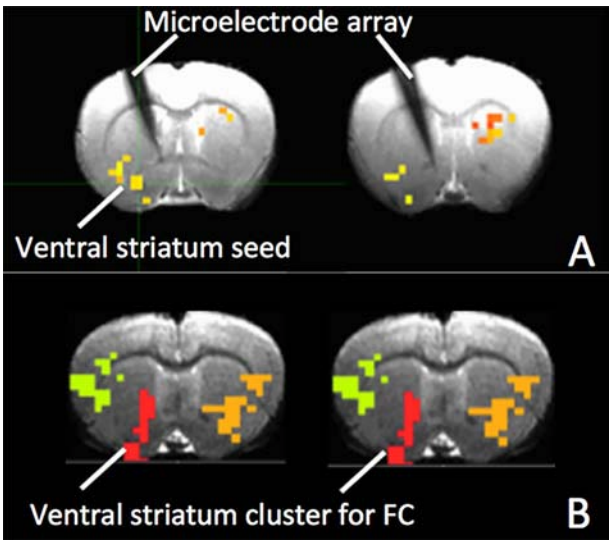

FIGURE 5 | (A) The electrode and clusters with significant fMRI MSE changes due to AMPA injection are shown on gradient echo (GRE) images of rat brain. The cluster in the ventral striatum is used as seed for FC; **(B)** Clusters with significant FC changes in response to VTA AMPA injection. The ventral striatum cluster (red) was used for calculation of mean FC.

smoking, heavy drinking, or recreational drug use without having experienced severe symptoms. All participants gave written informed consent as approved by the Washington University in St. Louis institutional review board.

Data were acquired at 3T with TR/TE = 720/33 ms, multiband-factor 8, FA = 52°, gradient-echo EPI readout and 2 mm isotropic resolution (Smith et al., 2013a). For each subject two sessions of rs-fMRI were analyzed with phase encoding from left to right (LR) and right to left (RL), respectively. Datasets were preprocessed according to HCP minimal preprocessing pipeline (Glasser et al., 2013). Additionally we regressed out physiological noise (white matter and cerebrospinal fluid signal fluctuations calculated as average signal fluctuations within eroded tissue probability maps) and motion parameters (3 translations and 3 rotations as well as their first derivatives). Preprocessed data was submitted to a group independent component analysis (GIFT toolbox; Calhoun et al., 2001) and four components were selected, which represent the Default Mode Network (DMN), Left and Right Executive Control Networks (L-/RECN), and the Salience Network (SAL).

For all nodes within these networks we computed FC between all nodes using conventional Pearson correlations. Second, MSE was calculated for 40 temporal scales (pattern length $m = 2$, matching threshold $r = 0.5$; McDonough and Nashiro, 2014; Smith et al., 2014). This allowed comparing FC to signal complexity at different temporal frequencies. Results from the LR and RL phase encoded rs-fMRI sessions were averaged for each subjects and the following tests were performed: (i) To test for potential relations between the local signal dynamics (MSE) and network coherence (FC) we correlated the overall network FC with overall network MSE across scales to identify a global association between network connectivity and network complexity. The overall network measures were computed by means of averaging across all node-to-node connections for FC and all nodes' MSE, respectively; (ii) We correlated MSE to the average FC of each node to identify the frequency range where MSE correlates to nodal connectivity.

On the network level, we found that the overall network FC is inversely related to the overall network MSE at higher temporal frequencies (0.347–0.694 Hz) across subjects while positively correlated to MSE at lower temporal frequencies (0.020–0.087 Hz; **Figure 7**). This result was found to be consistent for all four networks representing higher cognitive functions as well as when combining all nodes of all networks into a whole-brain network. This finding is consistent with previous reports (McDonough and Nashiro, 2014) and the theory that higher-frequency oscillations originate from smaller local neuronal populations, whereas low-frequency oscillations encompass larger long-range neuronal populations. Hence while MSE at higher frequencies represents local processing the association between FC and low frequency MSE represents the information transfer between distributed nodes of the network.

A more detailed analysis at the nodal level of the relationship between nodal MSE and the single node connectivity within the networks (average connectivity to all other nodes) revealed that the nodal signal complexity is positively correlated to average FC of a network node at low frequencies (0.020–0.087 Hz; **Figure 8**), similar to the pattern we observed at the network level. This finding suggest that the higher the complexity at a given node at low frequencies the more it is integrated into the network. Again this is in line with the theory that MSE at low frequencies might be related to information transfer between nodes of a network. Interestingly some nodes show very strong associations: for example the posterior cingulate cortex (PCC) in the DMN and the dorsal anterior cingulate cortex (dACC) in the SAL. We hypothesize that these areas represent hub areas in the respective networks that orchestrate the flow of information within these systems since their nodal complexity dominates the network's functional connectivity. This further indicates that complex and thus less regular signals in network nodes could allow for a more dynamic network reconfiguration and explorations of different FC states, and that network hub areas lie at the center of such reconfigurations and facilitate the information exchange between separate networks (Yang et al., 2013).

Last but not the least, conventional FC analysis often uses a band-pass filter limiting the frequency range from 0.001 to 0.1 Hz since this frequency range dominates long-range connections (Cordes et al., 2001). While higher frequencies are often contaminated by noise, there is increasing evidence that high frequency fMRI fluctuations also contribute to FC (Niazy et al., 2011; Smith et al., 2013b), especially since the advent of multiband fMRI acquisitions with sub-second temporal resolutions. Here we provide further evidence that the low-frequency fMRI fluctuations is strongly related to the long-range connectivity commonly investigated, while the MSE of high-frequency fMRI fluctuations

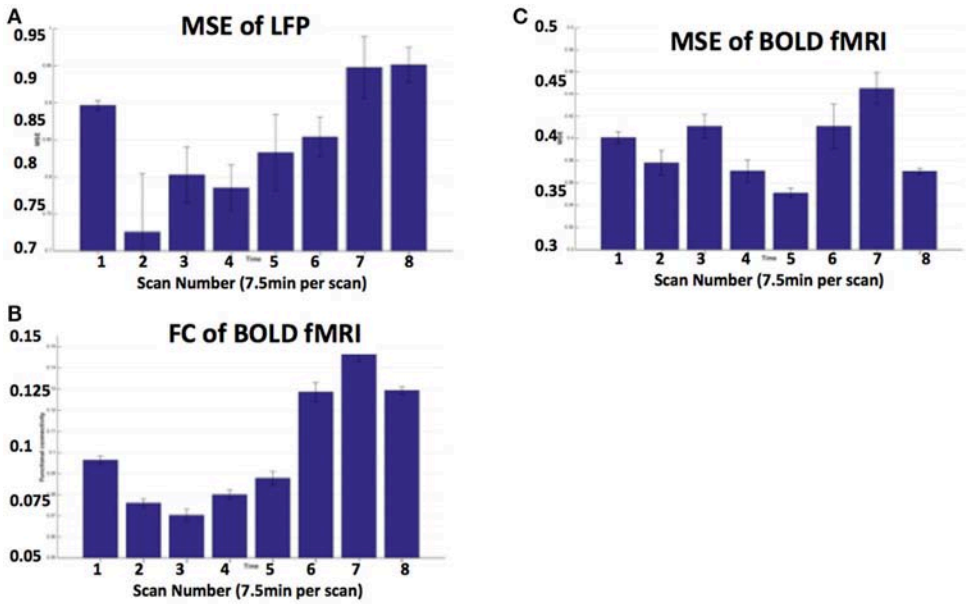

FIGURE 6 | (A) MSE of LFP recorded at electrode tip (close to ventral striatum); **(B)** BOLD FC using ventral striatum as a seed; **(C)** MSE of BOLD fMRI (0.04–0.07 Hz) in ventral striatum following VTA AMPA injection in 8 animals. Each scan is 7.5 min and scan 1 is baseline. FC is averaged within the ventral striatum cluster shown in **Figure 5B**.

TABLE 1 | Correlations between MSE of different frequency band of LFP and FC of BOLD fMRI signals (calculated with partial correlations controlling for effect of animals).

Frequency band (Hz)	*R*-value	*P*-value
Delta (1.25–4)	0.454	<0.001
Theta (4–7)	0.56	<0.001
Alpha (7–13)	0.545	<0.001
Beta (13–25)	0.505	<0.001
Gamma (25–50)	0.444	<0.001

may represent local signal processing that shows inverse correlations with FC. Our data suggest that high frequency fMRI fluctuations may also contribute to understanding the dynamic organization of brain networks in rs-fMRI (Cabral et al., 2017).

DISCUSSION

Complexity Analysis of Brain Signals

The self-similarity of neural signals across both temporal and spatial scales has been consistently observed in EEG, MEG, and fMRI studies of healthy volunteers, characterized by a power law of two-point correlation function (reviewed by Turkheimer et al., 2015). This observation indicates that a complex system such as the brain operates close to a critical point between two extreme states, one of excessive cortical integration, where long-range correlations dominate the dynamics of the system, and the other of complete segregation where activity is locally constrained. It has been suggested in brain models that operating at a point near criticality maximizes the dynamic range, sensitivity, and response time of networks to incoming information and is therefore ecologically advantageous (Beggs, 2008; de Arcangelis and Herrmann, 2010; Urban et al., 2012; Moretti and Munoz, 2013).

In electrophysiology, transient periods of synchronization of neuronal activities, typically mediated by gamma oscillations, are separated by moments of de-synchronization that mark the transition between perception and response (Rodriguez et al., 1999). Recent fMRI studies have shown that the temporal variation of FC is non-stationary with dynamic changes within time scales of seconds to minutes, and an rs-fMRI scan is characterized by frequent transitions between a repertoire of reoccurring short-term connectivity patterns termed "FC states" (Chang and Glover, 2010; Hutchison et al., 2013a,b; Allen et al., 2014). Such dynamic changes of reoccurring microstate sequences have also been observed in EEG (Van De Ville et al., 2010). There is evidence that temporal variability of FC and/or microstates is associated with behavioral performance, and may be affected by conscious and behavioral states (Thompson et al., 2013a,b; Barttfeld et al., 2015; Elton and Gao, 2015).

Based on such theory, characterizing the complexity of neural signals may indicate the brain's capacity for information processing, i.e., increased complexity of regional neural signals may indicate greater transition or exploration between different states of brain networks, thereby a greater propensity for information processing (McDonough and Nashiro, 2014;

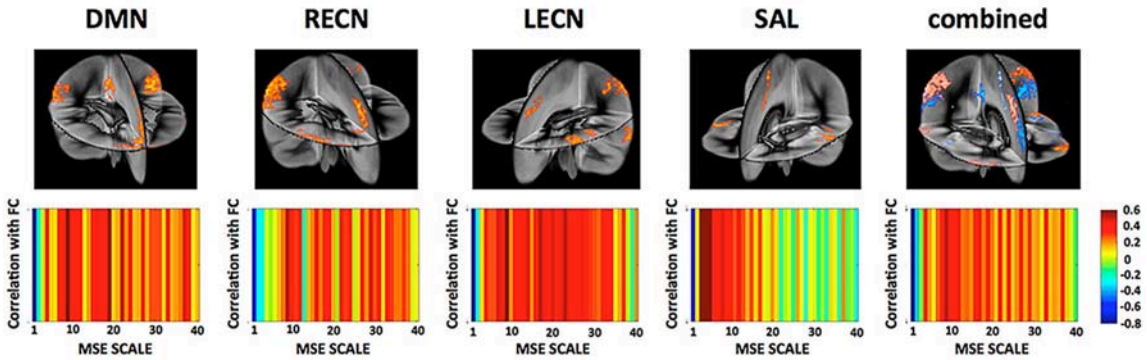

FIGURE 7 | (Top) Networks and their nodes as identified from group ICA displayed in a three dimensional rendering of the brain. [DMN, Default Mode Network; LECN, left executive control network; RECN, right executive control network]. **(Bottom)** Correlation between a network global FC and their MSE across all frequency scales. While network FC shows negative correlations between MSE and FC at higher frequencies (fine scales) there is indication that this relationship reverses at mid- to low-frequencies. This is in line with the view that MSE at high frequencies represents more local processing independent from other nodes whereas MSE at lower frequencies represents the information transfer between distributed nodes.

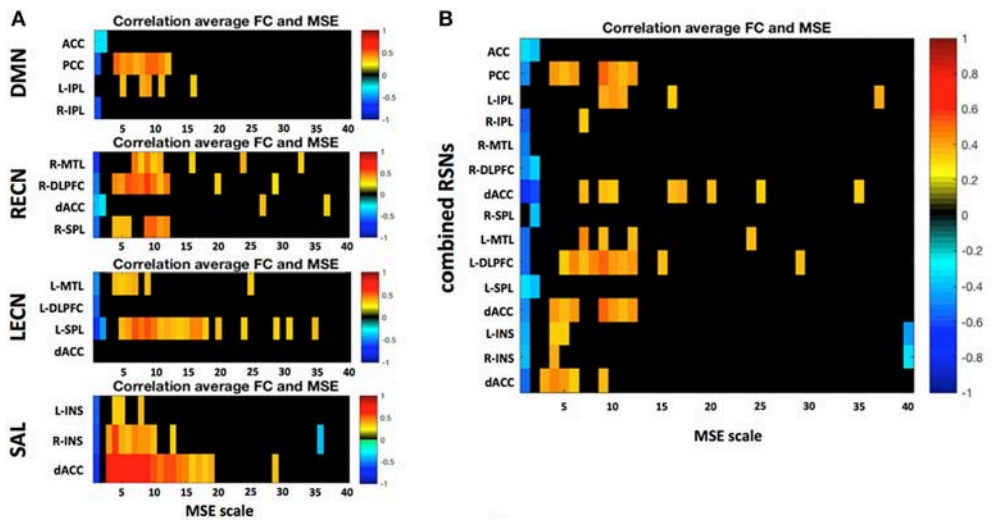

FIGURE 8 | (A) Correlation between a region's average FC to all other nodes within the respective resting state network (RSN) and its MSE across all frequency scales. **(B)** Same analysis but all four RSNs were combined into one global network. Only significant correlations ($p < 0.05$) are depicted. Static FC shows positive correlations between MSE and FC mid to low frequencies there.

Turkheimer et al., 2015). In this sense, model-free statistical metrics such as MSE are well suited for characterizing the non-stationary dynamic changes in neural signals across multiple measurement scales.

Relationship Between Neural Complexity and Network FC

In this paper, we investigated the relations between neural complexity (as measured by MSE) and network FC through theoretical simulations, animal models, and human rs-fMRI data. Both simulation and animal experiment showed positive correlations between MSE of regional neural signals (LFP and/or fMRI) and network FC. In human rs-fMRI, the positive association between MSE of regional fMRI signals and network FC is observed at low temporal frequencies (0.020–0.087 Hz).

The overall positive association between MSE of regional neural signals and network FC may counter the intuition that more complex neural signals interfere with phase relationships between network nodes, thereby decreasing overall FC. Nevertheless, our observation is consistent with the hypothesis that FC is mediated by a dynamic series of reoccurring "FC states" leading to an increased overall FC (averaged over a few minutes) with a greater level of regional neural complexity. Furthermore, our simulation and animal data showed a trend of decreasing associations between MSE and FC from the theta, alpha, beta, to gamma band. In rs-fMRI data, we observed positive associations between complexity and FC at low temporal frequencies

(0.020–0.087 Hz), and negative correlation between complexity and FC at high temporal frequencies (0.347–0.694 Hz). This is consistent with the theory that coarse time scales or lower temporal frequencies may reflect long-range interactions across distributed neural populations, while fine time scales or higher temporal frequencies may reflect interconnectivity among local neural populations (Vakorin et al., 2011; McIntosh et al., 2014). Hence MSE at high and low temporal frequencies may represent local and distributed information processing across nodes of the network respectively.

Another observation from our study is that the overall relationship between neural complexity and network FC is replicated across measurement scales from electrophysiology to fMRI, as well as across network scales such as the whole CoCoMac and its 5 modules, the 4 major human resting brain networks and their combined whole-brain network. This observation adds to increasing evidence of scale-invariant processes observed across a number of modalities such as electrophysiology, EEG, structural and functional MRI, as well as the hypothesis on the elementary spatial brain motif underlying computations across spatially organized neuronal ensembles (Turkheimer et al., 2015). Our data may also be interpreted in the context of non-equilibrium steady state (NESS) dynamics, self-organized criticality (SOC) and slowing (Stam and de Bruin, 2004; Shin and Kim, 2006; Kitzbichler et al., 2009). Critical slowing means that some modes of SOC systems decay slowly, compared to the stable fast modes, and show protracted correlations over time which are linked with the emergence of the intrinsic brain networks. This plausible interpretation may provide a link between the underlying neural complexity and the emergent large-scale functional connectivity. Overall, our results from dynamic network modeling, animal models, and human rs-fMRI suggest that characterizing the complexity of neural signals across spatial and temporal scales provides a valuable approach, alone or in conjunction with FC, to elucidate the mechanisms of local signal processing and relation to information transfer within functionally connected brain networks.

Potential Applications of Complexity Analysis

We expect potential applications of brain complexity analysis in the following areas: (1) Probing the excitatory/inhibitory (E/I) balance of regional neuronal populations; (2) Characterizing conscious and behavioral states including sleep, anesthesia, and vegetative states; (3) Diagnosing neurological disorders such as epilepsy and dementia.

The complexity of local signal fluctuations has been hypothesized to be sensitive to the coordinated firing of neuronal clusters, where increased excitability causes more irregular/complex activity and increased inhibition more regular/predictable patterns (Homayoun and Moghaddam, 2007; Haider and McCormick, 2009). Hence, quantifying the complexity of dynamic brain signals using non-linear statistics such as MSE may provide a unique and innovative approach to probe the underlying neuronal fluctuations and the E/I balance. In particular, electrophysiology and fMRI recording may be combined with noninvasive neuromodulation techniques such as transcranial magnetic stimulation (TMS) and transcranial direct current stimulation (tDCS) to manipulate the regional E/I state while observing concomitant changes in neural complexity (Liang et al., 2014).

The brain operates at a point near criticality between incoherence and synchrony that facilitates its fluid transition across a repertoire of quasi-stable states. Such self-organizing capability of the brain is affected by conscious and behavioral states including sleep, anesthesia, and vegetative state. Recently, complexity analysis has been successfully applied as a consciousness test by calculating the perturbational complexity index (PCI) of TMS induced EEG response (Massimini et al., 2005; Casali et al., 2013; Casarotto et al., 2016). The PCI exploits the common video compression algorithm (e.g., MPEG) to estimate the compressibility of TMS elicited EEG response. For spontaneous neural signals over relatively long measurement periods (e.g., minutes), MSE and its variants may be more suitable for characterizing conscious and behavioral states compared to PCI that was designed for transient responses.

MSE analysis may also have clinical value for diagnosing neurological disorders such as epilepsy and dementia. Epileptic seizures are characterized by relatively large-scale synchronization of the EEG signal into high amplitude and stereotyped bursts, reflecting the recruitment of millions of neurons to fire together in a patterned manner. In other words, epilepsy is an abnormal, and toxic, self-organizing state of the brain that may benefit from complexity analysis (Engel et al., 1998). Other neurologic and psychiatric disorders such as dementia and schizophrenia are characterized by abnormal E/I balance and network FC, therefore are suitable for complexity analysis. Indeed, recent studies reported reduced entropy measures of rs-fMRI and functional near-infrared spectroscopy (fNIRS) in subjects with mild cognitive impairment and Alzheimer's disease which are correlated with cognitive performance (Wang et al., 2017; Li et al., 2018). Several of these potential applications are also showcased in this special research topic.

Limitations and Caveats of Complexity Analysis

Complexity analysis of electrophysiology and fMRI is still in its infancy. Several issues remain to be addressed before it can be reliably applied to basic neuroscience and clinical applications: (1) Key parameters such as pattern length m and matching threshold r have been empirically determined in existing studies. We used m of 3 and r of 0.2 for simulated data with more data points and less noise, and m of 2 and r of 0.5 for experimental data with shorter time series and higher noise. It may be possible to adaptively determine these parameters based on the estimated noise level in the data (Smith et al., 2015); (2) The test-retest repeatability of MSE analysis needs to established; and (3) Quality control and preprocessing steps of the data are also key to reliable MSE analysis. Our experience is that MSE of electrophysiology data is more reliable than that of fMRI due to higher signal-to-noise ratio (SNR) and sampling points.

Nevertheless, recent development of simultaneous multislice (SMS) or multiband imaging allows high spatial and temporal resolution fMRI that is ideally suited for MSE and other complexity analysis. While community interest in complexity analysis is growing high, it can be difficult for the researchers to obtain high quality, validated, and accessible tools to perform the computationally complex analyses they require. To date, PhysioToolkit (https://physionet.org/physiotools/) (Goldberger et al., 2000) is the most comprehensive library of software for physiologic signal processing and analysis, including novel methods based on statistical physics and nonlinear dynamics (e.g., entropy), and analysis of non-equilibrium and non-stationary processes. However, PhysioToolKit was designed primarily for analyzing physiologic recordings from a single or a few channels (e.g., ECG), and therefore does not have the capability to handle high volume 4D neuroimaging data such as fMRI and EEG. Existing neuroimaging software packages such as EEGLAB, SPM, and FSL, on the other hand, lack specific modules for nonlinear complexity analysis. Our group has developed the Complexity Toolbox (http://www.fil.ion.ucl.ac.uk/spm/ext/#Complexity) as the first systematic and comprehensive software package dedicated to complexity analysis of neuroimaging data. The current version includes four metrics: Approximate Entropy (ApEn), Sample Entropy (SampEn), Multi-Scale Entropy (MSE), and Cross-ApEn for the analysis of fMRI. Further development includes wavelet based MSE and MSE of dynamic FC, as well as complexity analysis of neurophysiology data such as EEG and ECoG.

CONCLUSION

Our results from theoretical modeling, animal experiment and human fMRI suggest that (1) Regional neural complexity and network FC may be two related aspects of brain's information processing: the more complex regional neural activity, the higher FC this node has with rest network nodes; (2) MSE at high and low frequencies may represent local and distributed information processing across nodes of the network. Based on literature and our data, we propose that the complexity of regional neural signals may provide an index of the brain's capacity of information processing—increased complexity may indicate greater transition or exploration between different states of brain networks, thereby a greater propensity for information processing.

AUTHOR CONTRIBUTIONS

DW, KJ, Y-FZ, and YY contributed to the conceptualization of this paper. KJ, CF, YQ, and HL contributed data analysis. DW, KJ, Y-FZ, and YY contributed to the drafting of the manuscript.

ACKNOWLEDGMENTS

This work was partially supported by the Intramural Research Program of the National Institute on Drug Abuse, the National Institutes of Health (NIH). Data from the Human Connectome Project, WU-Minn Consortium (Principal Investigators: David Van Essen and Kamil Ugurbil; 1U54MH091657) were funded by the 16 NIH Institutes and Centers that support the NIH Blueprint for Neuroscience Research; This work was also supported by NIH grant (UH2-NS100614). The authors are grateful to Drs. Michael Breakspear and Stewart Heitmann for their help with the Brain Dynamic Toolbox. The authors are also grateful to Dr. Robert X. Smith for his contribution of **Figure 1**.

SUPPLEMENTARY MATERIAL

The Supplementary Material for this article can be found online at: https://www.frontiersin.org/articles/10.3389/fnins.2018.00352/full#supplementary-material

REFERENCES

Abásolo, D., Hornero, R., Espino, P., Poza, J., Sanchez, C. I., and De La Rosa, R. (2005). Analysis of regularity in the EEG background activity of Alzheimer's disease patients with approximate entropy. *Clin. Neurophysiol.* 116, 1826–1834. doi: 10.1016/j.clinph.2005.04.001

Alivisatos, A. P., Chun, M., Church, G. M., Greenspan, R. J., Roukes, M. L., and Yuste, R. (2012). The brain activity map project and the challenge of functional connectomics. *Neuron* 74, 970–974. doi: 10.1016/j.neuron.2012.06.006

Allen, E. A., Damaraju, E., Plis, S. M., Erhardt, E. B., Eichele, T., and Calhoun, V. D. (2014). Tracking whole-brain connectivity dynamics in the resting state. *Cereb. Cortex* 24, 663–676. doi: 10.1093/cercor/bhs352

Bak, P., Tang, C., and Wiesenfeld, K. (1987). Self-organized criticality: an explanation of the 1/f noise. *Phys. Rev. Lett.* 59, 381–384. doi: 10.1103/PhysRevLett.59.381

Barttfeld, P., Uhrig, L., Sitt, J. D., Sigman, M., Jarraya, B., and Dehaene, S. (2015). Signature of consciousness in the dynamics of resting-state brain activity. *Proc. Natl. Acad. Sci. U.S.A.* 112, 887–892. doi: 10.1073/pnas.1418031112

Bassett, D. S., and Bullmore, E. (2006). Small-world brain networks. *Neuroscientist* 12, 512–523. doi: 10.1177/1073858406293182

Beckmann, C. F., and Smith, S. M. (2004). Probabilistic independent component analysis for functional magnetic resonance imaging. *IEEE Trans. Med. Imaging* 23, 137–152. doi: 10.1109/TMI.2003.822821

Beggs, J. M. (2008). The criticality hypothesis: how local cortical networks might optimize information processing. *Philos. Trans. A Math. Phys. Eng. Sci.* 366, 329–343. doi: 10.1098/rsta.2007.2092

Bell, A. J., and Sejnowski, T. J. (1995). An information-maximization approach to blind separation and blind deconvolution. *Neural Comput.* 7, 1129–1159. doi: 10.1162/neco.1995.7.6.1129

Betzel, R. F., Erickson, M. A., Abell, M., O'donnell, B. F., Hetrick, W. P., and Sporns, O. (2012). Synchronization dynamics and evidence for a repertoire of network states in resting EEG. *Front. Comput. Neurosci.* 6:74. doi: 10.3389/fncom.2012.00074

Biswal, B., Yetkin, F. Z., Haughhton, V. M., and Hyde, J. S. (1995). Functional connectivity in the motor cortex of resting human brain using echo-planar imaging. *Magn. Reson. Med.* 34, 537–541. doi: 10.1002/mrm.1910340409

Breakspear, M. (2017). Dynamic models of large-scale brain activity. *Nat. Neurosci.* 20, 340–352. doi: 10.1038/nn.4497

Breakspear, M., Terry, J. R., and Friston, K. J. (2003). Modulation of excitatory synaptic coupling facilitates synchronization and complex dynamics in a biophysical model of neuronal dynamics. *Network* 14, 703–732. doi: 10.1088/0954-898X_14_4_305

Bullmore, E., Fadili, J., Maxim, V., Sendur, L., Whitcher, B., Suckling, J., et al. (2004). Wavelets and functional magnetic resonance imaging of the human brain. *NeuroImage* 23(Suppl. 1), S234–S249. doi: 10.1016/j.neuroimage.2004.07.012

Bullmore, E., and Sporns, O. (2009). Complex brain networks: graph theoretical analysis of structural and functional systems. *Nat. Rev. Neurosci.* 10, 186–198. doi: 10.1038/nrn2575

Cabral, J., Kringelbach, M. L., and Deco, G. (2017). Functional connectivity dynamically evolves on multiple time-scales over a static structural connectome: models and mechanisms. *Neuroimage* 160, 84–96. doi: 10.1016/j.neuroimage.2017.03.045

Calhoun, V. D., Adali, T., Pearlson, G. D., and Pekar, J. J. (2001). A method for making group inferences from functional MRI data using independent component analysis. *Hum. Brain Mapp.* 14, 140–151. doi: 10.1002/hbm.1048

Carr, J. (1981). *Applications of Centre Manifold Theory*. New York, NY: Springer-Verlag.

Casali, A. G., Gosseries, O., Rosanova, M., Boly, M., Sarasso, S., Casali, K. R., et al. (2013). A theoretically based index of consciousness independent of sensory processing and behavior. *Sci. Transl. Med.* 5:198ra105. doi: 10.1126/scitranslmed.3006294

Casarotto, S., Comanducci, A., Rosanova, M., Sarasso, S., Fecchio, M., Napolitani, M., et al. (2016). Stratification of unresponsive patients by an independently validated index of brain complexity. *Ann. Neurol.* 80, 718–729. doi: 10.1002/ana.24779

Chang, C., and Glover, G. H. (2010). Time-frequency dynamics of resting-state brain connectivity measured with fMRI. *Neuroimage* 50, 81–98. doi: 10.1016/j.neuroimage.2009.12.011

Cohen, M. S., and Bookheimer, S. Y. (1994). Localization of brain function using magnetic resonance imaging. *Trends Neurosci.* 17, 268–277. doi: 10.1016/0166-2236(94)90055-8

Cordes, D., Haughton, V. M., Arfanakis, K., Carew, J. D., Turski, P. A., Moritz, C. H., et al. (2001). Frequencies contributing to functional connectivity in the cerebral cortex in "resting-state" data. *Am. J. Neuroradiol.* 22, 1326–1333.

Costa, M., Goldberger, A. L., and Peng, C. K. (2002). Multiscale entropy analysis of complex physiologic time series. *Phys. Rev. Lett.* 89:068102. doi: 10.1103/PhysRevLett.89.068102

Damoiseaux, J. S., Rombouts, S. A., Barkhof, F., Scheltens, P., Stam, C. J., Smith, S. M., et al. (2006). Consistent resting-state networks across healthy subjects. *Proc. Natl. Acad. Sci. U.S.A.* 103, 13848–13853. doi: 10.1073/pnas.0601417103

de Arcangelis, L., and Herrmann, H. J. (2010). Learning as a phenomenon occurring in a critical state. *Proc. Natl. Acad. Sci. U.S.A.* 107, 3977–3981. doi: 10.1073/pnas.0912289107

Deco, G., Jirsa, V., McIntosh, A. R., Sporns, O., and Kötter, R. (2009). Key role of coupling, delay, and noise in resting brain fluctuations. *Proc. Natl. Acad. Sci. U.S.A.* 106, 10302–10307. doi: 10.1073/pnas.0901831106

Di Ieva, A., Esteban, F. J., Grizzi, F., Klonowski, W., and Martin-Landrove, M. (2015). Fractals in the neurosciences, part II: clinical applications and future perspectives. *Neuroscientist* 21, 30–43. doi: 10.1177/1073858413513928

Elton, A., and Gao, W. (2015). Task-related modulation of functional connectivity variability and its behavioral correlations. *Hum. Brain Mapp.* 36, 3260–3272. doi: 10.1002/hbm.22847

Engel, J., Pedley, T. A., and Aicardi, J. (1998). *Epilepsy : A Comprehensive Textbook*. Philadelphia, PA: Lippincott-Raven.

Feinberg, D. A., Moeller, S., Smith, S. M., Auerbach, E., Ramanna, S., Gunther, M., et al. (2010). Multiplexed echo planar imaging for sub-second whole brain FMRI and fast diffusion imaging. *PLoS ONE* 5:e15710. doi: 10.1371/journal.pone.0015710

Friston, K., Breakspear, M., and Deco, G. (2012). Perception and self-organized instability. *Front. Comput. Neurosci.* 6:44. doi: 10.3389/fncom.2012.00044

Friston, K. J., Li, B., Daunizeau, J., and Stephan, K. E. (2011). Network discovery with DCM. *Neuroimage* 56, 1202–1221. doi: 10.1016/j.neuroimage.2010.12.039

Garrett, D. D., Samanez-Larkin, G. R., Macdonald, S. W., Lindenberger, U., McIntosh, A. R., and Grady, C. L. (2013). Moment-to-moment brain signal variability: a next frontier in human brain mapping? *Neurosci. Biobehav. Rev.* 37, 610–624. doi: 10.1016/j.neubiorev.2013.02.015

Ghanbari, Y., Bloy, L., Christopher Edgar, J., Blaskey, L., Verma, R., and Roberts, T. P. (2015). Joint analysis of band-specific functional connectivity and signal complexity in autism. *J. Autism Dev. Disord.* 45, 444–460. doi: 10.1007/s10803-013-1915-7

Ghosh, A., Rho, Y., McIntosh, A. R., Kötter, R., and Jirsa, V. K. (2008). Noise during rest enables the exploration of the brain's dynamic repertoire. *PLoS Comput. Biol.* 4:e1000196. doi: 10.1371/journal.pcbi.1000196

Gilden, D. L. (2001). Cognitive emissions of 1/f noise. *Psychol. Rev.* 108, 33–56. doi: 10.1037/0033-295X.108.1.33

Ginzburg, V. L., and Landau, L. D. (1950). On the theory of superconductivity. *Zh. Eksp. Teor. Fiz.* 20:1064.

Gisiger, T. (2001). Scale invariance in biology: coincidence or footprint of a universal mechanism? *Biol. Rev. Camb. Philos. Soc.* 76, 161–209. doi: 10.1017/S1464793101005607

Glasser, M. F., Sotiropoulos, S. N., Wilson, J. A., Coalson, T. S., Fischl, B., Andersson, J. L., et al. (2013). The minimal preprocessing pipelines for the human connectome project. *Neuroimage* 80, 105–124. doi: 10.1016/j.neuroimage.2013.04.127

Goldberger, A. L. (1996). Non-linear dynamics for clinicians: chaos theory, fractals, and complexity at the bedside. *Lancet* 347, 1312–1314. doi: 10.1016/S0140-6736(96)90948-4

Goldberger, A. L., Amaral, L. A., Glass, L., Hausdorff, J. M., Ivanov, P. C., Mark, R. G., et al. (2000). PhysioBank, PhysioToolkit, and PhysioNet: components of a new research resource for complex physiologic signals. *Circulation* 101, E215–E220. doi: 10.1161/01.CIR.101.23.e215

Haider, B., and McCormick, D. A. (2009). Rapid neocortical dynamics: cellular and network mechanisms. *Neuron* 62, 171–189. doi: 10.1016/j.neuron.2009.04.008

Haken, H. (1983). *Synergistics: An Introduction, Non-Equilibrium Phase Transition and Self-Organisation in Physics, Chemistry and Biology*. Berlin; Heidelberg: Springer Verlag.

Harriger, L., van Den Heuvel, M. P., and Sporns, O. (2012). Rich club organization of macaque cerebral cortex and its role in network communication. *PLoS ONE* 7:e46497. doi: 10.1371/journal.pone.0046497

He, B. J., Zempel, J. M., Snyder, A. Z., and Raichle, M. E. (2010). The temporal structures and functional significance of scale-free brain activity. *Neuron* 66, 353–369. doi: 10.1016/j.neuron.2010.04.020

Heitmann, S., and Breakspear, M. (2017). *Handbook for the Brain Dynamics Toolbox*. Brisbane, QLD: QIMR Berghofer Medical Research Institute.

Homayoun, H., and Moghaddam, B. (2007). NMDA receptor hypofunction produces opposite effects on prefrontal cortex interneurons and pyramidal neurons. *J. Neurosci.* 27, 11496–11500. doi: 10.1523/JNEUROSCI.2213-07.2007

Honey, C. J., Kötter, R., Breakspear, M., and Sporns, O. (2007). Network structure of cerebral cortex shapes functional connectivity on multiple time scales. *Proc. Natl. Acad. Sci. U.S.A.* 104, 10240–10245. doi: 10.1073/pnas.0701519104

Honey, C. J., Sporns, O., Cammoun, L., Gigandet, X., Thiran, J. P., Meuli, R., et al. (2009). Predicting human resting-state functional connectivity from structural connectivity. *Proc. Natl. Acad. Sci. U.S.A.* 106, 2035–2040. doi: 10.1073/pnas.0811168106

Hutchison, R. M., Womelsdorf, T., Allen, E. A., Bandettini, P. A., Calhoun, V. D., Corbetta, M., et al. (2013a). Dynamic functional connectivity: promise, issues, and interpretations. *Neuroimage* 80, 360–378. doi: 10.1016/j.neuroimage.2013.05.079

Hutchison, R. M., Womelsdorf, T., Gati, J. S., Everling, S., and Menon, R. S. (2013b). Resting-state networks show dynamic functional connectivity in awake humans and anesthetized macaques. *Hum. Brain Mapp.* 34, 2154–2177. doi: 10.1002/hbm.22058

Jaime, S., Gu, H., Sadacca, B. F., Stein, E. A., Cavazos, J. E., Yang, Y., et al. (2017). Delta rhythm orchestrates the neural activity underlying the resting state BOLD signal via phase-amplitude coupling. *Cereb. Cortex* doi: 10.1093/cercor/bhx310. [Epub ahead of print].

Jirsa, V. K., Sporns, O., Breakspear, M., Deco, G., and McIntosh, A. R. (2010). Towards the virtual brain: network modeling of the intact and the damaged brain. *Arch. Ital. Biol.* 148, 189–205.

Kaplan, D. T., Furman, M. I., Pincus, S. M., Ryan, S. M., Lipsitz, L. A., and Goldberger, A. L. (1991). Aging and the complexity of cardiovascular dynamics. *Biophys. J.* 59, 945–949. doi: 10.1016/S0006-3495(91)82309-8

Kitzbichler, M. G., Smith, M. L., Christensen, S. R., and Bullmore, E. (2009). Broadband criticality of human brain network synchronization. *PLoS Comput. Biol.* 5:e1000314. doi: 10.1371/journal.pcbi.1000314

Kwong, K. K., Belliveau, J. W., Chesler, D. A., Goldberg, I. E., Weisskoff, R. M., Poncelet, B. P., et al. (1992). Dynamic magnetic resonance imaging of human brain activity during primary sensory stimulation. *Proc. Natl. Acad. Sci. U.S.A.* 89, 5675–5679. doi: 10.1073/pnas.89.12.5675

Leopold, D. A., Murayama, Y., and Logothetis, N. K. (2003). Very slow activity fluctuations in monkey visual cortex: implications for functional brain imaging. *Cereb. Cortex* 13, 422–433. doi: 10.1093/cercor/13.4.422

Li, X., Zhu, Z., Zhao, W., Sun, Y., Wen, D., Xie, Y., et al. (2018). Decreased resting-state brain signal complexity in patients with mild cognitive impairment and Alzheimer's disease: a multi-scale entropy analysis. *Biomed. Opt. Exp.* 9, 1916–1929. doi: 10.1364/BOE.9.001916

Liang, W. K., Lo, M. T., Yang, A. C., Peng, C. K., Cheng, S. K., Tseng, P., et al. (2014). Revealing the brain's adaptability and the transcranial direct current stimulation facilitating effect in inhibitory control by multiscale entropy. *Neuroimage* 90, 218–234. doi: 10.1016/j.neuroimage.2013.12.048

Lipsitz, L. A. (2004). Physiological complexity, aging, and the path to frailty. *Sci. Aging Knowl. Environ.* 16:pe16. doi: 10.1126/sageke.2004.16.pe16

Liu, C. Y., Krishnan, A. P., Yan, L., Smith, R. X., Kilroy, E., Alger, J. R., et al. (2013). Complexity and synchronicity of resting state blood oxygenation level-dependent (BOLD) functional MRI in normal aging and cognitive decline. *J. Magn. Reson. Imaging* 38, 36–45. doi: 10.1002/jmri.23961

Lowen, S. B., Cash, S. S., Poo, M., and Teich, M. C. (1997). Quantal neurotransmitter secretion rate exhibits fractal behavior. *J. Neurosci.* 17, 5666–5677. doi: 10.1523/JNEUROSCI.17-15-05666.1997

Massimini, M., Ferrarelli, F., Huber, R., Esser, S. K., Singh, H., and Tononi, G. (2005). Breakdown of cortical effective connectivity during sleep. *Science* 309, 2228–2232. doi: 10.1126/science.1117256

McDonough, I. M., and Nashiro, K. (2014). Network complexity as a measure of information processing across resting-state networks: evidence from the human connectome project. *Front. Hum. Neurosci.* 8:409. doi: 10.3389/fnhum.2014.00409

McIntosh, A. R., Vakorin, V., Kovacevic, N., Wang, H., Diaconescu, A., and Protzner, A. B. (2014). Spatiotemporal dependency of age-related changes in brain signal variability. *Cereb. Cortex* 24, 1806–1817. doi: 10.1093/cercor/bht030

Mejias, J. F., Murray, J. D., Kennedy, H., and Wang, X. J. (2016). Feedforward and feedback frequency-dependent interactions in a large-scale laminar network of the primate cortex. *Sci. Adv.* 2:e1601335. doi: 10.1126/sciadv.1601335

Milstein, J., Mormann, F., Fried, I., and Koch, C. (2009). Neuronal shot noise and Brownian 1/f2 behavior in the local field potential. *PLoS ONE* 4:e4338. doi: 10.1371/journal.pone.0004338

Moeller, S., Yacoub, E., Olman, C. A., Auerbach, E., Strupp, J., Harel, N., et al. (2010). Multiband multislice GE-EPI at 7 tesla, with 16-fold acceleration using partial parallel imaging with application to high spatial and temporal whole-brain fMRI. *Magn. Reson. Med.* 63, 1144–1153. doi: 10.1002/mrm.22361

Moretti, P., and Muñoz, M. A. (2013). Griffiths phases and the stretching of criticality in brain networks. *Nat. Commun.* 4:2521. doi: 10.1038/ncomms3521

Natarajan, K., Acharya, U. R., Alias, F., Tiboleng, T., and Puthusserypady, S. K. (2004). Nonlinear analysis of EEG signals at different mental states. *Biomed. Eng. Online* 3:7. doi: 10.1186/1475-925X-3-7

Niazy, R. K., Xie, J., Miller, K., Beckmann, C. F., and Smith, S. M. (2011). Spectral characteristics of resting state networks. *Prog. Brain Res.* 193, 259–276. doi: 10.1016/B978-0-444-53839-0.00017-X

Ogawa, S., Lee, T. M., Kay, A. R., and Tank, D. W. (1990). Brain magnetic resonance imaging with contrast dependent on blood oxygenation. *Proc. Natl. Acad. Sci. U.S.A.* 87, 9868–9872. doi: 10.1073/pnas.87.24.9868

Petermann, T., Thiagarajan, T. C., Lebedev, M. A., Nicolelis, M. A., Chialvo, D. R., and Plenz, D. (2009). Spontaneous cortical activity in awake monkeys composed of neuronal avalanches. *Proc. Natl. Acad. Sci. U.S.A.* 106, 15921–15926. doi: 10.1073/pnas.0904089106

Pincus, S. M. (1991). Approximate entropy as a measure of system complexity. *Proc. Natl. Acad. Sci. U.S.A.* 88, 2297–2301. doi: 10.1073/pnas.88.6.2297

Pincus, S. M. (2006). Approximate entropy as a measure of irregularity for psychiatric serial metrics. *Bipolar Disord.* 8, 430–440. doi: 10.1111/j.1399-5618.2006.00375.x

Pincus, S. M., and Keefe, D. L. (1992). Quantification of hormone pulsatility via an approximate entropy algorithm. *Am. J. Physiol.* 262, E741–E754. doi: 10.1152/ajpendo.1992.262.5.E741

Plenz, D., and Thiagarajan, T. C. (2007). The organizing principles of neuronal avalanches: cell assemblies in the cortex? *Trends Neurosci.* 30, 101–110. doi: 10.1016/j.tins.2007.01.005

Raichle, M. E., MacLeod, A. M., Snyder, A. Z., Powers, W. J., Gusnard, D. A., and Shulman, G. L. (2001). A default mode of brain function. *Proc. Natl. Acad. Sci. U.S.A.* 98, 676–682. doi: 10.1073/pnas.98.2.676

Ribeiro, T. L., Copelli, M., Caixeta, F., Belchior, H., Chialvo, D. R., Nicolelis, M. A., et al. (2010). Spike avalanches exhibit universal dynamics across the sleep-wake cycle. *PLoS ONE* 5:14129. doi: 10.1371/journal.pone.0014129

Richman, J. S., and Moorman, J. R. (2000). Physiological time-series analysis using approximate entropy and sample entropy. *Am. J. Physiol. Heart Circul. Physiol.* 278, H2039–H2049. doi: 10.1152/ajpheart.2000.278.6.H2039

Rodriguez, E., George, N., Lachaux, J. P., Martinerie, J., Renault, B., and Varela, F. J. (1999). Perception's shadow: long-distance synchronization of human brain activity. *Nature* 397, 430–433. doi: 10.1038/17120

Ryan, S. M., Goldberger, A. L., Pincus, S. M., Mietus, J., and Lipsitz, L. A. (1994). Gender- and age-related differences in heart rate dynamics: are women more complex than men? *J. Am. Coll. Cardiol.* 24, 1700–1707.

Schuckers, S. A. C., and Raphisak, P. (1999). Distinction of arrhythmias with the use of approximate entropy. *Comput. Cardiol.* 26, 347–350. doi: 10.1109/CIC.1999.825978

Shew, W. L., Yang, H., Petermann, T., Roy, R., and Plenz, D. (2009). Neuronal avalanches imply maximum dynamic range in cortical networks at criticality. *J. Neurosci.*29, 15595–15600. doi: 10.1523/JNEUROSCI.3864-09.2009

Shin, C. W., and Kim, S. (2006). Self-organized criticality and scale-free properties in emergent functional neural networks. *Phys. Rev. E* 74:045101. doi: 10.1103/PhysRevE.74.045101

Smith, R. X., Jann, K., Ances, B., and Wang, D. J. (2015). Wavelet-based regularity analysis reveals recurrent spatiotemporal behavior in resting-state fMRI. *Hum. Brain Mapp.* 36, 3603–3620. doi: 10.1002/hbm.22865

Smith, R. X., Yan, L., and Wang, D. J. (2014). Multiple time scale complexity analysis of resting state FMRI. *Brain Imaging Behav.* 8, 284–291. doi: 10.1007/s11682-013-9276-6

Smith, S. M., Beckmann, C. F., Andersson, J., Auerbach, E. J., Bijsterbosch, J., Douaud, G., et al. (2013a). Resting-state fMRI in the human connectome project. *Neuroimage* 80, 144–168. doi: 10.1016/j.neuroimage.2013.05.039

Smith, S. M., Miller, K. L., Moeller, S., Xu, J., Auerbach, E. J., Woolrich, M. W., et al. (2012). Temporally-independent functional modes of spontaneous brain activity. *Proc. Natl. Acad. Sci. U.S.A.* 109, 3131–3136. doi: 10.1073/pnas.1121329109

Smith, S. M., Vidaurre, D., Beckmann, C. F., Glasser, M. F., Jenkinson, M., Miller, K. L., et al. (2013b). Functional connectomics from resting-state fMRI. *Trends Cogn. Sci.* 17, 666–682. doi: 10.1016/j.tics.2013.09.016

Sokunbi, M. O., Fung, W., Sawlani, V., Choppin, S., Linden, D. E., and Thome, J. (2013). Resting state fMRI entropy probes complexity of brain activity in adults with ADHD. *Psychiatry Res.* 214, 341–348. doi: 10.1016/j.pscychresns.2013.10.001

Stam, C. J., and de Bruin, E. A. (2004). Scale-free dynamics of global functional connectivity in the human brain. *Hum. Brain Mapp.* 22, 97–109. doi: 10.1002/hbm.20016

Szaflarski, J. P., Altaye, M., Rajagopal, A., Eaton, K., Meng, X., Plante, E., et al. (2012). A 10-year longitudinal fMRI study of narrative comprehension in children and adolescents. *Neuroimage* 63, 1188–1195. doi: 10.1016/j.neuroimage.2012.08.049

Takahashi, K., Koyama, Y., Kayama, Y., Nakamura, K., and Yamamoto, M. (2004). Is state-dependent alternation of slow dynamics in central single neurons during sleep present in the rat ventroposterior thalamic nucleus? *Neurosci. Res.* 48, 203–210. doi: 10.1016/j.neures.2003.10.015

Takahashi, T. (2013). Complexity of spontaneous brain activity in mental disorders. *Prog. Neuropsychopharmacol. Biol. Psychiatry* 45, 258–266. doi: 10.1016/j.pnpbp.2012.05.001

Takahashi, T., Cho, R. Y., Mizuno, T., Kikuchi, M., Murata, T., Takahashi, K., et al. (2010). Antipsychotics reverse abnormal EEG complexity in drug-naive schizophrenia: a multiscale entropy analysis. *Neuroimage* 51, 173–182. doi: 10.1016/j.neuroimage.2010.02.009

Thompson, G. J., Magnuson, M. E., Merritt, M. D., Schwarb, H., Pan, W. J., McKinley, A., et al. (2013a). Short-time windows of correlation between

large-scale functional brain networks predict vigilance intraindividually and interindividually. *Hum. Brain Mapp.* 34, 3280–3298. doi: 10.1002/hbm.22140

Thompson, G. J., Merritt, M. D., Pan, W. J., Magnuson, M. E., Grooms, J. K., Jaeger, D., et al. (2013b). Neural correlates of time-varying functional connectivity in the rat. *Neuroimage* 83, 826–836. doi: 10.1016/j.neuroimage.2013.07.036

Tucker, D. M., Roth, D. L., and Bair, T. B. (1986). Functional connections among cortical regions: topography of EEG coherence. *Electroencephalogr. Clin. Neurophysiol.* 63, 242–250. doi: 10.1016/0013-4694(86)90092-1

Turkheimer, F. E., Leech, R., Expert, P., Lord, L. D., and Vernon, A. C. (2015). The brain's code and its canonical computational motifs. From sensory cortex to the default mode network: a multi-scale model of brain function in health and disease. *Neurosci. Biobehav. Rev.* 55, 211–222. doi: 10.1016/j.neubiorev.2015.04.014

Urban, A., Rancillac, A., Martinez, L., and Rossier, J. (2012). Deciphering the neuronal circuitry controlling local blood flow in the cerebral cortex with optogenetics in PV::Cre transgenic mice. *Front. Pharmacol.* 3:105. doi: 10.3389/fphar.2012.00105

Vakorin, V. A., Lippé, S., and McIntosh, A. R. (2011). Variability of brain signals processed locally transforms into higher connectivity with brain development. *J. Neurosci.* 31, 6405–6413. doi: 10.1523/JNEUROSCI.3153-10.2011

Valverde, S., Ohse, S., Turalska, M., West, B. J., and Garcia-Ojalvo, J. (2015). Structural determinants of criticality in biological networks. *Front. Physiol.* 6:127. doi: 10.3389/fphys.2015.00127

Van De Ville, D., Britz, J., and Michel, C. M. (2010). EEG microstate sequences in healthy humans at rest reveal scale-free dynamics. *Proc. Natl. Acad. Sci. U.S.A.* 107, 18179–18184. doi: 10.1073/pnas.1007841107

Van Essen, D. C., Smith, S. M., Barch, D. M., Behrens, T. E., Yacoub, E., Ugurbil, K., et al. (2013). The WU-Minn human connectome project: an overview. *Neuroimage* 80, 62–79. doi: 10.1016/j.neuroimage.2013.05.041

Wang, B., Niu, Y., Miao, L., Cao, R., Yan, P., Guo, H., et al. (2017). Decreased complexity in Alzheimer's disease: resting-state fMRI evidence of brain entropy mapping. *Front. Aging Neurosci.* 9:378. doi: 10.3389/fnagi.2017.00378

Wang, J., Aguirre, G. K., Kimberg, D. Y., Roc, A. C., Li, L., and Detre, J. A. (2003). Arterial spin labeling perfusion fMRI with very low task frequency. *Magn. Reson. Med.* 49, 796–802. doi: 10.1002/mrm.10437

Wang, Z., Li, Y., Childress, A. R., and Detre, J. A. (2014). Brain entropy mapping using fMRI. *PLoS ONE* 9:e89948. doi: 10.1371/journal.pone.0089948

Yang, A. C., Huang, C. C., Yeh, H. L., Liu, M. E., Hong, C. J., Tu, P. C., et al. (2013). Complexity of spontaneous BOLD activity in default mode network is correlated with cognitive function in normal male elderly: a multiscale entropy analysis. *Neurobiol. Aging* 34, 428–438. doi: 10.1016/j.neurobiolaging.2012.05.004

Zarahn, E., Aguirre, G. K., and D'esposito, M. (1997). Empirical analyses of BOLD fMRI statistics. I. Spatially unsmoothed data collected under null-hypothesis conditions. *Neuroimage* 5, 179–197. doi: 10.1006/nimg.1997.0263

Conflict of Interest Statement: The authors declare that the research was conducted in the absence of any commercial or financial relationships that could be construed as a potential conflict of interest.

frontiers in Neuroscience

CORRECTION
published: 30 July 2018
doi: 10.3389/fnins.2018.00539

Correction: Neurophysiological Basis of Multi-Scale Entropy of Brain Complexity and Its Relationship With Functional Connectivity

Danny J. J. Wang[1]*, *Kay Jann*[1], *Chang Fan*[1], *Yang Qiao*[2,3], *Yu-Feng Zang*[2], *Hanbing Lu*[3] *and Yihong Yang*[3]

[1] *Laboratory of FMRI Technology, Stevens Neuroimaging and Informatics Institute, Keck School of Medicine, University of Southern California, Los Angeles, CA, United States,* [2] *Department of Psychology, Center for Cognition and Brain Disorders, Hangzhou Normal University, Hangzhou, China,* [3] *Neuroimaging Research Branch, National Institute on Drug Abuse, National Institutes of Health, Baltimore, MD, United States*

Keywords: multiscale entropy (MSE), complexity, BOLD fMRI, electrophysiology, functional connectivity (FC)

A correction on

Neurophysiological Basis of Multi-Scale Entropy of Brain Complexity and Its Relationship With Functional Connectivity

by Wang, D. J. J., Jann, K., Fan, C., Qiao, Y., Zang, Y. F., Lu, H., et al. (2018). Front. Neurosci. 12:352. doi: 10.3389/fnins.2018.00352

In the original article, there was an error in Acknowledgements section. We need to add an acknowledgement of Dr. Robert X. Smith for his contributions towards Figure 1.

A correction has been made to the Acknowledgements section.

This work was partially supported by the Intramural Research Program of the National Institute on Drug Abuse, the National Institutes of Health (NIH). Data from the Human Connectome Project, WU-Minn Consortium (Principal Investigators: David Van Essen and Kamil Ugurbil; 1U54MH091657) were funded by the 16 NIH Institutes and Centers that support the NIH Blueprint for Neuroscience Research; This work was also supported by NIH grant (UH2-NS100614). The authors are grateful to Drs. Michael Breakspear and Stewart Heitmann for their help with the Brain Dynamic Toolbox. The authors are also grateful to Dr. Robert X. Smith for his contribution of Figure 1.

The authors apologize for this error and state that this does not change the scientific conclusions of the article in any way.

The original article has been updated.

Conflict of Interest Statement: The authors declare that the research was conducted in the absence of any commercial or financial relationships that could be construed as a potential conflict of interest.

OPEN ACCESS

Approved by:
Frontiers in Neuroscience Editorial Office, Frontiers Media SA, Switzerland

***Correspondence:**
Danny J. J. Wang
jwang71@gmail.com

Specialty section:
This article was submitted to Brain Imaging Methods, a section of the journal Frontiers in Neuroscience

Received: *11 July 2018*
Accepted: *17 July 2018*
Published: *30 July 2018*

Citation:
Wang DJJ, Jann K, Fan C, Qiao Y, Zang Y-F, Lu H and Yang Y (2018) Correction: Neurophysiological Basis of Multi-Scale Entropy of Brain Complexity and Its Relationship With Functional Connectivity. Front. Neurosci. 12:539. doi: 10.3389/fnins.2018.00539

frontiers in Neuroscience

ORIGINAL RESEARCH
published: 13 June 2018
doi: 10.3389/fnins.2018.00398

A Strategy to Reduce Bias of Entropy Estimates in Resting-State fMRI Signals

Albert C. Yang[1,2], Shih-Jen Tsai[3,4], Ching-Po Lin[2] and Chung-Kang Peng[1]*

[1] Division of Interdisciplinary Medicine and Biotechnology, Beth Israel Deaconess Medical Center, Harvard Medical School, Harvard University, Boston, MA, United States, [2] Institute of Brain Science, National Yang-Ming University, Taipei, Taiwan, [3] Department of Psychiatry, Taipei Veterans General Hospital, Taipei, Taiwan, [4] Division of Psychiatry, School of Medicine, National Yang-Ming University, Taipei, Taiwan

Complexity analysis of resting-state blood oxygen level-dependent (BOLD) signals using entropy methods has attracted considerable attention. However, investigation on the bias of entropy estimates in resting-state functional magnetic resonance imaging (fMRI) signals and a general strategy for selecting entropy parameters is lacking. In this paper, we present a minimizing error approach to reduce the bias of sample entropy (SampEn) and multiscale entropy (MSE) in resting-state fMRI data. The strategy explored a range of parameters that minimized the relative error of SampEn of BOLD signals in cerebrospinal fluids where minimal physiologic information was present, and applied these parameters to calculate SampEn of BOLD signals in gray matter regions. We examined the effect of various parameters on the results of SampEn and MSE analyses of a large normal aging adult cohort (354 healthy subjects aged 21–89 years). The results showed that a tradeoff between pattern length m and tolerance factor r was necessary to maintain the accuracy of SampEn estimates. Furthermore, an increased relative error of SampEn was associated with an increased coefficient of variation in voxel-wise statistics. Overall, the parameters $m = 1$ and $r = 0.20$–0.45 provided reliable MSE estimates in short resting-state fMRI signals. For a single-scale SampEn analysis, a wide range of parameters was available with data lengths of at least 97 time points. This study provides a minimization error strategy for future studies on the non-linear analysis of resting-state fMRI signals to account for the bias of entropy estimates.

Keywords: complexity, sample entropy, multiscale entropy, bias, resting-state fMRI

OPEN ACCESS

Edited by:
Bradley J. MacIntosh, Sunnybrook Research Institute, Canada

Reviewed by:
Federico Giove, Centro Fermi - Museo Storico della Fisica e Centro Studi e Ricerche Enrico Fermi, Italy
Roser Sala-Llonch, Universitat de Barcelona, Spain

****Correspondence:***
Albert C. Yang
cyang1@bidmc.harvard.edu

Specialty section:
This article was submitted to Brain Imaging Methods, a section of the journal Frontiers in Neuroscience

Received: *20 December 2017*
Accepted: *23 May 2018*
Published: *13 June 2018*

Citation:
Yang AC, Tsai S-J, Lin C-P and Peng C-K (2018) A Strategy to Reduce Bias of Entropy Estimates in Resting-State fMRI Signals. Front. Neurosci. 12:398. doi: 10.3389/fnins.2018.00398

INTRODUCTION

Since the inception of the resting-state blood oxygen level-dependent (BOLD) technique from functional magnetic resonance imaging (fMRI) (Biswal et al., 1995), an essential question emerged: What are the characteristics of the temporal dynamics of these seemingly noisy and spontaneous BOLD oscillations (Fox and Raichle, 2007)? The first piece of evidence is from the exhibition of $1/f$ frequency distribution of BOLD signals (Zarahn et al., 1997; Fox et al., 2007), which is an ubiquitous feature of the complex system (Schlesinger, 1987; Zang, 1991; Goldberger, 1996; Goldberger et al., 2002a), and has been observed in other neurophysiologic signals (Linkenkaer-Hansen et al., 2001; Stam and de Bruin, 2004). In complex systems, the $1/f$ noise is likely to

arise from underlying oscillatory components operating at multiple time scales and is distinct with uncorrelated randomness (Zang, 1991; Hausdorff and Peng, 1996; Goldberger et al., 2002a); thus, using the entropy measure to assess the complexity of seemingly noisy physiologic data may provide hints for understanding the dynamics of a physiologic system (Pincus, 1991; Richman and Moorman, 2000), and for delineating the dynamical changes in physiologic systems of healthy and pathologic states (Costa et al., 2002; Goldberger et al., 2002b; Lipsitz, 2002; Peng et al., 2009).

To develop a systemic approach for quantifying temporal dynamics of brain signal data in healthy and pathological states, we have proposed a loss of brain complexity hypothesis (**Figure 1**) to study mental and brain function in normal and pathological conditions (Yang and Tsai, 2013). The hypothesis is intuitively based on the observation that behavioral symptoms observed in patients often follow the pattern of order or randomness, and can be summarized as follows: (1) the complexity of a brain reflects its ability to adapt and function in an ever-changing environment, (2) brain operates across multiple scales of space (i.e., brain regions) and time (i.e., temporal changes), hence the complexity of brain oscillations is also multiscale and hierarchical, and (3) aging and a wide class of mental illness appear to reduce the adaptive capacity of the brain. Thus, loss of brain complexity may be a generic, defining feature of pathologic brain.

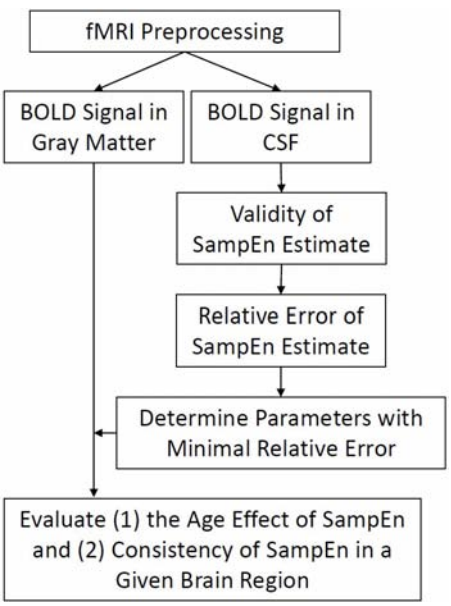

FIGURE 1 | Flow chart of analyses. Functional imaging data were preprocessed and BOLD signal in every gray matter and CSF voxels was extracted for subsequent SampEn/MSE analysis. The evaluation of SampEn of BOLD signal is twofold. First, we evaluated the validity of SampEn calculation using a variety of combinations of parameters m, r, and Scale Factors. Second, we evaluated the relative error of BOLD signal using a minimization strategy. Finally, we applied the obtained parameters to study the effect of age in SampEn of gray matter voxels and evaluated the consistency of SampEn in a given brain region.

A variety of entropy measures has been applied to study the brain complexity by measuring temporal dynamics of fMRI signals. Some of these studies have used Shannon entropy (de Araujo et al., 2003; Leite and Mandeville, 2006; Goni et al., 2011; Tobia et al., 2012) and related families (Sturzbecher et al., 2009) to quantify the activated patterns of BOLD signals in various fMRI task experiments. For resting-state fMRI signals, a Wavelet entropy has been applied to study the resting-state complexity in schizophrenia (Bassett et al., 2012), and recently, we and others introduced multiscale sample entropy (MSE) to study the complexity of resting-state fMRI signals of normal aging (Yang et al., 2013a; Siero et al., 2014), the effect of genetic polymorphism on resting-state fMRI complexity (Yang et al., 2014), the characteristics of BOLD signals in various brain regions (McDonough and Nashiro, 2014), and psychosis (Yang et al., 2015; Hager et al., 2017). Other studies have also applied single-scale approximate entropy (ApEn) (Sokunbi et al., 2011; Liu et al., 2013) or sample entropy (SampEn) to study the resting-state fMRI signals of normal aging (Sokunbi, 2014), attention deficit hyperactivity disorder (Sokunbi et al., 2013), and schizophrenia (Sokunbi et al., 2014).

Among these entropy methods, SampEn and a related family, MSE, have attracted considerable attention because of their simplicity and the advantage of being less dependent on the time series length than ApEn. However, abundant results of entropy analyses of resting-state fMRI signals also come with the inconsistency of parameter selection for entropy calculation. The calculation of SampEn requires a tolerance factor r (typically a fraction of the standard deviation, SD, of a given signal) to determine the number of matches of data points using a pattern length m. Selections of m in SampEn are sometimes based on theoretical calculations for ApEn which suggest that 10^m points should be sufficient, although 20^m–30^m points would be preferable for an accurate estimate (Pincus and Goldberger, 1994; Kirchner et al., 2012). However, there was no definite guideline to choose these parameters (Gow et al., 2015).

Generally, the selection of these parameters in fMRI studies have been based on maximizing the between-group difference in entropy estimates (Sokunbi et al., 2013, 2014; Yang et al., 2013a; Sokunbi, 2014), prior SampEn reports on other signals (Siero et al., 2014), or the conceptual notion that a sufficient pattern length was required to capture underlying dynamics (McDonough and Nashiro, 2014). Consequently, a variety of parameters have been reported, including $m = 1$, $r = 0.35$ (Yang et al., 2013a, 2014, 2015; Hager et al., 2017), $m = 2$, $r = 0.3$ (Siero et al., 2014; Sokunbi, 2014), $m = 2$, $r = 0.32$ (Sokunbi et al., 2014), $m = 2$, $r = 0.46$ (Sokunbi et al., 2013), or $m = 2$, $r = 0.50$ (McDonough and Nashiro, 2014).

The selection of SampEn parameters based on the approach of maximizing the between-group difference likely varies among studies and is not guaranteed to be more free from error or bias (McDonough and Nashiro, 2014). A general strategy for selecting SampEn parameters in resting-state fMRI signals is lacking. Although Lake et al. (2002) stated that one of the advantages of SampEn is its consistency, and that if one record showed lower SampEn than another with one set of m and r values,

then it would also show lower SampEn with different parameters; however, the problems in the selection of SampEn parameters are not trivial because the bias of SampEn has not been explored in previous fMRI studies, and errors may influence neuroimaging studies because of the relatively short BOLD signals and large volume of brain voxels to be analyzed.

In the study of physiologic time series such as heart rate, we will observe a variance of entropy estimates that results from different physiologic conditions, age, sex, or the error of entropy estimate itself. Likewise, the temporal dynamics of BOLD signal across brain voxels is associated with local post-synaptic potentials in gray matter and action potentials in white matter (Gawryluk et al., 2014). However, such neuronal-related variance of entropy measures from BOLD signal in gray matter may be also contaminated by non-neuronal hemodynamic responses or the error of entropy calculation. Therefore, minimizing the error of entropy estimate could potentially maximize the reliability and consistency of quantification of neuronal-related entropy in BOLD signal.

In accordance with Lake et al. (2002) to minimize the bias of entropy calculation in heart rate, this study developed a generic strategy to minimize the relative error of SampEn calculation for resting-state fMRI signals. A range of parameters was examined to minimize the relative error of SampEn in cerebrospinal fluids (CSFs) that had minimal physiologic information, and then the appropriate SampEn parameters with low relative error were determined for use in gray matter regions. We investigated the effect of various parameters on the results of SampEn and MSE in a large normal aging cohort of resting-state fMRI datasets.

MATERIALS AND METHODS

Participants

This study cohort comprised 354 healthy Han Chinese adult participants recruited from communities in Northern Taiwan (age range: 21–89 years; male/female: 185/169) (**Table 1**). The participants were selected from a larger cohort (502 subjects at the time of this study) based on a continuing effort of the Healthy Aging Project (Yang et al., 2013a, 2014) conducted in accordance with the Declaration of Helsinki. Approval was received from the institutional review board at Taipei Veterans General Hospital. Because we previously demonstrated that older subjects with Apolipoprotein-E (APOE) ε4 genotype had reduced BOLD complexity compared with APOE ε4 non-carriers (Yang et al., 2014), we did not include any APOE ε4 carriers in this study.

TABLE 1 | Normal aging cohort characteristics.

Age group (year)	No. of subjects	Females (%)	Total gray matter volume (cm^3)
20–29	65	32 (49.2)	651 ± 55
30–39	46	23 (50.0)	624 ± 60
40–49	47	27 (57.4)	575 ± 47
50–59	61	35 (57.4)	574 ± 59
60–69	66	40 (60.6)	524 ± 48
70–79	28	9 (32.1)	475 ± 52
80–89	41	3 (7.3)	447 ± 45

Each participant was evaluated by a trained research assistant using a mini-international neuropsychiatric interview to exclude those with Axis I psychiatric disorders (Sheehan et al., 1998). Older participants (age >59 years) were further assessed using the Clinical Dementia Rating (CDR) scale (Hughes et al., 1982) to exclude those with dementia (CDR > 0). The overall exclusion criteria for all participants consisted of the following: (a) the presence of dementia; (b) the presence of Axis I psychiatric disorders, such as schizophrenia, bipolar disorders, or unipolar depression; and (c) a history of neurological conditions, such as head injury, stroke, or Parkinson's disease.

Image Acquisition and Processing

Functional magnetic resonance imaging was performed at National Yang-Ming University by using a 3.0T Siemens MRI scanner (Siemens Magnetom Tim Trio, Erlangen, Germany) equipped with a 12-channel head coil. The scanning protocol was consistent with our prior reports (Yang et al., 2013a, 2014, 2015). For resting-state image scanning, T2*-weighted images with BOLD contrast were measured using a gradient echo-planar imaging (EPI) sequence (repetition time TR = 2,500 ms, echo time TE = 27 ms, FOV = 200 mm, flip angle = 77°, matrix size = 64 × 64, voxel size = 3.44 mm × 3.44 mm × 3.40 mm). For each run, 200 EPI volume images were acquired along the AC–PC plane. Structural T1 images were acquired with the 3D magnetization-prepared rapid gradient echo sequence (3D-MPRAGE; TR = 2,530 ms, TE = 3.5 ms, TI = 1,100 ms, FOV = 256 mm, flip angle = 7°). T1 images were segmented to estimate the total gray matter volume for each subject.

Resting-state fMRI data were preprocessed and analyzed using SPM8 (Wellcome Department of Imaging Neuroscience, London, United Kingdom) implemented in MATLAB ((MathWorks, Natick, MA, United States). The fMRI images were slice-time corrected, realigned, and normalized into the standard stereotaxic space of the Montreal Neurological Institute (MNI) EPI template, and resampled to a 3-mm cubic voxel. Covariates of the fMRI time series were regressed out, including the time courses of six head motion, white matter, and CSF. To avoid introducing distortions in the time series data, no global signal regression was performed (Murphy et al., 2009; Anderson et al., 2011). All participants included in this study exhibited a maximum displacement of less than 1.5 mm at each axis and an angular motion of less than 1.5° for each axis. The first five data points (12.5 s) in any fMRI time series were discarded because of the instability of the initial fMRI scanning, leaving 195 data points in the final data. Temporal low-pass filtering (0.01–0.08 Hz) was performed to reduce the influence of high-frequency noise from physiologic confounders.

Sample Entropy and Multiscale Entropy Analysis

SampEn (Richman and Moorman, 2000) was developed to reduce the bias of a related family, ApEn (Pincus, 1991), and has a

closer agreement with theoretical estimations than ApEn. Briefly, SampEn is defined by the negative natural logarithm of the conditional probability that a data set of length N, having repeated itself within a tolerance of r (similarity factor) for m points (pattern length), will also repeat itself for $m + 1$ points without allowing self-matches (Richman and Moorman, 2000). In practice, the number of matches of pattern length m within a tolerance of r was defined as B, and A was defined as the subset of B that also matched pattern length $m + 1$. Thus, SampEn was estimated by the negative natural logarithm of the ratio CP = A/B that SampEn = $-\log$ CP.

SampEn is a measure of regularity based on a single and shortest time scale (Richman and Moorman, 2000; Lake et al., 2002). Such a single-scale entropy measure produces higher values of entropy to uncorrelated noise, which is presumed to convey less information than $1/f$ noise (Goldberger et al., 2002a,b). Consequently, the MSE analysis (Costa et al., 2002) was introduced to estimate the entropy on multiple time scales based on the notion that complex dynamics typically arise from multiple time scales and that a generic approach to measure global complexity must account for the multiple time scales in a given physical system (Zang, 1991; Fogedby, 1992). The MSE calculation can be summarized in three steps: (1) construct a coarse-grained time series according to a range of scale factors, (2) quantify the SampEn of each coarse-grained time series, and (3) examine the MSE profile by using a range of scales. The length of each coarse-grained time series is equal to the length of the original time series divided by the scale factor. For Scale 1, the time series was simply the original time series.

A General Strategy for Selecting Parameters for the SampEn/MSE Analysis of fMRI Signals

As mentioned, three parameters were involved in the SampEn/MSE analysis, including the pattern length m, tolerance factor r, and the time scale factor. In principle, a sufficient pattern length m and a small r value is ideal for capturing underlying dynamics when the irregularity of a given signal is increased (Pincus, 1991). However, in practice, the confidence of the SampEn estimation was dependent on the number of pattern matches for lengths m and $m + 1$ (i.e., A and B). The stringent criteria for a large m and small r resulted in fewer pattern matches, and thus increased the statistical variation in calculating CP (i.e., A/B) and SampEn. By contrast, a relaxed criterion for a small m and large r resulted in more pattern matches in both A and B, thus causing the SampEn value to be close to 0 and reducing the ability of SampEn to discriminate dynamical processes (Lake et al., 2002).

Lake et al. (2002) proposed a general strategy to appropriately select m and r by (a) selecting m by using the autoregressive (AR) model order for a given signal and (b) minimizing the relative error of the SampEn calculation. In their study, the relative error of SampEn was estimated theoretically and applied to 200 randomly selected cardiac R-R interval time series (4096 data points). However, such a theoretical estimation is computationally exhausting and is unlikely to be practical for use with large amounts of resting-fMRI BOLD signals. Therefore, we adopted Lake et al.'s (2002) principle but used a straightforward strategy.

Empirically, the SampEn of BOLD signals can be computed directly in all brain voxels and the variance of SampEn can subsequently be estimated. However, the SampEn variance in gray matter contains not only error but also critical information related to neuronal signal dynamics. A direct minimization of the SampEn variance in the gray matter region will likely reduce the ability of SampEn to discriminate brain processes. By contrast, BOLD signals in CSFs have been considered as a nuisance and are routinely regressed out for contaminating gray matter BOLD signals (Biswal et al., 1995, 1997). Furthermore, recent reports showed that CSF signals exhibited the characteristics of uncorrelated noise (Wu et al., 2012; McDonough and Nashiro, 2014), thus opening the possibility of using CSF BOLD signals as the random control to minimize the bias of SampEn and to determine appropriate SampEn parameters.

Therefore, a general strategy was developed to explore a range of parameters that minimized the relative error of SampEn of BOLD signals in CSFs; the obtained parameters were then applied to study the SampEn of BOLD signals in gray matter. This minimization strategy considers the distinct BOLD signal properties between CSFs and gray matter and is presumed to be consistent across studies; thus, problems in prior approaches that maximize the between-group difference of entropy estimates in gray matter regions are avoided. In addition, a selection of pattern length m may be beneficial by studying the AR model order of the underlying structure of BOLD signals in gray matter, which is the primary brain region with functional relevance. However, we decided that this approach was less critical because the ability of SampEn to capture underlying dynamics is dependent not only on the pattern length m, but also on the tolerance factor r. Therefore, the selection of m and r in this study should be primarily based on minimizing the relative error of SampEn.

Adopting the methods proposed by Lake et al. (2002), we defined the relative error of SampEn as the 95% confidence interval (CI) of the SampEn estimate relative to the SampEn value. A relative error of 0.05 corresponds to a 95% CI that is 10% of the SampEn estimate (Lake et al., 2002). This relative error can be empirically estimated by calculating the mean and SD of SampEn of BOLD signals in all CSF voxels in a subject (i.e., $1.96 \times \frac{\sigma \text{SampEn}}{\text{SampEn}}/2$). This relative error metric is approximately the same as the coefficient of variation (CV), which is a measure of the dispersion of SampEn distribution. Because of short BOLD data (195 data points compared to 4096 RR intervals in Lake et al., 2002), we aimed for a relative error no higher than 0.1, which was approximately 10% of the CV value in SampEn estimates.

Statistical Analysis

A flow chart of analysis involved in this paper was shown in **Figure 1**. Briefly, functional imaging data were preprocessed and BOLD signal in every gray matter and CSF voxels was extracted for subsequent SampEn/MSE analysis. The evaluation of SampEn of BOLD signal is twofold. First, we evaluated the

validity of SampEn calculation using a variety of combinations of parameters *m*, *r*, and Scale Factors. The validity of SampEn indicated if a SampEn value can be derived from short BOLD signal using a given set of parameters. Second, we evaluated the relative error of BOLD signal using the aforementioned minimization strategy. Finally, we applied the obtained parameters to study the effect of age in SampEn/MSE of gray matter voxels and evaluated the consistency of SampEn in a given brain region.

The relative error was obtained from the CSF region of each subject, and a median value of the relative error of all subjects was reported for a given *m* and *r*. A CSF mask provided by a REST toolbox that contained 121 CSF voxels (3 mm × 3 mm × 3 mm) (Song et al., 2011) was used in this study. To maintain the consistency of fMRI signal characteristics across all brain voxels, we used postprocessed BOLD image data and normalized each BOLD time series for a zero mean and unit SD before conducting the SampEn/MSE analysis. We assess the relative error of SampEn for a wide range of combinations of *m* and *r*, and to examine the effect of BOLD data length (coarse-grained BOLD time series by various scale factors) on the relative error of SampEn. We also examined the AR model order for all gray matter voxels in the entire study cohort.

After determining a range of appropriate parameters for SampEn/MSE analyses, we applied these parameters to the SampEn calculation of BOLD signals in all gray matter voxels in each subject. A general linear model (GLM) controlling the effect of sex and total gray matter volume on SampEn was used to examine the primary effect of age on BOLD SampEn data. We used the GLM separately for the BOLD SampEn data of each scale factor, as well as for the overall average SampEn across all scale factors. We also compared the results of the GLM using various sets of SampEn parameters and evaluated the CV of t-statistics across gray matter voxels in a given brain region as a proxy of the consistency of SampEn calculation. Significant brain clusters with peak coordinates in the MNI space were reported if the *p*-value corrected for the family-wise error rate was less than 0.05 at the cluster level.

RESULTS

Characteristics of the SampEn/MSE Analysis

Figure 2A illustrates the coarse-graining of the BOLD time series in the MSE analysis. The coarse-graining averaged the data points within non-overlapping windows of increasing lengths of Scale Factors 1–5. SampEn for each scale factor was estimated from the coarse-grained time series. **Figures 2B,C** show the profile of SampEn from Scale Factors 1 to 5 averaged across all gray matter and CSF voxels in the entire study cohort, from using SampEn parameters reported in prior studies ($m = 1$, $r = 0.35$ and $m = 2$, $r = 0.50$). The mean SampEn across various scales revealed a consistent pattern with distinct parameters of *m* and *r*, but the 95% CI of SampEn increased with increasing scale factors.

The Valid Parameters for the SampEn/MSE Analysis in BOLD Signal

First, we examined how data length and selection of parameters *m* and *r* could result in invalid SampEn estimates due to the absence of pattern matches in BOLD signals. The absence of pattern matches could be due to short data length (i.e., lack of sufficient data sample for finding a match), large pattern length *m* (i.e., lack of the recurrence of complex pattern), or small *r* (i.e., unable to find a match within a narrow similarity criterion). We performed the experiment by calculating SampEn in CSF BOLD signals using a variety of combinations of *m*, *r* and Scale Factors.

Figure 3 shows the percentage of SampEn estimation failures that were caused by the absence of pattern matches in CSF BOLD signals. The percentage was calculated based on the CSF voxels with invalid SampEn estimates relative to all CSF voxels in the entire study cohort. The results showed that more stringent combinations of *m* and *r* (i.e., higher *m* and lower *r*) and shorter BOLD signals resulted in a higher percentage of invalid SampEn estimates. Ideally, a combination of *m* and *r* should be selected only when the BOLD signals of all voxels have valid SampEn estimates. Therefore, a range of combinations of *m* and *r*, including $m = 1$ and $r \geq 0.20$, $m = 2$ and $r \geq 0.35$, $m = 3$ and $r \geq 0.60$, and $m = 4$ and $r \geq 0.75$, was free for invalid SampEn calculation.

Estimation of the Relative Error of the SampEn/MSE Analysis

As aforementioned, the minimization of the relative error of SampEn was performed in CSF BOLD signals that contained minimal physiologic information and exhibited the characteristics of uncorrelated noise. The relative error of SampEn was empirically estimated by calculating the mean and SD of SampEn of BOLD signals in all CSF voxels in every subject. The relative error measured the dispersion of SampEn distribution in CSF regions, thereby provide a metric to evaluate the bias of SampEn estimates because the variance of entropy in CSF BOLD signal is presumably consistent across CSF voxels.

Figure 4 shows the color map of the relative error of SampEn calculation in CSF BOLD signals. The lower SampEn relative error indicates a higher consistency (i.e., lower variation) of SampEn among the CSF voxels. We set the criteria for the selection of *m* and *r* to have a relative error lower than 0.1. For Scale 1 (BOLD length = 195 time points), the acceptable range of *m* and *r* was $m = 1$, $0.05 \leq r \leq 0.70$, $m = 2$, $0.25 \leq r \leq 0.80$, $m = 3$, $0.35 \leq r \leq 0.80$, and $m = 4$, $0.55 \leq r \leq 0.80$. For Scale 2 (BOLD length = 97 time points), the acceptable range of *m* and *r* was $m = 1$, $0.10 \leq r \leq 0.80$, and $m = 2$, $0.40 \leq r \leq 0.80$. For Scale 3 (BOLD length = 65 time points), the acceptable range of *m* and *r* was $m = 1$, $0.15 \leq r \leq 0.80$. For Scale 4 (BOLD length = 48 time points), the acceptable range of *m* and *r* was $m = 1$, $0.30 \leq r \leq 0.35$. For Scale 5 (BOLD length = 39 time points), there was no error rate of SampEn below 0.1 for any *m* and *r*.

For the average relative error of Scales 1–5, the only range with an acceptable SampEn error was $m = 1$, $0.20 \leq r \leq 0.45$. The optimal *m* and *r* in this range was $m = 1$, $r = 0.30$ (relative

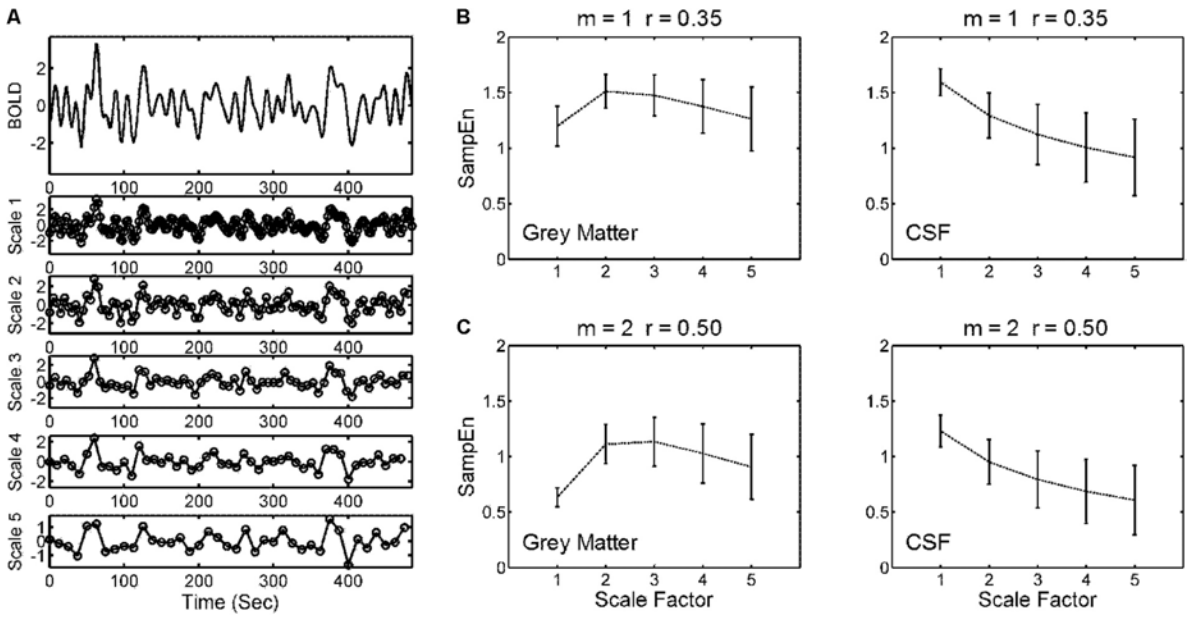

FIGURE 2 | Illustration of a multiscale sample entropy (SampEn; MSE) analysis. **(A)** Coarse-graining of a BOLD time series from a gray matter voxel of an individual was performed by averaging the data points within non-overlapping windows of increasing lengths of Scale Factors 1–5. Sample entropy for each scale factor was estimated from the coarse-grained time series. **(B)** Mean and 95% CI of MSE profiles across Scale Factors 1–5 from (left) all gray matter voxels and (right) all CSF voxels of the entire study cohort (354 subjects). The parameters for SampEn calculation were pattern length m = 1 and tolerance factor r = 0.35. **(C)** The same analysis as **(B)** but with distinct SampEn parameters (m = 2, r = 0.50). The strategy was to explore a range of parameters that minimized the relative error of SampEn of BOLD signals in CSFs where minimal physiologic information was present, and to apply these parameters to calculate the SampEn of BOLD signals in gray matter regions.

error = 0.087). When $m \geq 2$, the minimum error rate was beyond 0.1 for m = 2, r = 0.55 (relative error = 0.128) and m = 3, r = 0.70 (relative error = 0.162). When $m \geq 4$, the minimum error rate was beyond 0.2.

For comparison, we chose three sets of parameters with increasing levels of relative error: m = 1, r = 0.35 (relative error = 0.089), m = 2, r = 0.50 (relative error = 0.129), and m = 3, r = 0.70 (relative error = 0.162). The first two chosen sets of parameters were consistent with prior reports (Sokunbi et al., 2013; Yang et al., 2013a; McDonough and Nashiro, 2014) and were close to the minimum of relative error for a given m. Although the AR model order suggested a choice of $m \geq 3$, the error rate for $m \geq 3$ was beyond the acceptable error rate.

Effect of Entropy Parameters on the SampEn/MSE Analysis of BOLD Signals in Normal Aging Data

Figure 5 shows the voxel-wise correlation between age and MSE using the GLM to control the effect of sex and total gray matter volume on MSE values. The GLM was used separately for SampEn parameters of m = 1, r = 0.35; m = 2, r = 0.50; and m = 3, r = 0.70. For all three parameters, visual inspection of MSE brain topography suggested a similar pattern of brain regions with negative correlations between age and MSE. The results from parameters m = 2, r = 0.50, and m = 3, r = 0.70 showed larger brain clusters with negative correlations between age and MSE than parameter m = 1, r = 0.35.

Table 2 summarizes the statistical results by using the average MSE value of Scales 1–5. The results from the three parameters showed the same brain regions with significant negative correlations between age and MSE values, including the right and left parahippocampus and right and left superior temporal pole. Although the largest brain clusters and the strongest peak t value were found in the results of using m = 2, r = 0.50, there was no significant difference in the mean t value when comparing the t statistics of the same brain regions examined by using various parameters. Furthermore, the CV of t statistics within a given brain region was lower in the results of using m = 1, r = 0.35 than those in the results of using the other parameters, suggesting a higher consistency of brain voxels identified by SampEn using m = 1, r = 0.35. We averaged the MSE value within identified brain clusters; **Figure 6** shows the scattered plots with a consistent pattern of correlation between age and the average MSE using various parameters.

DISCUSSION

We systemically evaluated the relative error of SampEn in a wide range of pattern length m, tolerance factor r, and various time scales. The strategy was to minimize the relative error of SampEn in CSFs where minimal physiologic information was present, and determine appropriate SampEn parameters to be used in gray matter regions. Our estimations provided an array of parameters m and r in various scales of BOLD signals with relative errors

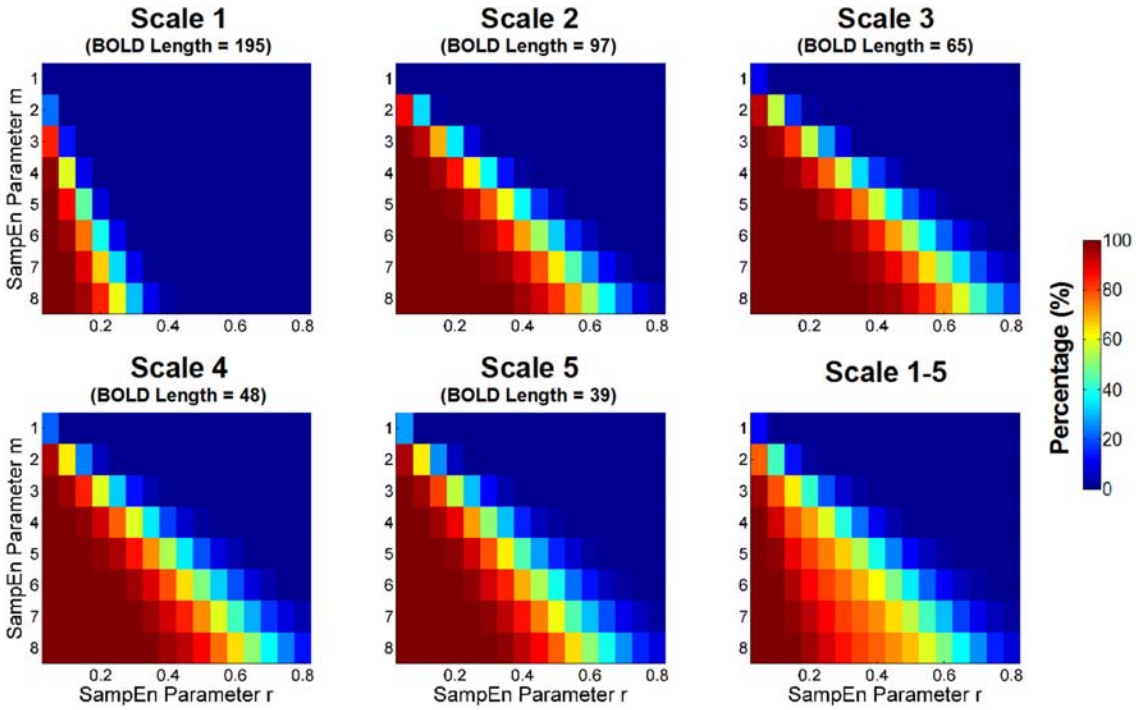

FIGURE 3 | Percentage of estimation failure for sample entropy (SampEn) because of the absence of pattern matches in CSF BOLD signals. The percentage was calculated based on the CSF voxels with invalid SampEn relative to all CSF voxels in the entire study cohort. The percentage was compared with those of various combinations of *m* and *r* across all scale factors with different BOLD signal lengths. The more stringent combinations of *m* and *r* (i.e., higher *m* and lower *r*) and shorter BOLD signals resulted in a higher percentage of invalid SampEn estimations. Ideally, the choice of *m* and *r* should have valid SampEn estimations in all voxels.

below 0.1. In general, a tradeoff between *m* and *r* was necessary to maintain the accuracy of SampEn calculation. In other words, an increased *m* value had to accompany an increased *r* value to maintain an acceptable error level in short fMRI time series.

For comparison, we chose $m = 1$, $r = 0.35$; $m = 2$, $r = 0.50$; and $m = 3$, $r = 0.70$ with increasing levels of error to evaluate the effect of SampEn parameters on the resting-state fMRI entropy analysis of a normal aging cohort. Qualitatively, the results from these three parameters consistently showed that the same brain regions had a significant negative correlation between age and SampEn at various time scales. These brain regions included the parahippocampus and superior temporal pole at both hemispheres. Quantitatively, $m = 1$, $r = 0.35$ resulted in smaller but more consistent brain clusters in terms of the CV value of *t* statistics. Larger brain clusters but also a reduced consistency of *t* statistics were shown in the results of using $m = 2$, $r = 0.50$, and $m = 3$, $r = 0.70$. These results suggested that an increased error of SampEn had a negative impact on the quantitative results of voxel-wise statistics, despite the qualitative results being the same in a large cohort. We expect that the adverse impact of such error on qualitative results will become apparent in a smaller dataset.

Overall, the parameters $m = 1$, $r = 0.20$–0.45 provided reliable MSE estimates for most scale factors, and the minimum error was found at $m = 1$, $r = 0.30$ for MSE analysis. For a single-scale SampEn analysis, a wide range of parameters is available with data lengths of at least 97 time points. We suggest that future studies on the complexity analysis of resting-state fMRI signals account for the relative error of SampEn. Our minimization strategy can also be generalized to other time domains and non-linear measures for fMRI data.

Strategies for Selecting SampEn and MSE Parameters

Few strategies exist for assessing the parameters of ApEn, SampEn, and even MSE analyses, and most of these strategies were developed for ApEn. In general, statistical estimates of conditional probabilities become less reliable as *m* increases, and the loss of system dynamics information also increases as *r* increases (Pincus and Goldberger, 1994). The early study of ApEn in cardiac R-R intervals established a guideline for selecting parameters of data length ≥ 100, $m \leq 3$, and $r = 0.1$–0.25 of SD of input data (Pincus and Goldberger, 1994). Many studies have arbitrarily adopted the parameter $m = 2$, $r = 0.1$–0.2 to ApEn, SampEn, and MSE analyses (Costa et al., 2002; Alcaraz et al., 2010; Yentes et al., 2013).

These commonly used parameters were typically applied to signals with slower dynamics such as heart rate; hence, some studies have suggested that these parameters are inappropriate for signals with faster dynamics, and proposed to use *r* values that maximize the ApEn value (Chen et al., 2005; Chon et al., 2009). However, this maximum entropy approach was shown to be invalid for SampEn estimates (Castiglioni et al., 2013).

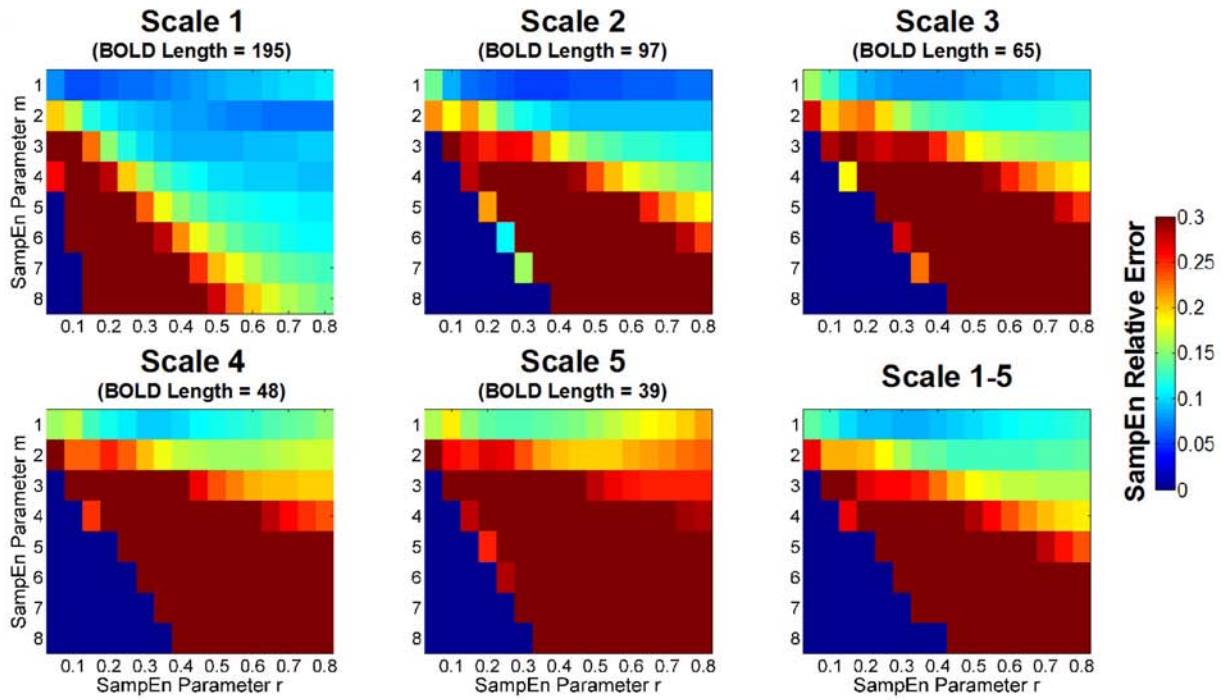

FIGURE 4 | Color map of the relative error of sample entropy (SampEn) of CSF BOLD data for appropriate selection of *m* and *r*. The SampEn relative error was defined in accordance with Lake et al. (2002) based on the 95% CI relative to the average SampEn in all CSF voxels; thus, the metric indicated the consistency of the SampEn calculation. A lower SampEn relative error indicated a higher consistency of SampEn. For example, a SampEn relative error value of 0.05 corresponds to a 95% CI, which is 10% of the average SampEn estimate. In this study, the goal was to minimize the relative error of SampEn in CSF BOLD signals because they exhibit characteristics of uncorrelated randomness and contain minimal physiologic information. The median value of the SampEn relative error for the entire study cohort is shown in color with various combinations of *m*, *r*, and scale factors.

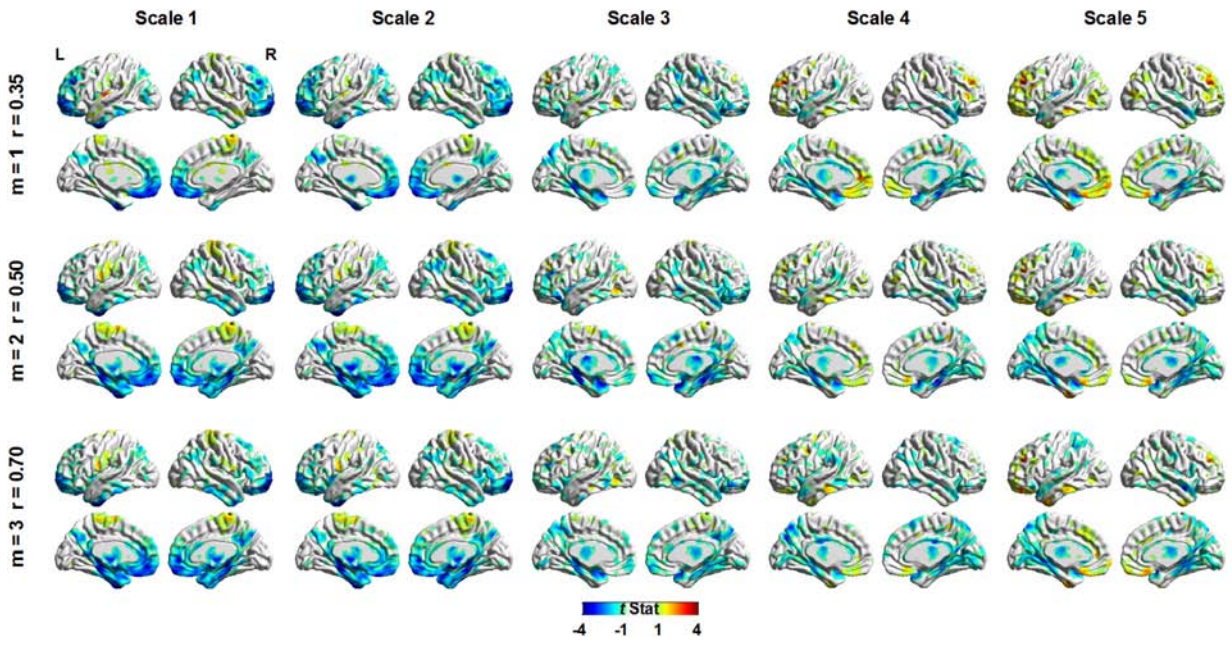

FIGURE 5 | Voxel-wise correlation between age and multiscale entropy using a general linear model (GLM) to control the effect of sex and total gray matter volume. The GLM was used separately for sample entropy parameters of $m = 1$, $r = 0.35$; $m = 2$, $r = 0.50$; and $m = 3$, $r = 0.70$.

TABLE 2 | Regions showing significant correlation of age with multiscale entropy in the normal aging cohort.

Brain region[a]	BA	MNI coordinates (mm)			Volume (mm^3)[b]	Peak *t*	Mean *t*	CV
		x	*y*	*z*				
***m* = 1, *r* = 0.35**								
Parahippocampus R		12	−30	0	1,404	−3.65	−3.27	0.039
Parahippocampus L		−21	−30	−12	1,404	−3.81	−3.35	0.052
Superior temporal pole R	38	42	−3	−15	2,781	−3.99	−3.46	0.057
Superior temporal pole L	38	−42	18	−21	2,943	−3.99	−3.40	0.054
***m* = 2, *r* = 0.50**								
Parahippocampus R		21	−30	−21	4,725	−3.84	−3.39	0.057
Parahippocampus L		−21	−30	−15	5,994	−4.62	−3.63	0.098
Superior temporal pole R	38	42	12	−18	6,588	−4.58	−3.62	0.102
Superior temporal pole L	38	−36	9	−21	5,157	−4.40	−3.52	0.084
***m* = 3, *r* = 0.70**								
Parahippocampus R		18	−36	−6	2,268	−3.71	−3.33	0.045
Parahippocampus L		−9	−27	6	4,239	−4.00	−3.40	0.068
Superior temporal pole R	38	42	0	−15	4,374	−4.60	−3.58	0.100
Superior temporal pole L	38	−36	9	−21	2,565	−4.01	−3.37	0.091

[a]L, left; R, right; BA, Brodmann area; CV, coefficient of variation. [b]Volume was computed from cluster size (3 mm × 3 mm × 3 mm voxel). All results had p-value less than 0.05 corrected for multiple comparisons using familywise error.

Lake et al. (2002) proposed a minimizing error approach for SampEn and found that $m = 3$, $r = 0.2$ was optimal for the cardiac R-R intervals at 4,096 time points. Lake et al.'s (2002) study also demonstrated a wide range of parameters with SampEn estimates that were within the acceptable error range, such as $r = 0.1$–0.8 for $m = 1$, and $r = 0.2$–0.5 for $m = 2$. These findings emphasized the advantage of SampEn for maintaining low error and consistency in a wide range of parameters.

Another approach is to maximize the differential ability of the entropy estimates for a certain dataset, such as finding optimal SampEn parameters to predict the termination and outcome of atrial fibrillation (Alcaraz et al., 2010). We and others also used similar approaches to maximize the ability of SampEn to differentiate the BOLD MSE between the older subjects with low and high cognitive scores (Yang et al., 2013a), and to differentiate healthy and ill subjects in various populations (Sokunbi et al., 2013, 2014; Yang et al., 2013b).

An obvious shortcoming of this approach is that the choices of parameters will be dependent on study populations. Furthermore, maximizing the between-group difference does not guarantee that those parameters are more free from error or bias (McDonough and Nashiro, 2014). The minimizing error approach we adopted from Lake et al. (2002) can eliminate the problems of the maximizing between-group difference approach.

Is a Larger Pattern Length *m* Superior to a Smaller *m* to Capturing Signal Dynamics?

Our results showed that there was no substantial difference in brain regions detected by SampEn or MSE analyses using $m = 1$, 2, or 3. This observation contradicted the results of the AR model and the long-standing idea that a choice of a larger m is superior to smaller m because it provides a more detailed reconstruction of system dynamics (Pincus and Goldberger, 1994; Groome et al., 1999; Lake et al., 2002). This notion formed when the development of entropy measures was influenced by the theories of phase space and embedding dimensions (Takens, 1981), and the empirical evidence for the notion was based on a relatively long time series (such as 4,096 data points in Lake et al., 2002), which allowed sufficient statistics of complex dynamics. Our findings suggested that this notion was compromised in short time series because a small m (i.e., $m = 1$) was as sufficient to capture the dynamics of short BOLD signals as $m = 2$ or 3. These results are similar to a prior report that a small $m = 1$ was sufficient to detect atrial fibrillation in short heartbeat time series (Lake and Moorman, 2011). Furthermore, we found that the effect of chosen parameters primarily reflected the SampEn error and quantitative results of brain clusters, suggesting that the effect of error in entropy estimates may outweigh the importance of selecting m and r for the reconstruction of underlying dynamics in short time series.

The choice of $m = 1$ and $r = 0.35$ in our data did not prevent the use of different parameters from other resting data with higher scanning volumes. For long resting-state fMRI time series (e.g., 1,200 time points) such as those from the Human Connectome Project (Van Essen et al., 2013), we suggested that the parameter $m = 2$, $r = 0.50$ may be too relaxed (McDonough and Nashiro, 2014), and we anticipate that $m = 2$ or 3 (according to the AR model) and $r < 0.5$ may help to uncover subtle dynamics in long-term resting data that are not otherwise apparent.

Time Series Length Constraints on Selecting Pattern Length *m* in SampEn

A critical but often overlooked parameter in entropy estimates is the time series length constraints. The accuracy of entropy estimates is dependent on the data length to accrue sufficient

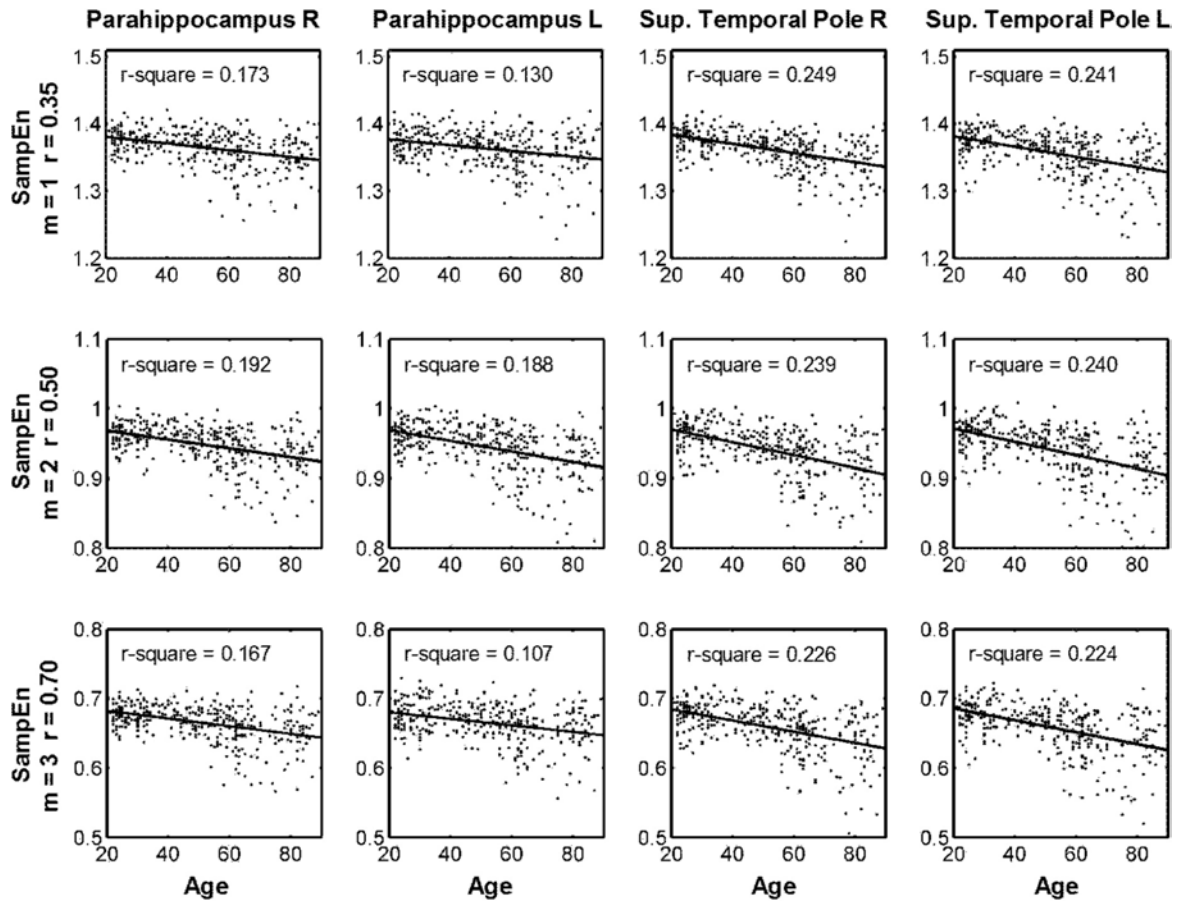

FIGURE 6 | Scattered plots of correlation between age and multiscale entropy (MSE) based on the average sample entropy (SampEn) with various parameters calculated in the four brain regions identified in **Table 2**.

statistics. Such data length constraints limit the selection of pattern length m because a large m will increase the chance of bias in entropy calculation. The theoretical work of time series length constraints on selecting m has been documented in ApEn that A time series with a length of at least 10^m to 20^m is necessary to obtain reliable ApEn estimates (Pincus and Goldberger, 1994). SampEn was developed to improve the consistency of entropy estimates in various data lengths (Richman and Moorman, 2000), and is therefore less vulnerable to time series length constraints than ApEn. However, Richman and Moorman (2000) also found that SampEn was unreliable for data lengths below 100 time points when using $m = 2$ (i.e., but the time series length effect with $m = 1$ was not tested). One recent study suggested that both ApEn and SampEn are extremely sensitive to parameter choices for short data sets $\leq$200 time points (Yentes et al., 2013). Because of the similarity between SampEn and ApEn, we adopted the same theoretical criteria of ApEn to estimate the time series length and pattern length m in the MSE analysis of short BOLD signals (Yang et al., 2013a).

While such a strategy may be questionable (Sokunbi, 2014), our results of relative error of SampEn in various scale factors may validate its reliability. The maximum pattern length m with a relative error below 0.1 for each scale factor was: $m = 4$ for Scale 1 (195 time points), $m = 2$ for Scale 2 (97 time points), $m = 1$ for Scales 3 and 4 (65 and 48 time points, respectively), and no pattern length m was able to maintain a relative error below 0.1 for Scale 5 (39 time points). The pattern of these results clearly suggested that SampEn was not subject to the theoretical constraints of ApEn (10^m–20^m) for data with at least 195 time points (i.e., m can be up to 4 in Scale Factor 1 with 195 time points). However, in a much shorter time series below 97 time points, the choices of pattern length m of SampEn may resemble that of ApEn and may be vulnerable to time series constraints.

Our results suggested that at a data length of approximately 97 time points, an r value larger than 0.4 was required for $m = 2$ to maintain a relative error below 0.1; this result was similar to the experimental data collected by Richman and Moorman (2000), using a data length 100 time points. Hence, although a resting-state fMRI study using single-scale SampEn may have a wide range of m and r available in short time series of at least 97 data points (**Figure 3**), the MSE analysis with a coarse-graining procedure has to consider these time series length constraints.

Effect of Normal Aging on Resting-State Brain Complexity

The normal aging data presented in this study were used as an attempt to improve our previous study (Yang et al., 2013a), which did not consider the between-age-group difference in the MSE analysis of the effect of gray matter volume loss in older people. Although we briefly studied this issue when examining the effect of APOE ε4 on MSE complexity (Yang et al., 2014), that study was based on younger and older groups and cannot be generalized to the adult lifespan. After regressing out the effect of age-related linear decline in total gray matter volume on MSE, the parahippocampus and superior temporal pole still showed a significant decline in MSE with increasing age, suggesting that a volume-independent functional change occurred in these two brain areas. Because both areas had neuropathologic changes caused by normal aging and Alzheimer's disease (Arnold et al., 1994; Mitchell et al., 2002), whether a reduced MSE in these areas can be explained by the accumulation of neurofibrillary tangles warrants further.

Limitations

This study was subject to certain limitations. First, the minimization strategy focused exclusively on the CSF region. Some studies have suggested that white matter also exerts some influences through noise (Liu et al., 2013; Siero et al., 2014). Second, neuronal activity is not always associated with changes in cerebral blood flows (Huo et al., 2014); thus, additional studies are required to examine the extent of neuronal activity that contributes to the complexity of BOLD fMRI data. Third, the removal of physiologic noise may be improved by a more advanced approach, such as component-based noise correction method (Behzadi et al., 2007). Future study is also warranted to explore the relationship between the bias of entropy calculation and mitigation of physiologic noise. Fourth, the relative error used in Lake et al. (2002) was consistent with the CV. We used a similar metric, but because our study showed that a CV with a threshold of 10% was approximately the same as a relative error of 0.1, using a CV to judge the bias of SampEn in future studies directly might be easier for interpretation. Finally, MSE is not merely a calculation of SampEn on multiple time scales (Peng et al., 2009). The substantial difference between MSE and single-scale SampEn in distinguishing complexity and irregularity was beyond the scope of this study and warrants a systemic investigation, using normal aging and disease population data.

CONCLUSION

We developed a general strategy to study the bias of the SampEn/MSE analysis of resting-state fMRI data and comprehensively examined the effect of various parameters on the relative error of SampEn estimates. Our results addressed the problems in the maximizing between-group difference approach and revealed a range of appropriate parameters that can be used in future resting-state fMRI studies with various data constraints. Finally, we expect that the bias minimization strategy can be generalized to other method of quantifying temporal dynamics of BOLD signal and improve the consistency of these methods to study abnormal brain activity in various brain diseases.

ETHICS STATEMENT

This study was carried out in accordance with the recommendations of the institutional review board at Taipei Veterans General Hospital, with written informed consent from all subjects. All subjects gave written informed consent in accordance with the Declaration of Helsinki. The protocol was approved by the institutional review board at Taipei Veterans General Hospital.

AUTHOR CONTRIBUTIONS

AY designed the experiment, analyzed the data, performed the statistical analyses, and wrote the paper. C-PL provided MRI resource and technical support of the experiment. S-JT and C-KP contributed the materials and critically commented the manuscript. All authors have approved the final article.

FUNDING

This work was supported by Taipei Veterans General Hospital, Taiwan (grants VGHUST100-G1-4-1, VGHUST102-G1-2-1, VGHUST103-G1-4-3, V99ER3-004, and V100C-013); Taipei Veterans General Hospital-National Yang-Ming University-Excellent Physician Scientists Cultivation Program, No.103-V-A-002; the Ministry of Science and Technology (MOST) of Taiwan (grants MOST 101-2314-B-075-041-MY3, MOST 103-2320-B-008-001, and MOST 104-2314-B-075-078-MY2).

ACKNOWLEDGMENTS

Part of this work has been published in the conference proceeding: Yang, A. C., Tsai, S. J., Lin, C. P., Peng, C. K. (2016). A Strategy to Reduce Bias of Entropy Estimates in fMRI Signal 38th Annual International Conference of the IEEE Engineering in Medicine and Biology Society Orlando, FL.

REFERENCES

Alcaraz, R., Abasolo, D., Hornero, R., and Rieta, J. J. (2010). Optimal parameters study for sample entropy-based atrial fibrillation organization analysis. *Comput. Methods Programs Biomed.* 99, 124–132. doi: 10.1016/j.cmpb.2010.02.009

Anderson, J. S., Druzgal, T. J., Lopez-Larson, M., Jeong, E. K., Desai, K., and Yurgelun-Todd, D. (2011). Network anticorrelations, global regression, and phase-shifted soft tissue correction. *Hum. Brain Mapp.* 32, 919–934. doi: 10.1002/hbm.21079

Arnold, S. E., Hyman, B. T., and Van Hoesen, G. W. (1994). Neuropathologic changes of the temporal pole in Alzheimer's disease and Pick's disease.

Arch. Neurol. 51, 145–150. doi: 10.1001/archneur.1994.00540140051014

Bassett, D. S., Nelson, B. G., Mueller, B. A., Camchong, J., and Lim, K. O. (2012). Altered resting state complexity in schizophrenia. *Neuroimage* 59, 2196–2207. doi: 10.1016/j.neuroimage.2011.10.002

Behzadi, Y., Restom, K., Liau, J., and Liu, T. T. (2007). A component based noise correction method (CompCor) for BOLD and perfusion based fMRI. *Neuroimage* 37, 90–101. doi: 10.1016/j.neuroimage.2007.04.042

Biswal, B., Yetkin, F. Z., Haughton, V. M., and Hyde, J. S. (1995). Functional connectivity in the motor cortex of resting human brain using echo-planar MRI. *Magn. Reson. Med.* 34, 537–541. doi: 10.1002/mrm.1910340409

Biswal, B. B., Van Kylen, J., and Hyde, J. S. (1997). Simultaneous assessment of flow and BOLD signals in resting-state functional connectivity maps. *NMR Biomed.* 10, 165–170. doi: 10.1002/(SICI)1099-1492(199706/08)10:4/5<165::AID-NBM454>3.0.CO;2-7

Castiglioni, P., Zurek, S., Piskorski, J., Kosmider, M., Guzik, P., Ce, E., et al. (2013). Assessing sample entropy of physiological signals by the norm component matrix algorithm: application on muscular signals during isometric contraction. *Conf. Proc. IEEE Eng. Med. Biol. Soc.* 2013, 5053–5056. doi: 10.1109/EMBC.2013.6610684

Chen, X., Solomon, I., and Chon, K. (2005). "Comparison of the use of approximate entropy and sample entropy: applications to neural respiratory signal," in *Proceedings of the 27th Annual International Conference of the Engineering in Medicine and Biology Society*, Shanghai, 4212–4215.

Chon, K., Scully, C. G., and Lu, S. (2009). Approximate entropy for all signals. *IEEE Eng. Med. Biol. Mag.* 28, 18–23. doi: 10.1109/MEMB.2009.934629

Costa, M., Goldberger, A. L., and Peng, C. K. (2002). Multiscale entropy analysis of complex physiologic time series. *Phys. Rev. Lett.* 89:068102. doi: 10.1103/PhysRevLett.89.068102

de, Araujo DB, Tedeschi, W., Santos, A. C., Elias, J Jr, Neves, U. P., and Baffa, O. (2003). Shannon entropy applied to the analysis of event-related fMRI time series. *Neuroimage* 20, 311–317. doi: 10.1016/S1053-8119(03)00306-9

Fogedby, H. C. (1992). On the phase space approach to complexity. *J. Stat. Phys.* 69, 411–425. doi: 10.1007/BF01053799

Fox, M. D., and Raichle, M. E. (2007). Spontaneous fluctuations in brain activity observed with functional magnetic resonance imaging. *Nat. Rev. Neurosci.* 8, 700–711. doi: 10.1038/nrn2201

Fox, M. D., Snyder, A. Z., Vincent, J. L., and Raichle, M. E. (2007). Intrinsic fluctuations within cortical systems account for intertrial variability in human behavior. *Neuron* 56, 171–184. doi: 10.1016/j.neuron.2007.08.023

Gawryluk, J. R., Mazerolle, E. L., and D'arcy, R. C. (2014). Does functional MRI detect activation in white matter? A review of emerging evidence, issues, and future directions. *Front. Neurosci.* 8:239. doi: 10.3389/fnins.2014.00239

Goldberger, A. L. (1996). Non-linear dynamics for clinicians: chaos theory, fractals, and complexity at the bedside. *Lancet* 347, 1312–1314. doi: 10.1016/S0140-6736(96)90948-4

Goldberger, A. L., Amaral, L. A., Hausdorff, J. M., Ivanov, P., Peng, C. K., and Stanley, H. E. (2002a). Fractal dynamics in physiology: alterations with disease and aging. *Proc. Natl. Acad. Sci. U.S.A.* 99(Suppl. 1), 2466–2472.

Goldberger, A. L., Peng, C. K., and Lipsitz, L. A. (2002b). What is physiologic complexity and how does it change with aging and disease? *Neurobiol. Aging* 23, 23–26. doi: 10.1016/S0197-4580(01)00266-4

Goni, J., Aznarez-Sanado, M., Arrondo, G., Fernandez-Seara, M., Loayza, F. R., Heukamp, F. H., et al. (2011). The neural substrate and functional integration of uncertainty in decision making: an information theory approach. *PLoS One* 6:e17408. doi: 10.1371/journal.pone.0017408

Gow, B. J., Peng, C. K., Wayne, P. M., and Ahn, A. C. (2015). Multiscale entropy analysis of center-of-pressure dynamics in human postural control: methodological considerations. *Entropy* 17, 7926–7947. doi: 10.3390/e17127849

Groome, L. J., Mooney, D. M., Holland, S. B., Smith, L. A., Atterbury, J. L., and Loizou, P. C. (1999). Human fetuses have nonlinear cardiac dynamics. *J. Appl. Physiol.* 87, 530–537. doi: 10.1152/jappl.1999.87.2.530

Hager, B., Yang, A. C., Brady, R., Meda, S., Clementz, B., Pearlson, G. D., et al. (2017). Neural complexity as a potential translational biomarker for psychosis. *J. Affect. Disord.* 216, 89–99. doi: 10.1016/j.jad.2016.10.016

Hausdorff, J. M., and Peng, C. (1996). Multiscaled randomness: a possible source of 1/f noise in biology. *Phys. Rev. E Stat. Phys. Plasmas Fluids Relat. Interdiscip. Topics* 54, 2154–2157. doi: 10.1103/PhysRevE.54.2154

Hughes, C. P., Berg, L., Danziger, W. L., Coben, L. A., and Martin, R. L. (1982). A new clinical scale for the staging of dementia. *Br. J. Psychiatry* 140, 566–572. doi: 10.1192/bjp.140.6.566

Huo, B. X., Smith, J. B., and Drew, P. J. (2014). Neurovascular coupling and decoupling in the cortex during voluntary locomotion. *J. Neurosci.* 34, 10975–10981. doi: 10.1523/JNEUROSCI.1369-14.2014

Kirchner, M., Schubert, P., Schmidtbleicher, D., and Haas, C. T. (2012). Evaluation of the temporal structure of postural sway fluctuations based on a comprehensive set of analysis tools. *Phys. A* 391, 4692–4703. doi: 10.1016/j.physa.2012.05.034

Lake, D. E., and Moorman, J. R. (2011). Accurate estimation of entropy in very short physiological time series: the problem of atrial fibrillation detection in implanted ventricular devices. *Am. J. Physiol. Heart Circ. Physiol.* 300, H319–H325. doi: 10.1152/ajpheart.00561.2010

Lake, D. E., Richman, J. S., Griffin, M. P., and Moorman, J. R. (2002). Sample entropy analysis of neonatal heart rate variability. *Am. J. Physiol. Regul. Integr. Comp. Physiol.* 283, R789–R797. doi: 10.1152/ajpregu.00069.2002

Leite, F. P., and Mandeville, J. B. (2006). Characterization of event-related designs using BOLD and IRON fMRI. *Neuroimage* 29, 901–909. doi: 10.1016/j.neuroimage.2005.08.022

Linkenkaer-Hansen, K., Nikouline, V. V., Palva, J. M., and Ilmoniemi, R. J. (2001). Long-range temporal correlations and scaling behavior in human brain oscillations. *J. Neurosci.* 21, 1370–1377. doi: 10.1523/JNEUROSCI.21-04-01370.2001

Lipsitz, L. A. (2002). Dynamics of stability: the physiologic basis of functional health and frailty. *J. Gerontol. A Biol. Sci. Med. Sci.* 57, B115–B125.

*Liu, C. Y., Krishnan, A. P., Yan, L., Smith, R. X., Kilroy, E., Alger, J. R., et al. (2013). Complexity and synchronicity of resting state blood oxygenation level-dependent (BOLD) functional MRI in normal aging and cognitive decline. *J. Magn. Reson. Imaging* 38, 36–45. doi: 10.1002/jmri.23961

McDonough, I. M., and Nashiro, K. (2014). Network complexity as a measure of information processing across resting-state networks: evidence from the human connectome project. *Front. Hum. Neurosci.* 8:409. doi: 10.3389/fnhum.2014.00409

Mitchell, T. W., Mufson, E. J., Schneider, J. A., Cochran, E. J., Nissanov, J., Han, L. Y., et al. (2002). Parahippocampal tau pathology in healthy aging, mild cognitive impairment, and early Alzheimer's disease. *Ann. Neurol.* 51, 182–189. doi: 10.1002/ana.10086

Murphy, K., Birn, R. M., Handwerker, D. A., Jones, T. B., and Bandettini, P. A. (2009). The impact of global signal regression on resting state correlations: are anti-correlated networks introduced? *Neuroimage* 44, 893–905. doi: 10.1016/j.neuroimage.2008.09.036

Peng, C. K., Costa, M., and Goldberger, A. L. (2009). Adaptive data analysis of complex fluctuations in physiologic time series. *Adv. Adapt. Data Anal.* 1, 61–70. doi: 10.1142/S1793536909000035

Pincus, S. M. (1991). Approximate entropy as a measure of system complexity. *Proc. Natl. Acad. Sci. U.S.A.* 88, 2297–2301. doi: 10.1073/pnas.88.6.2297

Pincus, S. M., and Goldberger, A. L. (1994). Physiological time-series analysis: what does regularity quantify? *Am. J. Physiol.* 266, H1643–H1656. doi: 10.1152/ajpheart.1994.266.4.H1643

Richman, J. S., and Moorman, J. R. (2000). Physiological time-series analysis using approximate entropy and sample entropy. *Am. J. Physiol. Heart Circ. Physiol.* 278, H2039–H2049. doi: 10.1152/ajpheart.2000.278.6.H2039

Schlesinger, M. F. (1987). Fractal time and 1/f noise in complex systems. *Ann. N. Y. Acad. Sci.* 504, 214–228. doi: 10.1111/j.1749-6632.1987.tb48734.x

Sheehan, D. V., Lecrubier, Y., Sheehan, K. H., Amorim, P., Janavs, J., Weiller, E., et al. (1998). The Mini-International Neuropsychiatric Interview (M.I.N.I.): the development and validation of a structured diagnostic psychiatric interview for DSM-IV and ICD-10. *J. Clin. Psychiatry* 59(Suppl. 20), 22–33.

Siero, J. C., Hermes, D., Hoogduin, H., Luijten, P. R., Ramsey, N. F., and Petridou, N. (2014). BOLD matches neuronal activity at the mm scale: a combined 7T fMRI and ECoG study in human sensorimotor cortex. *Neuroimage* 101, 177–184. doi: 10.1016/j.neuroimage.2014.07.002

Sokunbi, M. O. (2014). Sample entropy reveals high discriminative power between young and elderly adults in short fMRI data sets. *Front. Neuroinform.* 8:69. doi: 10.3389/fninf.2014.00069

Sokunbi, M. O., Fung, W., Sawlani, V., Choppin, S., Linden, D. E., and Thome, J. (2013). Resting state fMRI entropy probes complexity of brain activity in adults

with ADHD. *Psychiatry Res.* 214, 341–348. doi: 10.1016/j.pscychresns.2013.10.001

Sokunbi, M. O., Gradin, V. B., Waiter, G. D., Cameron, G. G., Ahearn, T. S., Murray, A. D., et al. (2014). Nonlinear complexity analysis of brain FMRI signals in schizophrenia. *PLoS One* 9:e95146. doi: 10.1371/journal.pone.0095146

Sokunbi, M. O., Staff, R. T., Waiter, G. D., Ahearn, T. S., Fox, H. C., Deary, I. J., et al. (2011). Inter-individual differences in fMRI entropy measurements in old age. *IEEE Trans. Biomed. Eng.* 58, 3206–3214. doi: 10.1109/TBME.2011.2164793

Song, X. W., Dong, Z. Y., Long, X. Y., Li, S. F., Zuo, X. N., Zhu, C. Z., et al. (2011). REST: a toolkit for resting-state functional magnetic resonance imaging data processing. *PLoS One* 6:e25031. doi: 10.1371/journal.pone.0025031

Stam, C. J., and de Bruin, E. A. (2004). Scale-free dynamics of global functional connectivity in the human brain. *Hum. Brain Mapp.* 22, 97–109. doi: 10.1002/hbm.20016

Sturzbecher, M. J., Tedeschi, W., Cabella, B. C., Baffa, O., Neves, U. P., and De Araujo, D. B. (2009). Non-extensive entropy and the extraction of BOLD spatial information in event-related functional MRI. *Phys. Med. Biol.* 54, 161–174. doi: 10.1088/0031-9155/54/1/011

Takens, F. (1981). "Detecting strange attractors in turbulence," in *Dynamical Systems and Turbulence*, eds D. A. Rand, and L.-S. Young (Berlin: Springer-Verlag).

Tobia, M. J., Iacovella, V., and Hasson, U. (2012). Multiple sensitivity profiles to diversity and transition structure in non-stationary input. *Neuroimage* 60, 991–1005. doi: 10.1016/j.neuroimage.2012.01.041

Van Essen, D. C., Smith, S. M., Barch, D. M., Behrens, T. E., Yacoub, E., Ugurbil, K., et al. (2013). The WU-Minn human connectome project: an overview. *Neuroimage* 80, 62–79. doi: 10.1016/j.neuroimage.2013.05.041

Wu, C. W., Gu, H., Zou, Q., Lu, H., Stein, E. A., and Yang, Y. (2012). TE-dependent spatial and spectral specificity of functional connectivity. *Neuroimage* 59, 3075–3084. doi: 10.1016/j.neuroimage.2011.11.030

Yang, A. C., Hong, C. J., Liou, Y. J., Huang, K. L., Huang, C. C., Liu, M. E., et al. (2015). Decreased resting-state brain activity complexity in schizophrenia characterized by both increased regularity and randomness. *Hum. Brain Mapp.* 36, 2174–2186. doi: 10.1002/hbm.22763

Yang, A. C., Huang, C. C., Liu, M. E., Liou, Y. J., Hong, C. J., Lo, M. T., et al. (2014). The APOE epsilon4 allele affects complexity and functional connectivity of resting brain activity in healthy adults. *Hum. Brain Mapp.* 35, 3238–3248. doi: 10.1002/hbm.22398

Yang, A. C., Huang, C. C., Yeh, H. L., Liu, M. E., Hong, C. J., Tu, P. C., et al. (2013a). Complexity of spontaneous BOLD activity in default mode network is correlated with cognitive function in normal male elderly: a multiscale entropy analysis. *Neurobiol. Aging* 34, 428–438. doi: 10.1016/j.neurobiolaging.2012.05.004

Yang, A. C., Wang, S. J., Lai, K. L., Tsai, C. F., Yang, C. H., Hwang, J. P., et al. (2013b). Cognitive and neuropsychiatric correlates of EEG dynamic complexity in patients with Alzheimer's disease. *Prog. Neuropsychopharmacol. Biol. Psychiatry* 47, 52–61. doi: 10.1016/j.pnpbp.2013.07.022

Yang, A. C., and Tsai, S. J. (2013). Is mental illness complex? From behavior to brain. *Prog. Neuropsychopharmacol. Biol. Psychiatry* 45, 253–257. doi: 10.1016/j.pnpbp.2012.09.015

Yentes, J. M., Hunt, N., Schmid, K. K., Kaipust, J. P., Mcgrath, D., and Stergiou, N. (2013). The appropriate use of approximate entropy and sample entropy with short data sets. *Ann. Biomed. Eng.* 41, 349–365. doi: 10.1007/s10439-012-0668-3

Zang, Y. C. (1991). Complexity and 1/f noise. A phase space approach. *J. Phys. I France* 1, 971–977. doi: 10.1186/s12911-016-0252-0

Zarahn, E., Aguirre, G. K., and D'esposito, M. (1997). Empirical analyses of BOLD fMRI statistics. I. Spatially unsmoothed data collected under null-hypothesis conditions. *Neuroimage* 5, 179–197. doi: 10.1006/nimg.1997.0263

Conflict of Interest Statement: The authors declare that the research was conducted in the absence of any commercial or financial relationships that could be construed as a potential conflict of interest.

frontiers in Neuroscience

PERSPECTIVE
published: 14 August 2018
doi: 10.3389/fnins.2018.00566

Developmental Trajectory of Infant Brain Signal Variability: A Longitudinal Pilot Study

Chiaki Hasegawa[1], Tetsuya Takahashi[2], Yuko Yoshimura[1,3], Sou Nobukawa[4], Takashi Ikeda[1], Daisuke N. Saito[1], Hirokazu Kumazaki[1], Yoshio Minabe[1] and Mitsuru Kikuchi[1]*

[1] Research Center for Child Mental Development, Kanazawa University, Kanazawa, Japan, [2] Health Administration Center, University of Fukui, Fukui, Japan, [3] Faculty of Education, Kanazawa University, Kanazawa, Japan, [4] Department of Computer Science, Chiba Institute of Technology, Narashino, Japan

The infant brain shows rapid neural network development that considerably influences cognitive and behavioral abilities in later life. Reportedly, this neural development process can be indexed by estimating neural signal complexity. However, the precise developmental trajectory of brain signal complexity during infancy remains elusive. This study was conducted to ascertain the trajectory of magnetoencephalography (MEG) signal complexity from 2 months to 3 years of age in five infants using multiscale entropy (MSE), which captures signal complexity at multiple temporal scales. Analyses revealed scale-dependent developmental trajectories. Specifically, signal complexity predominantly increased from 5 to 15 months of age at higher temporal scales, whereas the complexity at lower temporal scales was constant across age, except in one infant who showed decreased complexity. Despite a small sample size limiting this study's power, this is the first report of a longitudinal investigation of changes in brain signal complexity during early infancy and is unique in its application of MSE analysis of longitudinal MEG data during infancy. The results of this pilot study may serve to further our understanding of the longitudinal changes in the neural dynamics of the developing infant brain.

Keywords: infant development, magnetoencephalography (MEG), multiscale entropy, complexity, longitudinal change

OPEN ACCESS

Edited by:
Albert Yang,
Harvard Medical School,
United States

Reviewed by:
Vasily Vakorin,
Simon Fraser University, Canada
Chung-Kang Peng,
Harvard Medical School,
United States
Shih-Jen Tsai,
Taipei Veterans General Hospital,
Taiwan

***Correspondence:**
Tetsuya Takahashi
takahash@u-fukui.ac.jp

Specialty section:
This article was submitted to Brain Imaging Methods, a section of the journal Frontiers in Neuroscience

Received: *21 November 2017*
Accepted: *27 July 2018*
Published: *14 August 2018*

Citation:
Hasegawa C, Takahashi T, Yoshimura Y, Nobukawa S, Ikeda T, Saito DN, Kumazaki H, Minabe Y and Kikuchi M (2018) Developmental Trajectory of Infant Brain Signal Variability: A Longitudinal Pilot Study. Front. Neurosci. 12:566. doi: 10.3389/fnins.2018.00566

INTRODUCTION

Infancy is a period of remarkable neural development in the brain that is reflected by increasing cognitive and behavioral capacities for external circumstances or internal changes in later life (Cao et al., 2017). Recent advances in neuroimaging devices and analysis techniques have been used to visualize the development of brain functions. The human brain is a complex system that is characterized by its astonishing signal variability, which operates over a wide range of temporal and spatial scales. This brain signal variability facilitates learning and optimal environmental adaptation to the changing demands of a dynamic environment (Faisal et al., 2008). This complexity also conveys important information about neural system dynamics and their alterations (reviewed in Stam, 2005; Garrett et al., 2013; Takahashi, 2013).

Abbreviations: MEG, magnetoencephalography.

An entropy-based approach, multiscale entropy (MSE) analysis, has been proposed to estimate the physiological signal complexity on multiple temporal scales using coarse-graining procedures (Costa et al., 2005). This extension to multiple time scales enables the capture of long-range temporal correlations in a time series. MSE has been successfully applied in the investigation of developmental changes in brain signal complexity from infancy through adolescence and into adulthood (McIntosh et al., 2008; Lippe et al., 2009; Polizzotto et al., 2015; Takahashi et al., 2016). However, no study has explored the longitudinal changes in brain signal complexity during the early stages of development despite the significant importance of examining within-subject developmental trajectories (Giedd et al., 1999; Sowell et al., 2004; Shaw et al., 2008). This is due to the large variance in the developmental pattern during infancy (Landa et al., 2012), a period in which developmental disorders frequently emerge (Bolton et al., 2012; Lemcke et al., 2013).

We characterized the trajectory of brain signal complexity of typically developing infants, aged 5 to 36 months, using MSE applied to MEG. MEG is suited for measuring the infant brain because it offers a non-invasive and quiet environment during measurement. Additionally, MEG allows the mother to accompany the infant to provide encouragement and comfort, as well as enabling her to decide whether the experiment should be paused or continued. Furthermore, in the assessment of signal complexity, MEG can directly measure brain magnetic fields in the cortex with high temporal resolution (Kikuchi et al., 2011; Yoshimura et al., 2012; Takahashi et al., 2016).

METHODS

Data for the present study were obtained from an ongoing longitudinal study of infants. In this study, we analyzed five infants (one female and four males) who were 36 months of age at the time of analysis. They were recruited from Kanazawa University at 1 month old, and follow-up examinations and MEG experiments were conducted once a month (ideally every month). Participants had no history of developmental problems at the time of the latest measurement.

All mothers agreed to their infant's participation in the study and had full knowledge of the experimental nature of the research. Written informed consent was obtained prior to participation. The study was approved by the Ethics Committee of the Kanazawa University Hospital, and all procedures were performed in accordance with the Declaration of Helsinki.

EXPERIMENTAL PROCEDURE

Magnetoencephalography data were recorded using a 151-channel Superconducting Quantum Interference Device (SQUID) whole-head coaxial gradiometer MEG system for children (PQ 1151 R; Yokogawa/KIT, Kanazawa, Japan) installed at the MEG Center of Ricoh Company, Ltd. (Kanazawa, Japan). During recording, the participant lay supine on a bed in a magnetically shielded room (Daido Steel, Nagoya, Japan) with his or her head inside the MEG system helmet. The infant's mother and one research member remained in the shielded room to keep the infant comfortable and encourage the infant to maintain a steady body position when necessary. The infants were carefully monitored using a video monitoring system to assess their compliance with the instructions and to record any notable artifacts, such as head motion, inappropriate head position. Before recording, infants or their mother selected a video program according to their preference from a number of video programs (e.g., popular Japanese animations and TV programs). All infants viewed silent video programs projected onto a screen throughout the recording session to promote a consistent state and attention. MEG recordings were conducted every month when possible.

DATA ANALYSIS

Magnetic fields were sampled at 2000 Hz per channel (bandpass filter 0.16–200 Hz). Offline analysis was performed using a BrainVision Analyzer 2 (Brain Products GmbH, Gilching, Germany) and MATLAB (the MathWorks Inc., Natick, MA, United States). The raw MEG data were resampled at 500 Hz with 1.5–60-Hz bandpass and 60-Hz notch filters. MEG data were segmented for 5 s (2500 data points: 5 s × 500 Hz). Artifacts such as eye movements, blinks, cardiac activities, and muscle activities were visually identified and excluded from analyses. The children's head movements were video monitored throughout the session. At the epoch selection stage, clear head motion artifacts were eliminated by confirmation of head motion in the videos at the time of the MEG artifacts by an MEG expert who was blinded to the identity of the subjects. Contaminated data were also eliminated by an MEG expert who was blinded to the identity of the subjects. A minimum of 50 segments were recorded for each subject. Finally, we randomly selected 50 segments (i.e., a 250 s recording period) from all artifact-free segments of each recording. For each subject, MSE values were calculated separately for each of the selected segments and were then averaged into a single value as the mean MSE.

MSE ANALYSIS

Multiscale entropy analysis quantifies the complexity of a time series using different time scales (Costa et al., 2002). For the extension to multiple time scales, the original MEG time series $\{x_1, x_2, \ldots, x_N\}$ is coarse-grained to $\{y_1(\tau), y_2(\tau), \ldots, y_{N/\tau}(\tau)\}$ by the temporal scale τ with non-overlapping windows as follows.

$$y_j(\tau) = (1/\tau) \sum_{i=(j-1)\tau+1}^{j\tau} x_i, \qquad 1 \le j \le N/\tau.$$

The complexity of each scale can be measured through the calculation of sample entropy (SampEn), which assesses the predictability of a time series. The SampEn was calculated for each series $\{y_1(\tau), y_2(\tau), \ldots, y_{N/\tau}(\tau)\}$. The SampEn is the negative of the logarithmic conditional probability that two sequences of

m consecutive data points that are mutually similar (within a given tolerance r) will remain similar at the next point $(m + 1)$ in the dataset (N), where m is the space of the dimension and r is the effective filter for measuring the consistency of a time series (Richman and Moorman, 2000). Considering the MEG time series $\{x_1, x_2, \ldots, x_N\}$ as observations of a stochastic variable x, the dynamic SampEn is defined as

$$h_{\text{sample}}\ (r,\ m,\ N)\ =\ -\log_e\ [C_{m+1}\ (r)\ /\ C_m\ (r)],$$

where $C_m\ (r)$ = {number of pairs (i, j) with $|z_i^m - z_j^m| < r$, $i \neq j$}/{number of all probable pairs, i.e., $(N - m + 1)\ (N - m)$}. Therein, $z = y\ (\tau)$; z^m is a vector of an m sample time series of $(N - m)$ length, and $|z_i^m - z_j^m|$ denotes the distance between points z_i^m and z_j^m. In this study, we used m = 2 and r = 0.2. SampEn values were computed for 1–20 scales that correspond to 2–40 ms (Temporal scales in ms = tau * 1000 ms/sampling frequency).

POWER SPECTRAL ANALYSIS

Along with MSE calculations, spectral power analysis was performed for each epoch that was used for the MSE calculation as a comparative MSE analysis. We calculated the spectral density (amplitude) using a fast Fourier transform. A Hamming window was applied to each epoch for spectral power analysis.

SURROGATE ANALYSIS

We derived surrogate data using a Fourier transformation to the MEG data to detect non-linearity in the MEG data (Vakorin and McIntosh, 2012; Grandy et al., 2016). Specifically, the time-series of each epoch was Fourier transformed, and then its phase was randomized and applied to an inverse Fourier transform. Using 10 types of seeds for randomization, we derived 10 surrogate data per epoch and then calculated an average value among their SampEn values of surrogate data. We compared the SampEn values for the original time series to the SampEn values for the surrogate data.

RESULTS

Figure 1 shows the averaged (across all sensors into a single value) developmental trajectory of the spectral power (**Figure 1**, upper panels) and MSE (**Figure 1**, lower panels) across five infants aged from 5 to 36 months old. All infants demonstrated an increase in the MSE value with age. The Jonckheere-Terpstra test was used to test for an age-related trend in MSE values, and statistically significant age-related trends were identified for coarse time scales (31–40 ms, scales: 16–20) (T_{JT} = 459.0, standard error = 34.8, z = 5.6, $p < 0.001$). **Figure 2** shows the averaged developmental trajectory in each time scale bin (**Figure 2A**) and the topography of MSE values across different ages (**Figure 2B**). A more detailed examination of our results revealed that the remarkable increase in MSE identified for longer time scales (31–40 ms, scale: 16–20) was predominantly observed at ages up to 15 months and was found across brain regions (**Figure 2**). After 15 months of age, this increase tended to slow. However, the power spectral analysis also showed an increase in power in the theta and alpha bands. This increase was more prominent after 15 months of age, while the MSE change was more prominent during the earlier infancy periods. Regarding the shorter time scales (2–10 ms, scale: 1–5), the developmental trajectory of MSE varied across subjects. For instance, some infants showed constant MSE values across development, whereas one infant showed a gradual decrease (**Figure 1**, bottom panels).

In the surrogate analysis, we found region- and scale-specific entropy alterations in the surrogate data, which may suggest an inherent non-linearity in the MEG data (data not shown). Specifically, in the surrogate data, the SampEn increased near the frontal and temporo-occipital regions. Interestingly, this region-specific SampEn alteration was more prominent for smaller temporal scales (less than 20 ms) and was frequently identified during early infancy (5–10 months of age).

DISCUSSION

The neurodevelopmental trajectory of infancy has received much attention because infancy is a critical period of brain development in which cognitive and behavioral abilities are enhanced (Cao et al., 2017) and neurodevelopmental disorders, such as autism spectrum disorder (ASD), are predicted to develop. This is the first longitudinal investigation of how brain signal complexity, which represents neural system dynamics, changes during infancy. The analysis revealed scale-dependent developmental trajectories of MEG signal complexity. Specifically, we found an increase in signal complexity for longer time scales, whereas the changes in complexity varied across infants for shorter time scales.

Many studies have investigated age-related signal complexity changes from late childhood into adulthood. Polizzotto et al. (2015) examined the MSE of resting-state EEG results in healthy subjects aged 8–22 years old. They reported an age-related increase in entropy in lower scales and a decrease in entropy for higher scales. McIntosh et al. (2008) calculated MSE changes in EEG during a face recognition visual memory task in children (8–15 years old) and young adults (20–33 years old). They found an age-related increase in EEG complexity that was significantly correlated with the accuracy of task performance. This observation was replicated by the same group using MEG (Misic et al., 2010), confirming the characteristic shape of the MSE curve and its prominent task-dependent increase during development. We have also demonstrated an age-related increase in MEG signal complexity. However, enhanced complexity was identified in children with ASD, particularly in earlier childhood (Takahashi et al., 2016). Compared to the changes that occur during the period from childhood to adolescence, brain signal complexity during infancy has been addressed by few studies. Lippe et al. (2009) investigated EEG signal complexity in response to visual and auditory stimulation in children ranging from

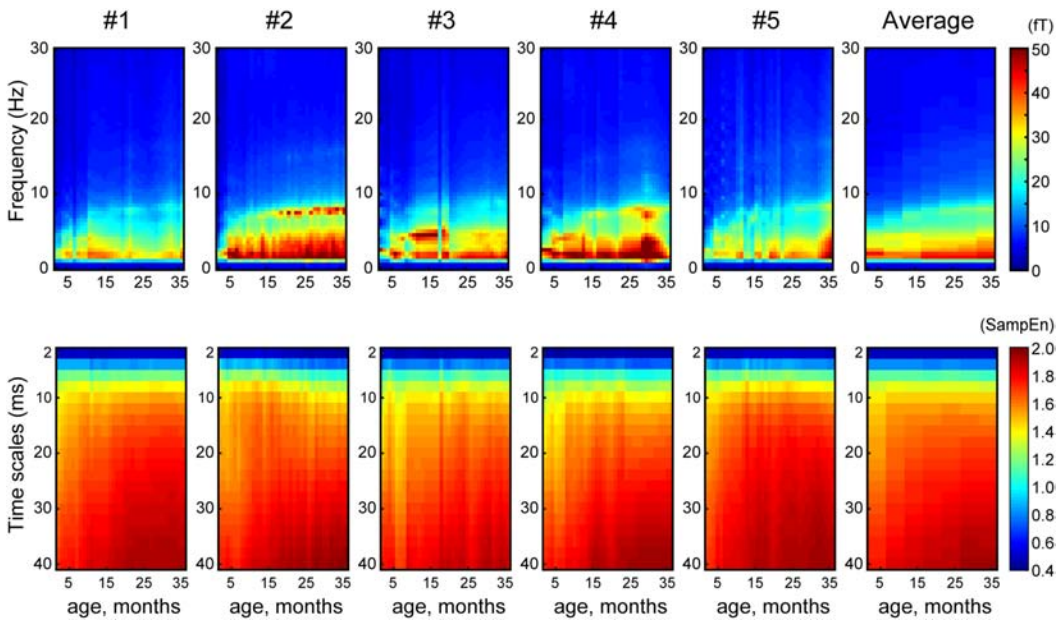

FIGURE 1 | Array plot showing the developmental trajectory of spectral power (top panels) and MSE (bottom panels) for each infant and their average (X-axis, age, months; Y-axis, frequency and time scales).

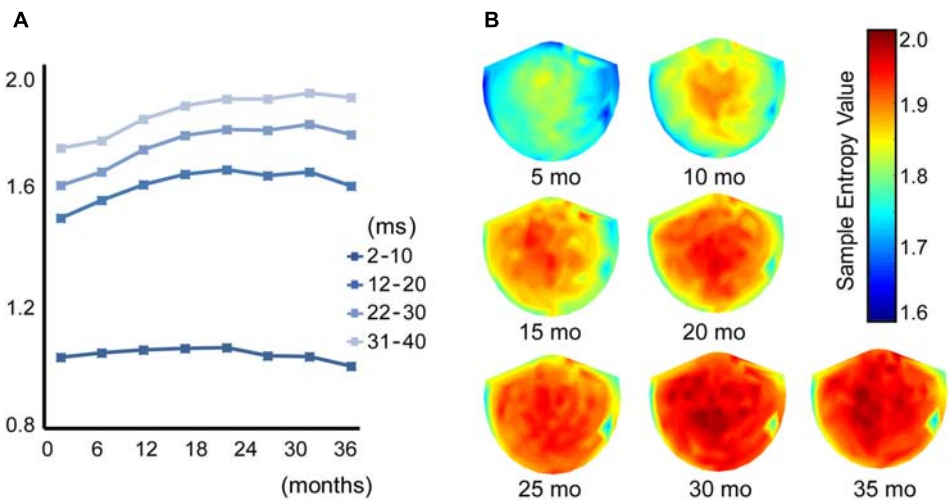

FIGURE 2 | (A) Each line shows the trajectory of the averaged MSE value across different time scales in 8 age bins (1–5, 6–10, 11–15, 16–20, 21–25, 26–30, 31–35, and 36–40 months of age). **(B)** Topography of the MSE value at a coarse time scale of 40 ms (scale = 20) across 7 age bins (5, 10, 15, 20, 25, 30, and 35 months of age).

1 month to 5 years of age. They found a task-dependent increase in EEG complexity with aging. However, these studies were based on a cross-sectional study design. Despite the small number of subjects, a unique aspect of this study is that we longitudinally investigated the development of MEG complexity during infancy.

In these contexts, our study provides the longitudinal underpinnings for the concept of significant shifts in brain signal complexity with aging (Garrett et al., 2013). Notably, for higher scales, we captured a robust developmental MSE profile across infants and across MEG sessions despite conditional inconsistencies (i.e., selected videos, emotions, or physical conditions), which may indicate the potential usefulness of MSE as a reliable and clinically useful trait biomarker of the infant brain. For instance, we have demonstrated a linear age-related increase in complexity at higher scales across 40–110 month-old children (Takahashi et al., 2016). Additionally, enhanced brain signal variability was observed in children with ASD, which was conformed for younger children. On the other hand, Bosl et al. (2011) examined resting-state EEG complexity by MSE in typically developing infants and infants with a high risk of ASD

across the ages of 6–24 months, and they found consistently lower EEG complexity at higher scales in the high-risk group, particularly at 9–12 months of age. These inconsistent results may be attributed to the different age ranges of these two previous studies on children with ASD.

Considering biological background, the observed rapid increase in MEG complexity in the high time scale (i.e., lower frequency range) at approximately 5–15 months old might demonstrate the development of long-range network-related cognitive processing. Given that long-range communication between multiple brain areas is driven by slow waves (i.e., theta and beta waves) (Wang, 2010), MEG complexity in a high time scale (i.e., lower frequency range) may be useful and a non-invasive biomarker of brain maturation in infants. Pujol et al. (2006) assessed myelination from birth to 3 years of age in children's brains using three-dimensional MRI imaging. Intriguingly, this volumetric study demonstrated that a period of rapid myelination started after the 5th month and reached the mature appearance by the 18th month, and the study revealed the relationship with vocabulary acquisition in children. This period of rapid myelination is almost the same as the period in which we observed a rapid change in the present study.

However, contrary to the developmental trajectory for higher scales, the developmental trajectory of MSE for lower scales is diverse across infants, and the reason for this difference remains unclear. Lippe et al. (2009) reported a rapid increase in complexity at lower scales, especially during the early stage of infancy (1–2 months old vs. 2–8 months old) that is followed by a gradual increase. This may suggest the possibility that complexity at lower scales (corresponding to $\leq$16 ms) saturates by 8 months of age. This may partially explain our finding of a constant complexity value across age after 5 months of age at lower scales. Theoretically, SampEn at finer (i.e., lower) time scales is based on wider frequencies, whereas coarser (i.e., higher) time scales are based on narrower frequencies (i.e., high frequency is filtered out). Signal variabilities in different frequencies must be reflected by differences in time scale. Therefore, a frequency-specific role in the differentiation of cognitive processing (Fries, 2015) and differences in maturational speed (Uhlhaas et al., 2009) may underlie these contradictory findings between the results from high and low time scales.

Surrogate analysis showed a region- and scale-specific increase in surrogate data compared to that in MSE from original data, which may suggest an inherent non-linearity in the MEG data. Furthermore, the developmental trajectory of the spectral power and MSE differed. Specifically, an increase in the power spectral seemed to be prominent after 12 months of age, whereas an increase in MSE emerged from early infancy until 15 months of age. Therefore, we assume that the enhancement in MSE with development may be associated with non-linear processes and may be independent of spectral power. In addition, as the outputs of neuronal networks are produced by interactions due to both local dense interconnectivity and sparse long-range excitatory projections (Friston et al., 1995), the resulting dynamics could be expected to operate at multiple scales.

Some potential limitations of the present study must be considered. First, despite frequent MEG recording, we were only able to follow five infants, which precluded statistical evaluation. Second, we did not correct for cognitive behavioral or psychological assessments, which might strengthen our claims. Third, the confounding influence of head motion cannot be excluded from potentially influencing the MSE results. Finally, as a technical consideration, the recent advent of cortical source localization techniques was not applied due to difficulties in performing MRI on infants. Although several limitations must be considered, our findings for the examination of MEG signal variability using MSE may add another dimension to the previously identified neural dynamics of development and may provide useful biomarkers for typically and abnormally developing brains.

AUTHOR CONTRIBUTIONS

YY, YM, and MK designed the study. CH, YY, and HK recruited the participants. CH, YY, TI, and DS performed the experiments. CH, SN, and TT analyzed the results and wrote the manuscript. All authors participated in revising the manuscript and approved the final draft of the manuscript.

FUNDING

This work was supported by JSPS KAKENHI Grant Number JP15K19717 to CH and JP16K10206 to TT and was partially supported by the Center of Innovation Program from the Japan Science and Technology Agency, JST and JST CREST Grant Number JPMJCR17A4, Japan.

ACKNOWLEDGMENTS

We wish to thank the study participants and their families. We also thank Sachiko Kitagawa for technical assistance and Wasin Hawaree from Fukui University of Technology for data analysis.

REFERENCES

Bolton, P. F., Golding, J., Emond, A., and Steer, C. D. (2012). Autism spectrum disorder and autistic traits in the avon longitudinal study of parents and children: precursors and early signs. *J. Am. Acad. Child Adolesc. Psychiatry* 51, 249 e25–260 e25. doi: 10.1016/j.jaac.2011.12.009

Bosl, W., Tierney, A., Tager-Flusberg, H., and Nelson, C. (2011). EEG complexity as a biomarker for autism spectrum disorder risk. *BMC Med.* 9:18. doi: 10.1186/1741-7015-9-18

Cao, M., Huang, H., and He, Y. (2017). Developmental connectomics from infancy through early childhood. *Trends Neurosci.* 40, 494–506. doi: 10.1016/j.tins.2017.06.003

Costa, M., Goldberger, A. L., and Peng, C. K. (2002). Multiscale entropy analysis of complex physiologic time series. *Phys. Rev. Lett.* 89:068102. doi: 10.1103/PhysRevLett.89.068102

Costa, M., Goldberger, A. L., and Peng, C. K. (2005). Multiscale entropy analysis of biological signals. *Phys. Rev. E Stat. Nonlin. Soft Matter Phys.* 71(2 Pt 1):021906. doi: 10.1103/PhysRevE.71.021906

Faisal, A. A., Selen, L. P., and Wolpert, D. M. (2008). Noise in the nervous system. *Nat. Rev. Neurosci.* 9, 292–303. doi: 10.1038/nrn2258

Fries, P. (2015). Rhythms for cognition: communication through coherence. *Neuron* 88, 220–235. doi: 10.1016/j.neuron.2015.09.034

Friston, K. J., Tononi, G., Sporns, O., and Edelman, G. M. (1995). Characterising the complexity of neuronal interactions. *Hum. Brain Mapp.* 3, 302–314. doi: 10.1002/hbm.460030405

Garrett, D. D., Samanez-Larkin, G. R., MacDonald, S. W., Lindenberger, U., McIntosh, A. R., and Grady, C. L. (2013). Moment-to-moment brain signal variability: a next frontier in human brain mapping? *Neurosci. Biobehav. Rev.* 37, 610–624. doi: 10.1016/j.neubiorev.2013.02.015

Giedd, J. N., Blumenthal, J., Jeffries, N. O., Castellanos, F. X., Liu, H., Zijdenbos, A., et al. (1999). Brain development during childhood and adolescence: a longitudinal MRI study. *Nat. Neurosci.* 2, 861–863. doi: 10.1038/13158

Grandy, T. H., Garrett, D. D., Schmiedek, F., and Werkle-Bergner, M. (2016). On the estimation of brain signal entropy from sparse neuroimaging data. *Sci. Rep.* 6:23073. doi: 10.1038/srep23073

Kikuchi, M., Shitamichi, K., Yoshimura, Y., Ueno, S., Remijn, G. B., Hirosawa, T., et al. (2011). Lateralized theta wave connectivity and language performance in 2- to 5-year-old children. *J. Neurosci.* 31, 14984–14988. doi: 10.1523/JNEUROSCI.2785-11.2011

Landa, R. J., Gross, A. L., Stuart, E. A., and Bauman, M. (2012). Latent class analysis of early developmental trajectory in baby siblings of children with autism. *J. Child Psychol. Psychiatry* 53, 986–996. doi: 10.1111/j.1469-7610.2012.02558.x

Lemcke, S., Juul, S., Parner, E. T., Lauritsen, M. B., and Thorsen, P. (2013). Early signs of autism in toddlers: a follow-up study in the danish national birth cohort. *J. Autism. Dev. Disord.* 43, 2366–2375. doi: 10.1007/s10803-013-1785-z

Lippe, S., Kovacevic, N., and McIntosh, A. R. (2009). Differential maturation of brain signal complexity in the human auditory and visual system. *Front. Hum. Neurosci.* 3:48. doi: 10.3389/neuro.09.048.2009

McIntosh, A. R., Kovacevic, N., and Itier, R. J. (2008). Increased brain signal variability accompanies lower behavioral variability in development. *PLoS Comput. Biol.* 4:e1000106. doi: 10.1371/journal.pcbi.1000106

Misic, B., Mills, T., Taylor, M. J., and McIntosh, A. R. (2010). Brain noise is task dependent and region specific. *J. Neurophysiol.* 104, 2667–2676. doi: 10.1152/jn.00648.2010

Polizzotto, N., Takahashi, T., Walker, C., and Cho, R. (2015). Wide range multiscale entropy changes through development. *Entropy* 18:12. doi: 10.3390/e18010012

Pujol, J., Soriano-Mas, C., Ortiz, H., Sebastián-Gallés, N., Losilla, J. M., and Deus, J. (2006). Myelination of language-related areas in the developing brain. *Neurology* 66, 339–343. doi: 10.1212/01.wnl.0000201049.66073.8d

Richman, J. S., and Moorman, J. R. (2000). Physiological time-series analysis using approximate entropy and sample entropy. *Am. J. Physiol. Heart Circ. Physiol.* 278, H2039–H2049. doi: 10.1152/ajpheart.2000.278.6.H2039

Shaw, P., Kabani, N. J., Lerch, J. P., Eckstrand, K., Lenroot, R., Gogtay, N., et al. (2008). Neurodevelopmental trajectories of the human cerebral cortex. *J. Neurosci.* 28, 3586–3594. doi: 10.1523/JNEUROSCI.5309-07.2008

Sowell, E. R., Thompson, P. M., Leonard, C. M., Welcome, S. E., Kan, E., and Toga, A. W. (2004). Longitudinal mapping of cortical thickness and brain growth in normal children. *J. Neurosci.* 24, 8223–8231. doi: 10.1523/jneurosci.1798-04.2004

Stam, C. J. (2005). Nonlinear dynamical analysis of EEG and MEG: review of an emerging field. *Clin. Neurophysiol.* 116, 2266–2301. doi: 10.1016/j.clinph.2005.06.011

Takahashi, T. (2013). Complexity of spontaneous brain activity in mental disorders. *Prog. Neuropsychopharmacol. Biol. Psychiatry* 45, 258–266. doi: 10.1016/j.pnpbp.2012.05.001

Takahashi, T., Yoshimura, Y., Hiraishi, H., Hasegawa, C., Munesue, T., Higashida, H., et al. (2016). Enhanced brain signal variability in children with autism spectrum disorder during early childhood. *Hum. Brain Mapp.* 37, 1038–1050. doi: 10.1002/hbm.23089

Uhlhaas, P. J., Roux, F., Singer, W., Haenschel, C., Sireteanu, R., and Rodriguez, E. (2009). The development of neural synchrony reflects late maturation and restructuring of functional networks in humans. *Proc. Natl. Acad. Sci. U.S.A.* 106, 9866–9871. doi: 10.1073/pnas.0900390106

Vakorin, V. A., and McIntosh, A. R. (2012). "Mapping the multi-scale information content of complex brain signals," in *Principles of Brain Dynamics: Global State Interactions*, eds M. Rabinovich, K. Friston, and P. Varona (Cambridge, MA: The MIT Press), 183–208.

Wang, X. J. (2010). Neurophysiological and computational principles of cortical rhythms in cognition. *Physiol. Rev.* 90, 1195–1268. doi: 10.1152/physrev.00035.2008

Yoshimura, Y., Kikuchi, M., Shitamichi, K., Ueno, S., Remijn, G. B., Haruta, Y., et al. (2012). Language performance and auditory evoked fields in 2- to 5-year-old children. *Eur. J. Neurosci.* 35, 644–650. doi: 10.1111/j.1460-9568.2012.07998.x

Conflict of Interest Statement: The authors declare that the research was conducted in the absence of any commercial or financial relationships that could be construed as a potential conflict of interest.

The reviewer C-KP and the handling Editor declared their shared affiliation.

frontiers in Neuroscience

ORIGINAL RESEARCH
published: 20 September 2018
doi: 10.3389/fnins.2018.00645

Do Complexity Measures of Frontal EEG Distinguish Loss of Consciousness in Geriatric Patients Under Anesthesia?

Sarah L. Eagleman[1†], Don A. Vaughn[2,3*†], David R. Drover[1], Caitlin M. Drover[4], Mark S. Cohen[2,5], Nicholas T. Ouellette[6] and M. Bruce MacIver[1]*

[1] Department of Anesthesiology, Perioperative and Pain Medicine, Stanford University, Palo Alto, CA, United States, [2] UCLA Semel Institute for Neuroscience and Human Behavior, Los Angeles, CA, United States, [3] Department of Psychology, University of Santa Clara, Santa Clara, CA, United States, [4] University of Washington, Seattle, WA, United States, [5] UCLA Departments of Psychiatry, Neurology, Radiology, Psychology, Biomedical Physics and Bioengineering, California Nanosystems Institute, Los Angeles, CA, United States, [6] Department of Civil and Environmental Engineering, Stanford University, Stanford, CA, United States

OPEN ACCESS

Edited by:
Kay Jann, University of Southern California, United States

Reviewed by:
Keiichiro Nishida, Kansai Medical University, Japan
Thomas Koenig, Universität Bern, Switzerland

***Correspondence:**
Sarah L. Eagleman
seagle@stanford.edu
Don A. Vaughn
donaldavaughn@gmail.com

[†] These authors have contributed equally to this work

Specialty section:
This article was submitted to Brain Imaging Methods, a section of the journal Frontiers in Neuroscience

Received: *10 June 2018*
Accepted: *29 August 2018*
Published: *20 September 2018*

Citation:
Eagleman SL, Vaughn DA, Drover DR, Drover CM, Cohen MS, Ouellette NT and MacIver MB (2018) Do Complexity Measures of Frontal EEG Distinguish Loss of Consciousness in Geriatric Patients Under Anesthesia? Front. Neurosci. 12:645. doi: 10.3389/fnins.2018.00645

While geriatric patients have a high likelihood of requiring anesthesia, they carry an increased risk for adverse cognitive outcomes from its use. Previous work suggests this could be mitigated by better intraoperative monitoring using indexes defined by several processed electroencephalogram (EEG) measures. Unfortunately, inconsistencies between patients and anesthetic agents in current analysis techniques have limited the adoption of EEG as standard of care. In attempts to identify new analyses that discriminate clinically-relevant anesthesia timepoints, we tested 1/*f* frequency scaling as well as measures of complexity from nonlinear dynamics. Specifically, we tested whether analyses that characterize time-delayed embeddings, correlation dimension (CD), phase-space geometric analysis, and multiscale entropy (MSE) capture loss-of-consciousness changes in EEG activity. We performed these analyses on EEG activity collected from a traditionally hard-to-monitor patient population: geriatric patients on beta-adrenergic blockade who were anesthetized using a combination of fentanyl and propofol. We compared these analyses to traditional frequency-derived measures to test how well they discriminated EEG states before and after loss of response to verbal stimuli. We found spectral changes similar to those reported previously during loss of response. We also found significant changes in 1/*f* frequency scaling. Additionally, we found that our phase-space geometric characterization of time-delayed embeddings showed significant differences before and after loss of response, as did measures of MSE. Our results suggest that our new spectral and complexity measures are capable of capturing subtle differences in EEG activity with anesthesia administration—differences which future work may reveal to improve geriatric patient monitoring.

Keywords: anesthesia, geriatric, electrophysiology (EEG), propofol, fentanyl, nonlinear dynamics, multiscale entropy, 1/*f*

INTRODUCTION

About 50% of geriatric patients aged 65 and older will require anesthesia for a surgical procedure at some time in their remaining years (Kim et al., 2015). It has been suggested that geriatric patients have an increased risk of dementia, delirium, and neurocognitive dysfunction after exposure to anesthetic agents (Avidan and Evers, 2011; Chen et al., 2013; Strøm et al., 2014; Purdon et al., 2015a; Yang and Fuh, 2015). Given this potential risk, several investigators have suggested that geriatric patients may benefit from maintenance at lighter anesthetic levels (Lindholm et al., 2009; Kalkman et al., 2011; Strøm et al., 2014; Petsiti et al., 2015), which may reduce the risks of developing dementia (Chen et al., 2014). However, a downside of light anesthesia is the possibility that a patient may not be unconscious during the procedure. It is estimated that 1–2 out of every 1000 patients undergoing general anesthesia for surgery are insufficiently anesthetized, and yet are immobilized and unable to respond (Bischoff and Rundshagen, 2011). There would be tremendous advantage in the ability to titrate an anesthetic dose accurately to balance an improved medical outcome against the risk of intraoperative awareness.

Electroencephalogram (EEG) signals, especially from the frontal cortex, exhibit stereotypical responses to some anesthetics. For example, loss of consciousness (LOC) correlates with a transition from low amplitude, high frequency EEG waveforms to high amplitude, low frequency patterns, resembling the transition to sleep. In anesthesia, low frequency delta (∼1–4 Hz) rhythms are replaced gradually by burst suppression patterns as patients transition to deeper surgical planes of anesthesia (Pilge et al., 2014). Since the 1990s, several monitoring devices have been developed to capitalize on these EEG frequency domain transitions (Fahy and Chau, 2018). Unfortunately, the resultant measures are inconsistent as EEG changes depend on the anesthesia and the patient (Akeju et al., 2015; Purdon et al., 2015a,b).

In particular, geriatric patients pose a unique challenge for electrophysiological monitoring because brain activity (as measured with EEG) attenuates with advancing age (Akeju et al., 2015; Purdon et al., 2015b; Lee et al., 2017). This makes it difficult to quantify the frequency changes between awake and anesthetized states accurately in individual patients. None of the EEG intraoperative monitoring methods account for the differences that exist in the geriatric population. In addition, geriatric surgical patients are often medicated with beta-adrenergic blockers (beta-blockers). Beta-blockers may hide the cardiovascular signs of inadequate anesthesia (tachycardia and hypertension) (Ghosh et al., 2008), and geriatric patients treated with beta-blockers may require less anesthesia (Zaugg et al., 2003; Ghosh et al., 2008). Importantly, beta-blockers themselves can cause changes in the EEG activity, and thus are likely to cause problems with anesthetic depth monitoring (Johansen, 2001; Zaugg et al., 2003; Ghosh et al., 2008). The result is that EEG monitoring has not been adopted as standard of care. The development of efficacious, anesthetic- and patient-invariant EEG processing techniques could mitigate this and provide a better way to monitor patients and improve outcomes. Thus, in the current study, we analyzed EEG data collected from geriatric patients who received beta-blockers for at least 24 h prior to surgery, and who were subsequently anesthetized with fentanyl and propofol.

Fentanyl and propofol are used in combination routinely to obtain balanced anesthesia for induction during surgical procedures. Fentanyl is a potent opioid that decreases the intensity of response to intubation and provides general pain relief during surgical procedures. Administration of fentanyl correlates with a shift in the EEG pattern from high frequency, low amplitude to low frequency, high amplitude (Scott et al., 1985). Propofol has been shown to increase frontal EEG activity in the alpha (8–14 Hz) and slow (0.1–1 Hz) bands after LOC (Gugino et al., 2001; Feshchenko et al., 2004; Purdon et al., 2013; Akeju et al., 2014). This change in activity occurs in both young and elderly patients (Purdon et al., 2015a); however, the reduction in amplitude with age causes more subtle differences in spectral characteristics with anesthesia onset, which may not be detected by modern EEG monitoring devices (Purdon et al., 2015b).

A potentially more sensitive spectral measure of anesthetic depth might be $1/f$. Electrophysiological signals demonstrate $1/f$-like frequency scaling (He, 2011): the power declines relative to increases in frequency composition. Importantly, this measure has demonstrated sensitivity to the electrophysiological brain state changes associated with sleep (Bédard et al., 2006). Further, $1/f$ scaling in EEG changes with age (Voytek et al., 2015). To our knowledge, $1/f$ frequency scaling has not been tested on EEG protocols that include anesthesia.

In addition to spectral measurements, previous studies have demonstrated that complexity measures from nonlinear dynamics correlate with anesthetic depth (Watt and Hameroff, 1988; Widman et al., 2000; van den Broek et al., 2006; Walling and Hicks, 2006; MacIver and Bland, 2014; Eagleman et al., 2018). Structural changes in time-delayed embeddings (attractors) of EEG signals have been reported in both rodents (MacIver and Bland, 2014) and humans (Watt and Hameroff, 1988; Widman et al., 2000; Walling and Hicks, 2006; Eagleman et al., 2018). The awake attractors appear in 3D as spheroids, and then flatten to ellipsoids with LOC (Watt and Hameroff, 1988; Walling and Hicks, 2006; MacIver and Bland, 2014; Eagleman et al., 2018). Previous work has quantified these attractor changes using the correlation dimension (CD) (Grassberger and Procaccia, 1983; Widman et al., 2000; Walling and Hicks, 2006) and a phase-space geometric fit called the ellipse radius ratio (ERR), which fits the attractor with an ellipsoid solid of revolution, and then reports the ratio of the lengths of the minimum and maximum symmetry axes (Eagleman et al., 2018). Another complexity measure, multiscale entropy (MSE), has also been reported to correlate well with existing anesthetic depth measures (Li et al., 2010; Liu et al., 2015). In the current study, we tested whether these complexity measures could distinguish between subtle changes in EEG activity occurring before and after LOC.

We performed a retrospective analysis of data collected from geriatric patients (aged 65 and older) who were on beta-adrenergic blockers at least 24 h prior to surgery. Patients were anesthetized with fentanyl and propofol. We identified and analyzed 20 s clips of frontal EEG from before and after loss

of response to verbal commands (LOR, considered here as loss of consciousness). We compared frequency-derived measures, as well as complexity measures, of the EEG signal in the before-and-after clips to identify measures that discriminated between the two states.

MATERIALS AND METHODS

Study Protocol

All procedures took place under an approved protocol from the Stanford School of Medicine Administrative Panel on Human Subjects in Medical Research (ClinicalTrials.gov, NCT00938782). The database consisted of 67 surgical patients all older than 65 years of age. Patients underwent anesthesia for non-cardiac procedures classified as status 1–3 by the American Society of Anesthesiologists. All patients in the original study were receiving beta-adrenergic treatment for a minimum of 24 h preoperatively and received their medication prior to surgery. We reviewed the database retrospectively and analyzed data under a separate Stanford-approved IRB. Out of the 67 patients, 28 patients were used for analysis (details of selection below). These 28 patients had an average age of 76 ($\pm$ 6) years and included 18 males and 10 females. They had an average body mass index (BMI) of 27.3 ($\pm$ 4.7). The healthy BMI range for patients aged 65 and older has been suggested as 23 to 30 (Porter Starr and Bales, 2015). Our analysis included 8 patients with a BMI greater than 30 and 5 patients with a BMI less than 23.

The surgical procedures and anesthetic administration have been described in detail previously (Drover et al., 2011). Briefly, patients were induced with fentanyl (1–3 mcg/kg), propofol (1–2 mg/kg), and muscle relaxant (if required) using either rocuronium (0–1 mg/kg) or vecuronium (0.1 mg/kg). After intubation, sevoflurane in oxygen with 50–60% nitrous oxide was initiated and used to maintain anesthesia. Medical staff recorded significant clinical events including induction, anesthetic administration and dosage, LOR to verbal commands, and time.

The average time of fentanyl use prior to LOR was 2.1 $\pm$ 1.6 min. With propofol, the average before LOR was 1.0 $\pm$ 0.6 min. A total of 6 patients received muscle relaxant before LOR. One patient received vecuronium 0.7 min before LOR, and 5 patients received rocuronium an average of 5.2 min before LOR. A total of 14 patients received muscle relaxant within a 4 min window following LOR. Three patients received vecuronium and 11 received rocuronium, both an average of 0.8 min following LOR. In addition, 18 patients were started on sevoflurane in oxygen with 50–60% nitrous oxide an average of 1.7 min following LOR.

EEG Recording and Preprocessing

Electroencephalogram recordings were acquired using a SedLine Legacy EEG monitor (Masimo, Irvine, CA, United States). The manufacturer's standard adhesive electrode was attached to the patient prior to starting the anesthetic, as per the manufacturer's instructions. EEGs were recorded at approximately F7 grounded to Fpz and referenced to ∼1 cm above Fpz (**Figure 1A**). Data was digitized at 250 Hz. Records of the surgical events including time stamps of start of induction, LOR to verbal stimuli, and administration and dosages were de-identified and then used for analysis. The EEG recordings were de-trended, and notch filtered using a second-order Butterworth Infinite Impulse Response (IIR) filter to remove 60 and 120 Hz noise prior to analysis. Additionally, a second-order Butterworth IIR filter was used to remove a 78.125 Hz impedance measurement pulse generated by the EEG monitor system.

We identified each subject's 20 s pre-LOR and post-LOR EEG clip via a two-step algorithm which was a mix of exclusion and inclusion criteria (**Figure 1A**). First, three of the authors (SLE, DRD, and MBM) visually inspected the EEG traces, spectrums, processed spectrograms to identify EEG periods containing burst suppression or artifacts (exclusion criteria). Second, given the fundamentally imprecise metric of LOR, from these remaining clips we used the clips most temporally-distant from the LOR timepoint (within a 2 min window) to obtain the clips most representative of pre-LOR and post-LOR (inclusion criteria). From the original 67 patients, 28 were selected who had LOR timestamps and artifact and noise free EEG clips for at least 20 continuous seconds before and after LOR.

Spectral Analyses

To visualize the spectral changes that occurred in our clips before and after LOR, we performed multitaper spectral analysis on the 20 s clips during pre and post LOR period using the MATLAB Chronux toolbox (**Figure 1B**; Mitra and Bokil, 2008).[1] Specifically, we used a time-bandwidth product of 5 with 9 tapers, limited the frequency ranges calculated to 0 to 50 Hz, and computed the theoretical error range at the 95% confidence interval. Power values were expressed in decibels.

To give an example of the temporal profile of the spectral changes that occurred during the windows surrounding the LOR transitions, we computed a normalized spectrogram (**Figure 1C**). We calculated the Fourier transform using Hann windows with half window overlaps. We then cutoff the frequencies above 50 Hz, converted the magnitude to decibels (dB), and scaled the spectrogram output by its maximum magnitude.

We calculated the spectral edge frequency (i.e., the frequency bounding 95% of the power from above) and total power using multitaper spectral analysis (Mitra and Bokil, 2008) without limiting the frequency range to below 50 Hz. We calculated the percentage of total power for individual frequency bands per condition. The percentage of total power was used because of prior reports of significant changes in total power with exposure to anesthetics. The ranges we used for the frequency bands were as follows: delta: 0.1 to 4 Hz; theta: 4 to 8 Hz; alpha: 8 to 14 Hz; beta: 14 to 30 Hz; and gamma: above 30 Hz (Gugino et al., 2001; Purdon et al., 2013). To test whether we observed similar changes in before and after clips compared to other studies, we calculated the slow frequency component (0.1–1 Hz) separately.

To determine whether $1/f$ characteristics change before and after LOR, we fit each patient's spectral power to c/f^{α}, where α and

[1] http://chronux.org/

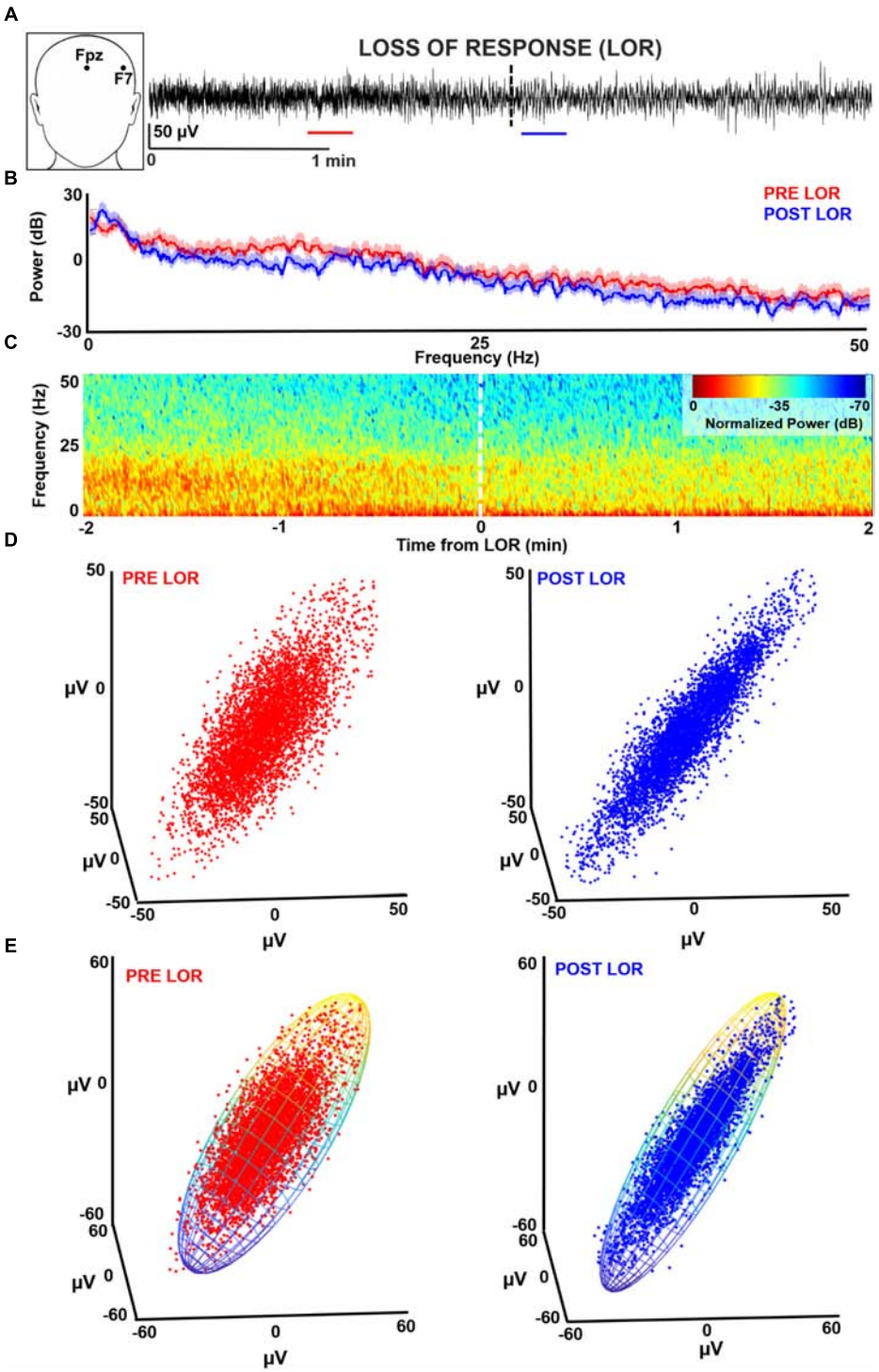

FIGURE 1 | Characterizing loss of response (LOR) using electroencephalogram (EEG) analysis. **(A)** EEGs were recorded from F7 during induction with propofol and fentanyl anesthesia in geriatric patients receiving beta-adrenergic blockade. We selected continuous artifact-free 20 s clips from before (red) and after (blue) patients lost response to verbal commands. **(B)** We analyzed these clips using multitaper spectral analysis. In this patient (PT09) an increase in lower frequencies and a decrease in higher frequencies from before to after LOR can be observed. **(C)** To view the dynamics of the spectral changes through time we plotted a normalized spectrogram starting 2 min before LOR to 2 min after LOR. We can see the increase in lower frequencies and decrease in higher frequencies coordinates well with the LOR timestamp. **(D)** We tested several complexity measures of time-delayed embeddings (attractors). An awake attractor (red) looks less ellipsoidal than the anesthetized attractor (blue). **(E)** One method we used to quantify change in attractors before and after LOR is by fitting the attractor with an ellipsoid solid of revolution. We then calculate the ratio of the minimum and maximum radii.

c were free parameters representing the quickness of frequency decay and an arbitrary constant, respectively. We determined α and *c* for each patient by minimizing the L_2 norm of the residuals between predicted and actual values.

Multiscale Entropy

As complex signals often have meaningful relationships at multiple timescales, we used MSE to characterize the relationship and complexity of the EEG time series. MSE utilizes an algorithm that calculates a traditional entropy metric at several timescales (Costa et al., 2002). In this case, we used sample entropy as our multiscale metric (Pincus, 1991) as it has been shown to extract meaningful complexity differences in a variety of physiological signals (Costa et al., 2003; Bian et al., 2009; Liu et al., 2013). We calculated MSE using custom MATLAB (The MathWorks, Inc.) scripts.

Characterization of Dynamical Attractors

Correlation Dimension

We constructed three-dimensional time-delayed embeddings (attractors) of the EEG signal before and after LOR using an 8 ms delay (**Figure 1D**) as previously described (Watt and Hameroff, 1988; Walling and Hicks, 2006; MacIver and Bland, 2014; Eagleman et al., 2018). We chose this delay as we observed shape changes in attractors when plotted at this timescale. We tested whether the CD captured this shape change with LOR. CD is used to determine the non-integer (fractal) dimensionality of irregular objects (e.g., a point cloud in our case) as described previously (Grassberger and Procaccia, 1983; Widman et al., 2000; Walling and Hicks, 2006). We also tested whether significant differences in CD could be observed when we increased the dimensionality of the embeddings from 3D to 5D.

We tested whether the embedding delay of the attractor impacted the estimate of the CD value. To estimate the optimal delay for creating the attractors we calculated the first zero-crossing of the autocorrelations of the pre-LOR and post-LOR signals. This is the first time lag that the EEG signal differs maximally with itself. We used this value to set our maximum range of embedding delays and tested multiple delays between the shortest time window (shifting the EEG by 1 point) to the largest (set by the autocorrelation zero crossing). We tested delays of 4, 8, 12, 52, 100, 500, 1000, 1500, 2000, and 2500 ms. We tested these delays for both 3D and 5D time-delayed embeddings. We tested whether a trend existed between embedding delay and CD using the Spearman correlation.

Ellipse Radius Ratio

We constructed three-dimensional time-delayed embeddings, as described above (**Figure 1D**). We quantified this shape change by fitting the three-dimensional attractor to an ellipsoidal solid of revolution (**Figure 1E**; Khachiyan, 1980; Eagleman et al., 2018). The lengths of the symmetry axes of the ellipsoid were calculated and the ratio of the minimum and maximum axes (which we term the ellipsoid radius ratio, ERR) was used to quantify the shape change. A radius ratio of 1 implies a sphere, while smaller ratios imply more strongly ellipsoidal shapes.

Similar to the CD, we tested also whether the ERR was changed by the embedding delay time. We created time delayed embeddings using the same delays as were used to calculate the CD. We tested whether a trend existed between embedding delay and ERR using the Spearman correlation statistic.

Correlations Between EEG Measures and Effect Size of EEG Measures

To test whether our EEG measures correlated with patient age or body-mass index (BMI), we calculated the Spearman correlation statistic between the change in ERR (LORpost–LORpre) at the shortest delay (4 ms) with corresponding patient ages and BMIs. We did the same for the MSE results.

To test whether our EEG measures correlated with each other or with spectral changes, we calculated the Spearman correlation statistic between the changes in these measures before and after LOR. Specifically, we tested the correlation between changes in ERR and MSE as well as between ERR or MSE and percentage of power change (LORpost–LORpre) in the individual frequency bands that we measured (delta, theta, alpha, beta, and gamma). For the change in ERR, we chose the values calculated at the shortest delay (4 ms) as these showed the most significant changes before and after LOR.

We calculated a paired-data Cohen's D on our EEG measures before and after LOR for the novel spectral ($1/f$) and complexity (MSE and ERR phase space analysis) measures that showed significant differences before and after LOR. We also calculated Cohen's D for the percentage of power in each of the frequency bands (delta, theta, alpha, beta, and gamma) for comparison.

Statistics

We corrected significance values for multiple univariate statistical comparisons within a particular analysis type, by using the Holm-Bonferroni method—a sequentially-rejective procedure (Holm, 1979). Specifically, we corrected p values for pre vs post metrics within each of the following analyses: (1) the power percentage across all 5 frequency bands (delta, theta, alpha, beta, gamma), (2) the CD across all 10 embedding delays, (3) the ERR across all 10 embedding delays, and (4) the correlation of MSE, ERR, and frequency band power. We report our results as medians (25, 75 percentiles), and significance values (p) are calculated from Wilcoxon Signed Rank Tests.

RESULTS

Spectral Analyses

We performed multitaper spectral analysis to quantify the changes that occur before and after LOR (**Figure 2A**). To compare our measures to previous reports, we computed a common spectral measure that correlates with anesthetic depth: the spectral edge frequency. We also tested whether total power differed from before and after LOR. We did not observe a significant change in spectral edge frequency before and after LOR (**Figure 2B**, pre-LOR 14.1 Hz [9.6, 19.4], post-LOR 13.0 Hz

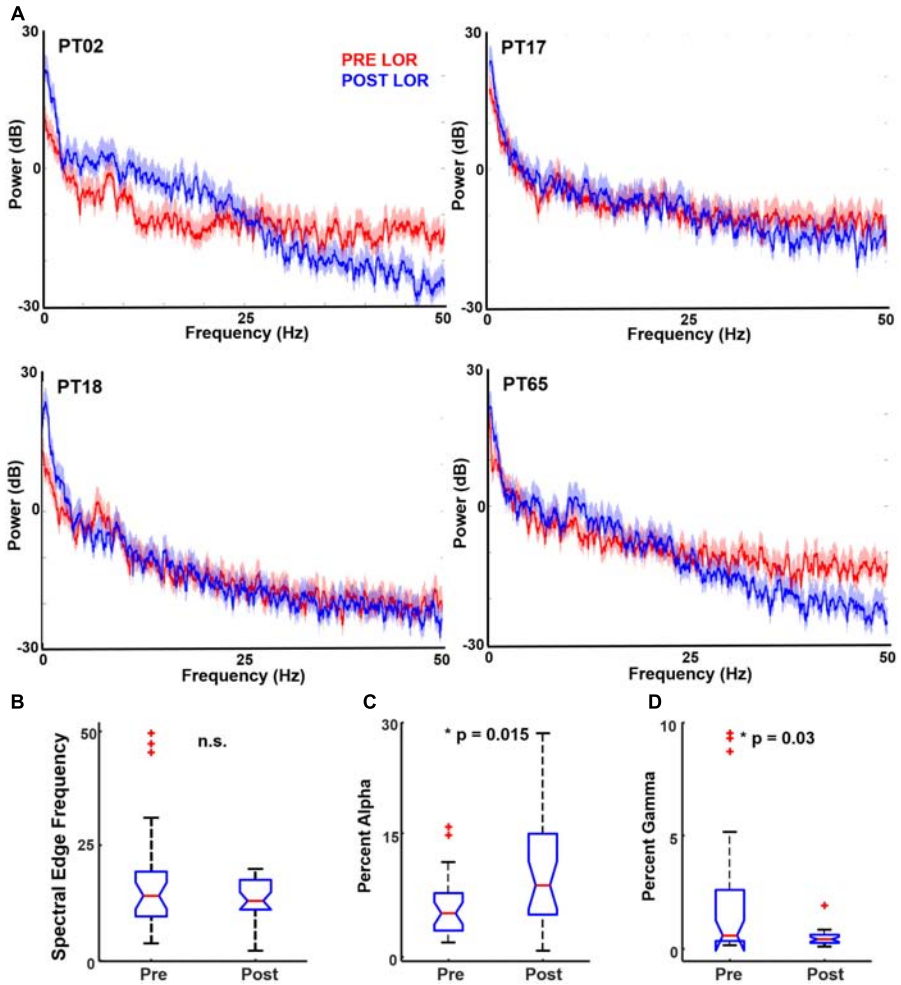

FIGURE 2 | Spectral characteristics before and after loss of response (LOR). **(A)** Example of multitaper spectrum from four patients pre- (red) and post- (blue) LOR. Note the increases in alpha and decrease in gamma activity following LOR. The shaded region represents the 95% confidence interval. We computed several standard spectral measures pre- and post-LOR. **(B)** Spectral edge frequency has been shown to correlate with anesthetic depth; however, we did not observe a significant difference. **(C)** We observed a significant increase in alpha activity after LOR (p = 0.015 corrected). **(D)** We observed a significant decrease in gamma activity after LOR (p = 0.03 corrected).

[11.1, 17.6], $p = 0.64$). We did not observe a significant difference in total power before and after LOR (pre-LOR 35.2 dB [33.0, 36.2], post-LOR 34.6 dB [32.8, 36.3], $p = 0.21$).

To determine the changes in frequency bands, we calculated the changes in delta (0.1–4 Hz), theta (4–8 Hz), alpha (8–14 Hz), beta (14–30 Hz), and gamma (above 30 Hz) ranges. Significant differences were found for alpha (**Figure 2C**) and gamma (**Figure 2D**), and all spectral results are summarized in **Table 1**. Similar to previous reports, we observed a significant increase in alpha from before to after LOR. In addition, we observed a significant decrease in gamma power from before to after LOR. In a separate analysis, we separated out the slow (0.1–1 Hz) frequency component from the EEG signal to see if the percentage of slow activity changed before to after LOR. We did not observe a significant difference in this frequency band (pre-LOR 48.6% [37.6, 62.9], post-LOR 54.3% [34.0, 64.4], $p = 0.57$).

To determine whether $1/f$ characteristics change before and after LOR, we fit each patient's spectral power to c/f^{α} (**Figure 3A**). Overall, 71% of the patients showed an increase in the value of α from pre-LOR to post-LOR (**Figure 3B**). This difference in α before and after LOR differed significantly from the null hypothesis of no change (median change = 0.17, $p < 10^{-3}$, **Figure 3C**).

Characterization of Dynamical Attractors

We began by testing whether significant differences could be observed in CD between 3D attractors plotted at an 8 ms embedding delay. We observed a similar flattening of the attractor and more ellipsoidal shapes after LOR (**Figure 4A**). We quantified the pre- to post-LOR changes in 3D attractors using CD. We did not observe a significant difference using this measure (**Figure 4B**). We also calculated the CD for 5 dimensional attractors. Here again we did

TABLE 1 | Summary of spectral changes from before and after loss of response (LOR).

Frequency band	Percentage of power PRE LOR	Percentage of power POST LOR	Significance value, corrected
Delta (0.1–4 Hz)	76.3% [66.5, 83.7]	74.1% [60.1, 82.8]	0.22
Theta (4–8 Hz)	4.8% [3.2, 7.1]	6.4% [4.3, 9.4]	0.34
Alpha (8–14 Hz)	5.3% [3.2, 7.7]	8.7% [5.1, 15.0]	0.015*
Beta (14–30 Hz)	3.8% [2.2, 5.3]	3.9% [2.8, 8.9]	0.26
Gamma (>30 Hz)	0.6% [0.4, 2.6]	0.4% [0.3, 0.6]	0.03*

*Percentage of power in individual frequency bands are reported as medians [25, 75 percentiles]. Significance values reported are from Wilcoxon signed rank tests, corrected for multiple comparisons. The * indicates the percentage of power change was significant at $p < 0.05$ corrected.*

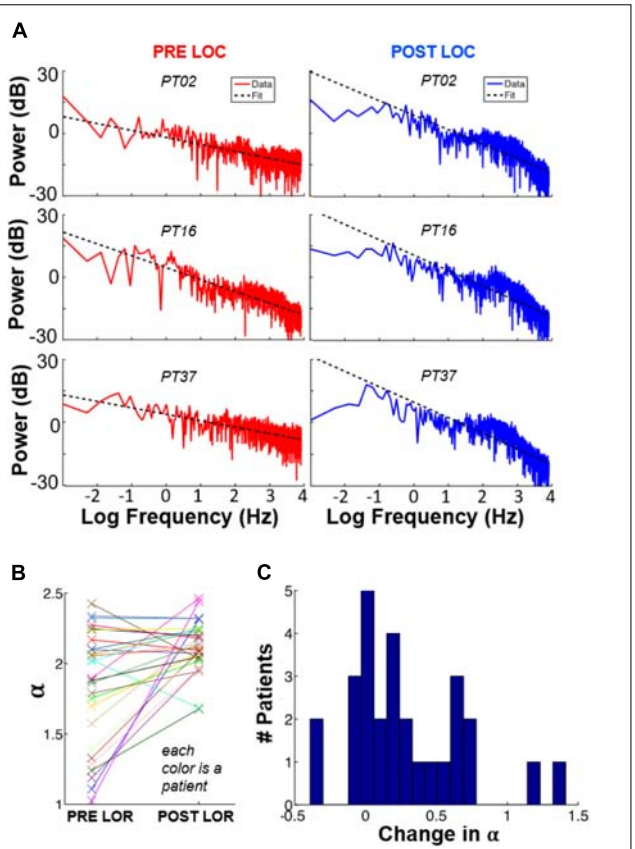

FIGURE 3 | 1/*f* spectral changes occur with loss of response. We fit each patient's spectral power to c/f^{α}, where α and *c* were free parameters representing the quickness of frequency decay and an arbitrary constant, respectively. Panel **(A)** shows these plots for three patients, before and after LOC. **(B)** Values of α for each subject, pre-LOR and post-LOR. **(C)** Overall, we observed that 71% of the patients show an increase in α after LOR.

not observe a significant difference pre- and post-LOR (**Figure 4C**).

We then tested our ERR with the 8 ms attractors before and after LOR. We found a significant difference between pre- and post-LOR (**Figure 4D**, $p = 0.04$ corrected).

To test the impact of the embedding delay on the attractor calculations we chose multiple embeddings delays between the smallest possible delay (4 ms, shifting the EEG by 1 point) and the largest (set by the first zero-crossing of the autocorrelation). We calculated the first zero-crossing for both the pre- and post-LOR period to see if there was a difference. We did not find a significant difference between the pre- and post-LOR values (pre-LOR 1800 ms [1392, 2856], post-LOR 2176 ms [1664, 2480], $p = 0.35$ corrected). Given these results, we decided to calculate CD using the following embedding delays: 4, 8, 12, 52, 100, 500, 1000, 1500, 2000, and 2500 ms. The impact of embedding delay on attractor shape is shown in **Figure 5A**. We did not observe a significant difference at any delay for 3D or 5D CD calculations, nor did we observe a significant correlation between CD and embedding delay (**Figure 5B**).

We performed the same test of different embedding delays with our ERR analysis. The ERR showed a significant positive relationship with the difference in post-LOR–pre-LOR conditions (**Figure 5C**, $p = 0.04$, Spearman correlation). This relationship likely was driven by a reduction in the ERR between the pre- and post-LOR states at short embedding delays: only embedding delays of only 4 and 8 ms showed a significant difference ($p_4 = 0.017$ corrected, $p_8 = 0.04$ corrected).

Multiscale Entropy

A MSE analysis between the pre-LOR and post-LOR conditions revealed a scale-dependent change in sample entropy (**Figure 6A**). Complexity decreased at short scale factors, showing a statistically significant trend toward increasing at medium scale factors ($r_{spearman} = 0.45$, $p < 10^{-3}$ percentile permutation test). The difference in sample entropy between post and pre conditions then showed a decreasing relationship with a further increase in scale factor ($r_{spearman} = -0.31$, $p < 10^{-3}$ percentile permutation test). The initial decrease in complexity at a scale factor of 1, which was not significantly different by median ($p = 0.48$), likely resulted from sharp decreases in MSE among several of the participants (**Figure 6B**).

Correlations Between EEG Measures and Effect Size of EEG Measures

Spearman correlation revealed no significant relationship in our ERR or MSE changes before and after LOR and with patient age or BMI (**Table 2**). Spearman correlation between our ERR (calculated at the shortest delay, 4 ms) and MSE changes before and after LOR revealed that they are correlated with each other (**Table 3**, $r = 0.54$, $p = 0.0034$ corrected). Additionally, a significant correlation between ERR change and change in percentage of gamma activity before and after LOR was observed ($r = 0.67$, $p = 0.00012$ corrected). Significant correlations are also observed between changes in MSE and changes in delta ($r = -0.60$, $p = 0.00084$ corrected), alpha ($r = 0.57$, $p = 0.0019$ corrected), beta ($r = 0.74$, $p = 10^{-5}$ corrected) and gamma power ($r = 0.64$, $p = 0.00034$ corrected). A summary of all of the measured values before and after LOR can be found in **Table 3**.

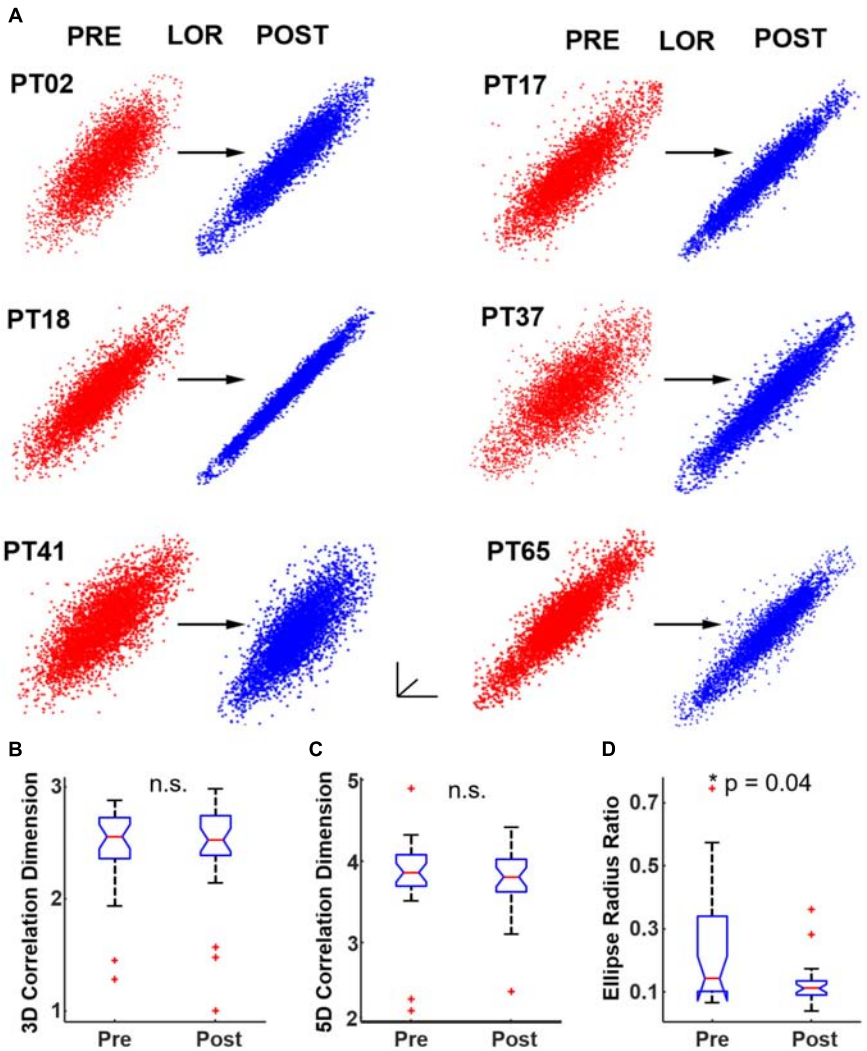

FIGURE 4 | Quantifying dynamical attractors before and after loss of response (LOR). **(A)** We created time-delayed embeddings (attractors) from 20 s continuous clips. A shape change from thicker, less-ellipsoidal attractors before LOR (red) to flatter, more ellipsoidal attractors after LOR (blue) was observed and is shown here for 6 patients. We quantified the difference in attractors using both correlation dimension and our ellipse radius ratio (ERR). **(B)** We did not observe a significant difference in correlation dimension in 3 dimensions, nor did we observe a significant difference in correlation dimension in 5 dimensions **(C)**. **(D)** We did observe a significant difference in our ERR measure from before to after LOR ($p = 0.04$ corrected). The * indicates significant difference between pre-LOR and post-LOR measures at $p < 0.05$ corrected.

Cohen's D values revealed medium effect sizes for both complexity measures: sample entropy and ERR (**Table 4**, $D_{MSE} = -0.55$, $D_{ERR} = -0.69$). Cohen's D values were also sizeable for percentage of power differences before and after LOR in alpha and gamma frequency bands (**Table 4**, $D_{1/f} = 0.68$, $D_{Alpha} = 0.61$, $D_{Gamma} = -0.55$). The rest of the frequency bands had small effect sizes (**Table 4**).

DISCUSSION

We found spectral results similar to those reported for propofol anesthesia (Gugino et al., 2001; John et al., 2001; Purdon et al., 2013, 2015a). Specifically, we saw increases in the percentage of alpha activity and decreases in the percentage of gamma activity with LOR. Conversely, we did not observe a significant difference in the percentage of slow (0.1–1 Hz) frequency from before to after LOR, nor did we observe a significant difference in spectral edge frequency before and after LOR. This is likely due to the overall reduced amplitudes of EEG signals in our elderly patients (Purdon et al., 2015b), which reduces the magnitude of the spectral changes. In addition, patients were sedated heavily before they lost consciousness, so EEG changes were subtle. Since we were doing a retrospective data analysis, we were not able to control the initiation of maintenance anesthesia, so some of our patients were on sevoflurane in oxygen with 50–60% nitrous during the post-LOR timepoints. This may have obscured a change in spectral edge frequency as nitrous oxide

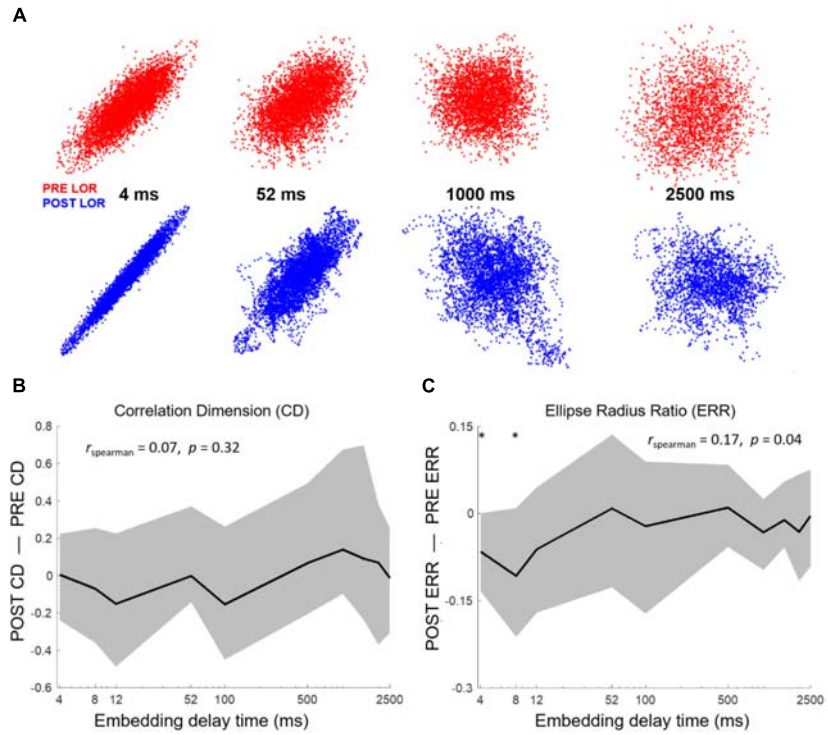

FIGURE 5 | Attractor shape changes are embedding delay dependent. **(A)** Attractors from PT02 shown at 4, 52, 1000, and 2500 ms. The shape change in the attractor is not observed at higher embedding delays. We tested whether our attractor characterization analyses correlated with embedding delay. We computed correlation dimension and ellipse radius ratio (ERR) at 10 different delays from 4 to 2500 ms. **(B)** No significant changes in correlation dimension were observed from before to after LOR for any embedding delay nor was correlation dimension correlated with the embedding delay. Here we show results from the 3D correlation dimension calculation. **(C)** We observed a significant correlation between the ERR and embedding delay ($r_{spearman}$ = 0.17, p = 0.04) and a significant difference in the ERR between pre- and post-LOR for 4 ms and 8 ms delays (p_4 = 0.017 corrected, p_8 = 0.04 corrected). The * indicates a significant difference between the measured values before and after loss of response at that embedding delay at $p < 0.05$ corrected.

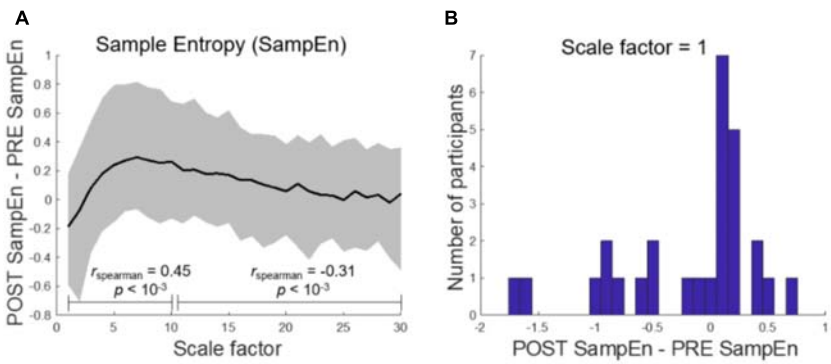

FIGURE 6 | Multiscale entropy reveals scale-dependent complexity change after loss of response. **(A)** Sample Entropy (SampEn) shows a decrease in complexity at short scale factors which monotonically increases until medium scale ($r_{spearman}$ = 0.45, $p < 10^{-3}$) and then decreases toward 0 ($r_{spearman} = -0.31$, $p < 10^{-3}$). Here, the solid black line represents the mean. **(B)** At the shortest scale, the difference in SampEn between post-LOR and pre-LOR conditions is not significantly different from chance as measured by the median, but is when measured by mean (p = 0.04, percentile permutation test).

maintains higher frequencies (Rampil et al., 1998). Sevoflurane, on the other hand, causes similar changes in EEG activity compared to propofol (Akeju et al., 2014; Purdon et al., 2015a). Overall, these nuances between common clinical anesthetics highlight the importance of developing new tools to better distinguish anesthetic states using EEG (Eagleman and Drover, 2018).

One interesting spectral analysis not previously applied to anesthesia EEG is the calculation of the $1/f$ frequency scaling. We chose this measure as it distinguishes different brain states

TABLE 2 | Summary of correlations between observed changes before and after loss of response (LOR) and patient demographics.

Parameter 1	Parameter 2	Spearman's Rho	Significance value, uncorrected
ERR	Age	0.10	0.60
ERR	BMI	0.09	0.66
MSE	Age	−0.28	0.15
MSE	BMI	0.22	0.25

The Spearman correlation between changes in the ellipse radius ratio (ERR, calculated from the shortest delay 4 ms) and multi-scale entropy (MSE) values before and after LOR (post – pre) with age and body-mass index (BMI) of patients used in the analysis is reported here. No correlations were significant.

TABLE 3 | Summary of correlations between measured changes before and after loss of response (LOR).

Parameter 1	Parameter 2	Spearman's Rho	Significance value, uncorrected
ERR	MSE	0.54	0.0034*
ERR	Delta	−0.24	0.22
ERR	Theta	0.12	0.53
ERR	Alpha	0.17	0.38
ERR	Beta	0.29	0.13
ERR	Gamma	0.67	0.00012*
MSE	Delta	−0.60	0.00084*
MSE	Theta	0.51	0.0061
MSE	Alpha	0.57	0.0019*
MSE	Beta	0.74	1.09e–05*
MSE	Gamma	0.64	0.00034*

*The Spearman correlation between changes in the ellipse radius ratio (ERR) and multi-scale entropy (MSE) values before and after LOR (post-pre) is reported here. Additionally, Spearman correlation between these values and the changes in percentage of power in individual frequency bands (delta, theta, alpha, beta, and gamma) before and after LOR (post–pre) are reported as well. The * indicates the correlation between the two parameters was significant at $p < 0.05$ corrected.*

TABLE 4 | Summary of Cohen's D for measured values before and after loss of response (LOR).

EEG measure	Cohen's D
$1/f^{\alpha}$ fit	0.68
SampEn	−0.55
ERR	−0.69
Delta	−0.20
Theta	0.15
Alpha	0.61
Beta	0.34
Gamma	−0.55

We calculated Cohen's D (sign convention: post-pre) to quantify the effect sizes of our EEG measures. We included all measures that showed significant differences before and after LOR, and the standard frequency bands for comparison. ERR value shown here is for the 4 ms delay.

(Bédard et al., 2006) and ages (Voytek et al., 2015). To our knowledge, we have demonstrated the first observation of a change in $1/f$ frequency scaling in EEGs in an anesthesia protocol. $1/f$ frequency scaling was sensitive to before and after LOR.

Previous studies reported differences in CD with anesthetic depth (Widman et al., 2000; Walling and Hicks, 2006), but our study differs in several important aspects. In these earlier studies, patients were anesthetized with sevoflurane to deep levels of anesthesia, but in our study, patients were anesthetized with propofol and fentanyl; further, we limited our analysis to 20 s before and after LOR. Additionally, we used a unique patient population consisting only of geriatric patients with beta-adrenergic blockade. We determined that our CD results were not based on embedding delay or differences between 3 and 5 dimensions.

There are several possibilities as to why we did not find significant differences in CD before and after LOR. For instance, the attractor might be better resolved with higher sampling frequency. Additionally, brain activity might be better represented in an even higher dimensionality embedding. Changes in CD also may not be observable due to age-related changes in complexity (Pierce et al., 2000; Müller and Lindenberger, 2012; Sleimen-Malkoun et al., 2014). The other possibility is that CD might not be sufficiently sensitive to detect the changes that occur during before and after LOR.

We did observe a change in attractor shape similar to what has been previously described (Watt and Hameroff, 1988; Walling and Hicks, 2006; MacIver and Bland, 2014; Eagleman et al., 2018). Additionally, our phase-space analysis based on the geometry of attractors showed significant differences before and after LOR at very short delays (shifting the EEG signal by 1 or 2 points), as previously reported (Eagleman et al., 2018). However, our results demonstrate variability in our population. To determine the source of this variation, better control and measurement of the anesthetics administered in a prospective study is needed. We noticed the magnitude of our results were reduced in the current study compared to our recently published results (Eagleman et al., 2018). This may be due to the current patient population being more sensitive to anesthetics and thus more sedated at our pre-LOR timepoint. We also tested the impact of the embedding delay on our analysis to explore whether changes in EEG signals before and after LOR existed at longer timescales. We found that shorter delays better distinguished before and after LOR and results were no longer significant when the signal was delayed by three points. Visual inspection of the attractor shapes supports this result. Further work is needed to elucidate whether calculations performed in real-time can classify anesthetic depth adequately.

In addition, we tested whether another complexity measure, MSE, could distinguish before- and after-LOR timepoints. We noticed that MSE values appear to converge within a smaller range in the post-LOR period. The distribution suggests that there is one group of patients that show a large decrease in this EEG measure with LOR, while another group does not. The differences between the groups were outside the scope of the current study; however, we plan to examine these differences in the future in a well-controlled prospective study. Additionally, previous reports that showed high correlation of MSE with existing anesthetic depth measures (BIS index and expert anesthesiologist assessment) used EEG data from the entirety of the surgery (induction through recovery), which exposed patients to deeper anesthetic levels than in our study

(Liu et al., 2015). Thus, further testing of this analysis on more clinically relevant timepoints is needed.

Since several EEG measures were applied here to an anesthetic dataset including some that have not been explored much previously (ERR), we calculated the Spearman correlation between the changes in EEG measures before and after LOR. We did this for the shortest delay of ERR, MSE, and the percentage of all the individual frequency bands we included. We found a significant correlation with the ERR and MSE values. This is interesting because it suggests that the ERR change, and thus attractor shape change, may be related to changes in the complexity of the signal (revealed by reduction in MSE with anesthesia onset). Additionally, a significant correlation between ERR and MSE with the percentage of gamma change was observed. These relationships are expected as both reductions in gamma activity and reductions in entropy with anesthetic administration have been previously reported (John et al., 2001; Li et al., 2010). The change in MSE is also correlated with changes in the percentages of delta, alpha, and beta power. This again is expected given the ability of MSE to capture all of the spectral changes observed with anesthesia onset (Li et al., 2010).

We tested the effect size of the EEG measures using Cohen's D. None of these measures had large effect sizes (> 1) indicating the challenge with detecting subtle EEG changes in geriatric patients. ERR and $1/f$ frequency scaling had the largest effect sizes, which were medium in magnitude. This indicates that supplementing complexity measures may improve geriatric patient monitoring. However, further testing of these analyses on more clinically relevant time points and on full EEG traces is needed to test this idea.

As with any study involving EEG, muscle contamination is a potentially important source of artifact. Three of the authors visually inspected all of the EEG clips as well as the processed EEG spectrum and spectrograms to ensure they were free of artifacts. Activity from facial and neck muscles can appear 20 Hz and above, and thus into the frequency ranges we used for analyses (Shackman et al., 2009; Claus et al., 2012; Muthukumaraswamy, 2013); however, as we have reasoned previously (Eagleman et al., 2018), it is important not to throw out higher frequency activity, as it plays an important role in brain-state dynamics (Muthukumaraswamy, 2013), especially in judging anesthetic depth (Sleigh et al., 2001). The measures that we have used have been tested in similar experimental paradigms on intracranial recordings free from EMG contamination (Bédard et al., 2006; MacIver and Bland, 2014; Voytek et al., 2015).

Since these results are only from retrospective analyses our work is limited in several ways. We were not able to control the timing of drug delivery (such as delivery of muscle relaxants); several anesthesiologists with potentially diverse clinical practices were involved, and consciousness measures were restricted to the first loss of response to verbal commands. However, all participating anesthesiologists were instructed to administer anesthesia and a small number of adjuvant agents as per strict protocol guidelines (Drover et al., 2011). Additionally, the protocol of anesthetic and adjuvant agent administration in this retrospective dataset is aligned with current clinical practice. Thus, our results are relevant to current practices of balanced anesthesia administration. Additionally, we tested whether any of our measured results were correlated with patient age or BMI and found no significant correlations. Future prospective work will include several measures to better titrate our analysis to anesthetic action. Collection of blood samples or exhaled vapor can help us correlate results with anesthetic delivery more accurately. Whenever possible, future work should control the delivery of muscle relaxants and the initiation of maintenance anesthetics to separate out the effects of individual anesthetic and adjuvant agents on our measures. Additionally, our results need to be tested on more clinically relevant timepoints, and alongside spectral measures on full EEG traces instead of clips, to better prepare our analyses for clinical application.

Nonetheless, we have observed significant differences before and after LOR using several techniques in a traditionally hard-to-monitor patient group. Future work will discern if these results are useful supplemental tools to better guide physicians in monitoring anesthetic depth in sensitive patient populations. Development of better EEG analysis techniques will hopefully encourage the wide adoption of EEG monitoring and improve the standard of care.

CONCLUSION

We found that frontal spectral changes before and after LOR in geriatric patients were limited to the alpha and gamma ranges. Further, we showed that $1/f$ frequency scaling differed before and after LOR. We tested the ability of several measures from nonlinear dynamics, including CD, MSE, and a geometric characterization of time-delayed embeddings, to distinguish LOR timepoints. Among these, MSE and the geometric characterization showed significant differences and had comparable or greater effect sizes to standard frequency measures. In the future, these results may enable the development of better methods of quantifying anesthetic depth in geriatric patients as they are able to significantly discriminate between the subtle EEG changes that occur before and after loss of response.

AUTHOR CONTRIBUTIONS

MM, DD, and SE conceived the study. DD acquired the data. SE, DD, and CD organized anesthesia records for analysis. SE and DV analyzed the data. MM, NO, and MC supervised the data analysis. SE and DV wrote the manuscript. All authors contributed to the intellectual content with rounds of review and approved the final version of the manuscript for publication.

FUNDING

This work was supported by a seed grant from the Department of Anesthesiology, Perioperative and Pain Medicine at Stanford University (SE, CD, DD, NO, and MM), the Anesthesia Training Grant in Biomedical Research (NIH T32 GM 089626-09, SE), and by the UCLA QCBio Collaboratory Postdoctoral Fellowship directed by Matteo Pellegrini (DV and MC).

REFERENCES

Akeju, O., Pavone, K. J., Thum, J. A., Firth, P. G., Westover, M. B., Puglia, M., et al. (2015). Age-dependency of sevoflurane-induced electroencephalogram dynamics in children. *Br. J. Anaesth.* 115(Suppl. 1), i66–i76. doi: 10.1093/bja/aev114

Akeju, O., Westover, M. B., Pavone, K. J., Sampson, A. L., Hartnack, K. E., Brown, E. N., et al. (2014). Effects of sevoflurane and propofol on frontal electroencephalogram power and coherence. *Anesthesiology* 121, 990–998. doi: 10.1097/ALN.0000000000000436

Avidan, M. S., and Evers, A. S. (2011). Review of clinical evidence for persistent cognitive decline or incident dementia attributable to surgery or general anesthesia. *J. Alzheimers Dis.* 24, 201–216. doi: 10.3233/JAD-2011-101680

Bédard, C., Kröger, H., and Destexhe, A. (2006). Does the 1 / f frequency scaling of brain signals reflect self-organized critical states? *Phys. Rev. Lett.* 97:118102. doi: 10.1103/PhysRevLett.97.118102

Bian, C. H., Ma, Q. L., Si, J. F., Wu, X. H., Shao, J., Ning, X. B., et al. (2009). Sign series entropy analysis of short-term heart rate variability. *Sci. Bull.* 54, 4610–4615. doi: 10.1007/s11434-009-0398-6

Bischoff, P., and Rundshagen, I. (2011). Awareness under general anesthesia. *Dtsch. Arztebl. Int.* 108, 1–7. doi: 10.3238/arztebl.2011.0001

Chen, C. W., Lin, C. C., Chen, K. B., Kuo, Y. C., Li, C. Y., and Chung, C. J. (2014). Increased risk of dementia in people with previous exposure to general anesthesia: a nationwide population-based case–control study. *Alzheimers Dement.* 10, 196–204. doi: 10.1016/j.jalz.2013.05.1766

Chen, P. L., Yang, C. W., Tseng, Y. K., Sun, W. Z., Wang, J. L., Wang, S. J., et al. (2013). Risk of dementia after anaesthesia and surgery. *Br. J. Psychiatry* 204, 188–193. doi: 10.1192/bjp.bp.112.119610

Claus, S., Velis, D., Lopes da Silva, F. H., Viergever, M. A., and Kalitzin, S. (2012). High frequency spectral components after secobarbital: the contribution of muscular origin–a study with MEG/EEG. *Epilepsy Res.* 100, 132–141. doi: 10.1016/j.eplepsyres.2012.02.002

Costa, M., Goldberger, A. L., and Peng, C.-K. (2002). Multiscale entropy analysis of complex physiologic time series. *Phys. Rev. Lett.* 89:068102. doi: 10.1103/PhysRevLett.89.068102

Costa, M., Peng, C. K., Goldberger, A. L., and Hausdorff, J. M. (2003). Multiscale entropy analysis of human gait dynamics. *Phys. A* 330, 53–60. doi: 10.1016/J.PHYSA.2003.08.022

Drover, D. R., Schmiesing, C., Buchin, A. F., Ortega, H. R., Tanner, J. W., Atkins, J. H., et al. (2011). Titration of sevoflurane in elderly patients: blinded, randomized clinical trial, in non-cardiac surgery after beta-adrenergic blockade. *J. Clin. Monit. Comput.* 25, 175–181. doi: 10.1007/s10877-011-9293-1

Eagleman, S. L., Drover, C. M., Drover, D. R., Ouellette, N. T., and MacIver, M. B. (2018). Remifentanil and nitrous oxide anesthesia produces a unique pattern of EEG activity during loss and recovery of response. *Front. Hum. Neurosci.* 12:173. doi: 10.3389/fnhum.2018.00173

Eagleman, S. L., and Drover, D. R. (2018). Calculations of consciousness: electroencephalography analyses to determine anesthetic depth. *Curr. Opin. Anaesthesiol.* 31, 431–438. doi: 10.1097/ACO.0000000000000618

Fahy, B. G., and Chau, D. F. (2018). The technology of processed electroencephalogram monitoring devices for assessment of depth of anesthesia. *Anesth. Analg.* 126, 111–117. doi: 10.1213/ANE.0000000000002331

Feshchenko, V. A., Veselis, R. A., and Reinsel, R. A. (2004). Propofol-induced alpha rhythm. *Neuropsychobiology* 50, 257–266. doi: 10.1159/000079981

Ghosh, I., Bithal, P. K., Dash, H. H., Chaturvedi, A., and Prabhakar, H. (2008). Both clonidine and metoprolol modify anesthetic depth indicators and reduce intraoperative propofol requirement. *J. Anesth.* 22, 131–134. doi: 10.1007/s00540-007-0606-y

Grassberger, P., and Procaccia, I. (1983). Characterization of strange attractors. *Phys. Rev. Lett.* 50, 346–349. doi: 10.1103/PhysRevLett.50.346

Gugino, L. D., Chabot, R. J., Prichep, L. S., John, E. R., Formanek, V., and Aglio, L. S. (2001). Quantitative EEG changes associated with loss and return of consciousness in healthy adult volunteers anaesthetized with propofol or sevoflurane. *Br. J. Anaesth.* 87, 421–428. doi: 10.1093/bja/87.3.421

He, B. J. (2011). Scale-free properties of the functional magnetic resonance imaging signal during rest and task. *J. Neurosci.* 31, 13786–13795. doi: 10.1523/JNEUROSCI.2111-11.2011

Holm, S. (1979). A simple sequentially rejective multiple test procedure. *Scand. J. Stat.* 6, 65–70. doi: 10.2307/4615733

Johansen, J. W. (2001). Esmolol promotes electroencephalographic burst suppression during propofol/alfentanil anesthesia. *Anesth. Analg.* 93, 1526–1531. doi: 10.1097/00000539-200112000-00039

John, E. R., Prichep, L. S., Kox, W., Valdés-Sosa, P., Bosch-Bayard, J., Aubert, E., et al. (2001). Invariant reversible QEEG effects of anesthetics. *Conscious. Cogn.* 10, 165–183. doi: 10.1006/CCOG.2001.0507

Kalkman, C. J., Peelen, L. M., and Moons, K. G. (2011). Pick up the pieces: depth of anesthesia and long-term mortality. *Anesthesiology* 114, 485–487. doi: 10.1097/ALN.0b013e31820c2ba2

Khachiyan, L. G. (1980). Polynomial algorithms in linear programming. *USSR Comput. Math. Math. Phys.* 20, 53–72. doi: 10.1016/0041-5553(80)90061-0

Kim, S., Brooks, A. K., and Groban, L. (2015). Preoperative assessment of the older surgical patient: honing in on geriatric syndromes. *Clin. Interv. Aging* 10, 13–27. doi: 10.2147/CIA.S75285

Lee, J. M., Akeju, O., Terzakis, K., Pavone, K. J., Deng, H., Houle, T. T., et al. (2017). A prospective study of age-dependent changes in propofol-induced electroencephalogram oscillations in children. *Anesthesiology* 127, 293–306. doi: 10.1097/ALN.0000000000001717

Li, D., Li, X., Liang, Z. L., Voss, J., and Sleigh, J. W. (2010). Multiscale permutation entropy analysis of EEG recordings during sevoflurane anesthesia. *J. Neural Eng.* 7:046010. doi: 10.1088/1741-2560/7/4/046010

Lindholm, M. L., Träff, S., Granath, F., Greenwald, S. D., Ekbom, A., Lennmarken, C., et al. (2009). Mortality within 2 years after surgery in relation to low intraoperative bispectral index values and preexisting malignant disease. *Anesth. Analg.* 108, 508–512. doi: 10.1213/ane.0b013e31818f603c

Liu, C. Y., Krishnan, A. P., Yan, L., Smith, R. X., Kilroy, E., Alger, J. R., et al. (2013). Complexity and synchronicity of resting state blood oxygenation level-dependent (BOLD) functional MRI in normal aging and cognitive decline. *J. Magn. Reson. Imaging* 38, 36–45. doi: 10.1002/jmri.23961

Liu, Q., Chen, Y. F., Fan, S. Z., Abbod, M. F., and Shieh, J. S. (2015). EEG signals analysis using multiscale entropy for depth of anesthesia monitoring during surgery through artificial neural networks. *Comput. Math. Methods Med.* 2015:232381. doi: 10.1155/2015/232381

MacIver, M. B., and Bland, B. H. (2014). Chaos analysis of EEG during isoflurane-induced loss of righting in rats. *Front. Syst. Neurosci.* 8:203. doi: 10.3389/fnsys.2014.00203

Mitra, P., and Bokil, H. (2008). *Observed Brain Dynamics*. Oxford: Oxford University Press.

Müller, V., and Lindenberger, U. (2012). Lifespan differences in nonlinear dynamics during rest and auditory oddball performance. *Dev. Sci.* 15, 540–556. doi: 10.1111/j.1467-7687.2012.01153.x

Muthukumaraswamy, S. D. (2013). High-Frequency brain activity and muscle artifacts in MEG/EEG: a review and recommendations. *Front. Hum. Neurosci.* 7:138. doi: 10.3389/fnhum.2013.00138

Petsiti, A., Tassoudis, V., Vretzakis, G., Zacharoulis, D., Tepetes, K., Ganeli, G., et al. (2015). Depth of anesthesia as a risk factor for perioperative morbidity. *Anesthesiol. Res. Pract.* 2015:829151. doi: 10.1155/2015/829151

Pierce, T. W., Kelly, S. P., Watson, T. D., Replogle, D., King, J. S., and Pribram, K. H. (2000). Age differences in dynamic measures of EEG. *Brain Topogr.* 13, 127–134. doi: 10.1023/A:1026659102713

Pilge, S., Jordan, D., Kreuzer, M., Kochs, E. F., and Schneider, G. (2014). Burst suppression-MAC and burst suppression-CP50 as measures of cerebral effects of anaesthetics. *Br. J. Anaesth.* 112, 1067–1074. doi: 10.1093/bja/aeu016

Pincus, S. M. (1991). Approximate entropy as a measure of system complexity. *Proc. Natl. Acad. Sci. U.S.A.* 88, 2297–2301. doi: 10.1073/pnas.88.6.2297

Porter Starr, K. N., and Bales, C. W. (2015). excessive body weight in older adults. *Clin. Geriatr. Med.* 31, 311–326. doi: 10.1016/j.cger.2015.04.001

Purdon, P. L., Pavone, K. J., Akeju, O., Smith, A. C., Sampson, A. L., Lee, J., et al. (2015a). The ageing brain: age-dependent changes in the electroencephalogram during propofol and sevoflurane general anaesthesia. *Br. J. Anaesth.* 115(Suppl. 1), i46–i57. doi: 10.1093/bja/aev213

Purdon, P. L., Sampson, A., Pavone, K. J., and Brown, E. N. (2015b). Clinical electroencephalography for anesthesiologists part I: background and basic signatures. *Anesthesiology* 123, 937–960. doi: 10.1097/ALN.0000000000000841

Purdon, P. L., Pierce, E. T., Mukamel, E. A., Prerau, M. J., Walsh, J. L., Wong, K. F. K., et al. (2013). Electroencephalogram signatures of loss and recovery of

consciousness from propofol. *Proc. Natl. Acad. Sci. U.S.A.* 110, E1142–E1151. doi: 10.1073/pnas.1221180110

Rampil, I. J., Kim, J. S., Lenhardt, R., Negishi, C., and Sessler, D. I. (1998). Bispectral EEG index during nitrous oxide administration. *Anesthesiology* 89, 671–677. doi: 10.1097/00000542-199809000-00017

Scott, J. C., Ponganis, K. V., and Stanski, D. R. (1985). EEG quantitation of narcotic effect: the comparative pharmacodynamics of fentanyl and alfentanil. *Anesthesiology* 62, 234–241. doi: 10.1097/00000542-198503000-00005

Shackman, A. J., McMenamin, B. W., Slagter, H. A., Maxwell, J. S., Greischar, L. L., and Davidson, R. J. (2009). Electromyogenic artifacts and electroencephalographic inferences. *Brain Topogr.* 22, 7–12. doi: 10.1007/s10548-009-0079-4

Sleigh, J. W., Steyn-Ross, D. A., Steyn-Ross, M. L., Williams, M. L., and Smith, P. (2001). Comparison of changes in electroencephalographic measures during induction of general anaesthesia: influence of the gamma frequency band and electromyogram signal. *Br. J. Anaesth.* 86, 50–58. doi: 10.1093/bja/86.1.50

Sleimen-Malkoun, R., Temprado, J. J., and Hong, S. L. (2014). Aging induced loss of complexity and dedifferentiation: consequences for coordination dynamics within and between brain, muscular and behavioral levels. *Front. Aging Neurosci.* 6:140. doi: 10.3389/fnagi.2014.00140

Strøm, C., Rasmussen, L. S., and Sieber, F. E. (2014). Should general anaesthesia be avoided in the elderly? *Anaesthesia* 69(Suppl. 1), 35–44. doi: 10.1111/anae.12493

van den Broek, P. L., van Rijn, C. M., van Egmond, J., Coenen, A. M., and Booij, L. H. (2006). An effective correlation dimension and burst suppression ratio of the EEG in rat. correlation with sevoflurane induced anaesthetic depth. *Eur. J. Anaesthesiol.* 23, 391–402. doi: 10.1017/S0265021505001857

Voytek, B., Kramer, M. A., Case, J., Lepage, K. Q., Tempesta, Z. R., Knight, R. T., et al. (2015). Age-related changes in 1/*f* neural electrophysiological noise. *J. Neurosci.* 35, 13257–13265. doi: 10.1523/JNEUROSCI.2332-14.2015

Walling, P. T., and Hicks, K. N. (2006). nonlinear changes in brain dynamics during emergence from sevoflurane anesthesia: preliminary exploration using new software. *Anesthesiology* 105, 927–935. doi: 10.1097/00000542-200611000-00013

Watt, R. C., and Hameroff, S. R. (1988). phase space electroencephalography (EEG): a new mode of intraoperative EEG analysis. *Int. J. Clin. Monit. Comput.* 5, 3–13. doi: 10.1007/BF01739226

Widman, G., Schreiber, T., Rehberg, B., Hoeft, A., and Elger, C. E. (2000). Quantification of depth of anesthesia by nonlinear time series analysis of brain electrical activity. *Phys. Rev. E Stat. Phys. Plasmas Fluids Relat. Interdiscip. Topics* 62(4 Pt A), 4898–4903. doi: 10.1103/PhysRevE.62.4898

Yang, C. W., and Fuh, J. L. (2015). Exposure to general anesthesia and the risk of dementia. *J. Pain Res.* 8, 711–718. doi: 10.2147/JPR.S55579

Zaugg, M., Tagliente, T., Silverstein, J. H., and Lucchinetti, E. (2003). Atenolol may not modify anesthetic depth indicators in elderly patients — a second look at the data. *Can. J. Anesth.* 50, 638–642. doi: 10.1007/BF03018703

Conflict of Interest Statement: DD is a consultant for Masimo Inc. The original study was conducted with financial support from Hospira, Inc.

The remaining authors declare that the research was conducted in the absence of any commercial or financial relationships that could be construed as a potential conflict of interest.

frontiers in Neuroscience

ORIGINAL RESEARCH
published: 01 October 2018
doi: 10.3389/fnins.2018.00677

Dynamic Complexity of Spontaneous BOLD Activity in Alzheimer's Disease and Mild Cognitive Impairment Using Multiscale Entropy Analysis

*Yan Niu[1†], Bin Wang[1,2†], Mengni Zhou[1], Jiayue Xue[1], Habib Shapour[1], Rui Cao[1], Xiaohong Cui[1], Jinglong Wu[3,4] and Jie Xiang[1]**

[1] College of Information and Computer, Taiyuan University of Technology, Taiyuan, China, [2] Department of Radiology, First Hospital of Shanxi Medical University, Taiyuan, China, [3] Key Laboratory of Biomimetic Robots and Systems, Ministry of Education, Beijing Institute of Technology, Beijing, China, [4] Graduate School of Natural Science and Technology, Okayama University, Okayama, Japan

Alzheimer's disease (AD) is characterized by progressive deterioration of brain function among elderly people. Studies revealed aberrant correlations in spontaneous blood oxygen level-dependent (BOLD) signals in resting-state functional magnetic resonance imaging (rs-fMRI) over a wide range of temporal scales. However, the study of the temporal dynamics of BOLD signals in subjects with AD and mild cognitive impairment (MCI) remains largely unexplored. Multiscale entropy (MSE) analysis is a method for estimating the complexity of finite time series over multiple time scales. In this research, we applied MSE analysis to investigate the abnormal complexity of BOLD signals using the rs-fMRI data from the Alzheimer's disease neuroimaging initiative (ADNI) database. There were 30 normal controls (NCs), 33 early MCI (EMCI), 32 late MCI (LMCI), and 29 AD patients. Following preprocessing of the BOLD signals, whole-brain MSE maps across six time scales were generated using the Complexity Toolbox. One-way analysis of variance (ANOVA) analysis on the MSE maps of four groups revealed significant differences in the thalamus, insula, lingual gyrus and inferior occipital gyrus, superior frontal gyrus and olfactory cortex, supramarginal gyrus, superior temporal gyrus, and middle temporal gyrus on multiple time scales. Compared with the NC group, MCI and AD patients had significant reductions in the complexity of BOLD signals and AD patients demonstrated lower complexity than that of the MCI subjects. Additionally, the complexity of BOLD signals from the regions of interest (ROIs) was found to be significantly associated with cognitive decline in patient groups on multiple time scales. Consequently, the complexity or MSE of BOLD signals may provide an imaging biomarker of cognitive impairments in MCI and AD.

Keywords: multiscale entropy, Alzheimer's disease, mild cognitive impairment, blood oxygen level-dependent signals, dynamic complexity

OPEN ACCESS

Edited by:
Danny J. J. Wang,
University of Southern California,
United States

Reviewed by:
Kay Jann,
University of Southern California,
United States
Albert Yang,
Harvard Medical School,
United States
Robert X. Smith,
Washington University in St. Louis,
United States
Hengyi Rao,
University of Pennsylvania,
United States

****Correspondence:***
Jie Xiang
xiangjie@tyut.edu.cn

[†]These authors are co-first authors

Specialty section:
This article was submitted to Brain Imaging Methods, a section of the journal Frontiers in Neuroscience

Received: *27 April 2018*
Accepted: *07 September 2018*
Published: *01 October 2018*

Citation:
Niu Y, Wang B, Zhou M, Xue J, Shapour H, Cao R, Cui X, Wu J and Xiang J (2018) Dynamic Complexity of Spontaneous BOLD Activity in Alzheimer's Disease and Mild Cognitive Impairment Using Multiscale Entropy Analysis. Front. Neurosci. 12:677. doi: 10.3389/fnins.2018.00677

INTRODUCTION

Functional connectivity (FC) of spontaneous blood oxygen level-dependent (BOLD) signals in functional magnetic resonance imaging (fMRI) has become an important tool for probing brain function changes in normal aging and neurodegenerative diseases. However, relatively few studies have investigated the temporal dynamics of BOLD signals and its relations with pathologic changes in neurophysiology (Sporns et al., 2000; Friston et al., 2003; Wu et al., 2012). As the most complex organ of the human body, the human brain regulates multifaceted actions with billions of neurons and synapses (Fox et al., 2007). Therefore, the BOLD signals possess complex temporal fluctuations, which could be imitated by nonlinear dynamical processes (Soltysik et al., 2004; Stephan et al., 2008; Yan et al., 2017).

Over the past few years, several statistical methods have been applied to quantify the temporal dynamics of physiological systems. A widely used non-linear statistical method is sample entropy (SE) proposed by Richman and Moorman (2000). SE improved approximate entropy (ApEn) proposed by Pincus (1991), by resolving the problem of erratic results due to vector self-matching. Many studies evidenced the effectiveness of SE in the complexity analysis of time series data of biological systems (Sokunbi et al., 2013, 2014). However, recent studies found that neural signals in the brain possess correlations over a wide range of temporal and spatial scales, stemming from long-range interactions (Costa et al., 2005; Peng et al., 2009; Morabito et al., 2012). Therefore, SE may not be adequate to fully capture the complexity of neural signals by only calculating signal entropy on a single scale.

The multiscale entropy (MSE) was proposed (Costa et al., 2002) to investigate the dynamic complexity of a time series across multiple temporal scales. Several studies have demonstrated the efficacy of MSE for quantifying the complexity of BOLD signals in aging (Yang et al., 2013; Smith et al., 2014). Yang et al. (2013) employed MSE analysis to investigate the complexity of BOLD signals between the younger and older groups, and found significant decreases in MSE in older subjects. Smith et al. (2014) explored the effect of healthy aging on the entropy of resting-state fMRI (rs-fMRI) using MSE analysis, and the results revealed enhanced contrast between healthy young and aged volunteers at longer time scales. However, the dynamic complexity of BOLD signals in neurodegenerative diseases across multiple temporal scales remains largely unexplored.

Alzheimer's disease (AD) is a neurodegenerative disease characterized by progressive deterioration of cognitive and behavioral function (Ballard et al., 2011). Mild cognitive impairment (MCI) is a neurological disorder occurring before the onset of early AD as an intermediate stage at a high risk of developing AD (Petersen et al., 1999; Belleville et al., 2011). A few studies found decreased complexity of BOLD signals in AD by using single-scale entropy analysis (Liu et al., 2013; Wang et al., 2017). However, the complexity alterations of BOLD signals in MCI and AD patients across multiple time scales remain unclear.

We obtained BOLD rs-fMRI data from the Alzheimer's disease neuroimaging initiative (ADNI[1]) database, including 30 normal control (NC), 33 early MCI (EMCI), 32 late MCI (LMCI), and 29 AD subjects. MSE maps of the four groups across multiple time scales were calculated and the clusters with significant MSE differences were identified. We then examined the relationships between MSE values and scores of cognitive assessments on all time scales. Finally, we investigated the relationship between MSE and gray matter volume (GMV) on all time scales.

MATERIALS AND METHODS

Participants

A total of 124 subjects were selected from ADNI-2 database, including 30 NC subjects (aged 74.18 ± 5.96 years; 19 females; education: 16.8 ± 2.0 years), 33 EMCI subjects (aged 72.01 ± 5.87 years; 16 females; education: 15.5 ± 2.4 years), 32 LMCI subjects (aged 72.57 ± 8.16 years; 13 females; education: 16.5 ± 2.1 years), and 29 AD subjects (aged 72.33 ± 7.26 years; 18 females; education: 16 ± 2.7 years). For each subject, there were cognitive assessments including Mini-Mental State Examination (MMSE), Clinical Dementia Rating (CDR), and Functional Activities Questionnaire (FAQ). **Table 1** summarizes the demographic and clinical characteristics of the participants.

Data Acquisition and Data Processing

All subjects went through resting-state BOLD fMRI scans with their eyes closed on a 3.0 T scanner (Philips Medical Systems)

[1]http://adni.loni.usc.edu/

TABLE 1 | Demographic and clinical characteristics of the participants.

	NC	EMCI	LMCI	AD	*p*-value
Age (years)	74.18 ± 5.96	72.01 ± 5.87	72.57 ± 8.16	72.33 ± 7.26	0.505
Sex (M/F)	11/19	17/16	19/13	11/18	0.732
Education (years)	16.8 ± 2.0	15.5 ± 2.4	16.5 ± 2.1	16 ± 2.7	0.418
MMSE	28.9 ± 1.7	27.59 ± 2.02	26.96 ± 2.69	21.0 ± 3.5	<0.001
FAQ	0.14 ± 0.44	3.03 ± 4.50	4.07 ± 4.70	15 ± 7.47	<0.001
CDR	0	0.5	0.5	0.84 ± 0.23	<0.001

Data are given as the mean ± standard deviation (SD).
The p-values were obtained by one-way ANOVA.

using the following parameters: repetition time (TR) = 3000 ms; echo time (TE) = 30 ms; slice thickness = 3.3 mm; flip angle = 80°; slice number = 48, and 140 time points.

Resting-state fMRI data were preprocessed using Statistical Parametric Mapping (SPM12[2]), Data Processing and Analysis for (Resting-State) Brain Imaging (DPABI; Yan et al., 2016) and the rs-fMRI Data Analysis Toolkit (REST 1.8; Song et al., 2011) packages. The following steps were performed: removing the first 10 time points; slice-timing correction; image realignment; normalization to the Montreal Neurological Institute (MNI) space (resampled into 3 mm × 3 mm × 3 mm voxels). The linear trends of time courses were removed, and the effect of nuisance covariates was removed by signal regression using the global signal, the motion parameters, the cerebrospinal fluid (CSF) and white matter (WM) signals. Temporal filtering ($0.01\ \text{Hz} < f < 0.2\ \text{Hz}$) was applied. Finally, each voxel time series was standardized to a mean of zero and standard deviation of unity.

The analysis of the GMV was performed according to the voxel-based morphometry (VBM) protocol using DPABI. The VBM procedure involves the segmentation of the original anatomic MRI images in gray matter (GM), WM, and CSF tissues, followed by GM image normalization to templates in stereotactic space to acquire optimized normalization parameters, which were applied to the raw images. Finally, GM images were smoothed using a 6-mm full-width at half-maximum (FWHM) Gaussian kernel.

MSE Theory

Multiscale entropy is based on the theory of SE over a range of scales and consists of two steps (Costa et al., 2002).

(1) The coarse-graining procedure of time series represents the system dynamics on different scale factors. Given time series $\{x_i, i = 1, 2, \ldots, N\}$, for the time scale l, the coarse-grained time series $\{y^l\}$ is calculated as follows:

$$y_j^l = \frac{1}{l} \sum_{i=(j-1)l+1}^{jl} x_i, 1 \le j \le N/l \quad (1)$$

The length of new time series is N/l. For scale 1, the new time series corresponds to the original time series.

(2) The SE for each coarse-grained time series is calculated.

Sample entropy (Richman and Moorman, 2000) is calculated as:

$$SE(m, r, N) = -\ln \frac{P_{m+1}(r)}{P_m(r)} \quad (2)$$

where m is the sequence length of time points to be compared, r is the radius of similarity, N is the length of the time series, and P is the probability that points falling within r.

Multiscale entropy consists of a set of SE values under multiple time scales, which reflects the complexity of time series on multiple scales. MSE can be used to compare the complexity of different time series, based on the specific trend of SE changes with scales (e.g., complex time series show constant entropy over various time scales, while random noise shows a marked decrease in entropy at longer time scales; Wang et al., 2018).

MSE Calculation

We used the Complexity Toolbox[3] [Laboratory of Functional MRI Technology (LOFT), Department of Neurology, University of Southern California] to calculate MSE of rs-fMRI data.

Three parameter values were set for the calculation of MSE, including pattern length m, distance threshold r, and time scale l. The point to be made is that the r value is generally correlated with the standard deviation of the original time series (Lu et al., 2015). Various theoretical and clinical applications have indicated that, $m = 1$ or 2 and $r = 0.1$–0.35 of the standard deviation of the original sequence, provides reasonable statistical validity for calculating SE (Richman and Moorman, 2000). Because no rigorous standard exists for choosing the parameters to calculate SE, prior studies on SE analysis of biomedical signals have shown inconsistent selection of parameters. For example, studies of fMRI used various parameters, including $m = 1$ and $r = 0.35$ (Yang et al., 2013), $m = 2$ and $r = 0.30$ (Smith et al., 2014), $m = 2$ and $r = 0.15$ (Yang et al., 2011). In addition, different parameters were also used in the studies of EEG, including $m = 2$ and $r = 0.15$ (Catarino et al., 2011), $m = 2$ and $r = 0.25$ (Xiang et al., 2015), $m = 1$ and $r = 0.25$ (Escudero et al., 2006). In this study, MSE was calculated for each BOLD time series based on different parameter pairs: ($m = 2$, $r = 0.15$), ($m = 2$, $r = 0.25$), ($m = 2$, $r = 0.30$), ($m = 2$, $r = 0.35$), ($m = 1$, $r = 0.25$), and ($m = 1$, $r = 0.35$) across the range of scales from 1 to 6.

Statistical Analyses

For every time scale, one-way analysis of variance (ANOVA) was used to assess differences in MSE maps of BOLD signals among four groups (NC, EMCI, LMCI, and AD) using REST 1.8. For multiple comparison corrections, a stringent statistical significance level was employed by setting a voxelwise threshold of $p < 0.001$ and a cluster threshold of $p < 0.05$ with a Gaussian random field (GRF) correction among four groups after adjusting for age, sex, and education differences.

Then, fivefold cross-validation was used for regions of interest (ROIs) analyses. We divided the data into five independent subsets. For each fold, we used one subset for selective analysis after using other four subsets for selection (ANOVA). According to the peak MNI coordinates (X Y Z), we extracted the average MSE and GMV by using DPABI toolbox to define ROIs and the radius of the spheres at all scales (8 mm). For each ROI, differences on MSE values among four groups at all scales were compared using ANOVA using Statistical Package for Social Sciences (SPSS 20.0) software. Bonferroni's *post hoc* pairwise test on ANOVA was performed.

Spearman's correlation was used to assess the relationship between MSE and MMSE, FAQ, CDR, and GMV for four groups using SPSS 20.0 software.

[2]http://www.fil.ion.ucl.ac.uk/spm

[3]http://loft-lab.org/index-5.html

RESULTS

Demographic and Clinical Characteristics

Table 1 summarizes the demographic and clinical characteristics of the participants. The *p*-values were obtained by one-way ANOVA. The results indicated no difference in age, sex, and education across four groups. Significant differences ($p < 0.001$) among four groups were found on the MMSE, FAQ, and CDR scores.

Parameter Selection for MSE Calculation

The comparison was made by calculating MSE using six different parameter combinations (m, r). All subjects' MSE maps were calculated across time scales from 1 to 6. We performed the one-way ANOVA on MSE maps of four groups on every time scale. Based on the final results, the findings using $m = 2$ and $r = 0.35$ as the optimal parameter were mainly reported in this study. Previous study has shown that the accuracy of the calculation results is least dependent on the sequence length N when $m = 2$ (Smith et al., 2014). Other results are presented in **Supplementary Data Sheet 1**. For $m = 2$ and $r = 0.15$, four clusters were significantly different among the four groups across multiple time scales on scale 2, scale 3, scale 4, and scale 6 (**Supplementary Table S1** and **Supplementary Figure S1**). Five clusters were found on scale 2, scale 4, and scale 6 when $m = 2$ and $r = 0.25$ (**Supplementary Table S2** and **Supplementary Figure S2**). For $m = 2$, $r = 0.30$ and $m = 2$, $r = 0.35$, similar results were found and nine clusters showed significant differences on scale 2, scale 4, scale 5, and scale 6 (**Supplementary Table S3** and **Supplementary Figure S3**). For $m = 1$, $r = 0.25$ and $m = 1$, $r = 0.35$, however, only one consistent cluster was found (left middle occipital gyrus) on scale 1 and no difference was found on the rest scales (**Supplementary Tables S4, S5** and **Supplementary Figures S4, S5**).

Significant Differences on MSE Among the Four Groups

Using $m = 2$ and $r = 0.35$, the result is presented in **Figure 1**. The detailed information is summarized in **Table 2**. Significant differences ($p < 0.001$, GRF correction) were found on the MSE maps among the four groups on scale 2, scale 4, scale 5, and scale 6. We found no significant difference on scale 1 and scale 3. On scale 2, one cluster was found: right thalamus (THA.R). On scale 4, one cluster was found: left superior frontal gyrus (SFGdor.L). We found two clusters on scale 5: right lingual gyrus (LING.R) and right insula (INS.R). For the scale 6, five clusters were found: right superior temporal gyrus (STG.R), left middle temporal gyrus (MTG.L), right olfactory cortex (OLF.R), left inferior occipital gyrus (IOG.L), and right supramarginal gyrus (SMG.R).

We also extracted the mean MSE of whole brain (WB), GM, WM, and CSF using the corresponding masks on all time scales. Then, one-way ANOVA was performed to examine the differences among the four groups. The result is presented in **Supplementary Table S6**. Only GM showed a trend of entropy difference ($F = 2.283$, $p = 0.083$) among four groups on scale 6. **Figure 2** shows the mean entropy curve of GM across the scale of 1–6 for four groups as well as the differences between each pair of the four groups on scale 6 ($p < 0.05$, two-sample t-test, uncorrected).

Time Scales Analysis on MSE From Scale 1 to Scale 6

We extracted the average MSE of 9 ROIs over multiple time scales. **Figure 3** displays the MSE curve across scale 1 to 6 among four groups (NC, EMCI, LMCI, and AD) for nine ROIs. Each group exhibited a drop in SE values with increasing scale. SE values on scale 1 showed no difference among the four groups for nine ROIs. For scale 2, there were two ROIs (THA.R and OLF.R) showing significant differences among four groups. SFGdor.L, INS.R, and OLF.R showed significant differences on scale 3. For scale 4, there were six ROIs (SFGdor.L, LING.R, INS.R, MTG.L, OLF.R, and SMG.R) showing significant differences among four groups. There were four ROIs showing significant differences (LING.R, INS.R, and IOG.L) on scale 5. On scale 6, there were six ROIs showing significant differences (THA.R, STG.R, MTG.L, OLF.R, IOG.L, and SMG.R) among four groups. Specifically, OLF.R showed significant differences on four time scales (scale 2, scale 3, scale 4, and scale 6).

Comparison of MSE Among the Four Groups

Multiscale entropy values of nine ROIs at all scales were compared among the four groups (NC, EMCI, LMCI, and AD) using ANOVA, and for MSE of ROIs with significant differences among the four groups, Bonferroni's *post hoc* pairwise test on ANOVA was performed. **Figure 4** displays the comparison of MSE of nine ROIs at different scales between any two groups. The results showed that, compared with NC subjects, patient groups demonstrated reduced complexity. Specifically, the AD group showed lower complexity than the NC group for all ROIs.

Compared with the NC group, the EMCI subjects had significantly reduced MSE of BOLD signals in INS.R. The LMCI subjects showed significantly decreased MSE in eight of the nine ROIs except THA.R. Compared with the EMCI group, the LMCI group showed decreased MSE in SFGdor.L while the AD group showed decreased MSE in three ROIs (THA.R, MTG.L, and OLF.R). In addition, THA.R had lower complexity in the AD group than that in the LMCI group.

Relationships Between MSE and Clinical Measurements

We performed Spearman's correlations between MSE values and the clinical measurements (MMSE, FAQ, and CDR) in patient groups (MCI and AD). After corrections for multiple comparisons, significant correlations were found.

Figure 5 shows the scatter plots between MSE values of BOLD signals and clinical measurement scores (MMSE, FAQ, and CDR) in patient groups in the significantly correlated brain regions. On scale 2, MMSE was positively correlated with the complexity of BOLD signals in THA.R ($r = 0.354$, $p = 0.006$). SFGdor.L

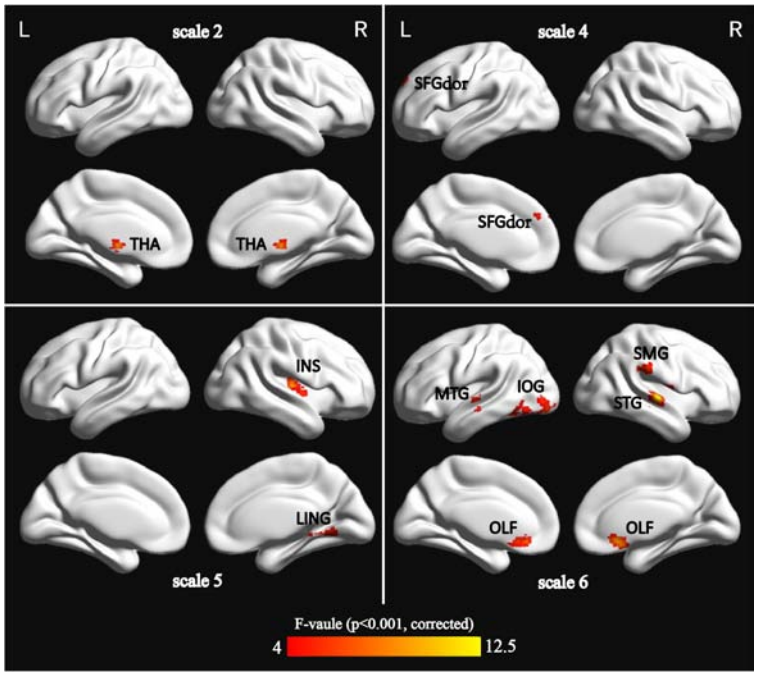

FIGURE 1 | Surface-rendered images showed the differences between the control and patient groups after adjusting for age, sex, and education. The regions showed significantly different brain regions among the four groups on scale 2, scale 4, scale 5, and scale 6. See **Table 2** for a complete list of these regions (threshold $p < 0.001$, GRF corrected).

TABLE 2 | Characteristics of the brain regions those were significantly different among the four groups across multiple time scales.

Scale	Brain Region	AAL.Abbr	Peak MNI (*X*, *Y*, *Z*)	Cluster voxels	Voxel *F*-value
Scale 2	Thalamus	THA.R	(0, −9, 0)	120	8.817
Scale 4	Superior frontal gyrus	SFGdor.L	(−18, 54, 42)	81	7.043
Scale 5	Lingual gyrus	LING.R	(15, −51, −9)	82	7.948
	Insula	INS.R	(33, −12, 6)	78	9.807
Scale 6	Superior temporal gyrus	STG.R	(60, −18, 0)	153	12.274
	Middle temporal gyrus	MTG.L	(−66, −18, −3)	95	8.258
	Olfactory cortex	OLF.R	(6, 21, −12)	139	10.959
	Inferior occipital gyrus	IOG.L	(−54, −69, −9)	203	7.434
	Supramarginal gyrus	SMG.R	(60, −33, 27)	81	7.177

The location coordinates are those of the peak significance in each region ($p < 0.001$, GRF corrected).

exhibited the significant positive correlation ($r = 0.293$, $p = 0.030$) between the MSE values and MMSE scores on scale 4. The four ROIs (INS.R, STG.R, IOG.L, and SMG.R) exhibited significant positive correlations ($r > 0.283$, $p < 0.048$) between MSE and MMSE scores on scale 6. Some trend correlations were also found ($p < 0.05$, uncorrected) and the results are shown in **Supplementary Table S7**.

As shown in **Figure 5**, the MSE values of THA.R exhibited significant negative correlations ($r = -0.344$, $p = 0.006$) with the FAQ scores on scale 2. OLF.R exhibited significant correlations ($r = -0.291$, $p = 0.042$) between FAQ scores and MSE values of BOLD signals in patient groups on scale 6. SFGdor.L, LING.R, INS.R, and IOG.L exhibited trend correlations ($p < 0.05$, uncorrected) between FAQ scores and MSE values on multiple time scales (**Supplementary Table S8**).

After corrections for multiple comparisons, MSE values of THA.R exhibited the significant negative correlation with the CDR scores on scale 2 ($r = -0.303$, $p = 0.024$) and scale 3 ($r = -0.286$, $p = 0.042$). LING.R showed the significant negative correlation between CDR scores and MSE values on scale 5 ($r = -0.331$, $p = 0.012$) and MSE values of SMG.R were negatively correlated with CDR scores on scale 6 ($r = -0.312$, $p = 0.018$; **Figure 5**). In addition, SFGdor.L, INS.R, STG.R, OLF.R, and IOG.L exhibited trend correlations ($p < 0.05$, uncorrected) between CDR scores and MSE values on multiple time scales. **Supplementary Table S9** summarizes the correlation results between CDR scores and MSE values of BOLD signals in patient groups.

We also performed Spearman's correlations between MSE values and the clinical measurements (MMSE, FAQ, and CDR)

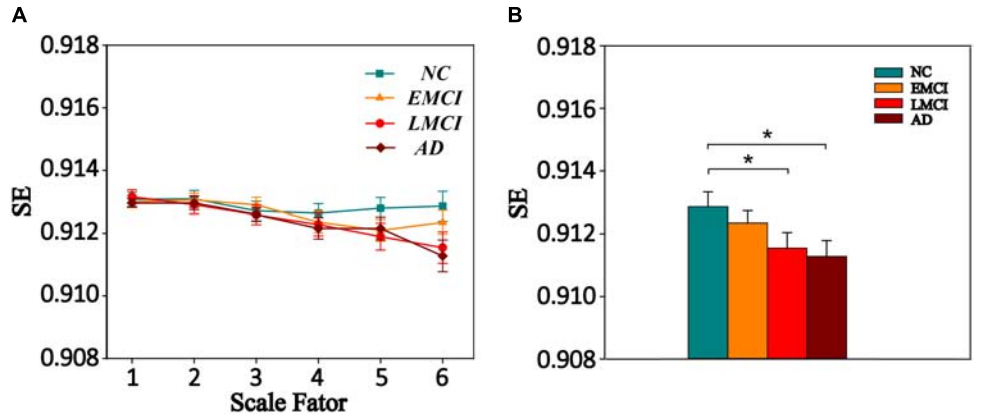

FIGURE 2 | (A) MSE curve across scale factor 1–6 in gray matter (GM) for four groups. Each point represents group average SE. **(B)** Mean SE values of GM in the NC, EMCI, LMCI, and AD subjects on scale 6. Significant differences between each pair of the four groups ($p < 0.05$, two-sample t-test, uncorrected) are indicated. The error bar represents the standard error of MSE within the group. * indicates $p < 0.05$.

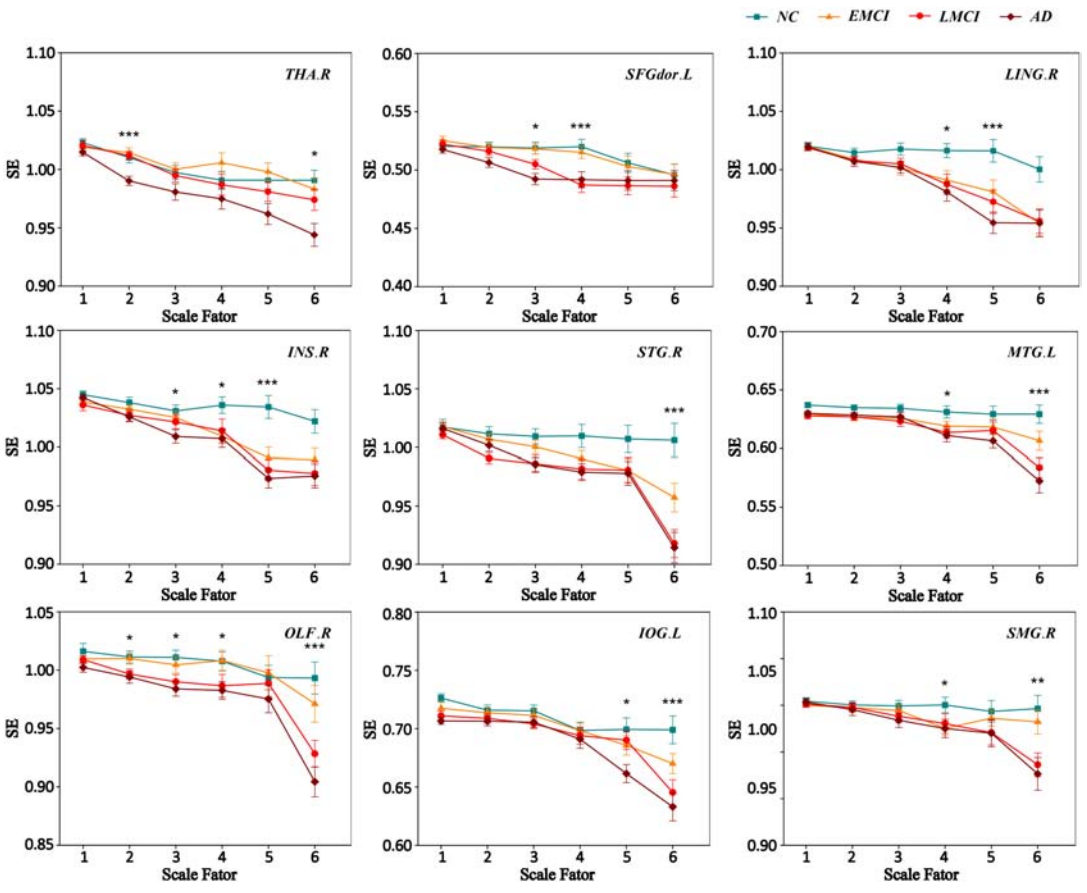

FIGURE 3 | MSE curve across scale factor 1–6 for four groups. Each point represents group average SE. The error bar represents the standard error of MSE within the group. * indicates $p < 0.05$. **indicates $p < 0.05$. *** indicates $p < 0.001$.

for each group (NC, EMCI, LMCI, and AD). After corrections for multiple comparisons, for the NC group, SMG.R exhibited the significant negative correlation ($r = -0.516$, $p = 0.048$) between MSE values and FAQ scores on scale 5. No correlation was found between MSE values and MMSE, FAQ, and CDR scores in the EMCI group on all scales. For the LMCI group, MSE values of STG.R were positively correlated ($r = 0.512$, $p = 0.030$) with MMSE scores and MSE values of MTG.R and IOG.L were

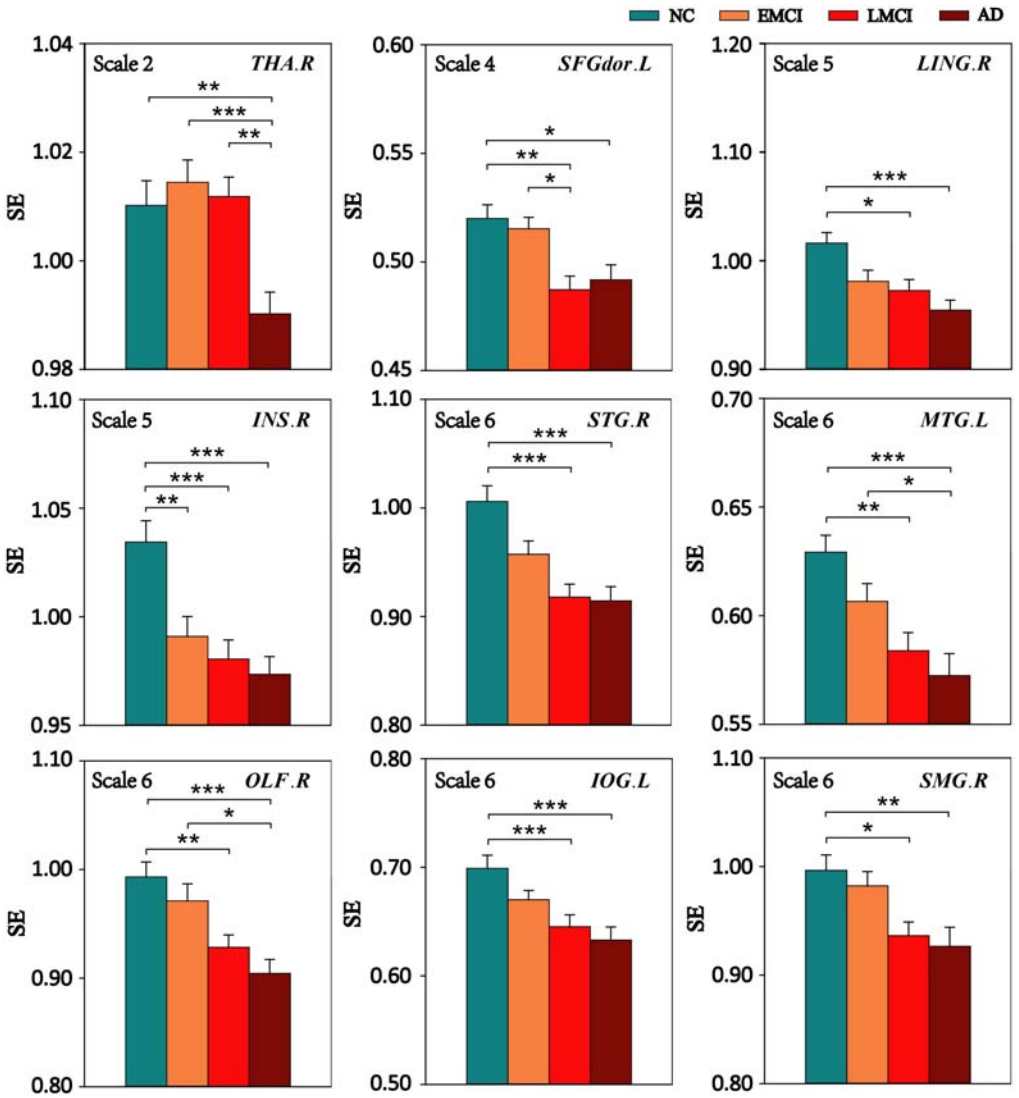

FIGURE 4 | Mean SE values of the nine ROIs in the NC, EMCI, LMCI, and AD subjects on four time scales. Significant differences between pairs of groups after Bonferroni correction ($p < 0.05$) are indicated. The error bar represents the standard error of MSE within the group. * indicates $p < 0.05$. ** indicates $p < 0.01$. *** indicates $p < 0.001$.

negatively correlated ($r < -0.485$, $p < 0.048$) with FAQ scores. STG.R exhibited the significant negative correlation(r = -0.488, $p = 0.048$ between MSE values and CDR scores in the AD group. Some trend correlations were also found ($p < 0.05$, uncorrected) and the results are shown in **Supplementary Tables S11–S14**.

Relationships Between MSE and GMV

We extracted the average GMV values of nine ROIs for four groups. Then, we explored the relationships between the MSE and the GMV in patient groups. After corrections for multiple comparisons, no significant correlation was found between the complexity of BOLD signals and GMV values. But the LING.R exhibited trend positive correlations ($r > 0.209$, $p < 0.043$, uncorrected) between the MSE and the GMV in patient groups on four time scales (scale 3, scale 4, scale 5, and scale 6). STG.R exhibited a positive correlation ($r = 0.203$, $p = 0.050$, uncorrected) between the MSE and the GMV on scale 6 and MTG.L showed a positive correlation ($r = 0.235$, $p = 0.023$, uncorrected) on scale 5. The results are presented in **Supplementary Table S10**.

Correlation analyses for each group (NC, EMCI, LMCI, and AD) were also performed between the MSE and the GMV on all time scales. After corrections for multiple comparisons, no significant correlation was found between the complexity of BOLD signals and GMV values in the NC, EMCI, and LMCI groups. Only SFGdor.L showed the significant positive correlations in the AD group on scale 6. Some brain regions exhibited trend positive correlations ($p < 0.05$, uncorrected) between MSE values and GMV values in each group and the results are presented in **Supplementary Tables S11–S14**.

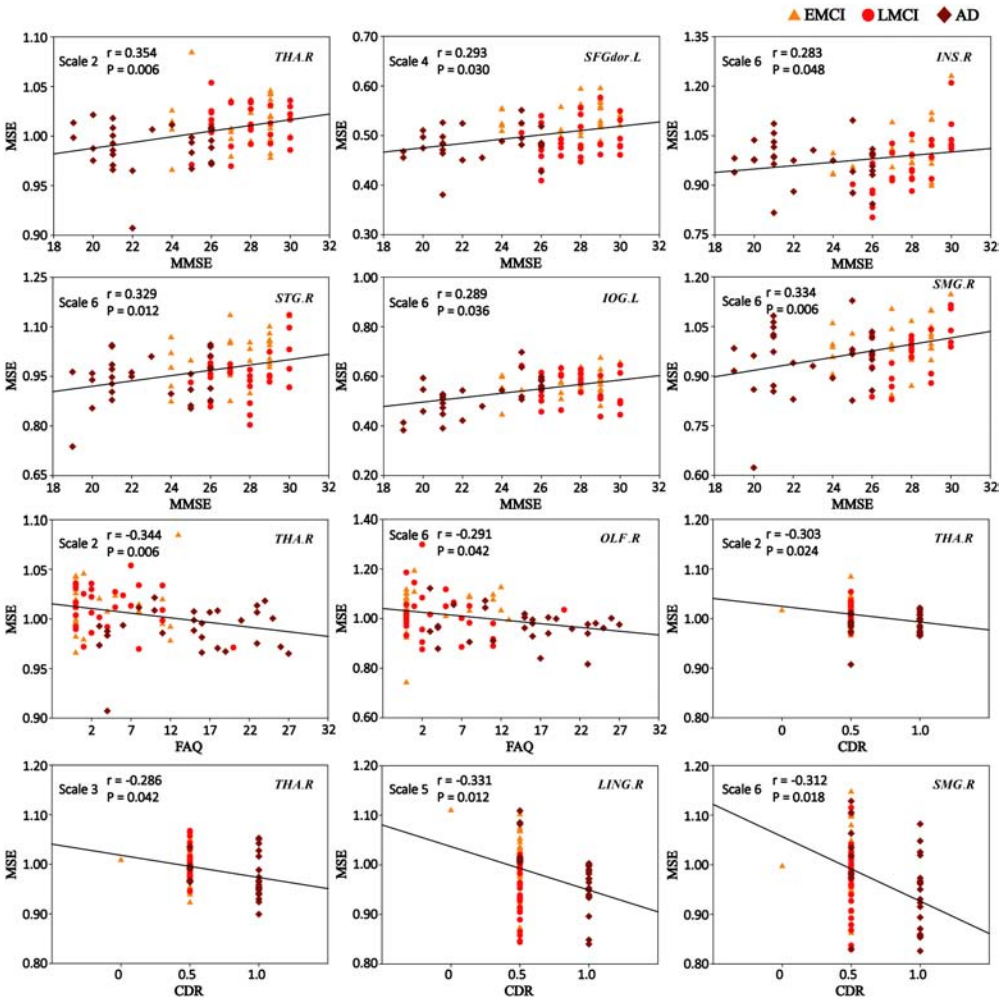

FIGURE 5 | Significant correlations between MSE of blood oxygen level-dependent (BOLD) signals and clinical measurement scores (MMSE, FAQ, and CDR) in patient groups ($p < 0.05$, corrected). r is the Spearman correlation coefficient, and p indicates the level of statistical significance.

DISCUSSION

In this study, we employed MSE analysis to assess the complexity of BOLD activity in AD and MCI patients from scale 1 to 6. We discovered that the spontaneous BOLD signals of nine clusters had significant differences among four groups on four time scales. The significant MSE differences were mainly detected in the occipital, frontal, temporal, limbic, and parietal lobes, which were significantly correlated with clinical measurements in patient groups from scale 2 to 6. These results suggest that the complexity analyses using MSE of BOLD signals can provide information on the temporal dynamics of neural signals across multiple scales that are relevant to the cognitive impairments in MCI and AD.

The MSE Differences Among Four Groups on Multiple Time Scales

This study found that MSE of BOLD activity exhibited significant contrasts among four groups on four time scales (scale 2, scale 4, scale 5, and scale 6; **Figure 1**), mainly distributed in the occipital lobe (IOG.L and LING.R), frontal lobe (SFGdor.L and OLF.R), parietal lobe (SMG.R), temporal lobe (STG.R and MTG.L), limbic lobe (INS.R), and the subcortical region (THA.R). In the MSE analysis for nine ROIs over all time scales, we found that three ROIs (SFGdor.L, INS.R, and OLF.R) had significant differences on scale 3 (**Figure 3**). This means that more useful information was found on multiple time scales. This is consistent with previous reports using MSE analysis on rs-fMRI and EEG signals that detected differences in entropy on multiple time scales (Mizuno et al., 2010; Liu et al., 2013; Yang et al., 2013; Mcbride et al., 2014; Smith et al., 2014; Michalopoulos and Bourbakis, 2017). Particularly, as **Figure 1** demonstrates, five clusters showed significant differences on scale 6. More significant differences were found among the four groups with increasing scales. As can be seen from **Figure 3**, six ROIs showed prominent differences among the four groups on scale 4 and 6. Based on the mechanism of MSE analysis, at the shortest scale, the entropy is dominated by the high

frequency fluctuations from random noise (Wang et al., 2018). By filtering out these random fluctuations, the contrast in entropy becomes larger at longer time scales (Smith et al., 2014).

In this study, each of the nine ROIs was observed on a single scale. In the process of calculating MSE, the key step is to coarse-grain the time series to reflect the system dynamics on different time scales, which means that, MSE mainly calculates the complexity of high frequencies at low scales, while the complexity of low frequencies is calculated at large scales. Our results showed that different brain regions displayed differences at different frequencies. Consisted with our result, Wang et al. (2018) investigated the neurophysiological underpinnings of complexity (MSE) of fMRI signals and their relations to FC and the results showed that the associations between MSE and FC were dependent on the temporal scales or frequencies It has been proposed that each frequency band is generated by different mechanisms and relates to different physiological functions, higher frequency oscillations are confined to a small neuronal space, whereas lower frequencies may reflect long-range interactions (Buzsáki and Draguhn, 2004; Zuo et al., 2010). More recently, studies on rs-fMRI have hypothesized that frequency-dependent effects in different brain regions which reflect different synaptic and functional characteristics that are affected by the progression of cognitive impairment (He et al., 2010; Yu et al., 2013; Wang et al., 2016; Zhou et al., 2016). Hence, we propose that the observed complexity changes on different time scales might represent different region or network-dependent neuropathophysiological mechanisms in MCI and AD.

We also analyzed the complexity of WB, GM, WM, and CSF on all time scales. Only GM showed a trend of entropy difference ($F = 2.283$, $p = 0.083$) among four groups on scale 6. Many studies on the complexity analysis of rs-fMRI data found global complexity differences in aging (Yang et al., 2013; Sokunbi et al., 2015) and AD (Liu et al., 2013; Wang et al., 2017). Smith et al. (2014) found greater age-related decline in average GM complexity of rs-fMRI at longer time scales, and Liu et al. (2013) found mean complexity of rs-fMRI in GM and WM decreased with normal aging. Thus, the complexity of global brain activity may decrease with age. For AD-related cognitive decline, Liu et al. (2013) found that mean ApEn of GM showed a significant positive correlation with MMSE scores in the cohort of familial AD subjects, and Wang et al. (2017) found significant differences ($p < 0.05$) in permutation entropy (PE) of GM and WM across the four groups of ADNI data. Possibly due to differences in data samples and complexity analysis methods, the MSE analysis used in this study was only able to reveal a trend of entropy difference ($p = 0.083$) among four groups in GM as well as decreased complexity in the AD and LMCI groups compared to that of the NC group at the statistical threshold of uncorrected $p < 0.05$. In contrast, we found highly significant MSE differences ($p < 0.001$, GRF corrected) in several brain regions on multiple time scales. This is not surprising as the pathological process of AD first affects the network of temporal, frontal, and parietal regions before progressing to the whole GM and brain level. Different complexity analyses may have different sensitivities in detecting global and regional changes of neural complexity with AD progression. This question awaits further investigation in future studies.

Decreased Complexity and Cognitive Decline in Patient Groups

Using the *post hoc* pairwise test on ANOVA, reduced complexity in the AD group was detected in all ROIs compared with the NC group ($p < 0.05$, Bonferroni corrected). In addition, MSE also showed strong sensitivity in differentiating NC from EMCI (one ROI), NC from LMCI (eight ROIs), EMCI from LMCI (one ROI), EMCI from AD (three ROIs), and LMCI from AD (one ROI). As can be seen from **Figure 4**, the complexity of BOLD signals in most ROIs showed a gradually decline from NC to EMCI to LMCI and to AD. Previous complexity studies of fMRI signals also consistently reported reduced complexity in AD patients compared to matched control subjects (Liu et al., 2013; Wang et al., 2017). Liu et al. (2013) reported decreased complexities in STG, MTG, and SMG in familial AD. Some of brain regions, such as SFGdor, MTG, and IOG, were also reported in our previous study using PE method to analyze the complexity of the same ADNI dataset (Wang et al., 2017).

We performed correlation analyses between complexity of BOLD signals in these brain regions with significant MSE differences and cognitive function scores (MMSE, FAQ, and CDR). These three clinical measurements provide quantitative assessments of cognitive function and are widely used (Ciesielska et al., 2016; Kaur et al., 2016; Kim et al., 2017). Higher scores of MMSE indicate higher aptitude of cognition; low functional performance is related to higher FAQ scores and the presence of dementia is indicated by higher CDR scores. Our correlation results showed that the average MSE of some brain regions was significantly positively correlated with the MMSE scores and significantly negatively correlated with FAQ scores and CDR scores in patient groups ($p < 0.05$, corrected). This means that lower MMSE and higher FAQ and CDR scores were observed in MCI and AD patients who exhibited lower MSE in some brain regions. Particularly, THA.R exhibited significant correlations between MSE values and three clinical measurement scores (MMSE, FAQ, and CDR) on scale 2. The MSE values of SMG.R showed significant correlations with the MMSE and CDR scores on scale 6. Previous fMRI studies suggested that THA and SMG are closely related to cognitive dysfunction in healthy aging and AD (Mevel et al., 2011; Yang et al., 2013; Xiaoying et al., 2014; Raczek et al., 2017). Studies found that activity in THA is associated with spatial working memory and memory processing (Jankowski et al., 2013; Saalmann and Kastner, 2015; Štillová et al., 2015; Hallock et al., 2016), and SMG is mainly involved in language perception, phonological processing and verbal working memory and processing (Hartwigsen et al., 2010; Kheradmand et al., 2013; Deschamps et al., 2014). In addition, as can be seen from **Figure 5**, significant correlations between MSE and cognitive measurements were dependent on the temporal scales. For example, we observed THA.R showed associations between complexity and MMSE at high temporal frequencies, and SMG.R exhibited significant correlations at low

temporal frequencies. The results showed that different brain regions displayed correlations at different frequencies and once again corroborated the MSE theory that high and low temporal frequencies may represent region or network-dependent different neuropathophysiological mechanisms (Buzsáki and Draguhn, 2004; Zuo et al., 2010).

Potential Physiological Underpinnings of Altered Complexity in Patient Groups

It has been suggested that physiological diseases are associated with a loss of complexity in healthy systems (Lipsitz, 2004; Pincus, 2010). AD is a neurodegenerative disorder characterized by dementia and cognitive decline (Querfurth and Laferla, 2010). The brain regions that we found to have reduced complexity play important roles for cognitive functions. For example, the lingual gyrus is believed to play a role in the analysis of logical conditions and encoding visual memories. The superior temporal gyrus is involved in social cognition processes and middle temporal gyrus is mainly involved in the recognition of known faces and episodic memory (Bigler et al., 2007; Acheson and Hagoort, 2013). Some fMRI experiments have found proof that the superior frontal gyrus is involved in self-awareness, sensory system, and social cognitive processes (Goldberg et al., 2006). The altered complexity of these brain regions in patient groups may be associated with deterioration of brain function in these important networks.

Further, AD is characterized by the presence of neuritic plaques and neurofibrillary tangles, accompanied by widespread cortical neuronal loss, and loss of connections between brain systems (Sankari, 2010). This may degrade cortical and sub-cortical connections, leading to cognitive and behavioral disturbances. Many studies have reported that disrupted FC in the AD group in THA, SFGdor, INS, STG, MTG, IOG, and SMG (Zhang et al., 2009; Wang et al., 2010; Dennis and Thompson, 2014). Thus, this degeneration of both local and long-range connections disrupts the functional coherence of brain activation, decreasing the complexity of spontaneous brain activity.

In addition, we examined the relationships between MSE and GMV in patient groups. After corrections for multiple comparisons, no significant correlation was found between the complexity of BOLD signals and GMV. But LING.R, STG.R, and MTG.L exhibited trend positive correlations ($p < 0.05$, uncorrected) between the MSE and the GMV in patient groups. Many studies have also reported GM atrophy in these brain regions in MCI and AD (Busatto et al., 2003; Karas et al., 2004; Guo et al., 2010; Möller et al., 2013). In our previous study, we also found that the complexity of these brain regions was related to GMV and was associated with glucose metabolism (Wang et al., 2017). More pathologies of AD may lead to lower complexity of brain regions still requires further study.

Comparison of SE, PE, MSE, and Multiscale PE

Sample entropy solved the problem of vector self-matching in the ApEn defined by the Heaviside function and has been widely used (Pincus, 1991; Richman and Moorman, 2000). PE is different from SE, as PE calculates the probability of a symbolic sequence of points in the phase space and the entropy value in the form of Shannon information entropy (Bandt and Pompe, 2002). Many researchers prefer to use SE and PE to study the complexity of time series and obtain findings on a single scale (Sokunbi et al., 2013; Berger et al., 2017; Wang et al., 2017; Aktaruzzaman, 2018). Compared with PE and SE, MSE and multiscale PE (MPE) investigate the dynamic complexity of time series data across multiple temporal scales, not only at the original time scale of 1 (Costa et al., 2002; Aziz and Arif, 2005; Ouyang et al., 2013).

In this study, we found significant complexity differences among four groups on multiple temporal scales, especially on longer time scales, due to MSE's capability to average out short time scale fluctuations (Smith et al., 2014; Yan et al., 2017). Thus, compared with SE, researchers performed MSE for complexity analysis obtained richer and more comprehensive information in aging and neurodegenerative diseases (Humeauheurtier, 2016; Shang, 2017). Our previous research investigated the abnormal complexity of BOLD signals in MCI and AD patients using PE analysis (Wang et al., 2017). Then, we also applied MPE to the same dataset, but no significant difference was found on longer scales ($p < 0.005$, GRF correction). Some studies demonstrated that PE had better anti-noise performance and thus, compared with SE, we got supplementary information in detecting differences among four groups on scale 1 (Bandt and Pompe, 2002; Nicolaou and Georgiou, 2012; Wang et al., 2017). The coarse-grained procedures in MPE with large scale factors may result in short data length, while PE requires more time points to contain more states of the reconstructed sequence (Bandt and Pompe, 2002). This may be the reason that we did not detect the significant PE difference at longer time scales. As a consequence, for our dataset, MPE had better performance at short time scales, while MSE could provide more information on multiple time scales. In the future, we will perform and compare SE and PE analysis across multiple time scales on more rs-fMRI datasets to further our understanding on this issue.

Limitation

A limitation of this study is the short BOLD time series used for MSE analysis which may lead to potentially erratic entropy estimation (Costa et al., 2002; Yang et al., 2013). In this study, we performed the parameter selection for MSE calculation by using 6 different parameter pairs based on previous studies, not all of the parameter pairs. The results of $m = 2$ and $r = 0.35$ were mainly reported in this study. The selection of parameters may be related to particular datasets, and different datasets may have different optimal parameters.

CONCLUSION

Multiscale entropy is a powerful tool to quantify the nonlinear information of a time series over multiple time scales through the SE algorithm. This study applied MSE analysis to investigate the abnormal complexity of BOLD signals across multiple time scales in MCI and AD patients. Enhanced MSE differences were detected among four groups which were significantly correlated

with clinical assessments in patient groups at multiple temporal scales. The MCI and AD patients demonstrated lower complexity than normal controls and AD patients showed lower complexity than MCI. These findings indicate that MSE of spontaneous BOLD signals may provide an imaging marker of cognitive impairment in MCI and AD.

ALZHEIMER'S DISEASE NEUROIMAGING INITIATIVE

The data used in preparation of this article were obtained from the Alzheimer's disease neuroimaging initiative (ADNI) database adni.loni.usc.edu. As such, the investigators within the ADNI contributed to the design and implementation of the ADNI and/or provided data but did not participate in analysis or writing of this report. A complete listing of the ADNI investigators can be found at http://adni.loni.usc.edu/wpcontent/uploads/how_to_apply/ADNI_Acknowledgement_List.pdf.

AUTHOR CONTRIBUTIONS

YN performed the experiment and completed the manuscript. BW, MZ, JX, HS, RC, and XC provided suggestions for this study. JX provided the guidance throughout the study.

FUNDING

This study was supported by the National Natural Science Foundation of China (61503272, 61305142, 61741212, and 61373101), the Natural Science Foundation of Shanxi Province (2015021090 and 201601D202042), a project funded by the China Postdoctoral Science Foundation (2016M601287), and the Shanxi Provincial Foundation for Returned Scholars, China (2016-037).

Data collection and sharing for this project was funded by the Alzheimer's disease neuroimaging initiative (ADNI) (National Institutes of Health Grant U01 AG024904) and DOD ADNI (Department of Defense award number W81XWH-12-2-0012). ADNI was funded by the National Institute on Aging and the National Institute of Biomedical Imaging and Bioengineering and through generous contributions from the following: AbbVie, Alzheimer's Association; Alzheimer's Drug Discovery Foundation; Araclon Biotech; BioClinica, Inc.;Biogen; Bristol-Myers Squibb Company; CereSpir, Inc.; Cogstate; Eisai Inc.; Elan Pharmaceuticals, Inc.; Eli Lilly and Company; EuroImmun; F. Hoffmann-La Roche Ltd and its affiliated company Genentech, Inc.; Fujirebio; GE Healthcare; IXICO Ltd.; Janssen Alzheimer Immunotherapy Research and Development, LLC.; Johnson & Johnson Pharmaceutical Research and Development LLC.; Lumosity; Lundbeck; Merck & Co., Inc.; Meso Scale Diagnostics, LLC.; NeuroRx Research; Neurotrack Technologies; Novartis Pharmaceuticals Corporation; Pfizer Inc.; Piramal Imaging; Servier; Takeda Pharmaceutical Company; and Transition Therapeutics. The Canadian Institutes of Health Research provides funds to support ADNI clinical sites in Canada. Private sector contributions are facilitated by the Foundation for the National Institutes of Health (www.fnih.org). The grantee organization is the Northern California Institute for Research and Education, and the study is coordinated by the Alzheimer's Therapeutic Research Institute at the University of Southern California. ADNI data are disseminated by the Laboratory for Neuro Imaging at the University of Southern California.

SUPPLEMENTARY MATERIAL

The Supplementary Material for this article can be found online at: https://www.frontiersin.org/articles/10.3389/fnins.2018.00677/full#supplementary-material

REFERENCES

Acheson, D. J., and Hagoort, P. (2013). Stimulating the brain's language network: syntactic ambiguity resolution after TMS to the inferior frontal gyrus and middle temporal gyrus. *J. Cogn. Neurosci.* 25, 1664–1677. doi: 10.1162/jocn_a_00430

Aktaruzzaman, M. (2018). Low computational cost for sample entropy. *Entropy* 20:61. doi: 10.3390/e20010061

Aziz, W., and Arif, M. (2005). "Multiscale permutation entropy of physiological time series," in *International Multitopic Conference* (New York, NY: IEEE INMIC), 1–6.

Ballard, C., Gauthier, S., Corbett, A., Brayne, C., Aarsland, D., and Jones, E. (2011). Alzheimer's disease. *Lancet* 377, 1019–1031. doi: 10.1016/S0140-6736(10)61349-9

Bandt, C., and Pompe, B. (2002). Permutation entropy: a natural complexity measure for time series. *Phys. Rev. Lett.* 88:174102.

Belleville, S., Clément, F., Mellah, S., Gilbert, B., Fontaine, F., and Gauthier, S. (2011). Training-related brain plasticity in subjects at risk of developing Alzheimer's disease. *Brain* 134, 1623–1634. doi: 10.1093/brain/awr037

Berger, S., Schneider, G., Kochs, E., and Jordan, D. (2017). Permutation entropy: too complex a measure for EEG time series? *Entropy* 19:692. doi: 10.3390/e19120692

Bigler, E. D., Mortensen, S., Neeley, E. S., Ozonoff, S., Krasny, L., Johnson, M., et al. (2007). Superior temporal gyrus, language function, and autism. *Dev. Neuropsychol.* 31, 217–238. doi: 10.1080/87565640701190841

Busatto, G. F., Garrido, G. E., Almeida, O. P., Castro, C. C., Camargo, C. H., Cid, C. G., et al. (2003). A voxel-based morphometry study of temporal lobe gray matter reductions in Alzheimer's disease. *Neurobiol. Aging* 24, 221–231. doi: 10.1016/S0197-4580(02)00084-2

Buzsáki, G., and Draguhn, A. (2004). Neuronal oscillations in cortical networks. *Science* 304, 1926–1929. doi: 10.1126/science.1099745

Catarino, A., Churches, O., Baron-Cohen, S., Andrade, A., and Ring, H. (2011). Atypical EEG complexity in autism spectrum conditions: a multiscale entropy analysis. *Clin. Neurophysiol.* 122, 2375–2383. doi: 10.1016/j.clinph.2011.05.004

Ciesielska, N., Sokołowski, R., Mazur, E., Podhorecka, M., Polak-Szabela, A., and Kędziora-Kornatowska, K. (2016). Is the montreal cognitive assessment (MoCA) test better suited than the mini-mental state examination (MMSE) in mild cognitive impairment (MCI) detection among people aged over 60? *Meta-Anal. Psychiatr. Polska* 50, 1039–1052. doi: 10.12740/PP/45368

Costa, M., Goldberger, A. L., and Peng, C. K. (2002). Multiscale entropy analysis of complex physiologic time series. *Phys. Rev. Lett.* 89:068102.

Costa, M., Goldberger, A. L., and Peng, C. K. (2005). Multiscale entropy analysis of biological signals. *Phys. Rev. E Statist. Nonlin. Soft Matter. Phys.* 71(2 Pt 1), 021906. doi: 10.1103/PhysRevE.71.021906

Dennis, E. L., and Thompson, P. M. (2014). Functional brain connectivity using fMRI in aging and Alzheimer's disease. *Neuropsychol. Rev.* 24, 49–62. doi: 10.1093/cercor/bhu259

Deschamps, I., Baum, S. R., and Gracco, V. L. (2014). On the role of the supramarginal gyrus in phonological processing and verbal working memory: evidence from rTMS studies. *Neuropsychologia* 53, 39–46. doi: 10.1016/j.neuropsychologia.2013.10.015

Escudero, J., Abásolo, D., Hornero, R., Espino, P., and López, M. (2006). Analysis of electroencephalograms in Alzheimer's disease patients with multiscale entropy. *Physiol. Measur.* 27:1091. doi: 10.1088/0967-3334/27/11/004

Fox, M. D., Snyder, A. Z., Vincent, J. L., and Raichle, M. E. (2007). Intrinsic fluctuations within cortical systems account for intertrial variability in human behavior. *Neuron* 56, 171–184. doi: 10.1016/j.neuron.2007.08.023

Friston, K. J., Harrison, L., and Penny, W. (2003). Dynamic causal modelling. *Neuroimage* 19, 1273–1302. doi: 10.1016/S1053-8119(03)00202-7

Goldberg, I. I., Harel, M., and Malach, R. (2006). When the brain loses its self: prefrontal inactivation during sensorimotor processing. *Neuron* 50, 329–339. doi: 10.1016/j.neuron.2006.03.015

Guo, X., Wang, Z., Li, K., Li, Z., Qi, Z., Jin, Z., et al. (2010). Voxel-based assessment of gray and white matter volumes in Alzheimer's disease. *Neurosci. Lett.* 468, 146–150. doi: 10.1016/j.neulet.2009.10.086

Hallock, H. L., Wang, A., and Griffin, A. L. (2016). Ventral midline thalamus is critical for hippocampal-prefrontal synchrony and spatial working memory. *J. Neurosci.* 36, 8372–8389. doi: 10.1523/JNEUROSCI.0991-16.2016

Hartwigsen, G., Baumgaertner, A., Price, C. J., Koehnke, M., Ulmer, S., and Siebner, H. R. (2010). Phonological decisions require both the left and right supramarginal gyri. *Proc. Natl. Acad. Sci. U.S.A.* 107, 16494–16499. doi: 10.1073/pnas.1008121107

He, B. J., Zempel, J. M., Snyder, A. Z., and Raichle, M. E. (2010). The temporal structures and functional significance of scale-free brain activity. *Neuron* 66, 353–369. doi: 10.1016/j.neuron.2010.04.020

Humeauheurtier, A. (2016). The multiscale entropy algorithm and its variants: a review. *Entropy* 17, 3110–3123. doi: 10.3390/e17053110

Jankowski, M. M., Ronnqvist, K. C., Marian, T., Vann, S. D., Wright, N. F., Erichsen, J. T., et al. (2013). The anterior thalamus provides a subcortical circuit supporting memory and spatial navigation. *Front. Syst. Neurosci.* 7:45. doi: 10.3389/fnsys.2013.00045

Karas, G., Scheltens, P., Rombouts, S., Visser, P., Van Schijndel, R., Fox, N., et al. (2004). Global and local gray matter loss in mild cognitive impairment and Alzheimer's disease. *Neuroimage* 23, 708–716. doi: 10.1016/j.neuroimage.2004.07.006

Kaur, N., Belchior, P., Gelinas, I., and Bier, N. (2016). Critical appraisal of questionnaires to assess functional impairment in individuals with mild cognitive impairment. *Int. Psychogeriatr.* 28, 1425–1439. doi: 10.1017/S104161021600017X

Kheradmand, A., Lasker, A., and Zee, D. S. (2013). Transcranial magnetic stimulation (TMS) of the supramarginal gyrus: a window to perception of upright. *Cereb. Cortex* 25, 765–771. doi: 10.1093/cercor/bht267

Kim, J. W., Min, S. B., Bo, K. S., Yi, D., Seo, E. H., Choe, Y. M., et al. (2017). Clinical dementia rating orientation score as an excellent predictor of the progression to Alzheimer's disease in mild cognitive impairment. *Psychiatry Investig.* 14, 420–426. doi: 10.4306/pi.2017.14.4.420

Lipsitz, L. A. (2004). Physiological complexity, aging, and the path to frailty. *Sci. Aging Knowl. Environ. Sage Ke* 2004:e16. doi: 10.1126/sageke.2004.16.pe16

Liu, C. Y., Krishnan, A. P., Yan, L., Smith, R. X., Kilroy, E., Alger, J. R., et al. (2013). Complexity and synchronicity of resting state blood oxygenation level-dependent (BOLD) functional MRI in normal aging and cognitive decline. *J. Magn. Reson. Imag. JMRI* 38, 36–45. doi: 10.1002/jmri.23961

Lu, W. Y., Chen, J. Y., Chang, C. F., Weng, W. C., Lee, W. T., and Shieh, J. S. (2015). Multiscale entropy of electroencephalogram as a potential predictor for the prognosis of neonatal seizures. *PLoS One* 10:e0144732. doi: 10.1371/journal.pone.0144732

Mcbride, J., Zhao, X., Munro, N., Jicha, G., Smith, C., and Jiang, Y. (2014). "EEG multiscale entropy dynamics in mild cognitive impairment and early Alzheimer's disease," in *Proceedings of the Biomedical Science and Engineering Center Conference* (New York, NY: IEEE), 1–4.

Mevel, K., Chételat, G., Eustache, F., and Desgranges, B. (2011). The default mode network in healthy aging and Alzheimer's disease. *Int. J. Alzheimer's Dis.* 2011:535816. doi: 10.4061/2011/535816

Michalopoulos, K., and Bourbakis, N. (2017). "Application of multiscale entropy on EEG signals for emotion detection," in *Proceeding of the IEEE Embs International Conference on Biomedical & Health Informatics* (New York, NY: IEEE).

Mizuno, T., Takahashi, T., Cho, R. Y., Kikuchi, M., Murata, T., Takahashi, K., et al. (2010). Assessment of EEG dynamical complexity in Alzheimer's disease using multiscale entropy. *Clin. Neurophysiol.* 121, 1438–1446. doi: 10.1016/j.clinph.2010.03.025

Möller, C., Vrenken, H., Jiskoot, L., Versteeg, A., Barkhof, F., Scheltens, P., et al. (2013). Different patterns of gray matter atrophy in early-and late-onset Alzheimer's disease. *Neurobiol. Aging* 34, 2014–2022. doi: 10.1016/j.neurobiolaging.2013.02.013

Morabito, F. C., Labate, D., Foresta, F. L., Bramanti, A., Morabito, G., and Palamara, I. (2012). Multivariate multi-scale permutation entropy for complexity analysis of Alzheimer's disease EEG. *Entropy* 14, 1186–1202. doi: 10.3390/e14071186

Nicolaou, N., and Georgiou, J. (2012). Detection of epileptic electroencephalogram based on permutation entropy and support vector machines. *Exp. Syst. Appl.* 39, 202–209. doi: 10.1016/j.eswa.2011.07.008

Ouyang, G., Li, J., Liu, X., and Li, X. (2013). Dynamic characteristics of absence EEG recordings with multiscale permutation entropy analysis. *Epilepsy Res.* 104, 246–252. doi: 10.1016/j.eplepsyres.2012.11.003

Peng, C. K., Costa, M., and Goldberger, A. L. (2009). Adaptive data analysis of complex fluctuations in physiologic time series. *Adv. Adap. Data Anal.* 1, 61–70. doi: 10.1142/S1793536909000035

Petersen, R. C., Smith, G. E., Waring, S. C., Ivnik, R. J., Tangalos, E. G., and Kokmen, E. (1999). Mild cognitive impairment: clinical characterization and outcome. *Arch. Neurol.* 56:303.

Pincus, S. M. (1991). Approximate entropy as a measure of system complexity. *Proc. Natl. Acad. Sci. U.S.A.* 88, 2297–2301. doi: 10.1073/pnas.88.6.2297

Pincus, S. M. (2010). Approximate entropy as a measure of irregularity for psychiatric serial metrics. *Bipolar Disord.* 8, 430–440. doi: 10.1111/j.1399-5618.2006.00375.x

Querfurth, H. W., and Laferla, F. M. (2010). Alzheimer's disease. *N. Engl. J. Med.* 362:329. doi: 10.1056/NEJMra0909142

Raczek, M., Cercignani, M., Gallaher, L. M., and Banerjee, S. (2017). Neural correlates of cognitive and functional impairment in alzheimer's disease: a community memory clinic cohORT. *Alzheimer's Dementia* 13(7, Suppl.), P1374. doi: 10.1016/j.jalz.2017.06.2118

Richman, J. S., and Moorman, J. R. (2000). Physiological time-series analysis using approximate entropy and sample entropy. *Am. J. Physiol. Heart Circul. Physiol.* 278:H2039. doi: 10.1152/ajpheart.2000.278.6.H2039

Saalmann, Y. B., and Kastner, S. (2015). The cognitive thalamus. *Front. Syst. Neurosci.* 9:39. doi: 10.3389/fnsys.2015.00039

Sankari, Z. T. (2010). Local and distal coherence as a measure of cortical connectivity in Alzheimer's disease, Alzheimers demen. *J. Alzheimers Assoc.* 6, S373–S373.

Shang, C. (2017). Time series complexity research based on multiscale sample entropy. *Modern Electron. Tech.* 40, 40–43.

Smith, R. X., Yan, L., and Wang, D. J. (2014). Multiple time scale complexity analysis of resting state FMRI. *Brain Imag. Behav.* 8:284. doi: 10.1007/s11682-013-9276-6

Sokunbi, M. O., Cameron, G. G., Ahearn, T. S., Murray, A. D., and Staff, R. T. (2015). Fuzzy approximate entropy analysis of resting state fMRI signal complexity across the adult life span. *Med. Eng. Phys.* 37, 1082–1090. doi: 10.1016/j.medengphy.2015.09.001

Sokunbi, M. O., Fung, W., Sawlani, V., Choppin, S., Linden, D. E., and Thome, J. (2013). Resting state fMRI entropy probes complexity of brain activity in adults with ADHD. *Psychiatry Res.* 214, 341–348. doi: 10.1016/j.pscychresns.2013.10.001

Sokunbi, M. O., Gradin, V. B., Waiter, G. D., Cameron, G. G., Ahearn, T. S., Murray, A. D., et al. (2014). Nonlinear complexity analysis of brain FMRI signals in schizophrenia. *PLoS One* 9:e95146. doi: 10.1371/journal.pone.0095146

Soltysik, D. A., Peck, K. K., White, K. D., Crosson, B., and Briggs, R. W. (2004). Comparison of hemodynamic response nonlinearity across primary cortical areas. *Neuroimage* 22, 1117–1127. doi: 10.1016/j.neuroimage.2004.03.024

Song, X. W., Dong, Z. Y., Long, X. Y., Li, S. F., Zuo, X. N., Zhu, C. Z., et al. (2011). REST: a toolkit for resting-state functional magnetic resonance imaging data processing. *PLoS One* 6:e25031. doi: 10.1371/journal.pone.0025031

Sporns, O., Tononi, G., and Edelman, G. M. (2000). Connectivity and complexity: the relationship between neuroanatomy and brain dynamics. *Neural Netw.* 13, 909–922. doi: 10.1016/S0893-6080(00)00053-8

Stephan, K. E., Kasper, L., Harrison, L. M., Daunizeau, J., den Ouden, H. E., Breakspear, M., et al. (2008). Nonlinear dynamic causal models for fMRI. *Neuroimage* 42, 649–662. doi: 10.1016/j.neuroimage.2008.04.262

Štillová, K., Jurák, P., Chládek, J., Chrastina, J., Halámek, J., Bočková, M., et al. (2015). The role of anterior nuclei of the thalamus: a subcortical gate in memory processing: an intracerebral recording study. *PLoS One* 10:e0140778. doi: 10.1371/journal.pone.0140778

Wang, B., Niu, Y., Miao, L., Cao, R., Yan, P., Guo, H., et al. (2017). Decreased complexity in Alzheimer's disease: resting-state fMRI evidence of brain entropy mapping. *Front. Aging Neurosci.* 9:378. doi: 10.3389/fnagi.2017.00378

Wang, D. J., Jann, K., Fan, C., Qiao, Y., Zang, Y.-F., Lu, H., et al. (2018). Neurophysiological basis of multi-scale entropy of brain complexity and its relationship with functional connectivity. *Front. Neurosci.* 12:352. doi: 10.3389/fnins.2018.00352

Wang, K., Liang, M., Wang, L., Tian, L., Zhang, X., Li, K., et al. (2010). Altered functional connectivity in early Alzheimer's disease: a resting-state fMRI study. *Hum. Brain Mapp.* 28, 967–978. doi: 10.1002/hbm.20324

Wang, P., Rui, L., Jing, Y., Huang, Z., and Li, J. (2016). Frequency-dependent brain regional homogeneity alterations in patients with mild cognitive impairment during working memory state relative to resting state. *Front. Aging Neurosci.* 8:60. doi: 10.3389/fnagi.2016.00060

Wu, J., Yan, T., Zhang, Z., Jin, F., and Guo, Q. (2012). Retinotopic mapping of the peripheral visual field to human visual cortex by functional magnetic resonance imaging. *Hum. Brain Mapp.* 33, 1727–1740. doi: 10.1002/hbm.21324

Xiang, J., Li, C., Li, H., Cao, R., Wang, B., Han, X., et al. (2015). The detection of epileptic seizure signals based on fuzzy entropy. *J. Neurosci. Methods* 243, 18–25. doi: 10.1016/j.jneumeth.2015.01.015

Xiaoying, T., Dominic, H., Dale, A. M., Laurent, Y., and Miller, M. I. (2014). Shape abnormalities of subcortical and ventricular structures in mild cognitive impairment and Alzheimer's disease: detecting, quantifying, and predicting. *Hum. Brain Mapp.* 35, 3701–3725. doi: 10.1002/hbm.22431

Yan, C. G., Wang, X. D., Zuo, X. N., and Zang, Y. F. (2016). DPABI: data processing & analysis for (resting-state) brain imaging. *Neuroinformatics* 14, 339–351. doi: 10.1007/s12021-016-9299-4

Yan, T., Feng, Y., Liu, T., Wang, L., Mu, N., Dong, X., et al. (2017). Theta oscillations related to orientation recognition in unattended condition: a vMMN study. *Front. Behav. Neurosci.* 11:166. doi: 10.3389/fnbeh.2017.00166

Yang, A. C., Huang, C. C., Yeh, H. L., Liu, M. E., Hong, C. J., Tu, P. C., et al. (2013). Complexity of spontaneous BOLD activity in default mode network is correlated with cognitive function in normal male elderly: a multiscale entropy analysis. *Neurobiol. Aging* 34, 428–438. doi: 10.1016/j.neurobiolaging.2012.05.004

Yang, A. C., Tsai, S. J., Yang, C. H., Kuo, C. H., Chen, T. J., and Hong, C. J. (2011). Reduced physiologic complexity is associated with poor sleep in patients with major depression and primary insomnia. *J. Affect. Disord.* 131, 179–185. doi: 10.1016/j.jad.2010.11.030

Yu, R., Hsieh, M. H., Wang, H. L. S., Liu, C. M., Liu, C. C., Tzung-Jeng, H., et al. (2013). Frequency dependent alterations in regional homogeneity of baseline brain activity in schizophrenia. *PLoS One* 8:e57516. doi: 10.1371/journal.pone.0057516

Zhang, H. Y., Wang, S. J., Xing, J., Liu, B., Ma, Z. L., Yang, M., et al. (2009). Detection of PCC functional connectivity characteristics in resting-state fMRI in mild Alzheimer's disease. *Behav. Brain Res.* 197, 103–108. doi: 10.1016/j.bbr.2008.08.012

Zhou, F., Huang, S., Zhuang, Y., Gao, L., and Gong, H. (2016). Frequency-dependent changes in local intrinsic oscillations in chronic primary insomnia: a study of the amplitude of low-frequency fluctuations in the resting state. *Neuroimage Clin.* 15:458.

Zuo, X. N., Martino, A. D., Kelly, C., Shehzad, Z. E., Gee, D. G., Klein, D. F., et al. (2010). The oscillating brain: complex and reliable. *Neuroimage* 49:1432. doi: 10.1016/j.neuroimage.2009.09.037

Conflict of Interest Statement: The authors declare that the research was conducted in the absence of any commercial or financial relationships that could be construed as a potential conflict of interest.

frontiers in Neuroscience

ORIGINAL RESEARCH
published: 04 October 2018
doi: 10.3389/fnins.2018.00685

Topological Pattern Recognition of Severe Alzheimer's Disease via Regularized Supervised Learning of EEG Complexity

Miaolin Fan[1], *Albert C. Yang*[2,3], *Jong-Ling Fuh*[4,5] *and Chun-An Chou*[1]*

[1] Department of Mechanical and Industrial Engineering, Northeastern University, Boston, MA, United States, [2] Division of Interdisciplinary Medicine and Biotechnology, Beth Israel Deaconess Medical Center, Harvard Medical School, Boston, MA, United States, [3] Institute of Brain Sciences, National Yang-Ming University, Taipei, Taiwan, [4] Neurological Institute, Taipei Veterans General Hospital, Taipei, Taiwan, [5] School of Medicine, National Yang-Ming University, Taipei, Taiwan

Alzheimer's disease (AD) is a progressive brain disorder with gradual memory loss that correlates to cognitive deficits in the elderly population. Recent studies have shown the potentials of machine learning algorithms to identify biomarkers and functional brain activity patterns across various AD stages using electroencephalography (EEG). In this study, we aim to discover the altered spatio-temporal patterns of EEG complexity associated with AD pathology in different severity levels. We employed the multiscale entropy (MSE), a complexity measure of time series signals, as the biomarkers to characterize the nonlinear complexity at multiple temporal scales. Two regularized logistic regression methods were applied to extracted MSE features to capture the topographic pattern of MSEs of AD cohorts compared to healthy baseline. Furthermore, canonical correlation analysis was performed to evaluate the multivariate correlation between EEG complexity and cognitive dysfunction measured by the Neuropsychiatric Inventory scores. 123 participants were recruited and each participant was examined in three sessions (length = 10 seconds) to collect resting-state EEG signals. MSE features were extracted across 20 time scale factors with pre-determined parameters ($m = 2, r = 0.15$). The results showed that comparing to logistic regression model, the regularized learning methods performed better for discriminating severe AD cohort from normal control, very mild and mild cohorts (test accuracy $\sim$ 80%), as well as for selecting significant biomarkers arcoss the brain regions. It was found that temporal and occipitoparietal brain regions were more discriminative in regard to classifying severe AD cohort vs. normal controls, but more diverse and distributed patterns of EEG complexity in the brain were exhibited across individuals in early stages of AD.

Keywords: Alzheimer's disease, EEG, complexity analysis, pattern recognition, LASSO

OPEN ACCESS

Edited by:
Laura Marzetti,
Università degli Studi G. d'Annunzio Chieti e Pescara, Italy

Reviewed by:
Elzbieta Olejarczyk,
Institute of Biocybernetics and Biomedical Engineering (PAN), Poland
Filippo Zappasodi,
Università degli Studi G. d'Annunzio Chieti e Pescara, Italy

***Correspondence:**
Chun-An Chou
ch.chou@northeastern.edu

Specialty section:
This article was submitted to Brain Imaging Methods, a section of the journal Frontiers in Neuroscience

Received: *28 April 2018*
Accepted: *12 September 2018*
Published: *04 October 2018*

Citation:
Fan M, Yang AC, Fuh J-L and Chou C-A (2018) Topological Pattern Recognition of Severe Alzheimer's Disease via Regularized Supervised Learning of EEG Complexity. Front. Neurosci. 12:685. doi: 10.3389/fnins.2018.00685

1. INTRODUCTION

Alzheimer's disease (AD) is a neurodegenerative disorder characterized by progressive loss of memory and cognitive dysfunctions. Despite of many efforts, the pathological mechanism of AD progression still remains unsettled. In recent decades, the emerging field of interdisciplinary studies between computational cognitive and data sciences has enabled data-driven knowledge discovery

systems for investigating multivariate patterns based on large-scale, complex brain data. More specifically, advances of machine learning techniques have contributed to the clinical science by not only improving the automated diagnostic/predictive tools, but also enhancing the understanding of pathological mechanism underlying AD progression. In the past years, there were studies to demonstrate the capability of machine learning algorithms in addressing the sophisticated patterns using various brain data, e.g., electroencephalography (EEG) and magnetic resonance imaging (MRI). Trambaiolli et al. (2011) identified the bipolar peaks of EEG signals as biomarkers for differentiating AD, mild cognitive impairments (MCI) and early dementia patients. Casanova et al. (2011) found that most informative voxels in structural MRI data locate in the gray and white matter tissues, which can discriminate patients from cognitive normal subjects accurately using large-scale regularization. Other studies encouraged the utilization of an integrative EEG biomarkers derived from various sources in order to provide predictive models with diverse and comprehensive information (Poil et al., 2013; Triggiani et al., 2017).

Among modern neuroimaging modalities, EEG as a non-invasive, inexpensive technique has drawn extensive attentions for investigating nonlinear dynamics of neuronal brain functions. It was reported that AD progression can be characterized by the reduced complexity in EEG signals, which is hypothesized to be related to the loss of neurons and possible connectivity caused by pathological aging process. A recent and comprehensive review is refered to Dauwels et al. (2010). In this study, we used Multiscale Entropy (MSE) for estimating the nonlinear complexity of EEG signals across multiple temporal scales (Costa et al., 2002). Previous studies investigated MSE as a measure of complexity for understanding AD pathology using univariate (Escudero et al., 2006; Park et al., 2007) and multivariate EEG dynamics (Labate et al., 2013). It was reported that the decreased complexity in short-time scale and increased complexity in long-time scale distinguish AD patients from normal controls (Mizuno et al., 2010; Yang et al., 2013). A recent study (Azami et al., 2017) also indicated the potentials of the second-order MSE features for characterizing EEG changes with AD progression. Moreover, correlation was found between MSE features from various brain regions and multiple neuropsychiatric symptoms, particularly in temporal and occipitoparietal electrodes (Yang et al., 2013). Since the previous study only assessed the bivariate correlation, we extend to investigate the relationships in a multivariate feature space by applying canonical correlation analysis (CCA) (Hotelling, 1936). CCA is a multivariate technique that is capable to capture multiple causes and effects to further investigate the relationship between MSE and neuropsychiatric symptoms.

One of the most challenging tasks for understanding AD pathology is to characterize the biomarkers and associated patterns that differentiate different AD severity levels. Considering the pathological aging of the brain is a highly heterogeneous process, the generalizability in many existing research studies is limited by the small sample size, large individual variability, and high-dimensional data structure. While most state-of-the-art machine learning algorithms suffered from over-fitting data and produced poor generalized prediction results, regularized learning methods attempt to address this over-fitting issue by adding a regularization term (called L_1-norm or L_2-norm) to the cost function. Least Absolute Shrinkage and Selection Operator (LASSO) (Tibshirani, 1996) is a classic method that builds a regression model of correlating input variables (MSE features in this study) to the prediction outcome (severe AD or not) while posing a penalty on the number of non-zero coefficients of input variables (L_1-norm feature selection). Later, Elastic net (ENet) was proposed by combining L_1-norm and L_2-norm for the purpose of addressing several drawbacks of LASSO, including the group effect among input variables in addition to feature selection. The flexibility and variability of regularization methods allow one to develop variants for specific purposes (Tibshirani et al., 2005; Bach, 2008). Specifically, the interpretability/stability of feature selection is desired for providing scientific insights, since consistent feature selection across different samples and individuals is more likely to suggest a meaningful pattern (Fan and Chou, 2016). Stability selection (Meinshausen and Bühlmann, 2010) is thus proposed based on the combination of feature selection method and repeated subsampling. For the cost of computational resources, the stability selection aims to provide a statistical control on the error rate of feature selection in a sparse dataset.

Based on the general concept of stability selection approach, the present study intends to provide a stability-based feature selection and identify important EEG biomarkers using the frequency of selection across multiple replicates in cross validation. The objective of our study is two fold. On one hand, we are interested in characterizing the functional brain activities with varying temporal scales that best discriminate severity levels of AD groups and normal controls based on EEG complexity. On the other hand, we aim to profile the topographic map of EEG biomarkers for various AD severity and investigate the multivariate correlation patterns to cognitive dysfunctions.

2. MATERIALS AND METHODS

2.1. Participants

One hundred and twenty-three participants were recruited from the Dementia Clinic at the Neurological Institute, Taipei Veterans General Hospital in Taiwan. The diagnosis for AD was based on the criteria of the National Institute of Neurological and Communicative Disorders and the Stroke/Alzheimer's Disease and Related Disorders Association (McKhann et al., 1984). All patients had received neurological examinations, laboratory tests, EEG monitoring, and neuroimaging evaluation during the diagnostic process. Our study was approved by the Institutional Review Board of Taipei Veterans General Hospital to conduct retrospective analysis of the patients' clinical and EEG data. We excluded patients who had other conditions that caused secondary dementia, such as vascular dementia, Parkinson's disease, hypothyroidism, vitamin B12 deficiency, syphilis, and prior history of major psychiatric illness (e.g., major depression, bipolar disorder, or schizophrenia). The participants were categorized into four groups according to their severity of dementia, assessed by the Clinical Dementia Rating (CDR) scale (Morris, 1993). In the following sections, we refer to these groups

as HC (healthy control; $N = 15$), AD1 (very mild, CDR = 0.5; $N = 15$), AD2 (mild, CDR = 1; $N = 69$), and AD3 (moderate to severe, CDR = 2; $N = 24$).

2.2. EEG Data Acquisition and Pre-processing

A routine EEG recordings were performed on all participants (Nicolet EEG, Natus Medical, Incorporated, San Carlos, CA, USA) in the EEG examination room at the Neurological Institute of Taipei Veterans General Hospital. The EEG recording protocol began with a 5-min habituation to the examining environment, followed by three consecutive sessions of 10–20 s with the eyes closed and then open, and a session of photo stimulation, while only the eye closed data was used in the present study. The recordings were performed using the international 10–20 system of 19 electrodes (Fp1, Fp2, F7, F3, Fz, F4, F8, T3, C3, Cz, C4, T4, T5, P3, Pz, P4, T6, O1, and O2) with linked ear reference, 256 Hz sampling rate and filtered at 0.05 Hz high-pass, 70 hZ low-pass and notch filter of 60 Hz, and impedance below 3 kΩ. Vigilance was monitored by the EEG technician, who alerted patients when signs of drowsiness appeared in the tracings. Vertical eyeball movement was detected from electrodes placed above and below the right eye, while the horizontal eyeball movement was detected from electrodes placed at the left outer canthus. EEG signals were preprocessed to remove the linear trend and visually inspected to ensure there were no eye movement artifacts. The EEG signals were exported in European Data Format and were processed using MATLAB 2016b (Mathworks, Inc.).

2.3. Multiscale Entropy Analysis (MSE)

In this study, we employed MSE (Costa et al., 2002) to measure the nonlinear complexity of EEG signal. Let us consider a single-channel EEG signals with length $= N$, denoted by $\{x_1, x_2, ...x_N\}$. MSE provides an estimate of the sample entropy over multiple time scales in two steps: (1) the construction of coarse-grained time series based on various scale factors, denoted by τ, and (2) the estimation of sample entropy for each time scale. In the first step, the range of τ need to be pre-defined as a set of increasing integers starting from 1. (i.e., [1, 2, ... T]). For each possible value of τ, the corresponding coarse-grained time series $y_j(\tau)$ is obtained by applying a non-overlapping sliding window with length $= \tau$ and taking the average of all values in each window, represented by the following equation ($1 \leq j \leq N/\tau$):

$$y_j(\tau) = \frac{1}{\tau} \sum_{i=(j-1)\tau+1}^{j\tau} x_i. \quad (1)$$

If we denote M as the largest integer such that $M \leq N/\tau$, the coarse-grained time series is then rewritten as $\{y_1(\tau), y_2(\tau), ..., y_j(\tau), ...y_M(\tau)\}$.

In the second step, the sample entropy (Richman and Moorman, 2000) is calculated for each coarse-grained time series as a function of τ. To calculate the sample entropy for a time series with length $= M$, two parameters need to be determined: the pattern length m and the similarity criterion r. Within the coarse-grained time series $\{y_1(\tau), y_2(\tau), ..., y_j(\tau), ...y_M(\tau)\}$, we denote a vector of pattern length $= m$ as $Y_m(k) = \{y_k(\tau), y_{k+1}(\tau), ..., y_{k+m-1}(\tau)\}$. Accordingly, the total number of pairs of vectors that satisfy $D(Y_m(k), Y_m(l)) < r(k \neq l)$ is denoted by N_m. The sample entropy $I(\tau)$ for this time series with parameters τ and r is defined as:

$$I(\tau, r) = -\log \frac{N_{m+1}}{N_m}. \quad (2)$$

In this study, we use $m = 2$ and $r = 0.15$, and the range of scale factors is [1, 20] by following our previous work (Yang et al., 2013). **Figure 1** shows the averaged raw EEG signals, spectral power and MSE scores across all groups; a cross-over is observed in the MSE curves with the increasing scale factors. In short-time scales (≤ 8), lower MSE features are observed from the severe AD group comparing to normal controls, but in long-time scales (> 8) an opposite pattern is observed.

2.4. Hybrid Machine Learning Model for Classification and Biomarker Identification

The objective of applying machine learning model to analyze the MSE features of EEG signals is two-fold: first, we intend to discriminate between control group and AD groups (AD1, AD2, and AD3) by performing a binary classification task in a one-to-one manner (exhaust all the possible combination of pairs). Second, we aim to examine the multivariate correlation patterns between MSE features and dementia symptoms rated by clinicians based on The Neuropsychiatric Inventory (NPI) (Cummings et al., 1994). After extracting MSE features from 19-channel EEG device using 20 scale factors, 380 ($= 19 \times 20$) dimensions were obtained for the feature space. The machine learning model may be over-fitted in training with the relatively less samples on this high dimensional feature space. Therefore, regularization learning methods are employed to perform classification tasks between different AD/HC groups while reducing the dimensionality of trained model. A logistic regression (LR) model is trained and fitted with a penalization on the number of features with non-zero coefficients. As a result, an automatic feature selection is performed by forcing some features to yield zero coefficients. In the following subsections, we present two classic types of regularized LR models. Furthermore, we implement canonical correlation analysis, a unsupervised learning method, for inferring the correlations among two sets of variables.

2.4.1. L_1-Norm and L_2-Norm Regularized Learning Methods

The original form of LASSO is a linear regression model with a penalty term that controls the number of non-zero coefficients for all variables. In a classification problem, LASSO is reformulated with the cost function of LR, which is rewritten as the following problem (Tibshirani, 1996; Friedman et al., 2001):

$$\max_{\beta_0,\beta} \left\{ \sum_{i=1}^{N} [y_i(\beta_0 + \beta^T x_i) - \log(1 + e^{\beta_0 + \beta^T x_i})] - \lambda \sum_{j=1}^{p} |\beta_j| \right\}, \quad (3)$$

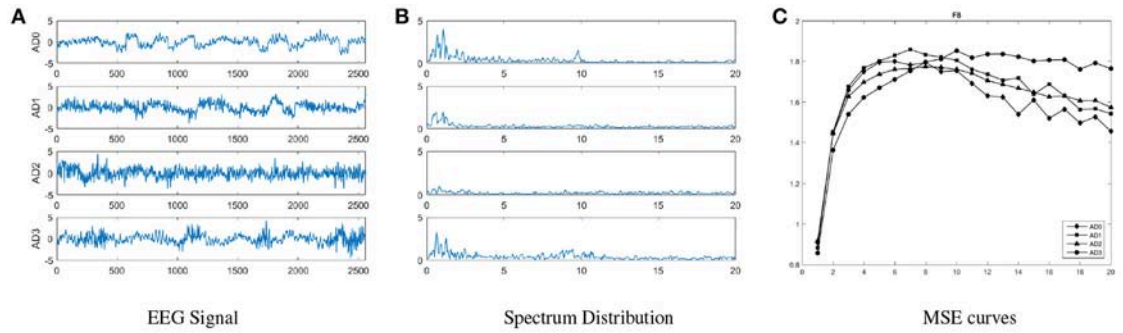

FIGURE 1 | An illustration of general distribution for each group, including **(A)** raw EEG signals, **(B)** spectral powers, and **(C)** MSE on channel F8 for all groups. These curves show that MSE curves are more distinguishable than EEG signals and spectral powers in overall, and the trend with increasing scale factors in the MSE curve of each AD group is different.

where $f(x_i) = \beta_0 + \beta^T x_i$ and y_i are the prediction and target class for the *ith* sample respectively. $\sum_{j=1}^{p} |\beta_j|$ is also known as L_1-norm penalty that controls the shrinkage with corresponding parameter λ selected via nested cross-validation.

However, LASSO attempts to addresses cluster information of correlated variables, which is referred to as grouping effect. It only selects one and drops the other variables when fitted with a group of related variables (Zou and Hastie, 2005). In this study, this grouping effect is observed among MSE features extracted from the same electrode; however, we may want to keep multiple correlated MSE variables in our model in order to characterize the correlation in spatial patterns of functional brain activity. Therefore, we used ENet, a variation of LASSO, to account for this grouping effect (Zou and Hastie, 2005). Similar to Equation (3), ENet is formulated with a penalty term but in a different format:

$$\lambda \sum_{j=1}^{p} \left[(1-\alpha)\|\beta_j\| + \alpha|\beta_j| \right], \tag{4}$$

where α is a trade-off parameter that controls the balance between L_1-norm and L_2-norm. As α approaches 1, the sparsity of solution will increase such that $\alpha = 1$ is equivalent to LASSO. On the other hand, $\alpha = 0$ is equivalent to ridge regression. As α approaches 0, the algorithm tends to encourage group selection of correlated features and stabilize the solution path. In our study, we choose the $\alpha = 0.7$ for ENet as a empirical choice.

2.4.2. CCA Between MSE and Cognitive Declines

In our study, we used CCA for analyzing the multivariate correlation patterns between MSE features and cognitive decline symptoms related to dementia. The NPI scores includes 12 symptoms: delusions (DEL), hallucinations (HAL), agitation (AG), dysphoria (DEP), anxiety (ANX), apathy (APA), irritability (IRR), euphoria (EUP), disinhibition (DIS), aberrant motor behavior (ABE), night-time behavior disturbances (NIG), and appetite and eating abnormalities (APP). CCA (Hotelling, 1936) is a multivariate analysis approach for finding the relationship between two sets of variables, **X** and **Y**, with the objective to maximize the Pearson correlation based on projections on new subspaces of **X** and **Y**. **Figure 2** illustrates the cencept. The new feature space is constructed by canonical variables set **U** and **V**, which correspond to original MSE and symptoms rating scales. CCA is formulated as follows:

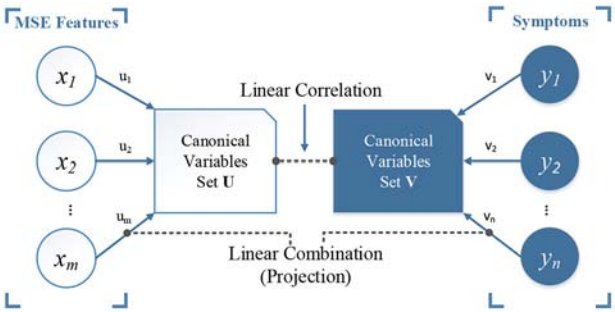

FIGURE 2 | An illustration of canonical correlation analysis. The objective is to find a linear combination (projection) of set ***X*** and ***Y***, or the rotated canonical space, by maximizing the linear correlation between the two sets of new canonical variables ***U*** and ***V*** ($\rho = 1$ in our case). In our study, we have MSE features as set ***X*** and the scores of 12 symptoms from NPI scale as set ***Y***.

$$\underset{\mathbf{u}\in R^p, \mathbf{v}\in R^q}{\arg\max} \quad \frac{\mathbf{u}^T\mathbf{X}^T\mathbf{Y}\mathbf{v}}{\sqrt{(\mathbf{u}^T\mathbf{X}^T\mathbf{X}\mathbf{u})(\mathbf{v}^T\mathbf{Y}^T\mathbf{Y}\mathbf{v})}}, \tag{5}$$

where **X** is a $n \times p$ matrix that represents n samples in p-dimensional space; **Y** is a $n \times q$ matrix that represents n samples in q-dimensional space; **X** and **Y** are two sets of paired variables that correspond to n samples. This problem is solved as a generalized eigen-decomposition problem.

2.4.3. Model Validation and Biomarker Identification

The evaluation of overall performance uses the following three metrics: (1) *accuracy* indicates the ratio of correctly classified patients in the entire sample; (2) *sensitivity* indicates the ratio of correctly identified AD patients; and (3) *specificity* indicates

the ratio of correctly identified normal controls, defined as follows:

$$\text{Accuracy} = \frac{\text{TN} + \text{TP}}{\text{TN} + \text{TP} + \text{FP} + \text{FN}}, \quad (6)$$

$$\text{Sensitivity} = \frac{\text{TP}}{\text{TP} + \text{FN}}, \quad (7)$$

$$\text{Specificity} = \frac{\text{TN}}{\text{TN} + \text{FP}}, \quad (8)$$

where TP = true positive, TN = true negative, FP = false positive, and FN = false negative. In particular, normal control group is treated as the negative class in the classification task of this study. If two groups are both AD patients, the less severe group is defined as the negative class. We reported the accuracy of both training and test set to show the potential risks of overfitting, indicated by the gap between training and testing accuracy.

The classifier will be impacted by the imbalanced data during training phase, and the trained model is usually more biased to the majority class. The Receiver Operating Characteristic (ROC) analysis is thus employed for performance evaluation. The area under ROC curve (or AUC) is used as an alternative metric without bias from the selection of threshold parameter (e.g., cut-point) in binary classification of logistic regression.

In addition, we use a leave-one-subject-out cross-validation design to minimize the bias introduced by sample variability. That is, the generalization error is estimated by leaving out samples collected from in the three sessions of one participant for testing and training the model on remaining samples. Validation repeats for all participants as testing samples. Furthermore, the importance of EEG biomarkers was assessed by overall selection frequency in all iterations.

3. RESULTS

3.1. Classification for AD Severity

Table 1 presents the classification performances of three algorithms. AD groups are considered as the target class. ENet classifier with $\alpha = 0.7$ (Enet 0.7) yields the best accuracy for classification tasks of HC vs. AD2 and AD1 vs. AD2, and LASSO classifier performs better in discriminating HC vs. AD1, AD1 vs. AD3, and AD2 vs. AD3. Neither model is able to classify AD1 vs. AD2 given the low specificity, although the AUC achieved $\sim$ 0.7. From the feature selection perspective, grouping effect is accounted for in ENet, which allows for multiple selection among correlated MSE features. This property, considering the high correlation among EEG biomarkers, may better describe the topological patterns for brain activity. Finally, LR with no regularization performed 100% accurate for the training tasks, but the model has poor generalizability because of low test set accuracy and AUC, which indicates the over-fitting issue. All the above results show that the regularized learning methods provide insights about EEG biomarkers with lower risks of over-fitting than LR models.

3.2. Multivariate Correlation Between MSE and Cognitive Declines

The structure coefficients in canonical variables for all channels and symptoms are presented in **Figure 3**. These structure coefficients can be interpreted as the loadings of each original variables (MSE features and cognitive declines) projected into the canonical space. In **Figure 3**, the left panel shows the coefficients of symptoms and right panel shows the absolute values of coefficients for MSE features across all channels. These figures describe how the MSE features and cognitive symptoms contributed to all canonical variables, which suggests a multivariate correlation pattern between clinician's rating and functional brain activity. Our study focus on canonical variables 1–6, since they have higher coefficients of MSE features. For example, in canonical variable 1, the combination of symptoms IRR, DIS, ANX and ABE is associated with channels P3, O1, O2 and central electrodes in short-term complexity, but associated with the frontal area in long-term complexity. In canonical variable 2, the combination of DIS, DEL and APA is associated with central-frontal region. In canonical variable 3, the combination of symptoms DEP, ANX, AG, APA and APP with is associated with frontal region. Canonical variables 4 and 5 present a similar correlation pattern between symptoms ANX, EUP, and APP, and frontal region, but with different signs (positive and negative). Canonical variable 6 presents a positive functional correlation between temporal regions with HAL and AG, but a negative correlation with DIS and IRR. We noted that most significant coefficients are assigned to low time factors (1–4), while very few non-zero coefficients are distributed in frontal regions for higher (5–8) time factors. In addition, canonical variables 7–12 yield relatively small coefficients comparing to canonical variables 1–6.

3.3. Topological Patterns of EEG Changes Associated With AD Severity

Figures 4, **5** display the frequency distribution of selected MSE features in all EEG channels across the brain regions. In the classification tasks of HC vs. AD1 and HC vs. AD2, the selected MSE features were concentrated in the low scale factors (1-4) and distributed diversely from frontal-central to temporal and occipital regions. In contrast, in the classification task of HC vs. AD3, a relatively consistent selection of channels was shown across subjects, mainly in channels T5, T6, O1, and O2.

4. DISCUSSION

4.1. Classification Results

In overall, we found the AD3 is most differentiable from any other groups, including both patients and controls. This result suggested a significant change in EEG complexity of moderate to severe AD patients comparing to early stage dementia. Furthermore, the mild AD patients can be discriminated from other groups in a moderate accuracy, indicating the presence of alteration in EEG dynamics can be captured ($\sim$ 70% accuracy). In contrast, none of our developed models can discriminate between control and very mild AD patients. However, the classification

TABLE 1 | Summary of classification performances for all classification tasks among three methods LASSO, Enet, and LR.

Method	Group	Sensitivity (%)	Specificity (%)	Test accuracy (%)	Train accuracy (%)	AUC
LASSO	HC vs. AD1	40.54	43.40	42.22	51.72	0.45
	HC vs. AD2	86.44	28.00	69.05	87.55	0.64
	HC vs. AD3	88.71	69.09	**79.49**	95.61	**0.83**
	AD1 vs. AD3	90.48	72.22	**82.05**	96.49	**0.87**
	AD2 vs. AD3	47.19	84.21	**72.40**	80.80	**0.71**
	AD1 vs. AD2	87.64	31.08	71.03	84.74	0.69
Enet ($\alpha = 0.7$)	HC vs. AD1	43.90	44.90	44.44	51.72	0.47
	HC vs. AD2	86.59	28.77	**69.84**	87.15	**0.64**
	HC vs. AD3	87.30	68.52	78.63	96.49	0.83
	AD1 vs. AD3	88.89	70.37	80.34	100.00	0.86
	AD2 vs. AD3	46.67	84.13	72.04	82.25	0.71
	AD1 vs. AD2	88.20	32.43	**71.83**	86.75	**0.70**
LR	HC vs. AD1	56.10	55.10	55.56	100.00	0.54
	HC vs. AD2	83.66	20.20	58.73	100.00	0.53
	HC vs. AD3	68.85	46.43	58.12	100.00	0.61
	AD1 vs. AD3	71.64	52.00	63.25	100.00	0.64
	AD2 vs. AD3	32.00	79.22	58.06	100.00	0.56
	AD1 vs. AD2	17.53	81.94	57.14	100.00	0.49

None of LR models has achieved 60% accuracy, so they are considered as ineffective models with no highlights. LASSO outperforms the other two methods for tasks HC vs. AD3, AD1 vs. AD3, and AD2 vs. AD3. Enet outperforms for tasks HC vs. AD2 and AD1 vs. AD2. The LR performs worst in all tasks. Bold highlights the best performances with accuracy at least 60%.

task of AD1 vs. AD3 yields the best accuracy (82.05%) using the LASSO classifier). This may imply that participants with less mild AD share very much complexity in common with healthy controls. In contrast, the classification task of HC vs. AD3 only yields accuracy = 79.49%. Although the classification performances in overall are not significantly high, our purpose is to utilize regularization methods to identify the brain activities patterns measured by nonlinear features of EEG collected from subjects including normal controls and AD cohorts at different severity levels. Limited by the inevitable data quality issues of EEG signals, the present study did not overemphasize the importance of accuracy because the models may learn false patterns as the result of achieving high performances on a noisy dataset. Instead, our study is focused on developing a robust model and providing scientific insights about a consistent pattern of EEG biomarkers across different individuals.

4.2. Functional Activity Patterns From Feature Selection of Regularization Models

From the classification task of HC vs. AD3, the LASSO classifier consistently selects MSE features from right temporal region across all folds in cross-validation. This finding may be consistent with prior studies that Alzheimer's disease is associated with rapid decline in the volume of medial temporal lobe (Jobst et al., 1994). It is possible that the atrophic changes in severe AD could result in prominent changes in functional brain activity so machine learning algorithm can consistently detect the difference between healthy elderly and patient with severe AD.

On the other hand, our results present that major changes with the progress to severe AD occur in occipital and parietal regions, in particular the right hemisphere with lower scale factors (1–4 and 5–8) and left hemisphere with higher scale factors (13–16 and 17–20). However, the classification task of HC vs. AD2 and HC vs. AD1 yields a unstable classification performances, and the selected channels are diversely distributed across different brain regions. This uncertainty may reflect the heterogeneous course of the disease observed in very early and mild AD. In other words, we should expect higher individual variability among patient from AD1 and AD2 comparing to AD3, and thus leads to a varying feature selection solution depending on the different partitioning of subsamples in cross-validation.

AD is known to have an insidious course of onset, with the functional decline leading the structural deficit during the course of illness. Previous studies of machine learning of AD focused mainly on structural brain imaging data, such as ADNI (Frisoni et al., 2010). Few studies have used functional brain activity data to classify AD. Therefore, our results may implicate in the early screening of AD in the future application using functional brain data. Our future direction may include more considerations for stabilizing the feature selection procedure across subjects during early developmental stages of AD. Variables from different sources, e.g., age, gender, spectral features, network metrics, asymmetry, synchrony patterns, can be introduced to build a more comprehensive model for classifying AD and normal control cohorts.

4.3. Neurological Insights for AD Progression

In our study, the regularization learning algorithms enable the discovery of meaningful associations between the model/feature

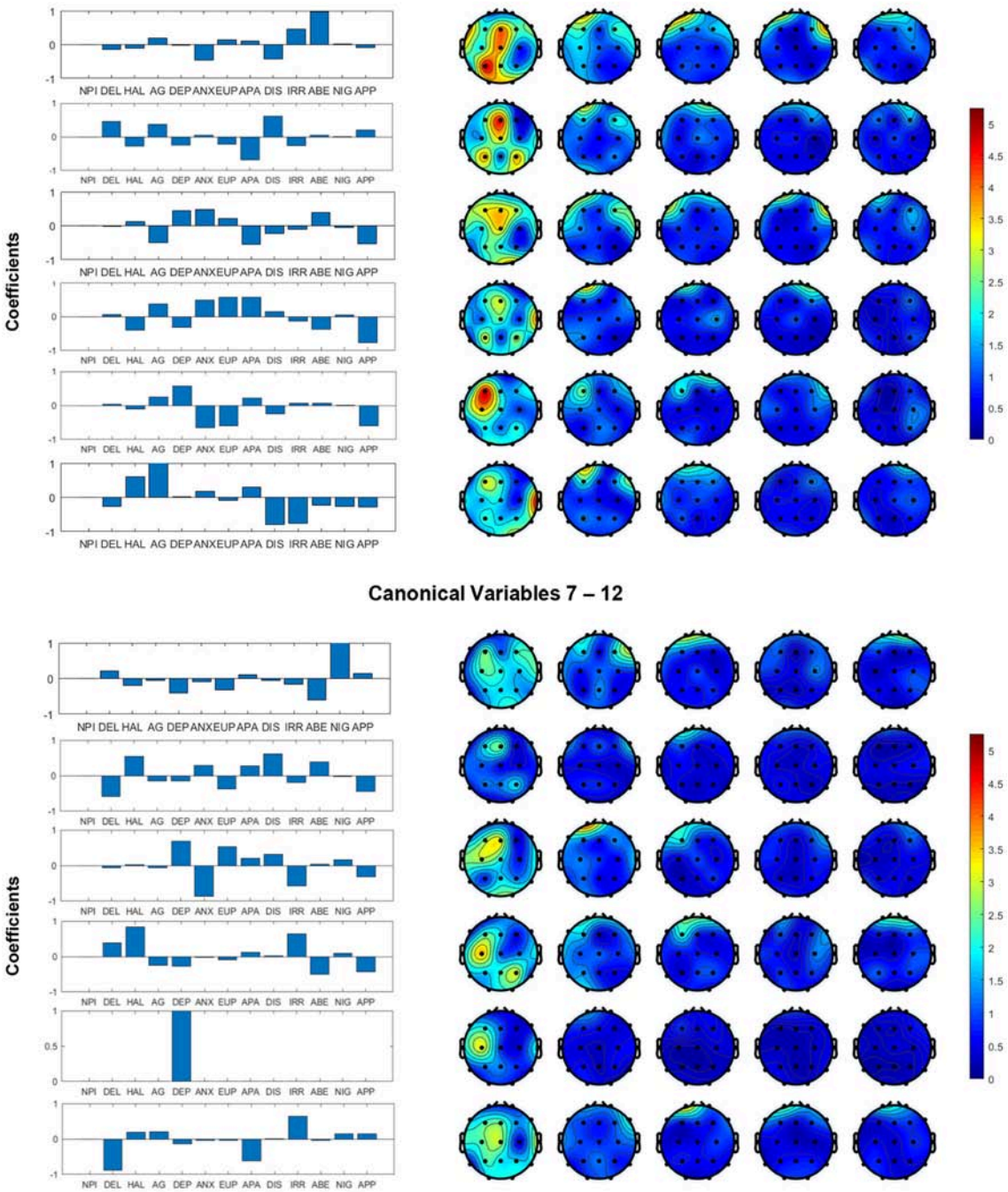

FIGURE 3 | Structural coefficients of canonical variables reformed from MSE and cognitive dysfunction symptoms. We decide to focus on the first six canonical variables because they yielded higher coefficients in the MSE features.

selection and the spatial/temporal functional brain activity patterns. Specifically, in the cross-validation, we assumed the frequency of being selected for each electrode/brain region and scale factor implies how much it accounts for the between-group differentiation. Our findings suggested the posterior brain regions as the most impacted areas from cognitive declines following dementia, which is consistent with previous quantitative EEG studies (Yang et al., 2013). The electrodes picked by regularized learning algorithm in our study also have some overlap with EEG biomarkers using a

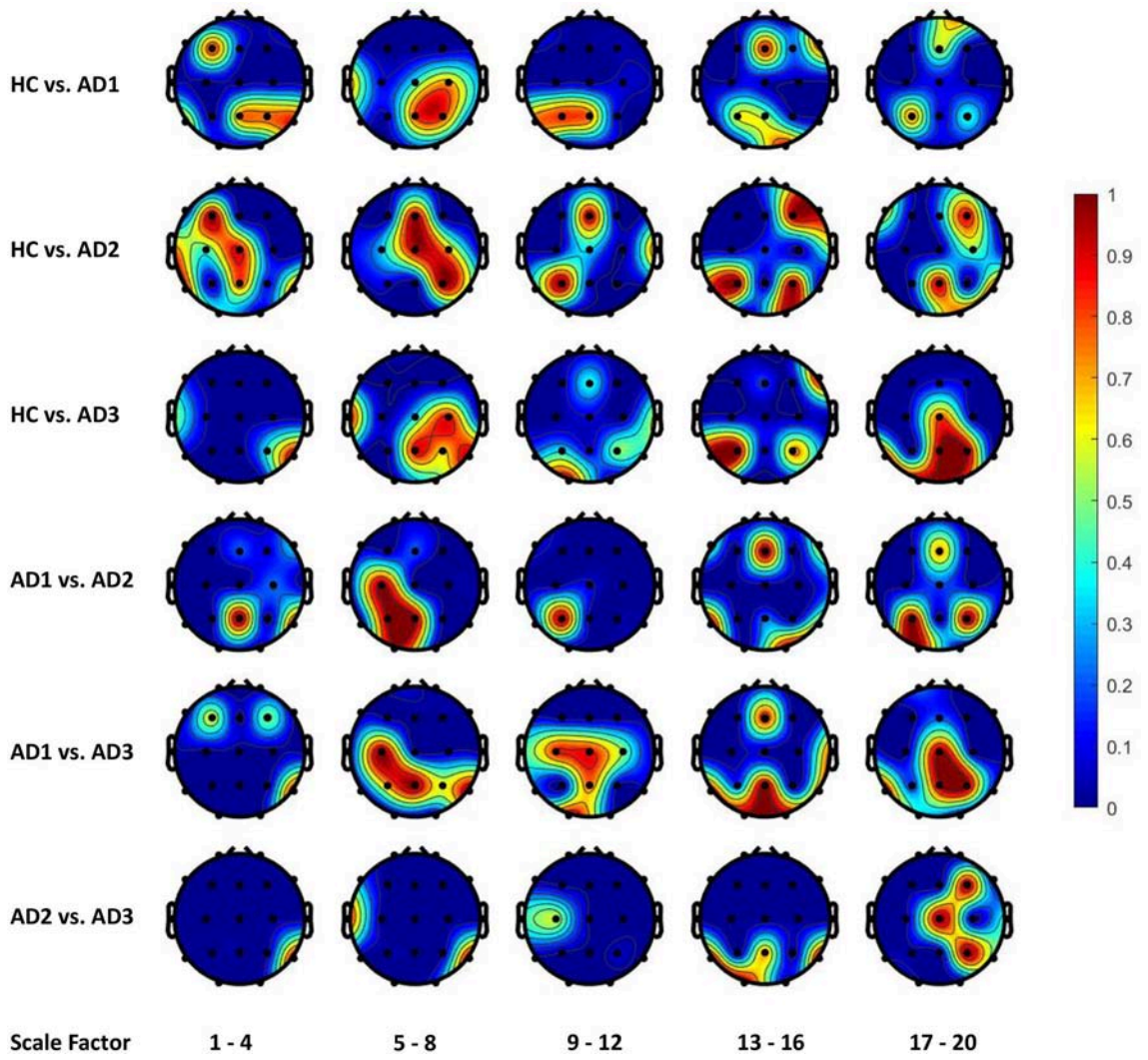

FIGURE 4 | The frequency distribution of MSE features selected by LASSO across brain regions. The plotted values are the ratio of being selected in cross validation for each electrode and scale factors; we categorize the 20 scale factors (MSE features) into 5 bins; the plotted value for each bin is the maximal frequency within the bin. For instance, if scale factors 1, 2, 3, and 4 computed using channel O1 is selected in 30, 50, 70, and 90% of all replications in cross-validation, the value assigned to channel O1 will be 0.9 for the scale factors 1–4.

multivariate extension of MSE in a recent study (Azami et al., 2017).

In addition, the multivariate correlation patterns obtained by CCA in our study suggest the grouped symptoms can provide rich information associated with MSE. We observed a collection of functional correlations of central parietal and left occipital brain regions with symptoms such as ABE and IRR, and a group of negative correlations between frontal regions with ANX, EUP, and APP. The sleep changes (reflected in NIG) were found associated with short-term complexity in occipitoparietal electrodes, which is consistent as reported by Yang et al. (2013). Our study further validated the potential of complex patterns of clustered neuropsychiatric symptoms that may be associated with EEG complexity in various regions at short- and long-term time scales.

4.4. Limitations and Future Work

The present study still has a few limitations. First, EEG data segments used in this study are relatively short (10 s), and therefore may not be able to provide long-term complexity information. Moreover, the number of trials is limited; to compromise this shortcoming, we collected multiple sessions for each participant in order to extend the sample size. Finally, since each channel was considered individually during feature extraction and classification, the interaction between electrodes may not be fully presented in our current dataset; the future work may consider connectivity patterns to give a comprehensive view of EEG alterations with AD progress. Furthermore, a multi-variate MSE (MMSE) analysis, proposed by Ahmed and Mandic (2011), that accounts for spatio-temporal dynamic brain patterns, i.e., both within-and cross-channel dependencies, will

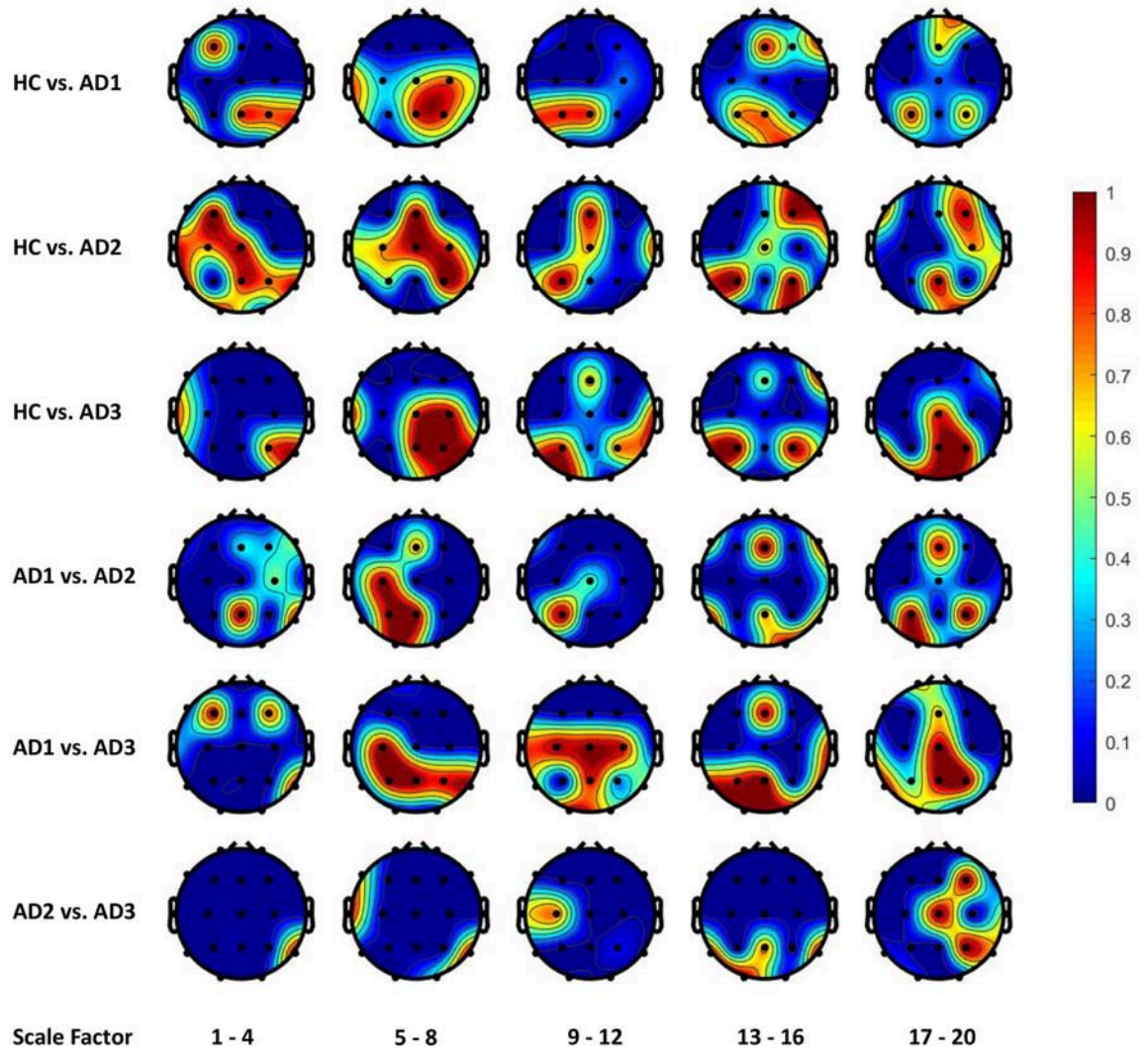

FIGURE 5 | The frequency distribution of MSE features selected by Elastic Net (alpha = 0.7) across brain regions.

be investigated and integrated in machine learning models in our AD study.

5. CONCLUSION

In this study, we examined the functional brain activity patterns in varying AD severity levels with a contrast to normal controls. MSE was used as a measure of nonlinear dynamic to represent the signals complexity using 10 seconds of resting EEG. Regularized logistic regression was applied to this supervised machine learning problem, in which we trained leave-one-subject-out cross-validated model with the MSE features for a comparison between AD cohorts and normal controls. We demonstrated ∼80% classification accuracy between severe AD cohorts and normal controls and found that the long-term complexity of EEG signals decreases with the severity of AD. Moreover, cognitive function declines can be analyzed in combination with the original MSE features to indicate the integrated correlation patterns of dementia symptoms and EEG complixity alternations. These findings relate neurological changes associated with different AD severity to the state-of-the-art assessment scales. On the other hand, regularized learning methods showed the capability for automatic selection of significant EEG biomarkers. Our future work will explore the integrative patterns including EEG complexity, synchrony and functional connectivity in this AD research direction.

AUTHOR CONTRIBUTIONS

ACY and J-LF contributed conception and design of the study, participants recruitment, experiment conduction,

and dataset collection and preprocessing. MF and C-AC are in charge of modeling and analysis methods. All authors contributed to manuscript writing and proofreading.

FUNDING

This study is supported by Northeastern University Staff Startup Funds.

REFERENCES

Ahmed, M. U., and Mandic, D. P. (2011). Multivariate multiscale entropy: a tool for complexity analysis of multichannel data. *Phys. Rev. E* 84:061918. doi: 10.1103/PhysRevE.84.061918

Azami, H., Abásolo, D., Simons, S., and Escudero, J. (2017). Univariate and multivariate generalized multiscale entropy to characterise EEG signals in Alzheimer's disease. *Entropy* 19:31. doi: 10.3390/e19010031

Bach, F. R. (2008). "Bolasso: model consistent lasso estimation through the bootstrap," in *Proceedings of the 25th International Conference on Machine Learning* (Helsinki: ACM), 33–40.

Casanova, R., Wagner, B., Whitlow, C. T., Williamson, J. D., Shumaker, S. A., Maldjian, J. A., et al. (2011). High dimensional classification of structural MRI Alzheimer's disease data based on large scale regularization. *Front. Neuroinformatics* 5:22. doi: 10.3389/fninf.2011.00022

Costa, M., Goldberger, A. L., and Peng, C.-K. (2002). Multiscale entropy analysis of complex physiologic time series. *Phys. Rev. Lett.* 89:068102. doi: 10.1103/PhysRevLett.89.068102

Cummings, J. L., Mega, M., Gray, K., Rosenberg-Thompson, S., Carusi, D. A., and Gornbein, J. (1994). The neuropsychiatric inventory: comprehensive assessment of psychopathology in dementia. *Neurology* 44, 2308–2308. doi: 10.1212/WNL.44.12.2308

Dauwels, J., Vialatte, F., and Cichocki, A. (2010). Diagnosis of alzheimer's disease from EEG signals: where are we standing? *Curr. Alzheimer Res.* 7, 487–505. doi: 10.2174/156720510792231720

Escudero, J., Abásolo, D., Hornero, R., Espino, P., and López, M. (2006). Analysis of electroencephalograms in Alzheimer's disease patients with multiscale entropy. *Physiol. Meas.* 27:1091. doi: 10.1088/0967-3334/27/11/004

Fan, M., and Chou, C.-A. (2016). Exploring stability-based voxel selection methods in mvpa using cognitive neuroimaging data: a comprehensive study. *Brain Informat.* 3, 193–203. doi: 10.1007/s40708-016-0048-0

Friedman, J., Hastie, T., and Tibshirani, R. (2001). *The Elements of Statistical Learning*, Vol. 1. New York, NY: Springer Series in Statistics.

Frisoni, G. B., Fox, N. C., Jack, C. R. Jr., Scheltens, P., and Thompson, P. M. (2010). The clinical use of structural MRI in alzheimer disease. *Nat. Rev. Neurol.* 6:67. doi: 10.1038/nrneurol.2009.215

Hotelling, H. (1936). Relations between two sets of variates. *Biometrika* 28, 321–377. doi: 10.1093/biomet/28.3-4.321

Jobst, K., Smith, A., Szatmari, M., Esiri, M., Jaskowski, A., Hindley, N., et al. (1994). Rapidly progressing atrophy of medial temporal lobe in Alzheimer's disease. *Lancet* 343, 829–830. doi: 10.1016/S0140-6736(94)92028-1

Labate, D., La Foresta, F., Morabito, G., Palamara, I., and Morabito, F. C. (2013). Entropic measures of EEG complexity in Alzheimer's disease through a multivariate multiscale approach. *IEEE Sens. J.* 13, 3284–3292. doi: 10.1109/JSEN.2013.2271735

McKhann, G., Drachman, D., Folstein, M., Katzman, R., Price, D., and Stadlan, E. M. (1984). Clinical diagnosis of Alzheimer's disease report of the nincds-adrda work group* under the auspices of department of health and human services task force on alzheimer's disease. *Neurology* 34, 939–939. doi: 10.1212/WNL.34.7.939

Meinshausen, N., and Bühlmann, P. (2010). Stability selection. *J. R. Stat. Soc. Ser. B (Stat. Methodol.)* 72, 417–473. doi: 10.1111/j.1467-9868.2010.00740.x

Mizuno, T., Takahashi, T., Cho, R. Y., Kikuchi, M., Murata, T., Takahashi, K., et al. (2010). Assessment of EEG dynamical complexity in Alzheimer's disease using multiscale entropy. *Clin. Neurophysiol.* 121, 1438–1446. doi: 10.1016/j.clinph.2010.03.025

Morris, J. C. (1993). The clinical dementia rating (CDR): current version and scoring rules. *Neurology*. 43, 2412–2414. doi: 10.1212/WNL.43.11.2412-a

Park, J.-H., Kim, S., Kim, C.-H., Cichocki, A., and Kim, K. (2007). Multiscale entropy analysis of EEG from patients under different pathological conditions. *Fractals* 15, 399–404. doi: 10.1142/S0218348X07003691

Poil, S.-S., De Haan, W., van der Flier, W. M., Mansvelder, H. D., Scheltens, P., and Linkenkaer-Hansen, K. (2013). Integrative EEG biomarkers predict progression to Alzheimer's disease at the MCI stage. *Front. Aging Neurosci.* 5:58. doi: 10.3389/fnagi.2013.00058

Richman, J. S., and Moorman, J. R. (2000). Physiological time-series analysis using approximate entropy and sample entropy. *Am. J. Physiol. Heart Circul. Physiol.* 278, H2039–H2049. doi: 10.1152/ajpheart.2000.278.6.H2039

Tibshirani, R. (1996). Regression shrinkage and selection via the lasso. *J. R. Stat. Soc. Ser. B (Methodol.).* 58, 267–288.

Tibshirani, R., Saunders, M., Rosset, S., Zhu, J., and Knight, K. (2005). Sparsity and smoothness via the fused lasso. *J. R. Stat. Soc. Ser. B (Stat. Methodol.)* 67, 91–108. doi: 10.1111/j.1467-9868.2005.00490.x

Trambaiolli, L. R., Lorena, A. C., Fraga, F. J., Kanda, P. A., Anghinah, R., and Nitrini, R. (2011). Improving Alzheimer's disease diagnosis with machine learning techniques. *Clin. EEG Neurosci.* 42, 160–165. doi: 10.1177/155005941104200304

Triggiani, A. I., Bevilacqua, V., Brunetti, A., Lizio, R., Tattoli, G., Cassano, F., et al. (2017). Classification of healthy subjects and Alzheimer's disease patients with dementia from cortical sources of resting state eeg rhythms: a study using artificial neural networks. *Front. Neurosci.* 10:604. doi: 10.3389/fnins.2016.00604

Yang, A. C., Wang, S.-J., Lai, K.-L., Tsai, C.-F., Yang, C.-H., Hwang, J.-P., et al. (2013). Cognitive and neuropsychiatric correlates of EEG dynamic complexity in patients with Alzheimer's disease. *Prog. Neuro-Psychopharmacol. Biol. Psychiatry* 47, 52–61. doi: 10.1016/j.pnpbp.2013.07.022

Zou, H., and Hastie, T. (2005). Regularization and variable selection via the elastic net. *J. R. Stat. Soc. (Stat. Methodol.).* 67, 301–320. doi: 10.1111/j.1467-9868.2005.00503.x

Conflict of Interest Statement: The authors declare that the research was conducted in the absence of any commercial or financial relationships that could be construed as a potential conflict of interest.

The Reviewer FZ and the handling editor declared their shared affiliation.

frontiers in Neuroscience

ORIGINAL RESEARCH
published: 23 October 2018
doi: 10.3389/fnins.2018.00770

Default Mode Network Complexity and Cognitive Decline in Mild Alzheimer's Disease

Matthias Grieder[1], Danny J. J. Wang[2], Thomas Dierks[1], Lars-Olof Wahlund[3] and Kay Jann[2]*

[1] Translational Research Center, University Hospital of Psychiatry, University of Bern, Bern, Switzerland, [2] USC Stevens Neuroimaging and Informatics Institute, Keck School of Medicine of USC, University of Southern California, Los Angeles, CA, United States, [3] Division of Clinical Geriatrics, Department of Neurobiology, Care Sciences and Society, NVS, Karolinska Institute, Stockholm, Sweden

The human resting-state is characterized by spatially coherent brain activity at a low temporal frequency. The default mode network (DMN), one of so-called resting-state networks, has been associated with cognitive processes that are directed toward the self, such as introspection and autobiographic memory. The DMN's integrity appears to be crucial for mental health. For example, patients with Alzheimer's disease or other psychiatric conditions show disruptions of functional connectivity within the brain regions of the DMN. However, in prodromal or early stages of Alzheimer's disease, physiological alterations are sometimes elusive, despite manifested cognitive impairment. While functional connectivity assesses the signal correlation between brain areas, multi-scale entropy (MSE) measures the complexity of the blood-oxygen level dependent signal within an area and thus might show local changes before connectivity is affected. Hence, we investigated alterations of functional connectivity and MSE within the DMN in fifteen mild Alzheimer's disease patients as compared to fourteen controls. Potential associations of MSE with functional connectivity and cognitive abilities [i.e., mini-mental state examination (MMSE)] were assessed. A moderate decrease of DMN functional connectivity between posterior cingulate cortex and right hippocampus in Alzheimer's disease was found, whereas no differences were evident for whole-network functional connectivity. In contrast, the Alzheimer's disease group yielded lower global DMN-MSE than the control group. The most pronounced regional effects were localized in left and right hippocampi, and this was true for most scales. Moreover, MSE significantly correlated with functional connectivity, and DMN-MSE correlated positively with the MMSE in Alzheimer's disease. Most interestingly, the right hippocampal MSE was positively associated with semantic memory performance. Thus, our results suggested that cognitive decline in Alzheimer's disease is reflected by decreased signal complexity in DMN nodes, which might further lead to disrupted DMN functional connectivity.

OPEN ACCESS

Edited by:
Vince D. Calhoun,
The University of New Mexico, United States

Reviewed by:
Yong Liu,
Institute of Automation (CAS), China
Rui Li,
Institute of Psychology (CAS), China

****Correspondence:***
Matthias Grieder
matthias.grieder@upd.unibe.ch

Specialty section:
This article was submitted to Brain Imaging Methods, a section of the journal Frontiers in Neuroscience

Received: *25 April 2018*
Accepted: *03 October 2018*
Published: *23 October 2018*

Citation:
Grieder M, Wang DJJ, Dierks T, Wahlund L-O and Jann K (2018) Default Mode Network Complexity and Cognitive Decline in Mild Alzheimer's Disease. Front. Neurosci. 12:770. doi: 10.3389/fnins.2018.00770

Additionally, altered entropy in Alzheimer's disease found in the majority of the scales indicated a disturbance of both local information processing and information transfer between distal areas. Conclusively, a loss of nodal signal complexity potentially impairs synchronization across nodes and thus preempts functional connectivity changes. MSE presents a putative functional marker for cognitive decline that might be more sensitive than functional connectivity alone.

Keywords: multi-scale entropy, complexity, functional connectivity, resting-state fMRI, default mode network, Alzheimer's disease, cognitive decline

INTRODUCTION

Brain activity during the human resting-state shows spatially coherent patterns at a low temporal frequency (Biswal et al., 1995; Raichle et al., 2001). Blood-oxygen level dependent (BOLD) resting-state functional MRI (rs-fMRI) revealed these so-called resting state networks (RSN), consisting of spatially segregated brain regions that are intrinsically co-activated and deactivated across time. The idea is widely accepted that these highly correlated brain regions are functionally connected, and the connectivity strength is represented by the correlation coefficient between given areas. Moreover, it has been shown that the RSNs or the functional connectivity (FC) are altered in subgroups of patients. In particular, FC appears to be related to disease severity or cognitive decline in dementia and normal aging (Petrella et al., 2011; Agosta et al., 2012; Brier et al., 2012).

The most widely studied RSN is the default mode network (DMN), which has been associated with mind wandering, autobiographic memory, future thinking, and introspection (for review, see Buckner and Carroll, 2007; Buckner et al., 2008). The core brain regions of the DMN are medial prefrontal cortex (MPFC), posterior cingulate cortex (PCC), left and right inferior parietal lobes (IPL), and left and right hippocampi (Hipp, Buckner et al., 2008). The DMN's integrity appears to play an important role for the health of mind, since DMN disruptions have been reported in schizophrenia spectrum disorder (Bluhm et al., 2007; Garrity et al., 2007), depression (Wise et al., 2017), autism (Padmanabhan et al., 2017; Hogeveen et al., 2018), and Alzheimer's disease (Jones et al., 2011; Cha et al., 2013). Specifically in Alzheimer's disease, disease progression severity has been associated with reduced DMN FC, as compared to age-matched controls (Lustig et al., 2003; Greicius et al., 2004; Zhang et al., 2010; Zhou et al., 2010). Furthermore, the temporal anti-correlation between task-positive (i.e., RSNs resembling functional networks engaged during task execution) and the task-negative RSN (increased activity in absence of a task, i.e., DMN), normally found in healthy subjects, is attenuated in progressed stages of AD (Fox et al., 2005; Weiler et al., 2017). This inability to switch between the task-positive RSNs and the DMN is hypothesized to be related to cognitive impairment in AD. Moreover, Koch et al. (2012) have corroborated the DMN's relevance in AD by demonstrating the diagnostic power of DMN connectivity strength to separate AD from healthy controls, while the prediction of mild cognitive impairment (MCI) was less obvious.

Despite the prospects of RSN-FC as a marker of cognitive decline, FC is an average measure of correlation between brain areas during a few minutes of fMRI scanning. FC has limited capability in characterizing the dynamic reorganization and regional activity of complex brain networks. Hence, assessing the dynamic properties of connections (network edges) between and within areas (network nodes) of the brain is a necessary step to further understand the normal brain function during resting state as well as putative disruptions of the functional organization in the course of a disease.

Non-linear statistical approaches have been applied for quantifying the regularity of biological signals such as approximate entropy (ApEn) or its variant sample entropy (SampEn; Pincus, 1991; Richman and Moorman, 2000; Liu et al., 2013; Sokunbi, 2014). When applied to several coarse-sampled scales from the original time series, SampEn can be extended to multi-scale entropy analysis (MSE; Costa et al., 2002). Smith et al. (2014) showed that healthy aging is associated with decreased MSE mainly in DMN regions such as middle temporal gyrus, MPFC, angular gyri, middle and superior medial frontal cortex, and Hipp. Smith et al. (2015) in a later study further showed that MCI is associated with reduced MSE in areas of the DMN. Such findings were confirmed by studies that reported a positive relationship between cognitive decline in familial AD and whole brain ApEn as well as regional entropy in precuneus, lateral parietal cortex, precentral gyrus, and paracentral gyrus (Liu et al., 2013; Wang et al., 2017). These preliminary studies suggest that MSE of rs-fMRI may provide a marker of cognitive decline in aging and dementia.

The purpose of the present study was to compare MSE of the DMN between a group of patients with mild AD and a group of age matched controls. We examined the added value of including a metric of regional (nodal) dynamics (MSE) to the inter-regional connectivity (edges) assessed with FC. We further tested the relation of MSE alteration and cognitive decline assessed by the mini-mental state examination (MMSE) as well as Boston Naming Task (BNT) scores. We expected generally lower MSE values in AD as compared to matched controls. More detailed hypotheses about regional DMN-MSE changes in AD were not made, since there is no comparable study available for hypothesis generation. However, we predicted a positive correlation between MSE and MMSE, which is in accordance with Liu et al. (2013). With focus on the standard FC analysis, we anticipated reduced FC in AD compared to HC, because most studies reported FC decreases in AD (Cha et al., 2013).

MATERIALS AND METHODS

Participants

All participants provided written informed consent according to a protocol approved by the Regional Ethics Committee of Stockholm, Sweden, in accordance with the Declaration of Helsinki. Only native speakers of Swedish were included and exclusion criteria were the presence of medical or psychiatric disorders (other than dementia), intake of drugs affecting the nervous system, or any contraindications for MRI procedures. Fourteen healthy elderly control (HC) participants (aged 62–73 years) were included into data analysis after exclusion of one participant due to excessive movement artifacts in the MR-images. The mild Alzheimer's disease (AD) group consisted of 15 patients (aged 53–83) after discarding two artifact-contaminated data-sets (**Table 1**). The patients were recruited at the Memory Clinic of the Geriatric Department at Karolinska University Hospital in Huddinge, Sweden. Hence, their diagnosis was performed by expert clinicians and were in accordance with the ICD-10 criteria. The patients with AD included in this study underwent a standard clinical procedure which consisted of examinations such as structural neuroimaging, lumbar puncture, blood analyses, and a neuropsychological assessment. Further inclusion criteria for all patients were a Global Deterioration Scale smaller than 6 (i.e., moderate dementia, or milder) and the Cornell Depression Scale below 8. Controls were screened with a neuropsychological test battery, comprised MMSE and BNT.

Image Acquisition and Preprocessing

Data were acquired on a 3T Siemens Magnetom Trio MR Scanner (Siemens AG, Erlangen, Germany). GE EPI fMRI BOLD was recorded with 26 transversal slices; 3.0 × 3.0 in-plane and 4 mm slice thickness; TR/TE = 1600/35 ms, FA 90°; FoV = 240 × 240 mm; matrix = 92 × 92, 400 volumes acquired in 10 min 40 s. A structural T1-weighted MPRAGE was recorded with 176 sagittal slices, 0.9 × 0.9 in-plane and 1 mm slice thickness, TR/TE = 1900/2.57 ms; FoV = 230 × 230 mm; matrix = 256 × 256.

TABLE 1 | Demographics and descriptive statistics.

	HC (n = 14)	AD (n = 15)	HC-AD	
	Mean (SD)	Mean (SD)	U	p-Value
Age, years	67.5 (3.5)	67.3 (8.6)	95.5	n.s.
Gender (F:M)	10:4	8:7		
Education, years	13.3 (3.0)	12.9 (3.0)	103.0	n.s.
MMSE (max 30)	28.8 (0.9)	25.0 (3.8)	16.5	<0.001
BNT (max 60)	53.7 (3.7)	45.8 (6.6)	30.5	0.001
GDS	n/a	2.9 (0.8)		
CDS	n/a	1.3 (1.2)		

Group-wise statistics were performed using the non-parametric Mann–Whitney U-test.

Preprocessing of fMRI data involved motion-realignment, linear drift correction (detrending), regression of motion (six motion parameters and first derivatives; Power et al., 2014) and physiological noise (WM and CSF signal fluctuations extracted from T1 image based tissue probability masks from SPM Dartel segmentation; Chang and Glover, 2009; Birn et al., 2014) followed by co-registration of functional to individual structural images and normalization to MNI standard space and final smoothing with a Gaussian Kernel (FWHM 6 mm).

Data Analysis

Data analysis was based on predefined parcellated regions of interest (ROIs) selected from a functional connectivity atlas (Shirer et al., 2012) delineating the DMN. As explained in the introduction, the DMN undergoes pathology characteristic structural and functional alterations related to cognitive decline in AD. We selected the DMN nodes in medial prefrontal cortex (MPFC), posterior cingulate cortex (PCC), left and right inferior parietal lobes (L-IPL/R-IPL) as well as left and right hippocampi (L-Hipp/R-Hipp). Average BOLD signal fluctuations from all these ROIs were extracted from the individual subjects' fMRI data and submitted to further analyses.

Multi-Scale Entropy (MSE) Computation

Entropy was computed for each ROI after averaging the signal fluctuations across all voxels within the respective ROI. We employed sample entropy (SampEn, Richman and Moorman, 2000; Smith et al., 2014) to compute complexity at each scale with pattern matching threshold r = 0.2 and pattern length m = 2 (Smith et al., 2014; Sokunbi, 2014; Li et al., 2018). Scales were created by coarse sampling of the original time series data into 40 scales; i.e., scale 1 is the original time series and 2 is created by averaging every two consecutive, non-overlapping time points, and similarly for all other scales n the time series was subsampled as averages of n consecutive non-overlapping time points. To identify the scales with reliable entropy values, we statistically compared SampEn at each scale against 0. MSE is the average across all scales considered (Costa et al., 2002; Smith et al., 2014). We further calculated the global DMN complexity as mean MSE across all scales and all nodes. Comparison of entropy between the AD and HC group was performed by two-sample, one-sided t-test (significance level $p < 0.05$) on nodal and global DMN level (scales 1–10, 0.625–0.063 Hz).

Functional Connectivity (FC) Analysis

Seed-to-Seed functional connectivity between every ROI pair was calculated by the Pearson correlation between the average ROI signal fluctuations. For group comparison we considered node-to-node connectivity as well as global DMN connectivity, which was defined as mean FC across all node-to-node correlations (upper-triangle in cross correlation matrix). Comparison of FC between the AD and HC group was performed by two-sample, one-sided t-test (significance level $p < 0.05$) on node-to-node and global DMN level.

Relationship Between MSE, FC, and Cognitive Impairment (MMSE)

First, we calculated the Pearson correlation between DMN FC and DMN-MSE at scales 1–20 (0.625–0.031 Hz) across all participants to elucidate the relationship between network complexity and connectivity. To examine potential associations of MSE with cognitive abilities, partial Pearson correlation coefficients were assessed, corrected for age and gender. Concretely, the global DMN-MSE (MSE averaged across scales 1–10; 0.625–0.063 Hz) was correlated with the MMSE reflecting a general measure of mental health as well as the BNT score mirroring semantic memory retrieval. Unfortunately, no utilizable episodic memory score was available for statistical analysis. Furthermore, we also performed the same correlations with nodal MSE and the neuropsychological tests, for DMN nodes showing significant MSE alteration in the AD group.

RESULTS

Functional Connectivity (FC)

There were no significant DMN-FC differences between the groups. This was true for whole DMN FC, which is the averaged FC across all node-to-node correlations, as well as for individual node-to-node connections (**Figure 1**). However, FC to the hippocampal nodes appeared reduced (non-significant, **Figure 1**). Using one-sided *t*-test assuming that FC is lower in AD than controls we found a significantly reduced connection between PCC and R-Hipp ($t = 1.90$, $p = 0.034$).

Multi-Scale Entropy (MSE)

The validity analysis for entropy at every scale revealed that for scales 1–20 (0.625–0.031 Hz) we observed a complex behavior of signal fluctuations (**Supplementary Figure 1**). This is comprehensible since our fMRI comprised 400 volumes and thus coarse sampling at scales 20 and above would produce very short time-series for MSE computation (20 time-points at scale 20) which renders it unreliable. Therefore, for further analysis we restricted entropy values to scales 10 and below to ascertain that entropy values are reliable.

Network and Nodal MSE Differences

We found significantly lower global network level DMN-MSE ($t = -1.81$, one-sided $p = 0.041$) in AD as compared to HC. **Figure 2A** displays the entropy for DMN at each scale. On a nodal level and across all scales, we found reduced MSE for R-Hipp ($t = -1.87$, $p = 0.036$, **Figure 2B**) and a trend for MPFC ($t = -1.42$, $p = 0.083$). Detailed analysis of effects for all nodes separated for different scales revealed that the effects for entropy are most pronounced in L-Hipp and R-Hipp which showed

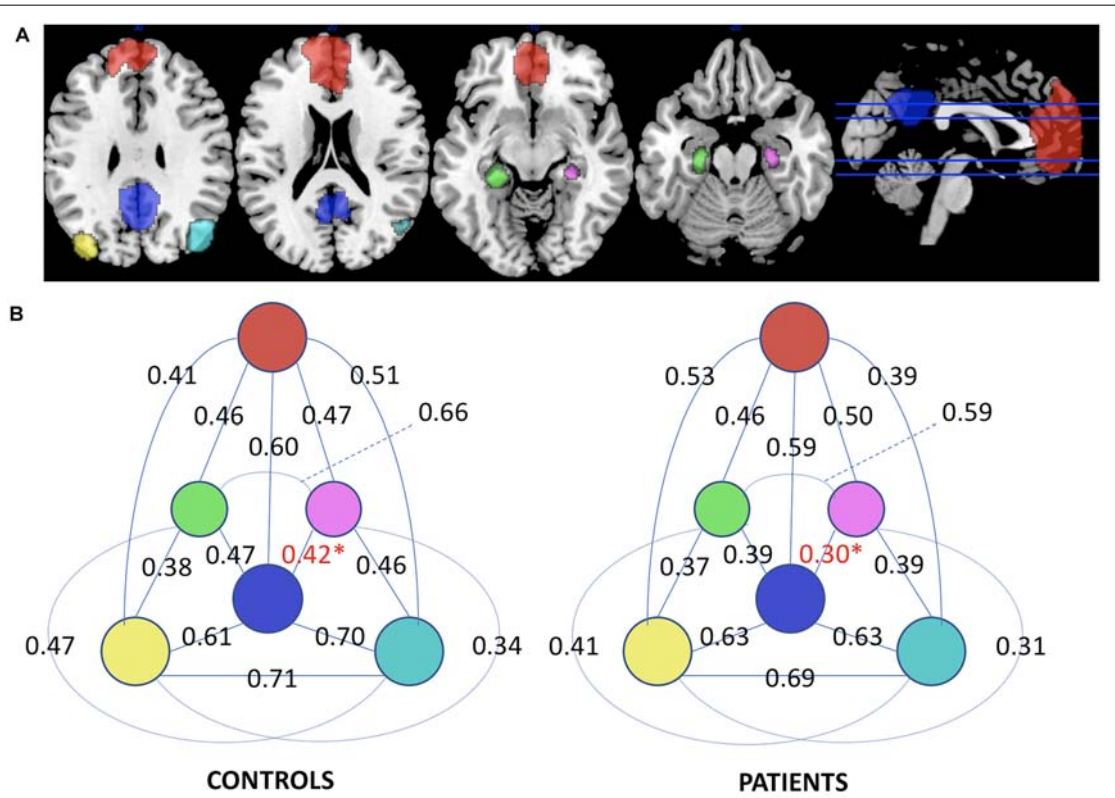

FIGURE 1 | (A) Nodes delineating the default mode network. **(B)** Functional Connectivity diagram displaying the correlations between the nodes of the DMN in control and Alzheimer's disease groups. Significant difference in the R-Hipp/PCC edge for one-sided *t*-test is marked in red and with asterisk (Red: MPFC, blue: PCC, yellow: L-IPL, cyan: R-IPL, green: L-Hipp, purple: R-Hipp).

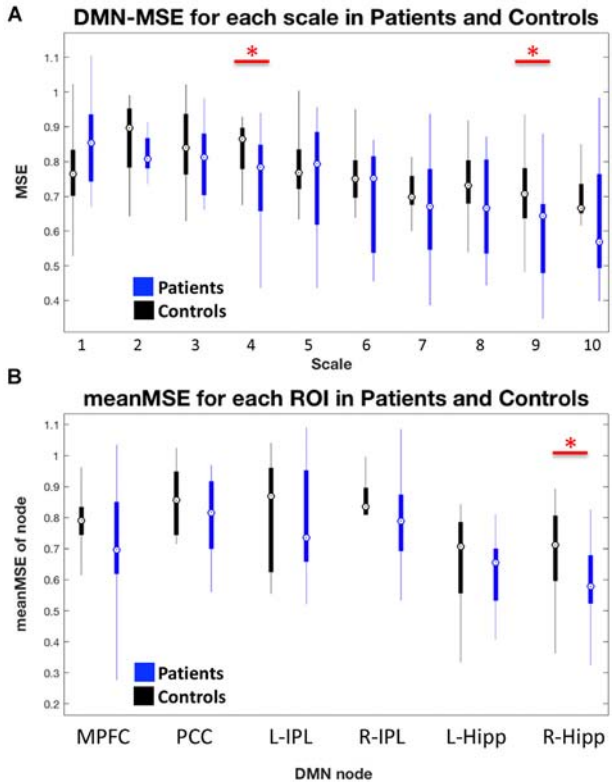

FIGURE 2 | (A) Box-plot of entropy values at each scale for whole DMN in HC and AD. **(B)** Box-plot of mean MSE within each node of the DMN. Red horizontal bars with red asterisks above boxes indicate significant differences between patients and controls. Generally, AD had reduced entropy within the DMN and specifically the right hippocampus showed decreased MSE on a nodal level.

consistently reduced entropy for most scales (**Supplementary Figure 2**). We further found some effects at single scales in MPFC, PCC and R-IPL.

Correlation Between MSE and FC or MMSE

Across all scales there was a significant positive association between network connectivity and entropy, with significant effects in the AD group in scales 1 and 2 (0.63–0.31 Hz) and in the control group in scale 16 (0.039 Hz, **Figure 3A**). Moreover, the global DMN-MSE correlated significantly with MMSE in AD patients ($r = 0.65$, $p = 0.032$), but not with the BNT. In contrast, nodal MSE of the R-Hipp showed no association with the MMSE, but with the BNT ($r = 0.67$, $p = 0.033$, **Figure 3B**). Thus, the lower cognitive abilities of the AD group were associated with a lower overall DMN-MSE, and their declined semantic memory performance was related to a decreased nodal MSE in the R-Hipp. Note that correlational analyses using nodal MSE was only performed with the R-Hipp, because as elucidated in the previous section, this was the only DMN node that yielded a significant MSE change in the AD group across all scales.

DISCUSSION

In this study, we investigated rs-fMRI signal complexity in DMN nodes in cohorts of mild AD and HC. We additionally compared the outcome of the MSE analysis with the results of the more commonly applied FC analysis.

Functional Connectivity

First of all, the standard FC analysis did not yield any compelling results. As outlined in the introduction, DMN alterations in AD have been reported repeatedly, yet only moderate to severe disease stages appear to produce reliable results (Buckner et al., 2008; Brier et al., 2012; Cha et al., 2013; Gardini et al., 2015). In the case of our mild AD sample, we merely found indices of reduced FC, mainly between R-Hipp and PCC, and even to a lower magnitude between L-Hipp and PCC, and R-IPL and MPFC (**Figure 1**). Studies that showed reduced FC of the PCC in AD have raised the hypothesis that cortical hubs such as the PCC are prone to functional deterioration due to their relatively high resting metabolism that is no longer maintained as a consequence of amyloid deposition, which co-occurs in these hubs (Buckner et al., 2005; Sorg et al., 2007; Vlassenko et al., 2010; Franciotti et al., 2013). Notwithstanding the consistency with the literature of the observed FC results indicating lower connectivity in AD, we did not find reduced DMN network FC, nor were the FC differences we observed statistically significant on a robust level.

Multi-Scale Entropy

In contrast, the AD group showed a lower global DMN-MSE, as compared to HC. This confirmed our hypothesis and implied that the DMN-related signal fluctuation was less complex in AD than HC, which is in line with a previous report about whole brain MSE (Liu et al., 2013). Similarly, Wang et al. (2017) reported lower rs-fMRI-derived complexity in AD than MCI and HC, and Li et al. (2018) found reduced fNIRS-signal complexity in DMN-nodes in AD as compared to controls. By inspecting the DMN-MSE at each scale (**Figure 2A**), we observed a trend of decreasing entropy with increasing scale in AD. In the HC group, there was an entropy increase from scales 1–4, followed by a decrease from scales 5–10. This distinct pattern between patients and controls might reflect a disturbed local functional integrity in AD, as it has been proposed that smaller scales (i.e., higher frequencies) are related to intra-regional processing, whereas larger scales (i.e., lower frequencies) are thought to be closely associated with inter-regional FC (Vakorin et al., 2011; McDonough and Nashiro, 2014; McIntosh et al., 2014; Wang et al., 2018). The statistical analysis of DMN-MSE revealed a significant MSE-reduction in AD at both scales 4 and 9, supporting that mild AD is characterized by a disturbance of signal complexity (i.e., entropy), which is associated with local and distal information processing. With regard to the mean MSE for each DMN node, we found a significant AD-related decrease in the R-Hipp. This is different to the findings of Wang et al. (2017), who reported decreased complexity in AD in other brain regions (only MPFC of the DMN regions, among others). However, they used permutation entropy analysis (as compared to SampEn in the current study) and the patients with AD they included in the study were

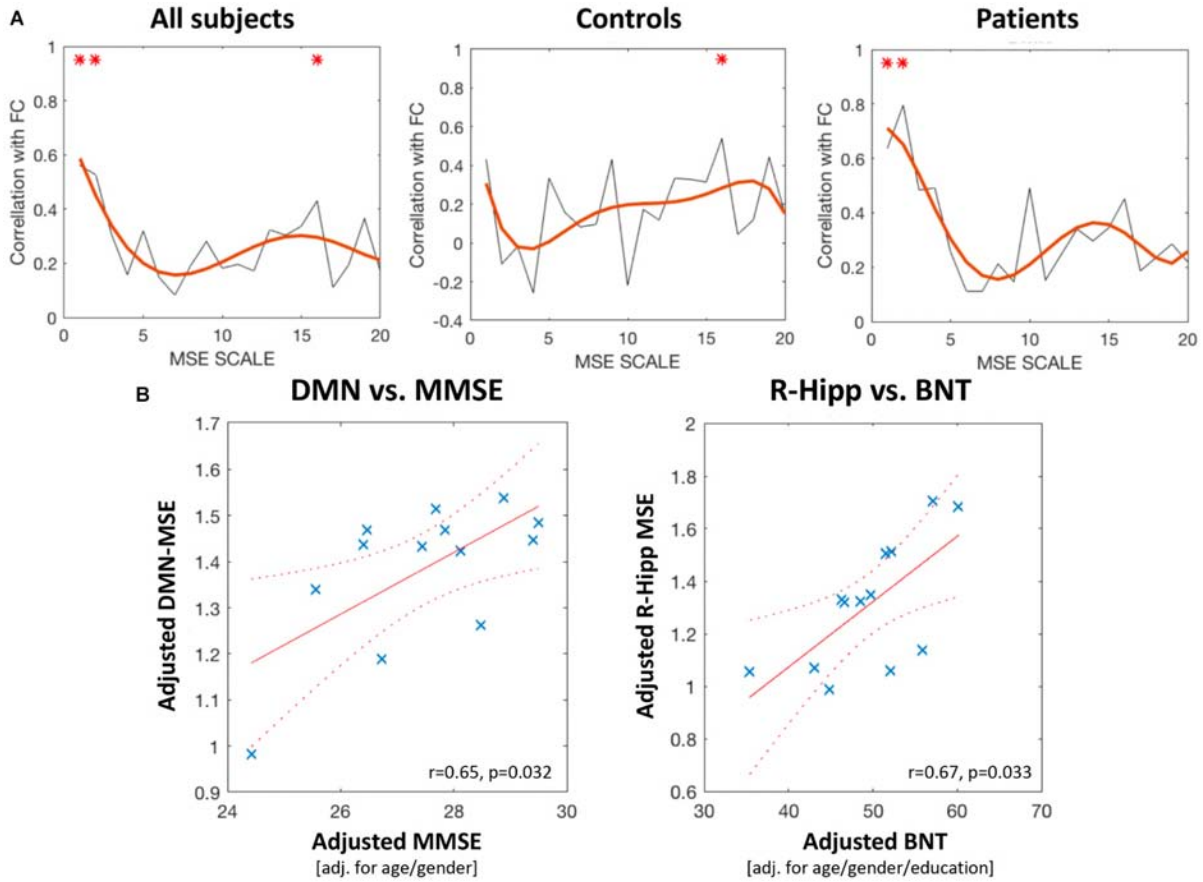

FIGURE 3 | (A) Correlation between DMN-FC and DMN-entropy at scales 1–20. The left panel depicts correlations for all subjects, the middle panel for the controls, and the right panel for the Alzheimer's disease group. Red asterisks mark scales that showed a significant correlation coefficient. **(B)** The left panel shows a scatterplot of the significant positive correlation between global-level DMN entropy (scales 1–10) and MMSE score. The right panel shows the significant positive correlation between R-Hipp entropy (scales 1–10) and BNT score (both panels include patients with AD only).

cognitively more impaired than those in this study (MMSE 21 vs. 25).

To this point, we can recapitulate that the main results of the current study were a decreased global DMN-MSE in mild AD, a constant reduction of entropy with increasing scales in AD, and a mean-MSE group comparison that showed decreased R-Hipp MSE in AD compared to HC. While these findings fit well into literature and our hypothesis, thoroughly elucidating the MSE differences between AD and HC for each DMN-node for each scale was more challenging.

With reference to **Supplementary Figure 2**, we identified the MPFC, L-Hipp, and R-Hipp as nodes with decreased MSE in AD in all significant scales. In MPFC and R-Hipp, the differences were located in fine scales, which indicated a local processing disturbance as circumscribed above. In the L-Hipp, significant differences were found at scales 4–8 (except scale 6). We interpreted this as a deterioration of hippocampal processing in general. Our view is supported by studies that described the Hipp (predominantly left-lateralized) as a crucial region for AD not only as an atrophy hot spot, but also with regard to its functional role in episodic and semantic memory, both of which are affected in AD (Burianova et al., 2010; La Joie et al., 2014). Hence, the decreased entropy in the L-Hipp at the smaller scale 4 might be related to the impaired episodic memory encoding. On the other hand, the attenuated entropy found in the larger scales (i.e., 5, 7, and 8) might mirror a disconnection of the L-Hipp within episodic and semantic networks (Allen et al., 2007). Two additional DMN-nodes, namely the PCC and R-IPL, presented a more complicated image. Increased entropy was found at scale 8 in the R-IPL, whereas at scale 2, MSE was reduced. This pattern might have reflected a discrepant change of signal processing at local and network level. As outlined before, the PCC serves as a hub and has been found to be vulnerable to functional change in AD. It occurred thus unexpected to find increased MSE in scale 3, while neighboring scale 4 showed the opposite. There is some evidence from EEG, which, however, is on a different temporal scale, that increased complexity might also be related to cognitive decline in AD (Mizuno et al., 2010). In our view, future research on MSE is needed in order to resolve such findings. Finally, the L-IPL did not evince significant changes at any particular scale.

Correlation Between Complexity, Connectivity, and Cognitive Decline

In order to investigate the potential link between FC and MSE, we correlated the DMN-MSE at each scale with FC. As can be seen in **Figure 3A**, correlations were positive throughout the scales. Two peak correlations at scales 1/2 and 16 could be observed. Group-wise correlation uncovered that the second peak in slow frequency entropy was significant only in HC, whereas in AD, this relationship did not reach significance. In contrast, the AD group showed significant associations with higher frequency entropy and FC. Note that from scales 5–20, the corresponding frequencies range from 0.125 to 0.031 Hz which are commonly associated with the low frequency fluctuations of functional connectivity networks (Damoiseaux et al., 2006; De Luca et al., 2006; Shehzad et al., 2009). However, the second peak suggests that not only slow but also fast processes influence FC. Accordingly, even in the higher frequency spectrum of BOLD signal some physiologic information is contained. This aligns with the hypothesis of distinct information contained in high vs. low frequency MSE where the former represents local processing while the latter reflects information transfer between areas and both are critical properties of distributed processing within cortical networks.

Changes of FC as well as entropy measures have been found to accompany cognitive changes related to healthy aging or disease (Jones et al., 2011; Brier et al., 2012; Liu et al., 2013). The positive correlation between global DMN-MSE and the MMSE score in our AD cohort is in accordance with these previous findings and our predictions. This result also corroborated previous studies suggesting that a high signal complexity in general, or particularly in the DMN, is important for cognitive functionality (Sokunbi et al., 2011; Yang et al., 2013). Interestingly, BNT scores correlated positively specifically with the R-Hipp, but not for example with the global DMN-MSE. As discussed above, the hippocampus has been found to play a role in semantic memory retrieval, which endorses our finding. Moreover, La Joie et al. (2014) proposed that the R-Hipp might be a crossroad between episodic and semantic memory networks. Thus, we not only found supporting evidence for the findings of these studies, but additional indication that apart from the well described FC alterations in the R-Hipp in AD, the local information processing is disturbed, which is associated with an impaired memory performance.

Limitations

The main limitation of the present study is the small sample size (15 AD, 14 HC). This should be taken into account when interpreting the findings. Considering the mild disease state of the AD group, the small MSE and FC effects were statistically underpowered to apply a correction for multiple comparisons. We feel that despite the small sample size, we could show that MSE is sensitive enough to find differences between HC and mild AD. For a first proof of concept study, we highlighted the usefulness of MSE as a new characteristic for BOLD signal fluctuations in AD.

CONCLUSION

We found DMN-MSE in AD was reduced as compared to matched controls and that MSE is related to FC as well as cognitive abilities. Our results further suggest that cognitive decline in AD is reflected by decreased signal complexity in network nodes, which might further lead to disrupted DMN-FC. We hypothesize that a loss of nodal (i.e., right hippocampal) signal complexity potentially impairs synchronization across nodes and preempts FC changes. Thus, MSE presents a putative functional marker for cognitive decline that might be more sensitive than FC in mild AD.

DATA AVAILABILITY

Data can be requested from the corresponding author. The entropy toolbox and all subroutines can be downloaded from the USC Laboratory of Functional MRI Technology website: http://loft-lab.org/index-5.html.

AUTHOR CONTRIBUTIONS

MG contributed to the study design, the data acquisition and analysis, and the manuscript writing. DW contributed to the writing and reviewing of the manuscript. TD contributed to the study design. L-OW contributed to the study design and data acquisition. KJ contributed to the data analysis and the manuscript writing.

FUNDING

This work was supported by the University of Bern, the Swedish Alzheimerfonden, the Swiss Synapsis Foundation and NIH grant (UH2-NS100614).

SUPPLEMENTARY MATERIAL

The Supplementary Material for this article can be found online at: https://www.frontiersin.org/articles/10.3389/fnins.2018.00770/full#supplementary-material

REFERENCES

Agosta, F., Pievani, M., Geroldi, C., Copetti, M., Frisoni, G. B., and Filippi, M. (2012). Resting state fMRI in Alzheimer's disease: beyond the default mode network. *Neurobiol. Aging* 33, 1564–1578. doi: 10.1016/j.neurobiolaging.2011.06.007

Allen, G., Barnard, H., Mccoll, R., Hester, A. L., Fields, J. A., Weiner, M. F., et al. (2007). Reduced hippocampal functional connectivity in Alzheimer disease. *Arch. Neurol.* 64, 1482–1487. doi: 10.1001/archneur.64.10.1482

Birn, R. M., Cornejo, M. D., Molloy, E. K., Patriat, R., Meier, T. B., Kirk, G. R., et al. (2014). The influence of physiological noise correction on test-retest

reliability of resting-state functional connectivity. *Brain Connect.* 4, 511–522. doi: 10.1089/brain.2014.0284

Biswal, B., Yetkin, F. Z., Haughton, V. M., and Hyde, J. S. (1995). Functional connectivity in the motor cortex of resting human brain using echo-planar MRI. *Magn. Reson. Med.* 34, 537–541. doi: 10.1002/mrm.1910340409

Bluhm, R. L., Miller, J., Lanius, R. A., Osuch, E. A., Boksman, K., Neufeld, R. W. J., et al. (2007). Spontaneous low-frequency fluctuations in the BOLD signal in schizophrenic patients: anomalies in the default network. *Schizophr. Bull.* 33, 1004–1012. doi: 10.1093/schbul/sbm052

Brier, M. R., Thomas, J. B., Snyder, A. Z., Benzinger, T. L., Zhang, D., Raichle, M. E., et al. (2012). Loss of intranetwork and internetwork resting state functional connections with Alzheimer's disease progression. *J. Neurosci.* 32, 8890–8899. doi: 10.1523/JNEUROSCI.5698-11.2012

Buckner, R. L., Andrews-Hanna, J. R., and Schacter, D. L. (2008). The brain's default network: anatomy, function, and relevance to disease. *Ann. N. Y. Acad. Sci.* 1124, 1–38. doi: 10.1196/annals.1440.011

Buckner, R. L., and Carroll, D. C. (2007). Self-projection and the brain. *Trends Cogn. Sci.* 11, 49–57. doi: 10.1016/j.tics.2006.11.004

Buckner, R. L., Snyder, A. Z., Shannon, B. J., Larossa, G., Sachs, R., Fotenos, A. F., et al. (2005). Molecular, structural, and functional characterization of Alzheimer's disease: evidence for a relationship between default activity, amyloid, and memory. *J. Neurosci.* 25, 7709–7717. doi: 10.1523/JNEUROSCI.2177-05.2005

Burianova, H., Mcintosh, A. R., and Grady, C. L. (2010). A common functional brain network for autobiographical, episodic, and semantic memory retrieval. *Neuroimage* 49, 865–874. doi: 10.1016/j.neuroimage.2009.08.066

Cha, J., Jo, H. J., Kim, H. J., Seo, S. W., Kim, H. S., Yoon, U., et al. (2013). Functional alteration patterns of default mode networks: comparisons of normal aging, amnestic mild cognitive impairment and Alzheimer's disease. *Eur. J. Neurosci.* 37, 1916–1924. doi: 10.1111/ejn.12177

Chang, C., and Glover, G. H. (2009). Effects of model-based physiological noise correction on default mode network anti-correlations and correlations. *Neuroimage* 47, 1448–1459. doi: 10.1016/j.neuroimage.2009.05.012

Costa, M., Goldberger, A. L., and Peng, C. K. (2002). Multiscale entropy analysis of complex physiologic time series. *Phys. Rev. Lett.* 89:068102. doi: 10.1103/PhysRevLett.89.068102

Damoiseaux, J. S., Rombouts, S. A., Barkhof, F., Scheltens, P., Stam, C. J., Smith, S. M., et al. (2006). Consistent resting-state networks across healthy subjects. *Proc. Natl. Acad. Sci. U.S.A.* 103, 13848–13853. doi: 10.1073/pnas.0601417103

De Luca, M., Beckmann, C. F., De Stefano, N., Matthews, P. M., and Smith, S. M. (2006). fMRI resting state networks define distinct modes of long-distance interactions in the human brain. *Neuroimage* 29, 1359–1367. doi: 10.1016/j.neuroimage.2005.08.035

Fox, M. D., Snyder, A. Z., Vincent, J. L., Corbetta, M., Van Essen, D. C., and Raichle, M. E. (2005). The human brain is intrinsically organized into dynamic, anticorrelated functional networks. *Proc. Natl. Acad. Sci. U.S.A.* 102, 9673–9678. doi: 10.1073/pnas.0504136102

Franciotti, R., Falasca, N. W., Bonanni, L., Anzellotti, F., Maruotti, V., Comani, S., et al. (2013). Default network is not hypoactive in dementia with fluctuating cognition: an Alzheimer disease/dementia with Lewy bodies comparison. *Neurobiol. Aging* 34, 1148–1158. doi: 10.1016/j.neurobiolaging.2012.09.015

Gardini, S., Venneri, A., Sambataro, F., Cuetos, F., Fasano, F., Marchi, M., et al. (2015). Increased functional connectivity in the default mode network in mild cognitive impairment: a maladaptive compensatory mechanism associated with poor semantic memory performance. *J. Alzheimers Dis.* 45, 457–470. doi: 10.3233/JAD-142547

Garrity, A. G., Pearlson, G. D., Mckiernan, K., Lloyd, D., Kiehl, K. A., and Calhoun, V. D. (2007). Aberrant "default mode" functional connectivity in schizophrenia. *Am. J. Psychiatry* 164, 450–457. doi: 10.1176/ajp.2007.164.3.450

Greicius, M. D., Srivastava, G., Reiss, A. L., and Menon, V. (2004). Default-mode network activity distinguishes Alzheimer's disease from healthy aging: evidence from functional MRI. *Proc. Natl. Acad. Sci. U.S.A.* 101, 4637–4642. doi: 10.1073/pnas.0308627101

Hogeveen, J., Krug, M. K., Elliott, M. V., and Solomon, M. (2018). Insula-retrosplenial cortex overconnectivity increases internalizing via reduced insight in autism. *Biol. Psychiatry* 84, 287–294. doi: 10.1016/j.biopsych.2018.01.015

Jones, D. T., Machulda, M. M., Vemuri, P., Mcdade, E. M., Zeng, G., Senjem, M. L., et al. (2011). Age-related changes in the default mode network are more advanced in Alzheimer disease. *Neurology* 77, 1524–1531. doi: 10.1212/WNL.0b013e318233b33d

Koch, W., Teipel, S., Mueller, S., Benninghoff, J., Wagner, M., Bokde, A. L., et al. (2012). Diagnostic power of default mode network resting state fMRI in the detection of Alzheimer's disease. *Neurobiol. Aging* 33, 466–478. doi: 10.1016/j.neurobiolaging.2010.04.013

La Joie, R., Landeau, B., Perrotin, A., Bejanin, A., Egret, S., Pelerin, A., et al. (2014). Intrinsic connectivity identifies the hippocampus as a main crossroad between Alzheimer's and semantic dementia-targeted networks. *Neuron* 81, 1417–1428. doi: 10.1016/j.neuron.2014.01.026

Li, X., Zhu, Z., Zhao, W., Sun, Y., Wen, D., Xie, Y., et al. (2018). Decreased resting-state brain signal complexity in patients with mild cognitive impairment and Alzheimer's disease: a multi-scale entropy analysis. *Biomed. Opt. Express* 9, 1916–1929. doi: 10.1364/BOE.9.001916

Liu, C. Y., Krishnan, A. P., Yan, L., Smith, R. X., Kilroy, E., Alger, J. R., et al. (2013). Complexity and synchronicity of resting state blood oxygenation level-dependent (BOLD) functional MRI in normal aging and cognitive decline. *J. Magn. Reson. Imaging* 38, 36–45. doi: 10.1002/jmri.23961

Lustig, C., Snyder, A. Z., Bhakta, M., O'brien, K. C., Mcavoy, M., Raichle, M. E., et al. (2003). Functional deactivations: change with age and dementia of the Alzheimer type. *Proc. Natl. Acad. Sci. U.S.A.* 100, 14504–14509. doi: 10.1073/pnas.2235925100

McDonough, I. M., and Nashiro, K. (2014). Network complexity as a measure of information processing across resting-state networks: evidence from the human connectome project. *Front. Hum. Neurosci.* 8:409. doi: 10.3389/fnhum.2014.00409

McIntosh, A. R., Vakorin, V., Kovacevic, N., Wang, H., Diaconescu, A., and Protzner, A. B. (2014). Spatiotemporal dependency of age-related changes in brain signal variability. *Cereb. Cortex* 24, 1806–1817. doi: 10.1093/cercor/bht030

Mizuno, T., Takahashi, T., Cho, R. Y., Kikuchi, M., Murata, T., Takahashi, K., et al. (2010). Assessment of EEG dynamical complexity in Alzheimer's disease using multiscale entropy. *Clin. Neurophysiol.* 121, 1438–1446. doi: 10.1016/j.clinph.2010.03.025

Padmanabhan, A., Lynch, C. J., Schaer, M., and Menon, V. (2017). The default mode network in autism. *Biol. Psychiatry Cogn. Neurosci. Neuroimaging* 2, 476–486. doi: 10.1016/j.bpsc.2017.04.004

Petrella, J. R., Sheldon, F. C., Prince, S. E., Calhoun, V. D., and Doraiswamy, P. M. (2011). Default mode network connectivity in stable vs progressive mild cognitive impairment. *Neurology* 76, 511–517. doi: 10.1212/WNL.0b013e31820af94e

Pincus, S. M. (1991). Approximate entropy as a measure of system-complexity. *Proc. Natl. Acad. Sci. U.S.A.* 88, 2297–2301. doi: 10.1073/pnas.88.6.2297

Power, J. D., Mitra, A., Laumann, T. O., Snyder, A. Z., Schlaggar, B. L., and Petersen, S. E. (2014). Methods to detect, characterize, and remove motion artifact in resting state fMRI. *Neuroimage* 84, 320–341. doi: 10.1016/j.neuroimage.2013.08.048

Raichle, M. E., Macleod, A. M., Snyder, A. Z., Powers, W. J., Gusnard, D. A., and Shulman, G. L. (2001). A default mode of brain function. *Proc. Natl. Acad. Sci. U.S.A.* 98, 676–682. doi: 10.1073/pnas.98.2.676

Richman, J. S., and Moorman, J. R. (2000). Physiological time-series analysis using approximate entropy and sample entropy. *Am. J. Physiol. Heart Circ. Physiol.* 278, H2039–H2049. doi: 10.1152/ajpheart.2000.278.6.H2039

Shehzad, Z., Kelly, A. M., Reiss, P. T., Gee, D. G., Gotimer, K., Uddin, L. Q., et al. (2009). The resting brain: unconstrained yet reliable. *Cereb. Cortex* 19, 2209–2229. doi: 10.1093/cercor/bhn256

Shirer, W. R., Ryali, S., Rykhlevskaia, E., Menon, V., and Greicius, M. D. (2012). Decoding subject-driven cognitive states with whole-brain connectivity patterns. *Cereb. Cortex* 22, 158–165. doi: 10.1093/cercor/bhr099

Smith, R. X., Jann, K., Ances, B., and Wang, D. J. (2015). Wavelet-based regularity analysis reveals recurrent spatiotemporal behavior in resting-state fMRI. *Hum. Brain Mapp.* 36, 3603–3620. doi: 10.1002/hbm.22865

Smith, R. X., Yan, L., and Wang, D. J. (2014). Multiple time scale complexity analysis of resting state FMRI. *Brain Imaging Behav.* 8, 284–291. doi: 10.1007/s11682-013-9276-6

Sokunbi, M. O. (2014). Sample entropy reveals high discriminative power between young and elderly adults in short fMRI data sets. *Front. Neuroinform.* 8:69. doi: 10.3389/fninf.2014.00069

Sokunbi, M. O., Staff, R. T., Waiter, G. D., Ahearn, T. S., Fox, H. C., Deary, I. J., et al. (2011). Inter-individual differences in fMRI entropy measurements in old age. *IEEE Trans. Biomed. Eng.* 58, 3206–3214. doi: 10.1109/TBME.2011.2164793

Sorg, C., Riedl, V., Muhlau, M., Calhoun, V. D., Eichele, T., Laer, L., et al. (2007). Selective changes of resting-state networks in individuals at risk for Alzheimer's disease. *Proc. Natl. Acad. Sci. U.S.A.* 104, 18760–18765. doi: 10.1073/pnas.0708803104

Vakorin, V. A., Lippe, S., and Mcintosh, A. R. (2011). Variability of brain signals processed locally transforms into higher connectivity with brain development. *J. Neurosci.* 31, 6405–6413. doi: 10.1523/JNEUROSCI.3153-10.2011

Vlassenko, A. G., Vaishnavi, S. N., Couture, L., Sacco, D., Shannon, B. J., Mach, R. H., et al. (2010). Spatial correlation between brain aerobic glycolysis and amyloid-beta (Abeta) deposition. *Proc. Natl. Acad. Sci. U.S.A.* 107, 17763–17767. doi: 10.1073/pnas.1010461107

Wang, B., Niu, Y., Miao, L. W., Cao, R., Yan, P. F., Guo, H., et al. (2017). Decreased complexity in Alzheimer's disease: resting-state fMRI evidence of brain entropy mapping. *Front. Aging Neurosci.* 9:378. doi: 10.3389/fnagi.2017.00378

Wang, D. J. J., Jann, K., Fan, C., Qiao, Y., Zang, Y. F., Lu, H., et al. (2018). Neurophysiological basis of multi-scale entropy of brain complexity and its relationship with functional connectivity. *Front. Neurosci.* 12:352. doi: 10.3389/fnins.2018.00352

Weiler, M., De Campos, B. M., Teixeira, C. V. L., Casseb, R. F., Carletti-Cassani, A., Vicentini, J. E., et al. (2017). Intranetwork and internetwork connectivity in patients with Alzheimer disease and the association with cerebrospinal fluid biomarker levels. *J. Psychiatry Neurosci.* 42, 366–377. doi: 10.1503/jpn.160190

Wise, T., Marwood, L., Perkins, A. M., Herane-Vives, A., Joules, R., Lythgoe, D. J., et al. (2017). Instability of default mode network connectivity in major depression: a two-sample confirmation study. *Transl. Psychiatry* 7:e1105. doi: 10.1038/tp.2017.40

Yang, A. C., Huang, C. C., Yeh, H. L., Liu, M. E., Hong, C. J., Tu, P. C., et al. (2013). Complexity of spontaneous BOLD activity in default mode network is correlated with cognitive function in normal male elderly: a multiscale entropy analysis. *Neurobiol. Aging* 34, 428–438. doi: 10.1016/j.neurobiolaging.2012.05.004

Zhang, H. Y., Wang, S. J., Liu, B., Ma, Z. L., Yang, M., Zhang, Z. J., et al. (2010). Resting brain connectivity: changes during the progress of Alzheimer disease. *Radiology* 256, 598–606. doi: 10.1148/radiol.10091701

Zhou, J., Greicius, M. D., Gennatas, E. D., Growdon, M. E., Jang, J. Y., Rabinovici, G. D., et al. (2010). Divergent network connectivity changes in behavioural variant frontotemporal dementia and Alzheimer's disease. *Brain* 133, 1352–1367. doi: 10.1093/brain/awq075

Conflict of Interest Statement: The authors declare that the research was conducted in the absence of any commercial or financial relationships that could be construed as a potential conflict of interest.

frontiers in Neuroscience

ORIGINAL RESEARCH
published: 30 October 2018
doi: 10.3389/fnins.2018.00758

Measuring Brain Complexity During Neural Motor Resonance

Brandon M. Hager[1]*, *Albert C. Yang*[2] *and Jennifer N. Gutsell*[3]

[1] *Department of Psychology, Brandeis University, Waltham, MA, United States,* [2] *Division of Interdisciplinary Medicine and Biotechnology, Beth Israel Deaconess Medical Center, Harvard Medical School, Boston, MA, United States,* [3] *Department of Psychology, Neuroscience Program, and Volen National Center for Complex Systems, Brandeis University, Waltham, MA, United States*

Background: EEG mu-desynchronization is an index of motor resonance (MR) and is used to study social interaction deficiencies, but finding differences in mu-desynchronization does not reveal how nonlinear brain dynamics are affected during MR. The current study explores how nonlinear brain dynamics change during MR. We hypothesized that the complexity of the mu frequency band (8–13 Hz) changes during MR, and that this change would be frequency specific. Additionally, we sought to determine whether complexity at baseline and changes in complexity during action observation would predict MR and changes in network dynamics.

Methods: EEG was recorded from healthy participants ($n = 45$) during rest and during an action observation task. Baseline brain activity was measured followed by participants observing videos of hands squeezing stress balls. We used multiscale entropy (MSE) to quantify the complexity of the mu rhythm during MR. We then performed *post-hoc* graph theory analysis to explore whether nonlinear dynamics during MR affect brain network topology.

Results: We found significant mu-desynchronization during the action observation task and that mu entropy was significantly increased during the task compared to rest, while gamma, beta, theta, and delta bands showed decreased entropy. Moreover, resting-state entropy was significantly predictive of the degree of mu desynchronization. We also observed a decrease in the clustering coefficient in the mu band only and a significant decrease in global alpha efficiency during action observation. MSE during action observation was strongly correlated with alpha network efficiency.

Conclusions: The current findings suggest that the desynchronization of the mu wave during MR results in a local increase of mu entropy in sensorimotor areas, potentially reflecting a release from alpha inhibition. This release from inhibition may be mediated by the baseline MSE in the mu band. The dynamical complexity and network analysis of EEG may provide a useful addition for future studies of MR by incorporating measures of nonlinearity.

Keywords: motor resonance, complexity, network connectivity, EEG, mu suppression

OPEN ACCESS

Edited by:
Xiaoping Philip Hu,
University of California, Riverside, United States

Reviewed by:
Marco Iacoboni,
University of California, Los Angeles, United States
Dezhong Yao,
University of Electronic Science and Technology of China, China
Elzbieta Olejarczyk,
Institute of Biocybernetics and Biomedical Engineering (PAN), Poland

***Correspondence:**
Brandon M. Hager
bhager@brandeis.edu

Specialty section:
This article was submitted to Brain Imaging Methods, a section of the journal Frontiers in Neuroscience

Received: *31 May 2018*
Accepted: *02 October 2018*
Published: *30 October 2018*

Citation:
Hager BM, Yang AC and Gutsell JN (2018) Measuring Brain Complexity During Neural Motor Resonance. Front. Neurosci. 12:758. doi: 10.3389/fnins.2018.00758

INTRODUCTION

There has been great interest in the idea of neural mirroring–neural simulation of the actions and experiences of others while observing them–as a central process contributing to action understanding and experience sharing. Using electroencephalogram (EEG) to record the desynchronization of the mu wave (8–13 Hz) over sensorimotor regions is gaining popularity as a measure of neural simulation (e.g., Cheng et al., 2008; Pineda and Hecht, 2009; Gutsell and Inzlicht, 2010; Perry et al., 2010; Fabi and Leuthold, 2017; Li et al., 2017), including in the clinical setting (Oberman et al., 2008, 2013; Fan et al., 2010; Mitra et al., 2014; Minichino et al., 2016). Several researchers have used mu desynchronization to investigate impaired social and emotional processing in disorders like schizophrenia and autism (Oberman et al., 2005; McCormick et al., 2012; Horan et al., 2014; Brown et al., 2016). However, studies using mu desynchronization during action observation, have relied solely on measuring attenuation of the mu power spectrum. Utilizing the Fast Fourier transform (FFT) to obtain the average power of pre-selected frequency components or the Morlet wavelet transform to obtain frequency information at a specific moment in time, can only provide information on power spectrum changes and fails to address potentially important changes to nonlinear brain dynamics. The current study measured changes to neural complexity and network connectivity that occur during action observation, and sought to assess how these changes are related to, and might supplement, the linear changes observed in the mu power spectrum.

Viewing the actions of another person triggers neural representations similar to when actually performing the same action (di Pellegrino et al., 1992; Rizzolatti and Craighero, 2004; Rizzolatti, 2005), and such motor resonance (MR) is thought to transform visual information about the action including basic intentions into knowledge (Rizzolatti et al., 2009; Liu et al., 2016). EEG mu desynchronization is considered a valid measure of MR (see Fox et al., 2015 for a meta-analysis and Hobson and Bishop, 2016, for a critical perspective). The mu-rhythm can be picked up over the sensorimotor cortex at central electrodes (C3, C1, CZ, C2, and C4 electrodes), and its desynchronization is correlated with activation in areas thought to be part of the human mirror system, including the dorsal premotor cortex, the primary somatosensory cortex, and the inferior parietal lobe (Perry and Bentin, 2009; Arnstein et al., 2011; Yin et al., 2016). Since the decrease in mu amplitude during mu desynchronization occurs because the number of synchronously active neurons firing at a frequency of 8–13 Hz decreases during action and action observation (Lopes da Silva, 1991), the underlying nonlinear patterns of activity should become more complex (non-randomly varying), and may provide information on the adaptability of a system or network of connections to a stimulus (McIntosh et al., 2008; Manor et al., 2010; Vakorin et al., 2011). Such nonlinear patterns contain information that is not accessible by spectral measures (Meyer-Lindenberg et al., 1998; Abásolo et al., 2006; Park et al., 2007; Mizuno et al., 2010), and the current study is a novel investigation of EEG signal during action observation.

A promising approach to analyzing nonlinear dynamics in the brain is multi scale entropy (MSE), which measures entropy over multiple time scales inherent in a time series (Costa et al., 2002). Sample entropy of each coarse-grained time series serves as an index of signal complexity by evaluating the occurrence of repetitive patterns. Thus, using MSE analysis in this study allows us to extract meaningful information about the changes to nonlinear dynamics that occur in the EEG signal during action observation. Moreover, changes in entropy indexed using MSE, are likely to indicate, to some degree, a change in the neural underpinnings of connectivity (Friston et al., 1995; Sporns et al., 2000; Takahashi et al., 2010). To validate this assumption, we also measured changes in connectivity across the scalp using graph theoretical analysis and tested their link to changes in entropy. More specifically, we used global efficiency and the cluster coefficient (graph theoretical measures), to provide information on local and global changes to functional connectivity that result from local changes in nonlinear dynamics.

In sum, the first goal of the current study was to capture changes in the complexity of the signal measured over the sensorimotor area during MR using MSE analysis. The second goal was to determine how resting state MSE relates to mu desynchronization during MR. Resting-state complexity has been previously used as a predictor for risk of developing ASD (Bosl et al., 2011), as well as predicting cognitive function in Alzheimer's disease (Mizuno et al., 2010). The finding by Mizuno et al. (2010), suggests that complexity at rest can predict one's adaptability to a future "engaged" or active state. Along the same lines, we expected the level of resting MSE measured in the mu frequency band, to be predictive of the amount of decrease, if any, in the mu power spectrum during action observation. The final goal of the study was to assess whether MR changes network communication in the gamma, beta, alpha, theta, and delta bands, and its relationship to the MSE measured over the sensorimotor area.

THE CURRENT RESEARCH

We measured MR during action observation, using mu desynchronization, as part of a larger study that tested how perceptions of warmth and competence of target individuals affect MR. Participants first viewed personality ratings of varying combinations of the warmth and competence of a target person followed by a short video of ostensibly that person performing an action. We collapsed the action observation data across all warmth and competence conditions to assess mu desynchronization, MSE change, and network changes. We hypothesized that the level of MSE (average entropy across all scale factors) measured in the mu frequency band would increase during action observation relative to baseline, and that an increase would be linked to mu desynchronization, such that stronger desynchronization would be associated with a larger increase in MSE. Additionally, we tested whether changes to MSE during action observation was frequency-band specific by analyzing change in the MSE values in four other frequency bands (gamma, beta, theta, and delta). We

hypothesized that the level of baseline MSE would predict the degree of mu desynchronization, thereby being a determinant of adaptability during action observation. Finally, we used graph theory analysis to assess the effect of mu desynchronization on network communication by analyzing global efficiency in the five mentioned frequency bands, and the cluster coefficient over the sensorimotor area, respectively.

METHODS

Participants

Participants ($n = 66$) right-handed undergraduate college students had normal or corrected vision, and the ability to read and write fluently in English. Participants were all right-handed to ensure analogous cortical responses to videos of right hands performing simple motor activities.

All participants provided informed consent and participated in the research for course credit or financial compensation. Participants were excluded due to equipment failure resulting in too many non-functioning electrodes (cutoff of 5 non-functioning electrodes; $N = 4$), excessive EEG artifacts in the C3 electrode ($N = 12$; such as blinks, electromyogram (EMG), line noise, and visible signal drift), and visually excessive frontal alpha activity ($N = 4$) which suggests a participant might be sleeping, leading to a final sample of 45 participants (mean age = 18.814, SD = 0.958; 33 female).

Procedure

The experimental protocol and data acquisition procedure were approved by the Brandeis Institutional Review Board. After EEG setup was complete, participants were asked to repeatedly squeeze a stress ball using their right hand for 15 s while we filmed their hand. This both created a baseline for brain activity during actual hand movement and reinforced the cover story that participants would be watching videos previously recorded from other participants. Participants then underwent a measure of baseline neural activity for which they sat completely still, first with their eyes closed for 1.5 min, then open for 1.5 min, then while watching a video of white noise for 1 min. The baseline recorded with eyes open was used to calculate the complexity of the mu rhythm at rest.

Following the baseline recording, participants were told that they would be taking a personality test. The test required them to rate themselves on a list of adjectives related to warmth and competence. They were then told that nine other people had previously taken the same test and had their hand movement recorded. EEG was recorded while participants viewed the action videos following the warmth and competence information. Finally, participants filled out a demographic questionnaire, were debriefed, thanked, and dismissed.

Action Observation Task

The task consisted of 135 trials. During each trial, participants were first presented with a video of white noise for 2,000–2,300 ms followed by a fixation cross for 500 ms. They then viewed a screen with a target's name (e.g., "Participant A"), a simple silhouette and warmth/competence scores (e.g., "Warmth: High, Competence: Low") for 4,000 ms, followed by a video of what was ostensibly that person's hand squeezing a yellow stress ball for 2,000 ms at the rate of approximately one squeeze per second (see **Figure 1** for a depiction of a typical trial). Each hand was always paired with the same identity; all hands were White and with an even gender split (five female). The task was split into two blocks of ∼15 min in length divided by a short break of a duration determined by the participant.

EEG Recording and Processing

EEG was recorded from 32 active electrodes embedded in a stretch-lycra cap (ActiCap, BrainProducts GmbH, Munich, Germany) arranged per the 10–20 system with the impedances kept below 10 kΩ. The EEG was digitized at 500 Hz using BrainAmp amplifiers and BrainVision recorder software (BrainProducts GmbH, Munich, Germany) with an initial reference at FCz. The data was then re-referenced offline using the Reference Electrode Standardization Technique to standardize the reference of scalp EEG recordings to a point at infinity that, being far from all possible neural sources, acts like a neutral virtual reference (Yao, 2001; Dong et al., 2017). To avoid corrupting the raw data, we manually extracted segments of artifact-free EEG data by visually identifying and then removing vertical eye movements, blinks, muscle activity, and other artifact sources. From 40,000 data points, we extracted at least 20,000 artifact-free data points from the resting state task, and from 14,000 data points we extracted at least 12,000 artifact-free data points from the action observation task. For each of the 2-s action observation segments, we then computed the integrated power in the 8–13 Hz range using a Fast Fourier Transform (FFT) performed at 0.2 s intervals with an overlap of 0.25 s (using a Hamming window with 25% overlap). Finally, we averaged the segments over all trials and calculated Mu desynchronization scores with the following formulas: $(\ln(\mu_{task\ power}) - \ln(\mu_{pre-task\ resting\ power}))/\ln(\mu_{pre-task\ resting\ power})^{*}100$.

Multiscale Entropy (MSE) Analysis

MSE analysis (Costa et al., 2002, 2005) was developed to estimate sample entropy in multiple time scales by using a coarse-graining procedure. MSE analysis uses sample entropy (SE) because it provides greater consistency and is less dependent on a given signal length compared with other entropy methods (Richman and Moorman, 2000). MSE calculation can be summarized in the following three steps: (a) constructing coarse-grained time series per different scale factors (SF); (b) quantifying the SE of each coarse-grained time series; and (c) examining the sample entropy profile over a range of scales. Per this method, the length of each coarse-grained time series is equal to the length of the original time series divided by the SF. For Scale 1, the time series is merely the original time series.

The MSE analysis of EEG signal has been described previously (Catarino et al., 2011) using parameters of $m = 2$, $r = 0.15$, and a SF up to 40. In this study, we used $m = 2$, $r = 0.15$ standard deviation (SD), $N = 14{,}000$ data points and SF of 20 for resting state, and $N = 14{,}000$ data points and SF of 20 for the action observation task. We $N/SF = 14{,}000/20 = 700$ data points,

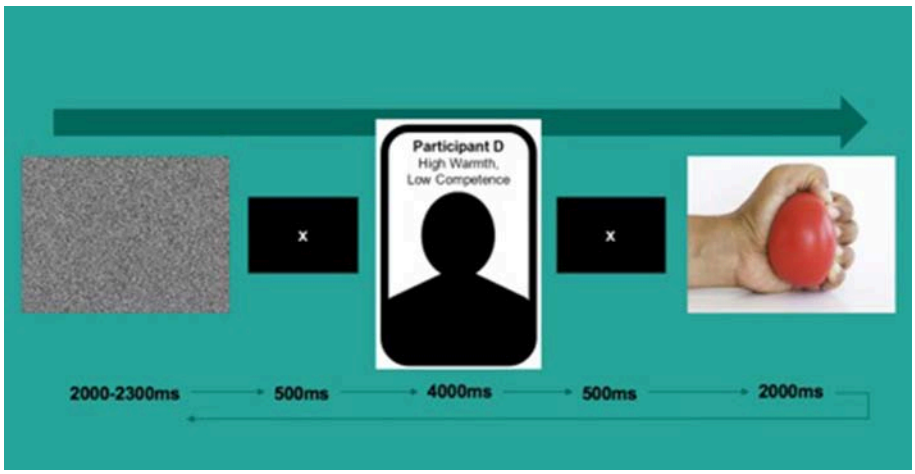

FIGURE 1 | Depiction of a typical task trial.

which is enough to obtain a reliable estimation of the SE values (Richman and Moorman, 2000).

Using the MSE of resting-state EEG signal as the reference, we classified MSE profiles into three types: (1) increased complexity (i.e., increased entropy in all scales), (2) reduced complexity toward regularity (i.e., decreased entropy in all scales), or (3) reduced complexity toward randomness (i.e., increased entropy in fine scales followed by decay in entropy as the scale factors increase; Yang et al., 2015). The random type of MSE profile quantifies uncorrelated randomness that cannot be fully captured by single-scale entropy.

Network Analysis

We used the first 2 s from the eyes-open baseline and the first of seven segments from the action observation task, for analysis. We then calculated the respective phase coherences (rPCs) for every electrode pair to obtain network measures (please see **Figure 2** for a graphical illustration of the procedure). The method used for obtaining the rPC is the phase-locking index (Tass et al., 1998). Once the rPC values between all the electrode-pairs were calculated, we obtained an undirected and weighted network by regarding each electrode as a node and the rPC values as the weight between two corresponding nodes. Then we considered two network measures, clustering coefficient (CC; Rubinov and Sporns, 2010) and global efficiency (GE; Rubinov and Sporns, 2010) to investigate the topological characteristics of the network. Based on graph theory, in the undirected and weighted network with n nodes in a nodes' set $\boldsymbol{N}$, CC of a node j is obtained by the ratio of geometric mean of triangles around the node to the maximum possible number of the connections between all the neighbors of the node, as

$$CC_j = \frac{1}{k_j(k_j-1)} \sum_{i,m=1}^{N} (w_{ij} w_{im} w_{jm})^{1/3}, \quad (1)$$

where

$$k_j = \sum_{i=1}^{N} w_{ij} \quad (2)$$

is the weighted degree of node j, w_{ij} are connection weights which are normalized between 0 and 1 for all i and j related to edges (i, j), and N is the number of all nodes. Importantly, the clustering coefficient can indicate the degree of local interconnectedness of a node and applied to evaluate the local structure of a graph (Rubinov and Sporns, 2010; Miraglia et al., 2017; Wang and Tao, 2017). The average value of all nodes' CC (denoted as aver_CC in this paper) is the average clustering coefficient CC over all nodes, as expressed in Equation (1).

The global efficiency that allows the existence of isolated points is the reciprocal of the shortest path, and not only reflects the global traffic capacity and integration, but also evaluates the performance of the graph effectively (Achard and Bullmore, 2007). The definition of global efficiency (denoted as GE) is given in Equation (3):

$$GE = \frac{1}{N(N-1)} \sum_{i,j,i\neq j}^{N} \frac{1}{d_{ij}}, \quad (3)$$

The shortest weighted path length between node i and j is defined as Equation (2):

$$d_{ij} = \sum\nolimits_{a_{uv} \in gi \overset{w}{\longleftrightarrow} j} f(w_{uv}), \quad (4)$$

where f is a map (e.g., an inverse) from weight (w_{uv}) to length, and g_{ij} is the shortest weighted path between node i and j (Rubinov and Sporns, 2010).

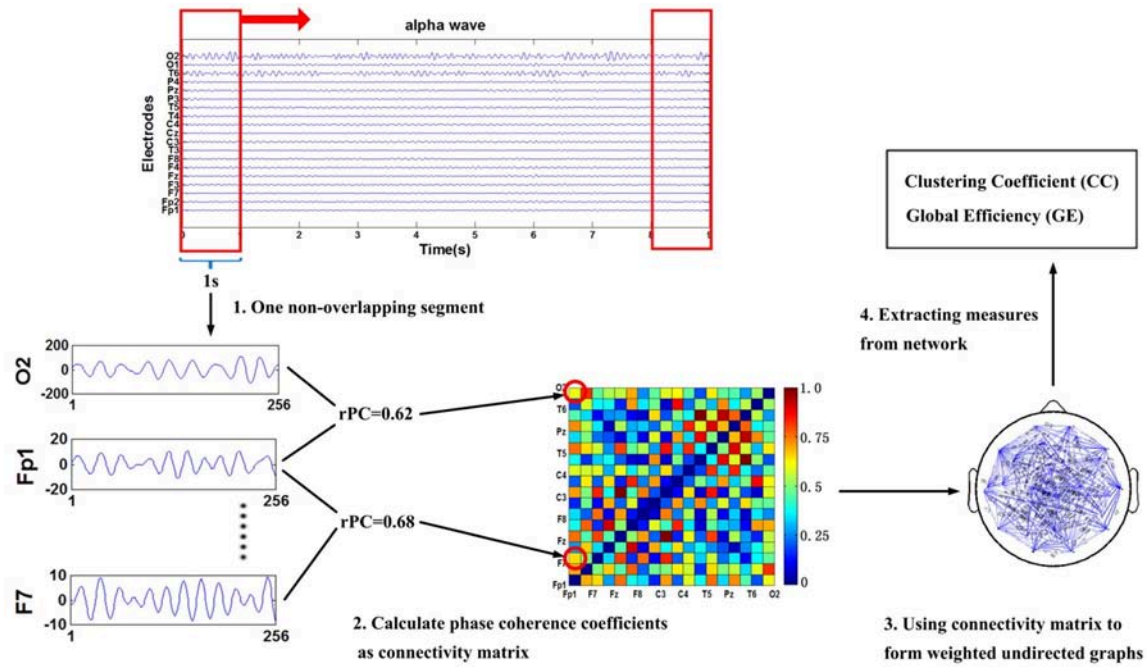

FIGURE 2 | The multi-step illustration of the procedure for extracting networks' measures from EEG time series to sub-network. To be noted, the EEG series given in this graph are the 10th subject's resting state data set and the electrode Fp1, F7, and O2 are shown as an example of the phase synchronization coefficients computed between two electrodes in the alpha band. Additionally, the graph is fully connected. Abbreviation: rPC: respective phase coherence.

Statistical Analysis

Statistical analyses were carried out using R version 3.3.2 (R Core Team, 2016). We set the alpha significance value at .05 and confirmed the normal distribution of the MSE values using the Kolmogorov–Smirnov normality test and by examining skewness and kurtosis values, for the (C3, C4, CZ, F3, F4, FZ, P3, P4, PZ, O1, O2, and OZ) electrodes. We found all MSE scores to be normally distributed. To determine the complexity score of the mu signal, we calculated the average sample entropy across all scale factors. All analyses were performed on a subset of electrodes reflecting neural activation in the sensorimotor cortex (C3, C4, and CZ as a control), which have been shown to produce the strongest mu signal, and frontal (F3, FZ, and F4), parietal (P3, PZ, and P4), and occipital (O1, OZ, and O2) areas as control regions. Repeated measures ANOVAs were carried out using the "car" package (Fox et al., 2012). Collapsing across the original experimental task conditions, we averaged MSE and mu power across all warmth/competence conditions to collapse the data into a single motor observation condition. We used Bonferroni correction to control for multiple comparisons, for 12 electrode comparisons the corrected $p\text{-}value = 0.05/12 = 0.004$.

RESULTS

Mu Desynchronization

We confirmed that significant mu desynchronization had occurred in our region of interest using a series of one sample *t*-tests on desynchronization scores obtained from electrodes C3 [$t_{(44)} = -5.209,\ p < 0.001,\ d = 0.759$] and C4 [$t_{(44)} = -3.117,\ p = 0.003,\ d = 0.465$], and that no significant alpha desynchronization occurred in the occipital electrodes O1 [$t_{(44)} = -0.421,\ p = 0.676$], *Oz* [$t_{(44)} = 0.043,\ p = 0.966$], or O2 [$t_{(44)} = 1.526,\ p = 0.134$]. These findings suggest that we indeed picked up mu desynchronization due to MR and not changes in alpha related to attentional shifts. Additionally, we performed a 3-way repeated measures ANOVA with Mu/alpha desynchronization as the dependent variable, and electrode centrality [frontal (F3, F4, Fz), central (C3, C4, Cz), parietal (P3, P4, Pz), and occipital (O1, O2, and Oz) electrodes], and electrode lateralization (left, central, right) as the within-subject factors. We found a significant main effect of lateralization [$F_{(2,\ 88)} = 40.733,\ p < 0.001$], no effect of centrality [$F_{(3,\ 132)} = 1.152,\ p = 0.331$], and a significant interaction effect between lateralization and centrality [$F_{(6,\ 264)} = 37.557,\ p < 0.001$]. Unpacking the interaction using simple effects, we found significantly more desynchronization at the C3 electrode compared to posterior P3, [$F_{(1,\ 44)} = 9.133,\ p = 0.004$], Pz [$F_{(1,\ 44)} = 32.023,\ p < 0.001$], P4, [$F_{(1,\ 44)} = 40.321,\ p < 0.001$], occipital, O1, [$F_{(1,\ 44)} = 42.602,\ p < 0.001$], Oz, [$F_{(1,\ 44)} = 18.302,\ p < 0.001$], and O2, [$F_{(1,\ 44)} = 28.230,\ p < 0.001$], and frontal, Fz [$F_{(1,\ 44)} = 28.161,\ p < 0.001$], F4 [$F_{(1,\ 44)} = 30.646,\ p < 0.001$], F3 [$F_{(1,\ 44)} = 28.336,\ p < 0.001$] electrodes, further confirming that mu-desynchronization was region specific. An additional one sample *t*-test was performed to check for beta desynchronization and no significant beta desynchronization was found [$t_{(44)} = -1.101,\ p = 0.277$]. In sum, these findings suggest

that desynchronization of mu was primarily localized to the C3 electrode–our region of interest.

Multiscale Entropy (MSE) Analysis

To test for changes in entropy in the mu frequency band during MR, we performed a paired *t*-test on our electrode of interest (C3). We found average entropy to be higher during the task (*mean = 1.057, SD = 0.097*) compared to rest [*mean = 1.004, SD = 0.129, $t_{(44)} = 3.524$, p = 0.001, d = 0.525*], indicating increased complexity of the mu signal. To determine whether entropy change during MR was frequency-band specific, we performed a series of paired *t*-tests on the five frequency bands (gamma = 30–60 Hz, beta = 13–30 Hz, alpha = 8–13 Hz, theta = 4–8 Hz, and delta = 1–4 Hz) between rest and task. After Bonferroni correction, we found significant changes in entropy for all frequency bands, as shown in **Figure 3**. Gamma *(baseline, m = 0.936, SD = 0.085; task, m = 0.846, SD = 0.106)* [$t_{(44)} = 5.892$, $p < 0.001$, $d = 0.878$], beta *(baseline, m = 1.352, SD = 0.073; task, m = 1.311, SD = 0.073)* [$t_{(44)} = 3.279$, $p = 0.002$, $d = 0.489$], theta *(baseline, m = 1.124, SD = 0.051; task, m = 1.029, SD = 0.071)* [$t_{(44)} = 7.636$, $p < 0.001$, $d = 1.138$], and delta *(baseline, m = 0.704, SD = 0.041; task, m = 0.626, SD = 0.063)* [$t_{(44)} = 8.307$, $p < 0.001$, $d = 1.238$] all showed a decrease in entropy for task compared to rest. These findings indicate that complexity change has a unique increase in the alpha band while all other frequencies showed a significant decrease in complexity.

To determine whether MSE change in the alpha band during MR was region specific, we performed a 3-way repeated-measures ANOVA with average entropy as the dependent variable, and condition (resting vs. task) and electrode (C3, C4, Cz, F3, F4, Fz, P3, P4, Pz, O1, O2, and Oz) as the within-subject factors. We found significant main effects for electrode [$F_{(11, 484)} = 10.981$, $p < 0.001$], condition [$F_{(1, 44)} = 8.791$, $p = 0.005$], and an interaction between condition and electrode [$F_{(11, 484)} = 2.003$, $p = 0.026$]. To unpack the interaction, we performed pairwise comparisons for each electrode showing significant increases in average entropy in the C3 [$F_{(1, 44)} = 12.468$, $p < 0.001$, $\eta_p^2 = 0.220$] and C4 [$F_{(1, 44)} = 17.953$, $p < 0.001$, $\eta_p^2 = 0.290$] electrodes. This finding suggests that changes in MSE in the Mu frequency band between baseline and task only occur in the bilateral sensorimotor area, with no changes to occipital regions with alpha activity.

To determine whether entropy change in the alpha band during MR was dependent on the SF, we performed a 3-way repeated-measures ANOVA with entropy as the dependent variable, and condition (resting vs. task) and SF (1 through 20) as the within-subject factors. A significant condition by SF interaction effect was found [$F_{(19, 798)} = 15.397$, $p < 0.001$]. This finding indicates that the sample entropy curves of each condition presented a different slope as the scale factor increased. Although the difference between conditions is not noticeable for smaller scale factors, the curves for both conditions become distinguishable for higher scale factors, representing greater differences in sample entropy at higher scale factors.

To determine whether complexity of the mu signal predicts MR, we used multiple linear regression models to examine the relationship between MR and baseline entropy. Using general linear hypothesis testing on mu desynchronization scores, the best model fit was found for model 1 with a significant regression equation [$F_{(1, 43)} = 11.73$, $p = 0.001$, *with an* R^2 *of 0.214*], as shown in **Table 1**. The model indicates that resting state entropy is significantly predictive of MR such that higher baseline entropy predicts less mu desynchronization, indicating less MR.

Efficiency Analysis

To explore the relationship between network efficiency and MR, we performed a 3-way repeated measures ANOVA with global

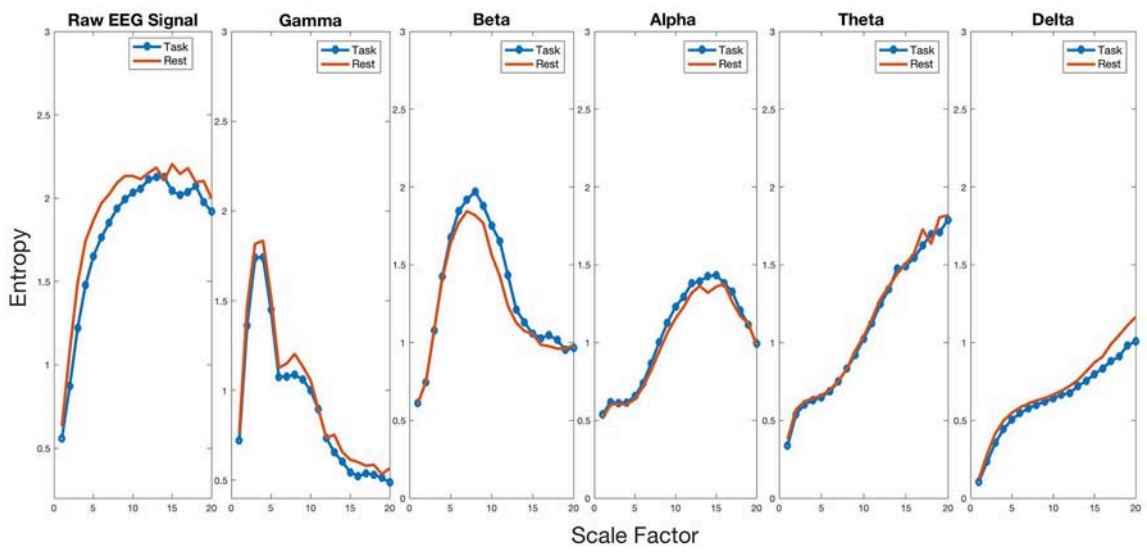

FIGURE 3 | Complexity profiles of the raw signal and all frequency bands for baseline and task.

efficiency as the dependent variable, and condition (resting vs. observation), and frequency band (gamma, beta, alpha, theta, delta) as the within-subject factors. We found a significant main effect for frequency [$F_{(4,\ 176)} = 64.452,\ p < 0.001,\ \eta_p^2 = 0.593$] and condition [$F_{(1,\ 44)} = 5.723,\ p = 0.021,\ \eta_p^2 = 0.113$] and no significant interaction effect for condition and frequency [$F_{(4,\ 176)} = 0.934,\ p = 0.446$]. We decided to perform pairwise comparisons for each frequency band to determine whether global efficiency modification was frequency specific during MR. The analysis revealed a significant decrease in efficiency in the alpha [$F_{(1,\ 44)} = 15.509,\ p < 0.001,\ \eta_p^2 = 0.260$] frequency band only. These findings indicate that global efficiency decreases during action observation in the alpha network only. As shown in **Figure 4**, alpha connectivity was reduced in frontal, central and parietal areas.

To explore the relationship between the cluster coefficient over the sensorimotor area and MR, we performed pairwise comparisons for the alpha frequency band. A significant decrease in the CC was shown in the alpha band [$t_{(44)} = 2.879,\ p = 0.006,\ d = 0.439$] during the task condition. These findings indicate that the local efficiency over the C3 electrode decreases during action observation in the mu frequency band.

TABLE 1 | Parameter estimates, approximate *p*-values, and associated goodness-of-fit statistics for a series of models depicting the relationship between mu desynchronization scores (as an index of motor resonance) and complexity of the mu rhythm.

Predictor	Model 1 ß(SE)	Model 2 ß(SE)	Model 3 ß(SE)
Intercept	−77.88*** (19.29)	−41.90 (29.16)	−4.929 (7.597)
C3 resting complexity	65.17** (19.03)		
C3 task complexity		27.95 (27.43)	
Baseline Mu power			−3.839 (3.708)
MODEL FIT STATISTICS			
R^2	0.214	0.024	0.024
RMSE	15.98	17.82	17.81
DF	43	43	43

****p < 0.001, **p < 0.01. RMSE, root mean square error; SE, standard error of the mean; DF, degrees of freedom.*

Finally, to determine whether there is a relationship between complexity change, measured as the percent change in entropy from baseline to task, and percent change in task efficiency in the alpha band, we performed a simple correlation, finding that there is a significant negative relationship between entropy and global efficiency during the task [$t_{(43)} = -2.653,\ p = 0.011,\ r = -0.375$] suggesting that there may be a direct relationship between efficiency change and complexity change.

DISCUSSION

The change in amplitude in the mu frequency band over the sensorimotor area, resulting from the observation of object-oriented actions, has been used as a marker of MR (Fox et al., 2015). The intention of this study was to explore how nonlinear brain dynamics change during MR, and how these changes are related to the linear changes observed in the mu power spectrum. We found that MSE measured from the C3 electrode over the sensorimotor area during action observation, increases in the mu frequency band only. At the same time, the MSE of the raw signal and other frequency bands decreases in response to action observation. These findings confirm our hypothesis that a decrease in the mu power spectrum results in increased complexity in that same frequency band, and the increase is frequency specific. We did not predict decreased complexity in the other frequency bands and this phenomenon should be addressed in future studies. The respective decrease in global efficiency in the alpha band during MR, may indicate greater local information processing due to a release from so-called alpha inhibition. The increased complexity in the mu band and decreased global alpha efficiency may underlie an increase to local functional integration (Sporns et al., 2000). Further supporting the link between increased complexity and MR, we found that larger decreases in mu power are associated with greater increases to the MSE of that signal.

Oscillations within specific frequency bands h ave been considered to be associated with information processing (Başar et al., 2001; Ghanbari et al., 2015), and our findings suggest that information processing increases in the mu band during MR. Interestingly, Ghanbari et al. (2015) found a significantly negative relationship between change in alpha connectivity and change in

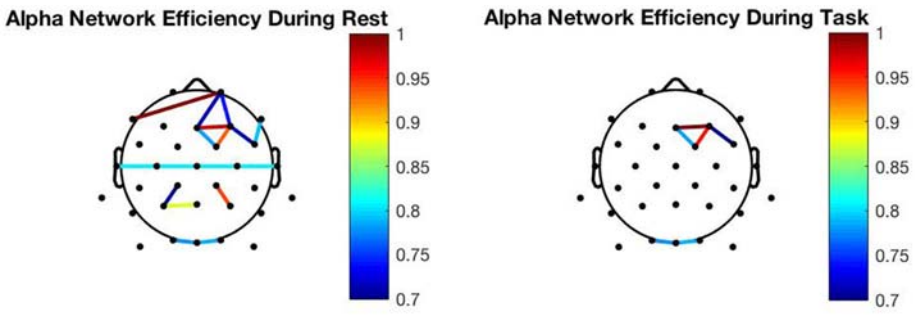

FIGURE 4 | Network changes: Resting alpha network connectivity (Left) Alpha network connectivity during action observation (Right). To be noted, the graphs presented are from the 10th subject.

MSE in patients with ASD, but no such relationship in the healthy controls. We did not find any significant relationship between complexity change and network efficiency change, confirming this finding for healthy controls. It is important to note, that the decrease in entropy within the other frequency bands does not necessarily indicate a reduction in information processing (McDonough and Nashiro, 2014), but instead may reflect that the flow of information in the sensorimotor area being mainly regulated by the alpha band during action observation.

Interestingly, the differences in the alpha complexity profiles of rest and task condition appear to be mainly in the higher time scales. Greater entropy at high scale factors are believed to capture long-range temporal correlations (Bhattacharya et al., 2005). Bhattacharya et al. (2005) found that neurons that showed long-range correlations also showed statistically significantly correlated firing, suggesting that the presence of long-range correlations indicates a memory of the firing pattern. The decrease in long-range correlations in the mu band reflects we found, may therefore reflect greater non-random variability in the underlying neuronal firing patterns, and therefore greater complexity.

Can EEG Complexity Predict Motor Resonance?

We expected MSE measured in the mu band over the sensorimotor area to increase during action observation due to less synchronous firing, reflecting an increase of the non-random variability within the underlying patterns of activity. Our analyses confirmed this hypothesis showing that a greater percent increase in MSE from baseline to action observation in the mu band was significantly associated with a greater decrease in the mu power spectrum, indicating greater MR. We also hypothesized that resting MSE measured in the mu band would predict decreases in the mu power spectrum during action observation, reflecting adaptability. Complexity may be a reflection of the adaptability to a constantly changing environment (Hager et al., 2016), and it may be that the level of MSE at rest predicts the adaptability to information processing when viewing an action. Specifically, we found that higher levels of resting MSE in the mu band were predictive of less mu desynchronization during action observation. This finding suggests that measuring signal complexity in the mu band at rest may have the potential to serve as a predictor of adaptability to a stimulus intended to trigger mu desynchronization.

EEG Network Changes

The observed increase in MSE during action observation was related to a decrease in global efficiency of the alpha network. If the role of the alpha rhythm is indeed inhibitory (Klimesch et al., 2007; Jensen and Mazaheri, 2010; Klimesch, 2012), this finding may suggest that signal complexity measured in the mu band in the sensorimotor area acts as a mediator of release from alpha inhibition. We found decreased network efficiency in the alpha band during MR, and no change in the gamma, theta, and delta bands. The reduced global efficiency in the alpha band suggests a reduction in the exchange of information across the brain in that band. Klimesch (2012), posited that the magnitude of alpha desynchronization reflects the degree of cortical activation because lower alpha power releases inhibition, and we found a stronger relationship between MSE and mu desynchronization when global alpha efficiency was lower during action observation. Since alpha oscillations are associated with inhibiting neural networks (Klimesch et al., 2007; Jensen et al., 2014), our finding of increased complexity in the mu band during mu desynchronization and decreased global alpha network efficiency, may indicate decreased alpha inhibition during action observation; an unattainable observation when looking at the power spectrum alone.

CONCLUSIONS

Our current study suggests that the desynchronization of mu over the sensorimotor area during the observation of an object-oriented action results in previously unexplored changes to nonlinear brain dynamics. The degree to which MSE measured in the mu band increases during action observation, may be related to individual differences in basal complexity leading to a dampening of local alpha and global alpha inhibition. Our findings suggest that increased complexity in the sensorimotor area reflects an increase of local information capacity, thus enabling successful processing of stimulus-related information, by triggering a decrease in alpha inhibition. These findings encourage future incorporation of measures of nonlinearity into analysis of MR to improve understanding of how the brain processes information.

AUTHOR CONTRIBUTIONS

BH and JG conceived of the presented idea. BH developed the theory and performed the computations. AY and JG verified the analytical methods. JG supervised the findings of this work. BH spearheaded writing the manuscript. All authors discussed the results and contributed to the final manuscript.

FUNDING

This work was supported by a grant from the National Institutes of Health, USA (NIH grant 5T32GM084907-09).

REFERENCES

Abásolo, D., Hornero, R., Espino, P., Álvarez, D., and Poza, J. (2006). Entropy analysis of the EEG background activity in Alzheimer's disease patients. *Physiol. Measure.* 27, 241–253. doi: 10.1088/0967-3334/27/3/003

Achard, S., and Bullmore, E. (2007). Efficiency and cost of economical brain functional networks. *PLoS Comput. Biol.* 3:e17. doi: 10.1371/journal.pcbi.0030017

Arnstein, D., Cui, F., Keysers, C., Maurits, N. M., and Gazzola, V. (2011). μ-suppression during action observation and execution correlates with BOLD in

dorsal premotor, inferior parietal, and SI cortices. *J. Neurosci.* 31, 14243–14249. doi: 10.1523/JNEUROSCI.0963-11.2011

Başar, E., Başar-Eroglu, C., Karakaş, S., and Schürmann, M. (2001). Gamma, alpha, delta, and theta oscillations govern cognitive processes. *Int. J. Psychophysiol.* 39, 241–248. doi: 10.1016/S0167-8760(00)00145-8

Bhattacharya, J., Edwards, J., Mamelak, A. N., and Schuman, E. M. (2005). Long-range temporal correlations in the spontaneous spiking of neurons in the hippocampal-amygdala complex of humans. *Neuroscience* 131, 547–555. doi: 10.1016/j.neuroscience.2004.11.013

Bosl, W., Tierney, A., Tager-Flusberg, H., and Nelson, C. (2011). EEG complexity as a biomarker for autism spectrum disorder risk. *BMC Med.* 9:18. doi: 10.1186/1741-7015-9-18

Brown, E. C., Gonzalez-Liencres, C., Tas, C., and Brüne, M. (2016). Reward modulates the mirror neuron system in schizophrenia: a study into the mu rhythm suppression, empathy, and mental state attribution. *Soc. Neurosci.* 11, 175–186. doi: 10.1080/17470919.2015.1053982

Catarino, A., Churches, O., Baron-Cohen, S., Andrade, A., and Ring, H. (2011). Atypical EEG complexity in autism spectrum conditions: a multiscale entropy analysis. *Clin. Neurophysiol.* 122, 2375–2383. doi: 10.1016/j.clinph.2011.05.004

Cheng, Y., Yang, C. Y., Lin, C. P., Lee, P. L., and Decety, J. (2008). The perception of pain in others suppresses somatosensory oscillations: a magnetoencephalography study. *NeuroImage* 40, 1833–1840. doi: 10.1016/j.neuroimage.2008.01.064

Costa, M., Goldberger, A. L., and Peng, C.-K. (2002). Multiscale entropy analysis of complex physiologic time series. *Phys. Rev. Lett.* 89:68102. doi: 10.1103/PhysRevLett.89.068102

Costa, M., Goldberger, A. L., and Peng, C. K. (2005). Multiscale entropy analysis of biological signals. *Phys. Rev. E Stat. Nonlinear Soft Matter Phys.* 71, 1–18. doi: 10.1103/PhysRevE.71.021906

di Pellegrino, G., Fadiga, L., Fogassi, L., Gallese, V., and Rizzolatti, G. (1992). Understanding motor events: a neurophysiological study. *Exp. Brain Res.* 91, 176–180. doi: 10.1007/BF00230027

Dong, L., Li, F., Liu, Q., Wen, X., Lai, Y., Xu, P., et al. (2017). MATLAB toolboxes for reference electrode standardization technique (REST) of scalp EEG. *Front. Neurosci.* 11:601. doi: 10.3389/fnins.2017.00601

Fabi, S., and Leuthold, H. (2017). Empathy for pain influences perceptual and motor processing: evidence from response force, ERPs, and EEG oscillations. *Soc. Neurosci.* 12, 701–716. doi: 10.1080/17470919.2016.1238009

Fan, Y.-T., Decety, J., Yang, C.-Y., Liu, J.-L., and Cheng, Y. (2010). Unbroken mirror neurons in autism spectrum disorders. *J. Child Psychol. Psychiatry* 51, 981–988. doi: 10.1111/j.1469-7610.2010.02269.x

Fox, J., Weisberg, S., Bates, D., and Fox, M. J. (2012). Package 'car'. Vienna: R Foundation for Statistical Computing.

Fox, N. A, Bakermans-Kranenburg, M. J., Yoo, K. H., Bowman, L. C., Cannon, E. N., Vanderwert, R. E., et al. (2015). Assessing human mirror activity with EEG mu rhythm: a meta-analysis. *Psychol. Bull.* 2016:31. doi: 10.1037/bul0000031

Friston, K. J., Tononi, G., Sporns, O., and Edelman, G. M. (1995). Characterising the complexity of neuronal interactions. *Hum. Brain Mapp.* 3, 302–314. doi: 10.1002/hbm.460030405

Ghanbari, Y., Bloy, L., Christopher Edgar, J., Blaskey, L., Verma, R., and Roberts, T. P. L. (2015). Joint analysis of band-specific functional connectivity and signal complexity in autism. *J. Autism Dev. Disord.* 45, 444–460. doi: 10.1007/s10803-013-1915-7

Gutsell, J. N., and Inzlicht, M. (2010). Empathy constrained: prejudice predicts reduced mental simulation of actions during observation of outgroups. *J. Exp. Soc. Psychol.* 46, 841–845. doi: 10.1016/j.jesp.2010.03.011

Hager, B., Yang, A. C., Brady, R., Meda, S., Clementz, B., Pearlson, G. D., et al. (2016). Neural complexity as a potential translational biomarker for psychosis. *J. Affect. Disord.* 20, 1–11. doi: 10.1016/j.jad.2016.10.016

Hobson, H. M., and Bishop, D. V. M. (2016). Mu suppression–a good measure of the human mirror neuron system? *Cortex* 82, 290–310. doi: 10.1016/j.cortex.2016.03.019

Horan, W. P., Pineda, J. A., Wynn, J. K., Iacoboni, M., and Green, M. F. (2014). Some markers of mirroring appear intact in schizophrenia: evidence from mu suppression. *Cogn. Affect Behav. Neurosci.* 14, 1049–1060. doi: 10.3758/s13415-013-0245-8

Jensen, O., Gips, B., Bergmann, T. O., and Bonnefond, M. (2014). Temporal coding organized by coupled alpha and gamma oscillations prioritize visual processing. *Trends Neurosci.* 37, 357–369. doi: 10.1016/j.tins.2014.04.001

Jensen, O., and Mazaheri, A. (2010). Shaping functional architecture by oscillatory alpha activity: gating by inhibition. *Front. Hum. Neurosci.* 4:186. doi: 10.3389/fnhum.2010.00186

Klimesch, W. (2012). α-band oscillations, attention, and controlled access to stored information. *Trends Cogn. Sci.* 16, 606–617. doi: 10.1016/j.tics.2012.10.007

Klimesch, W., Sauseng, P., and Hanslmayr, S. (2007). EEG alpha oscillations: the inhibition–timing hypothesis. *Brain Res. Rev.* 53, 63–88. doi: 10.1016/J.BRAINRESREV.2006.06.003

Li, X., Meng, X., Li, H., Yang, J., and Yuan, J. (2017). The impact of mood on empathy for pain: evidence from an EEG study. *Psychophysiology* 54, 1311–1322. doi: 10.1111/psyp.12882

Liu, N., Mok, C., Witt, E., Pradhan, A. H., Chen, J. E., and Reiss, A. L. (2016). NIRS-based hyperscanning reveals inter-brain neural synchronization during cooperative Jenga game with face-to-face communication. *Front. Hum. Neurosci.* 10:82. doi: 10.3389/fnhum.2016.00082

Lopes da Silva, F. (1991). Neural mechanisms underlying brain waves: from neural membranes to networks. *Electroencephalogr. Clin. Neurophysiol.* 79, 81–93. doi: 10.1016/0013-4694(91)90044-5

Manor, B., Costa, M. D., Hu, K., Newton, E., Starobinets, O., Kang, H. G., et al. (2010). Physiological complexity and system adaptability: evidence from postural control dynamics of older adults. *J. Appl. Physiol. (1985)* 109, 1786–1791. doi: 10.1152/japplphysiol.00390.2010

McCormick, L. M., Brumm, M. C., Beadle, J. N., Paradiso, S., Yamada, T., and Andreasen, N. (2012). Mirror neuron function, psychosis, and empathy in schizophrenia. *Psychiatry Res.* 201, 233–239. doi: 10.1016/j.pscychresns.2012.01.004

McDonough, I. M., and Nashiro, K. (2014). Network complexity as a measure of information processing across resting-state networks: evidence from the Human Connectome Project. *Front. Hum. Neurosci.* 8:409. doi: 10.3389/fnhum.2014.00409

McIntosh, A. R., Kovacevic, N., and Itier, R. J. (2008). Increased brain signal variability accompanies lower behavioral variability in development. *PLoS Comput. Biol.* 4:106. doi: 10.1371/journal.pcbi.1000106

Meyer-Lindenberg, A., Bauer, U., Krieger, S., Lis, S., Vehmeyer, K., Schüler, G., et al. (1998). The topography of non-linear cortical dynamics at rest, in mental calculation and moving shape perception. *Brain Topogr.* 10, 291–299. doi: 10.1023/A:1022227108139

Minichino, A., Singh, F., Pineda, J., Friederich, E., and Cadenhead, K. S. (2016). Biological Motion induced mu suppression is reduced in Early Psychosis (EP) patients with active negative symptoms and Autism Spectrum Disorders (ASD). *Psychiatry Res.* 238, 374–377. doi: 10.1016/j.psychres.2016.01.057

Miraglia, F., Vecchio, F., and Rossini, P. M. (2017). Searching for signs of aging and dementia in EEG through network analysis. *Behav. Brain Res.* 317, 292–300. doi: 10.1016/j.bbr.2016.09.057

Mitra, S., Nizamie, S. H., Goyal, N., and Tikka, S. K. (2014). Mu-wave activity in schizophrenia: evidence of a dysfunctional mirror neuron system from an Indian study. *Indian J. Psychol. Med.* 36, 276–281. doi: 10.4103/0253-7176.135380

Mizuno, T., Takahashi, T., Cho, R. Y., Kikuchi, M., Murata, T., Takahashi, K., et al. (2010). Assessment of EEG dynamical complexity in Alzheimer's disease using multiscale entropy. *Clin. Neurophysiol.* 121, 1438–1446. doi: 10.1016/j.clinph.2010.03.025

Oberman, L. M., Hubbard, E. M., McCleery, J. P., Altschuler, E. L., Ramachandran, V. S., and Pineda, J. A. (2005). EEG evidence for mirror neuron dysfunction in autism spectrum disorders. *Cogn. Brain Res.* 24, 190–198. doi: 10.1016/j.cogbrainres.2005.01.014

Oberman, L. M., McCleery, J. P., Hubbard, E. M., Bernier, R., Wiersema, J. R., Raymaekers, R., et al. (2013). Developmental changes in mu suppression to observed and executed actions in autism spectrum disorders. *Soc. Cogn. Affect. Neurosci.* 8, 300–304. doi: 10.1093/scan/nsr097

Oberman, L. M., Ramachandran, V. S., and Pineda, J. A. (2008). Modulation of mu suppression in children with autism spectrum disorders in response to familiar or unfamiliar stimuli: the mirror neuron hypothesis. *Neuropsychologia* 46, 1558–1565. doi: 10.1016/j.neuropsychologia.2008.01.010

Park, J.-H., Kim, S., Kim, C.-H., and Kim, K. (2007). Multiscale Entropy Analysis of EEG From Patients Under Different Pathological Conditions. *Fractals* 15:4. doi: 10.1142/S0218348X07003691

Perry, A., and Bentin, S. (2009). Mirror activity in the human brain while observing hand movements: a comparison between EEG desynchronization in the μ-range and previous fMRI results. *Brain Res.* 1282, 126–132. doi: 10.1016/j.brainres.2009.05.059

Perry, A., Troje, N. F., and Bentin, S. (2010). Exploring motor system contributions to the perception of social information: evidence from EEG activity in the mu/alpha frequency range. *Soc. Neurosci.* 5, 272–284. doi: 10.1080/17470910903395767

Pineda, J. A., and Hecht, E. (2009). Mirroring and mu rhythm involvement in social cognition: are there dissociable subcomponents of theory of mind? *Biol. Psychol.* 80, 306–314. doi: 10.1016/j.biopsycho.2008.11.003

R Core Team (2016). R: A Language and Environment for Statistical Computing. Vienna: R Foundation for Statistical Computing. Available online at: http://www.R-project.org/

Richman, J. S., and Moorman, J. R. (2000). Physiological time-series analysis using approximate entropy and sample entropy. *Am. J. Physiol.* 278, H2039–H2049. doi: 10.1152/ajpheart.2000.278.6.H2039

Rizzolatti, G. (2005). The mirror neuron system and its function in humans. *Anat. Embryol.* 210, 419–421. doi: 10.1007/s00429-005-0039-z

Rizzolatti, G., and Craighero, L. (2004). The mirror-neuron system. *Annu. Rev. Neurosci.* 27, 169–192. doi: 10.1146/annurev.neuro.27.070203.144230

Rizzolatti, G., Fabbri-Destro, M., and Cattaneo, L. (2009). Mirror neurons and their clinical relevance. *Nat. Clin. Pract. Neurol.* 5, 24–34. doi: 10.1038/ncpneuro0990

Rubinov, M., and Sporns, O. (2010). Complex network measures of brain connectivity: uses and interpretations. *NeuroImage* 52, 1059–1069. doi: 10.1016/j.neuroimage.2009.10.003

Sporns, O., Tononi, G., and Edelman, G. (2000). Connectivity and complexity: the relationship between neuroanatomy and brain dynamics. *Neural Netw.* 13, 909–922. doi: 10.1016/S0893-6080(00)00053-8

Takahashi, T., Cho, R. Y., Mizuno, T., Kikuchi, M., Murata, T., Takahashi, K., et al. (2010). Antipsychotics reverse abnormal EEGcomplexity in drug-naive schizophrenia: a multiscale entropy analysis. *NeuroImage* 51, 173–182. doi: 10.1016/j.neuroimage.2010.02.009

Tass, P., Rosenblum, M. G., Weule, J., Kurths, J., Pikovsky, A., Volkmann, J., et al. (1998). Detection of n : m phase locking from noisy data: application to magnetoencephalography. *Phys. Rev. Lett.* 81, 3291–3294. doi: 10.1103/PhysRevLett.81.3291

Vakorin, V. A., Lippé, S., and McIntosh, A. R. (2011). Variability of brain signals processed locally transforms into higher connectivity with brain development. *J. Neurosci.* 31, 6405–6413. doi: 10.1523/JNEUROSCI.3153-10.2011

Wang, C., and Tao, J. (2017). Graphs in scientific visualization: a survey. *Comput. Graph. Forum* 36, 263–287. doi: 10.1111/cgf.12800

Yang, A. C., Hong, C.-J., Liou, Y.-J., Huang, K.-L., Huang, C.-C., Liu, M.-E., et al. (2015). Decreased resting-state brain activity complexity in schizophrenia characterized by both increased regularity and randomness. *Hum. Brain Mapp.* 36, 2174–2186. doi: 10.1002/hbm.22763

Yao, D. (2001). A method to standardize a reference of scalp EEG recordings to a point at infinity. *Physiol. Measure.* 22, 693–711. doi: 10.1088/0967-3334/22/4/305

Yin, S., Liu, Y., and Ding, M. (2016). Amplitude of sensorimotor Mu rhythm is correlated with BOLD from multiple brain regions: a simultaneous EEG-fMRI study. *Front. Hum. Neurosci.* 10, 1–12. doi: 10.3389/fnhum.2016.00364

Conflict of Interest Statement: The authors declare that the research was conducted in the absence of any commercial or financial relationships that could be construed as a potential conflict of interest.

The reviewer MI and handling Editor declared their shared affiliation.

frontiers in Neuroscience

ORIGINAL RESEARCH
published: 06 November 2018
doi: 10.3389/fnins.2018.00812

Disentangling Multispectral Functional Connectivity With Wavelets

Jacob C. W. Billings[1,2], Garth J. Thompson[2,3], Wen-Ju Pan[2], Matthew E. Magnuson[2], Alessio Medda[4] and Shella Keilholz[1,2]**

[1] Graduate Division of Biological and Biomedical Sciences – Program in Neuroscience, Emory University, Atlanta, GA, United States, [2] Biomedical Engineering, Georgia Institute of Technology and Emory University, Atlanta, GA, United States, [3] iHuman Institute, ShanghaiTech University, Pudong, China, [4] Aerospace Transportation and Advanced Systems, Georgia Tech Research Institute, Atlanta, GA, United States

The field of brain connectomics develops our understanding of the brain's intrinsic organization by characterizing trends in spontaneous brain activity. Linear correlations in spontaneous blood-oxygen level dependent functional magnetic resonance imaging (BOLD-fMRI) fluctuations are often used as measures of functional connectivity (FC), that is, as a quantity describing how similarly two brain regions behave over time. Given the natural spectral scaling of BOLD-fMRI signals, it may be useful to represent BOLD-fMRI as multiple processes occurring over multiple scales. The wavelet domain presents a transform space well suited to the examination of multiscale systems as the wavelet basis set is constructed from a self-similar rescaling of a time and frequency delimited kernel. In the present study, we utilize wavelet transforms to examine fluctuations in whole-brain BOLD-fMRI connectivity as a function of wavelet spectral scale in a sample ($N = 31$) of resting healthy human volunteers. Information theoretic criteria measure relatedness between spectrally-delimited FC graphs. Voxelwise comparisons of between-spectra graph structures illustrate the development of preferential functional networks across spectral bands.

Keywords: resting state, functional magnetic resonance imaging, functional connectivity, wavelet packet transform, mutual information, clustering

OPEN ACCESS

Edited by:
Albert Yang,
Harvard Medical School,
United States

Reviewed by:
Chun-Yi Lo,
Fudan University, China
Shih-Jen Tsai,
Taipei Veterans General Hospital,
Taiwan

***Correspondence:**
Alessio Medda
alessio.medda@gtri.gatech.edu
Shella Keilholz
shella.keilholz@bme.gatech.edu

Specialty section:
This article was submitted to Brain Imaging Methods, a section of the journal Frontiers in Neuroscience

Received: *31 May 2018*
Accepted: *18 October 2018*
Published: *06 November 2018*

Citation:
Billings JCW, Thompson GJ, Pan W-J, Magnuson ME, Medda A and Keilholz S (2018) Disentangling Multispectral Functional Connectivity With Wavelets. Front. Neurosci. 12:812. doi: 10.3389/fnins.2018.00812

INTRODUCTION

The advent of functional magnetic resonance imaging (fMRI) offers an unprecedented view into normal brain function (Ogawa et al., 1990; Bandettini, 2012). One of the earliest uses of fMRI was to localize areas of the brain involved in experimentally defined tasks. Changes in blood-oxygen level dependent (BOLD) signals were statistically compared between task and control states (Belliveau et al., 1991). However, these task-related activations account for relatively small deviations (5–10%) from baseline metabolism (Raichle and Mintun, 2006). Biswal et al. (1995) analyzed the structure of the BOLD signal's spontaneous fluctuations to discover that temporal correlations in the low-frequency BOLD signal demarcate the same regions of the brain as activated during certain tasks. Mapping networks of "functional connectivity" (FC) based on intrinsic BOLD correlations has since become a powerful tool for neuroscience research. Among normal adults, contiguous brain networks (visual network, somatomotor network, cerebellar network, etc.) and networks composed of multiple disconnected regions (the default mode network, the dorsal attention network, etc.) are non-invasively identified through FC-fMRI (Fox et al., 2005; Vincent et al., 2008; Smith et al., 2009; Yeo et al., 2011).

Spontaneous BOLD fluctuations have been shown to match a 1/f-type scaling of frequency, f, to power spectral density, S: $S(f) \propto 1/f^{\gamma}$ (He, 2014). The spectral exponent, γ, has a value of between 0.5 and 1 in BOLD data (Bullmore et al., 2004; Herman et al., 2011). The physiological significance of 1/f-type scaling of brain signals is hotly debated. Conceptually, natural 1/f-type systems emerge as large-scale realizations of many granular and self-similar details. For instance, the 1/f-distributed BOLD signal has been demonstrated to be a convolution of discrete neural signaling events with a hemodynamic response function (Logothetis et al., 2001). Some authors discount multispectral features from 1/f-type signals as "scale-free" organization—that is, the 1/f-type scaling indicates that a finite set of properties describes the systems structures at all scales (Goldberger et al., 2002; Mandelbrot, 2013). Other authors point to fluctuations in the spectral exponent across brain regions and between task and rest conditions as an indication that variance in the multispectral evolution of brain signals bears useful information (He et al., 2008; He, 2011, 2014). The fact of the BOLD signal's mean and deviant 1/f-type structure motivates domain transformation that model spectral variability (Medda et al., 2016; Bielczyk et al., 2017; Billings, 2017; Shakil et al., 2017).

Perfectly scale-free systems may be constructed via tessellations of self-similar fractals. Wavelet transforms offer theoretically optimal domains for investigating 1/f-type signals because of the self-similarity properties of some wavelet basis sets (Ciuciu et al., 2012). For instance, multispectral wavelet filters may be constructed by simply dilating and translated a compactly supported kernel (a wavelet function, ψ). Such continuous wavelet transforms facilitate a time-frequency signal decomposition across a continuous range of scales (Grossmann and Morlet, 1984; Kronland-Martinet et al., 1987; Billings and Keilholz, 2018). Orthonormal wavelet bases (ψ, and the scaling functions, ϕ) may also be constructed to afford a discrete segmentation, and a perfect reconstruction, of an input signal across multiple resolutions (Daubechies, 1988, 1992). Since their development, wavelets have become an important tool in fMRI analysis (Bullmore et al., 2004). Several methodological studies have shown the usefulness of combining wavelet filtering with various connectivity metrics to better characterize FC networks (Achard and Bullmore, 2007; Sato et al., 2007; Chang and Glover, 2010; Eryilmaz et al., 2011; Guo et al., 2012; Schröter et al., 2012). These and other methods have been extended into investigations of fMRI based biomarkers for neurological diseases such as addiction (Salomon et al., 2012; Lam et al., 2013), depression (Salomon et al., 2011; Meng et al., 2013), Parkinson's (Skidmore et al., 2011), Alzheimer's (Supekar et al., 2008; Wang et al., 2013), and schizophrenia (Alexander-Bloch et al., 2010; Bassett et al., 2012).

Abbreviations: FC, functional connectivity; fMRI, functional magnetic resonance imaging; FC-fMRI, functional connectivity of functional magnetic resonance imaging data; *TR*, repetition time; LFF, low-frequency fluctuations (0.01–0.1 Hz); MFF, mid-frequency fluctuations (0.1–0.2 Hz); WPT, wavelet packet transform; D*i*P*j*, indices for the wavelet decomposition depth (D) *i* and position (P) *j*; HC, hierarchical clustering; VI, variation in information.

The present study seeks to characterize the BOLD signal's functional connectivity across multiple spectral scales. The study is motivated by findings from multiple sources citing patterns in FC-fMRI organization at in frequency bands within and beyond the habitually sampled low-frequency fluctuation (LFF) range (0.01–0.1 Hz). For instance, Kalcher et al. (2014) demonstrated large FC network variations among tissue types and gray-matter seed-regions when tissues and ROIs were filtered into different passbands (<0.1 Hz; 0.1–0.25 Hz; 0.25–0.75 Hz; 0.75–1.4 Hz). Wu et al. (2008) showed that cortical networks tend to organize in the frequency range between 0.01 and 0.06 Hz while limbic networks organize between 0.01 and 0.14 Hz. Chang and Glover (2010) showed that the frequency band harboring maximal correlation strength within the default mode network changed over time. Billings et al. (2017) mapped these multispectral fluctuations onto a 2-dimensional neighborhood embedding. The present study uses a series of data-driven techniques to observe how BOLD FC networks differ across a multiscale wavelet bases.

MATERIALS AND METHODS

Data Acquisition

Neuroimaging data were downloaded from the 1000 Functional Connectomes Project website (Milham, 2013), specifically, the *Enhanced Rockland Sample Multiband Imaging Test-Retest Pilot Dataset* uploaded by the Nathan Kline Institute for Psychiatric Research (Nooner et al., 2012; Nathan Kline Institute for Psychiatric Research, 2013). This dataset was chosen as it was one of the first to make use of multiband imaging (Feinberg et al., 2010) to produce BOLD scans with short repetition times ($TR = 0.645$ s). Study data were derived from 32 individuals randomly chosen from the database (n. female = 22, n. right handed = 31, n. no handedness = 1, mean age = 44 y, std. age = 18 year). One volunteer's data was excluded after becoming corrupted during preprocessing.

Each volunteer's dataset consisted of whole-brain BOLD-weighted functional scans acquired on a 3T Siemens Magnetome TriTom (multiband EPI; TR 645 ms; TE 30 ms; 40 slices; FOV 22.2 cm × 22.2 cm; 3 mm isotropic voxels; 900 images). A 32-channel anterior/posterior head coil facilitated multiband EPI imaging at high temporal resolution. An MPRAGE scan was acquired to facilitate alignment (TR 1900 ms; TE 2.52 ms; 176 slices; FOV 25 cm × 25 cm; 1 mm isotropic voxels).

Preprocessing

A series of preprocessing steps were carried out over the entire data set to bring data points into temporal and spatial alignment. These steps were conducted using revision 6,470 of the Statistical Parametric Mapping MATLAB toolbox (Friston et al., 2011). Slice timing mismatches were corrected per each slice's multiband acquisition time. Within-scan images were realigned to correct for movement between repetitions. Each scan's mean realigned image was co-registered to the volunteer's structural image. Structural images were segmented into 5 tissue classes: gray matter, white matter, cerebrospinal fluid (CSF), bone, and soft tissue. A warping matrix was evaluated and

used to normalize each scan from subject space to MNI space. Images were smoothed by an 8 × 8 × 8 mm Gaussian kernel. Volunteer images were realigned to the group mean of the functional images. A gray-matter mask was applied to all images. Voxels included in the mask were required to have at least a 50% probability of containing gray matter across all volunteers. Finally, motion terms were regressed from voxel time-series.

Multispectral Decomposition, the Wavelet Packet Transform

The wavelet packet transform (WPT) is a generalization of domain transforms utilizing orthonormal wavelet bases (Daubechies, 1988; Coifman and Wickerhauser, 1992; Coifman et al., 1992). The WPT is conducted via iterative convolutions of an input signal, $x(t)$, with paired high-pass and low-pass filters, h and g. The filters are quadrature mirrors of one another and divide the input into orthogonal subbands. Successive filtering operations produce trees of wavelet packet coefficients over $d \in [0, 1, 2, \ldots, \infty]$ sets of 2^{d} evenly segmented subbands. Application of the WPT filtering schema d times is called the decomposition's "depth." The set of "positions," $p \in [0, \ldots, 2^d]$, denote frequency ranges of packets at depth d. The zeroth depth is the space of the broadband signal. Each of the zeroth positions is a fully low-pass filter of variable width. The range of each packet's passband is roughly equivalent to $\left[\frac{p\left(\frac{f_s}{2}\right)}{2^d}, \frac{(p+1)\left(\frac{f_s}{2}\right)}{2^d}\right](Hz)$, where f_s is the sampling frequency. In the present study, the filtered data existing at depth d_i and position p_j is given the shorthand notation "Dd_iPp_j." Thus, the D2P0 signal is quarter-band signal covering the lowest frequencies, and the D2P3 signal is the quarter-band signal covering the highest frequencies.

For the present study, we generated a filterbank from Daubechies' 7-tap wavelet. The Daubechies family of wavelets offers the highest number of vanishing moments, or taps, for a given support width. Increasing the number of taps sharpens the filter edges in the Fourier domain at the cost of increased filter length (i.e., blurring in the time domain). Daubechies' 7-tap wavelet produces short duration filters with good spectral separation. Each voxel signal was filtered into packet coefficients at all positions of WPT depths 0 through 6, generating a total of 127 subbands. For more details on WPT theory and usage, the reader is referred to **Supplemental Figure S1**, the works of Coifman (Coifman et al., 1992), Daubechies (Daubechies, 1988, 1992), Mallat (Mallat, 1989, 1999), and Meyer (Meyer, 1993), as well as the technical notes of Misiti et al. (2013).

Data Structure

Reorganization of individual datasets for multi-subject hierarchical clustering was performed by concatenating the coefficients of a single wavelet packet, voxel-by-voxel, from all brain voxels, and from all volunteers, into spectrally-delimited group-level datasets.

Hierarchical Clustering (HC)

HC organizes a collection of data into distinctive groups through a deterministic algorithm. First, a distance metric, $S1\left(i,j\right)$, is calculated between all i and j indices of voxel signals. In the present study, we followed the practice of defining functional connectivity via the Pearson correlation distance over real valued wavelet coefficients. Voxels and/or clusters of voxels are then clustered together, beginning with the closest voxels/clusters, and continuing until only a single cluster exists. After each clustering step, an updated distance metric, the linkage distance, $S2\left(a,b\right)$, is calculated between all clusters a and b. For the present study, the linkage distance is defined as the average of the correlation distances between voxels in each cluster:

$$S2\left(a,b\right) = \frac{1}{(n_a n_b)} \sum_{i=1}^{n_a} \sum_{j=1}^{n_b} S1\left(i \in a, j \in b\right). \quad (1)$$

Variables n_a and n_b are the number of voxels contained within clusters a and b. Further details on hierarchical clustering may be found in **Supplemental Figure S2**.

FC Networks Clustered Against Dendrogram Inconsistencies

An HC map's hierarchy may be visualized by plotting successive links as a dendrogram. For the dendrograms of the present study, voxels are ordered along the abscissa, and the linkage distance numbers the ordinate axis. Horizontal lines are plotted between clusters joined at a given linkage distance. Vertical lines measure the linkage distance between 'successive clusters. Voxels are ordered along the abscissa in such a way as to minimize the length of each horizontal link. This arrangement results in the most related clusters being arranged adjacent to one another along the abscissa, i.e., the order of voxels along the abscissa is a linear projection of cluster similarity. A pictorial description of this process may be found in **Supplemental Figure S2**.

Concrete clusterings are produced by pruning links between intermediate clusters in the HC dendrogram. One method of dendrogram pruning identifies a threshold linkage distance that demarcates a specified number of clusters. For this study, the choice of how to prune the HC map was informed by calculating the inconsistency value of each link in the HC map. The inconsistency value of each link quantifies the relative change in linkage distance(s) between each link and up to $g - 1$ previous links. The higher the inconsistency value, the more dissimilar are the elements connected at that particular link relative to the elements connected beneath that link (Zahn, 1971). Small values for the variable g bring the inconsistency algorithm to focus on locally inconsistent links in the HC map. Alternatively, larger values of g will search the area below each link to provide a more globally representative assessments of cluster inconsistency. For a given HC map, the k^{th} link's inconsistency value is calculated as $Y_4\left(k\right) = \left(z\left(k\right) - Y_1\left(k\right)\right)/Y_2\left(k\right)$. Where $Y_1\left(k\right)$ is the mean of the linkage distances for the k^{th} link and the first $g - 1$ links beneath it. The quantity $Y_2\left(k\right)$ is the standard deviation of the k^{th} set of linkage distances. The quantity $z(k)$ is the linkage distance of the k^{th} link. Having set the g-value to perform either a local ($g = 2$) or a global search ($g \gg 2$), we select a threshold level of inconsistency values above which to remove all of the most inconsistent links, and all of their dependents. By pruning the

HC tree along natural cleavage points, natural clusterings may be better resolved.

Quantifying FC Network Similarity

We utilized a mutual information-based criterion to compare parcellations of FC networks. Specifically, we use Marina Meila's normalization for mutual information between clusterings called the variation in information *(VI)* (Meilă, 2007):

$$VI\left(C', C''\right) = \left[H\left(C'\right) - I\left(C', C''\right)\right] + \left[H\left(C''\right) - I\left(C', C''\right)\right]. \quad (2)$$

Here, H is the entropy of a clustering, $H(C) = -\sum_{i=1}^{k} P(i)\, log_2 P(i)$, with $P(i)$ the probability, $\frac{|C_i|}{n}$, of choosing a voxel from the ith cluster in C from all n voxels. The term I is the mutual information between clusterings, $I\left(C', C''\right) = \sum_{i=1}^{k}\sum_{j=1}^{l} P\left(i,j\right) log_2 \frac{P(i,j)}{P(i)P(j)}$, where $P\left(i,j\right) = \frac{|C'_i \cap C''_j|}{n}$. The first term in equation (2) may be thought of as how much information is lost when going from clustering C' to C". The second term is then how much information is left to be gained when going from C' to C" (Wagner and Wagner, 2007).

Voxelwise Comparisons of FC Networks

One important question to ask when comparing multispectral realizations of FC networks is how specific brain regions contribute to whole-brain network variability. The approach used in the present study characterized voxelwise connectivity as the degree of overlap between each voxel's nearest neighbors, as expanded between spectrally delimited FC graphs. Specifically, the Jaccard distance compared how similar the nearest 5% of correlating voxels are in each subband network:

$$JD_{vw} = \frac{\#\left[\left(v_j \neq w_j\right) \cap \left(\left(v_j \neq 0\right) \cup \left(w_j \neq 0\right)\right)\right]}{\#\left[\left(v_j \neq 0\right) \cup \left(w_j \neq 0\right)\right]}. \quad (3)$$

The Jaccard distance quantifies the percentage of binary elements that differ between sets v and w. Results were reported as the average voxel-wise Jaccard distance across volunteers. Analysis was limited to the D6P1 (12–24 mHz), D5P1 (24–48 mHz), D4P1 (48–97 mHz), D5P4 (97–121 mHz), D5P5 (121–143 mHz), and D4P3 (141–194 mHz) packets because potentially divergent FC networks were consistently produced by packets in these ranges (see Discussion and Results). Each packet graph was compared to the graph constructed from wideband BOLD images. Wideband images were generated from the inverse WPT of only the six aforementioned packets (coefficients from other packets were set to zero before taking the inverse).

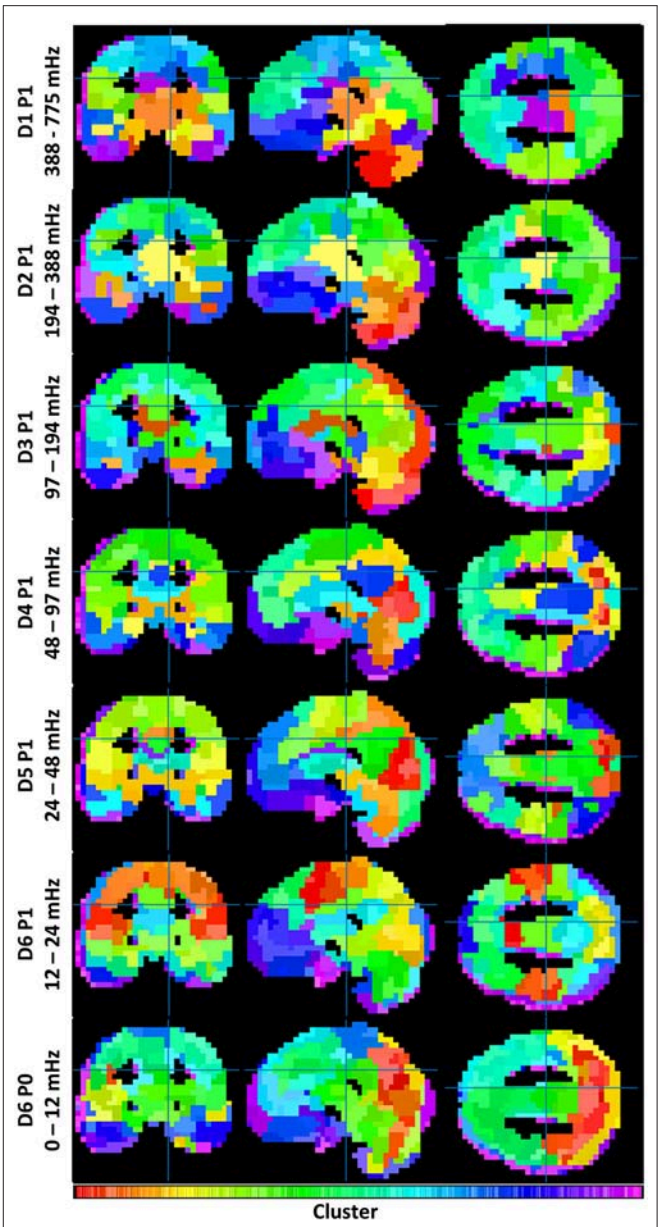

FIGURE 1 | Illustrates the similarities and differences between functional connectivity networks across spectra. Each clustering contains 355 ± 4 clusters (see **Supplemental Figure 3**). Coloration is a projection from each cluster's location on its dendrogram onto a 1D colorbar (see **Supplemental Figure 2**).

RESULTS

Functional Connectivity Maps Across Spectra

To understand the overall variation of FC-fMRI networks across spectra, **Figure 1** displays their cross-sectional views. Owing to space limitations, only a subset of packet networks are shown. Displayed packets follow the discrete wavelet transform schema, a multiresolution filter bank spanning the full spectral range without overlap. Each subband network was realized as a clustering with 355 ± 4 clusters. The number of clusters was derived upon consultation with the inconsistency values across packets ($g >> 2$, for a global search). These data are provided in **Supplemental Figure S3**.

Both similarities and differences exist in the networks produced within each subband. Whereas FC networks in the LFF range possess many of the networks expected from previous studies—including a default mode network, a somatomotor network, frontal and visual networks, etc.—such networks

become less defined at frequencies above 0.2 Hz. Rather, these frequencies produce FC networks with increased segmentation among midbrain and brainstem regions, and with reduced segmentation among cortical regions. A category of mid-frequency fluctuations (MFF) (0.1 – 0.2 Hz) displays a mixture of increased midbrain/brainstem segmentation with some cortical segmentation (e.g., the bilateral angular gyri of the default mode). DC frequency information also resembles known cortical brain networks; however, the networks appear blurred by comparison to networks constructed with LFF's.

Variation in Information (VI) Across Spectra

We can quantify the relatedness between spectrally delimited functional connectivity networks by assessing the *VI* between clusterings. A triangle plot of inter-spectral FC BOLD network VI distances is provided in **Supplemental Figure S4**. These distances are used in a hierarchical clustering (**Supplemental Figure S5**). Links were quantified via the "average" linkage metric. The plots in **Figure 2** show the results from pruning the dendrogram in two ways. Part A of the figure shows a coarse clustering from pruning the link having the single highest local inconsistency value (g=2). Part B of the figure shows a finer clustering that removes the first inconsistency value (g>>2) between any two packets in the LFF range.

Part A of the figure shows that the single largest jump in linkage distance occurs when connecting the D5P4 and D5P5 packets. This is an indication that sharp differences exist between FC networks above and below approximately 0.12 Hz. Alternatively, if inconsistency values are stabilized by averaging the change in linkage distances over a large number of previous links (g>>2), FC networks are shown to segment into a multiresolution filterbank of passbands (i.e., the set of wavelet packets in the first position of each depth). In both clusterings, FC networks containing DC frequencies form a separate group.

Taken as a whole, FC networks appear to segment into at least four types when drawing from different spectral components: (1) networks of 0.01 to 0.1 Hz LFF's, (2) networks of >0.2 Hz high-frequency fluctuations, (3) networks of 0.1–0.2 Hz MFFs, and (4) networks of DC frequency fluctuations. Additional varieties of FC networks may exist within finer passbands in the LFF and MFF ranges.

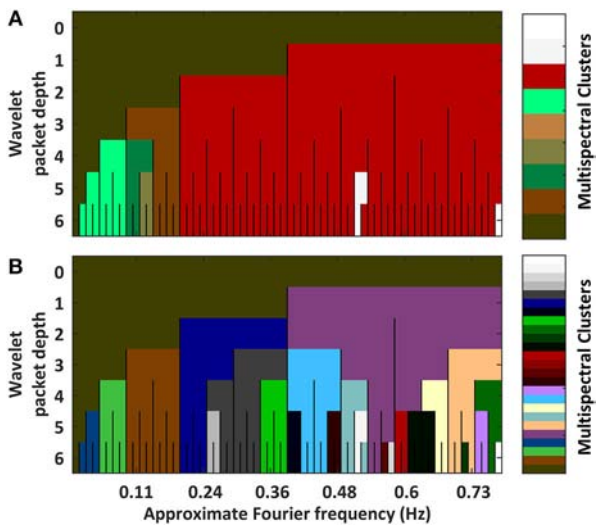

FIGURE 2 | Plots hierarchical clusterings of the similarities between functional connectivity networks across spectra. The distance metric was variation in information between concrete clusterings (Intermediate results are provided in **Supplemental Figures 3, 4**). To better assess the decomposition's natural segmentation, the dendrogram was pruned at a coarse scale **(A)** and at a fine scale **(B)** (Associated dendrograms are displayed in **Supplemental Figure 5**). Overall, networks segment into passbands. Sub-bands containing DC frequencies self-associate. Granular differences among high frequency packets are likely artifactual owing to increased noise at high frequencies.

Voxelwise Connectivity Between Spectra

A good way to assess differences between multispectral FC-fMRI networks is to observe differences in the group membership of individual voxels. To this end, we calculated Jaccard distances between the nearest neighbors (via correlation) of each voxel, in each spectral subband, vs. the correspond voxel from wideband filtered images. Slice representations of voxelwise network comparisons are shown in **Figure 3**. A series of tables detailing the 20 regions with the most similar and the least similar connectivity patterns from each subband are provided in **Supplemental Tables 1–6**. Histograms of the mean Jaccard distances are provided in **Supplemental Figure S6**. **Supplemental Figure S7** displays standard deviations of Jaccard distances for reference.

Regions showing marked similarity across spectra include many areas of the cerebral cortex, including, the intracalcerine cortex, the lateral occipital cortex, the lingual gyrus, precuneous, precentral gyrus, frontal pole, and post-central gyrus. LFFs from the D5P1 packet (0.24 and 0.48 Hz) show the strongest voxelwise similarity with the spectral average (mean $JD \cong 0.5$). Networks produced by frequencies above and below the D5P1 band show less similar voxelwise correlation in cortical regions. Additionally, these spectra show many differences in the correlation neighborhood of voxels in regions of the midbrain, basal ganglia, and the temporal lobe, including, the globus palladus, the thalamus, the hippocampus, the caudate, and the temporal pole. The most extreme deviations from the spectral average are observed from MFF packets above 0.12 Hz. The mean voxelwise Jaccard distance is ∼0.8 for packets D5P5 (121–143 mHz) and D4P3 (141–194 mHz). The the mean *JD* is ∼0.6 for the four other lower frequency packets (see **Supplemental Figure S6**).

DISCUSSION

It is common practice in fMRI studies to band-pass filter signals to the LFF range (Biswal et al., 1996; Murphy et al., 2013). The present study confirms the utility of this practice while providing insights into its limitations. **Figure 2A** Demonstrates that the connectivity structure of BOLD fluctuations can form a homogenous LFF group. But this LFF group structure is seen as homogenous only relative to a sharp change in network structure occurring at ∼0.12 Hz. An alternative perspective which takes more information about the evolution of each cluster into

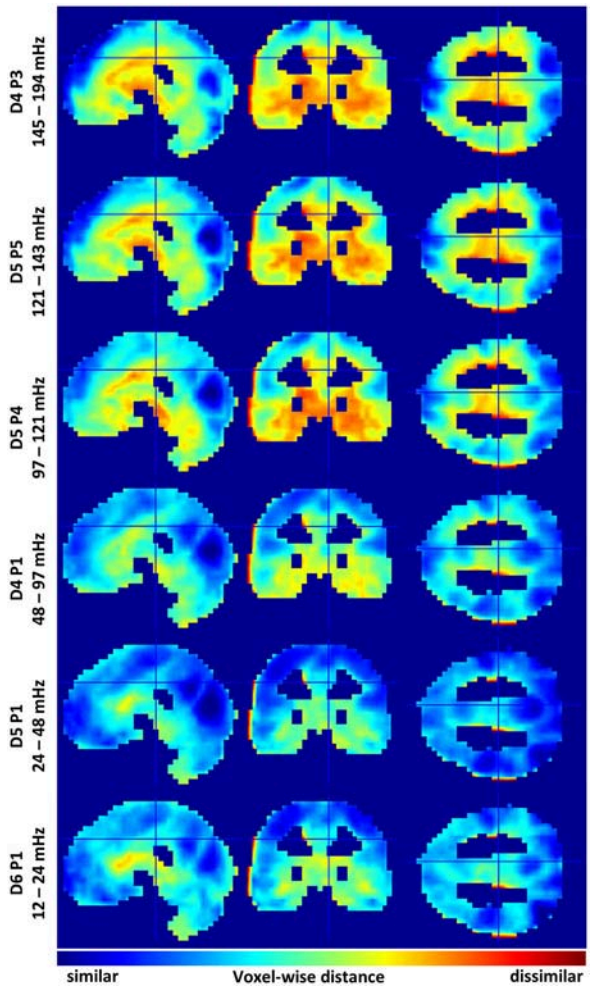

FIGURE 3 | Identifies similarities and differences in voxelwise functional connectivity graphs among selected sub bands. Variations are relative to the mean across the six sub bands. Cool colors indicate voxels sharing similar functional connectivity graphs. Warm colors demarcate dis-similarly connected voxels. Data histograms are provided in **Supplemental Figure 6**. Images displaying data standard deviations are provided in **Supplemental Figure 7**. The supplemental tables provide neuroanatomical labels for the most similar and dissimilar regions.

account (**Figure 2B**) demonstrates that LFF networks may form two distinct networks before differences in an MFF network are observed. A look at the associate dendrogram shows that both ways to segment networks in the 0.01–0.2 Hz range may be equally valid (**Supplemental Figure S6**). Indeed, the LFF and MFF networks cluster together later in the dendrogram. Similar trends are observed in previous studies using images from the same volunteers but with different EPI parameter choices (Billings, 2017).

While heterogeneous network properties across spectra are often observed in electroencephalographic measurements (Lu et al., 2007; Mantini et al., 2007), the presence of multispectral network diversity in the BOLD signal is only recently beginning to emerge. Zuo et al. (2010) and Xue et al. (2014) observed differential activation patterns in slow-4 (0.027–0.073 Hz ∼ D5P1) vs. slow-5 (0.01–0.027 Hz ∼ D6P1) FC-fMRI activity. Similarly, Thompson and Fransson (2015) demonstrated that the centers of graph-theoretic hubs in cortical networks are frequency dependent.

Having oversampling multispectral BOLD FC clusterings, the present study selected a set of 6 passbands with potentially distinct network properties (**Figure 3**). From these 6 passbands, it appeared that a subband of the LFF range—the D5P1 packet network—was very similar to the wideband average. As found by Wu et al. (2008), networks in higher (MFF) frequencies tended to hold unique connectivity structures in limbic regions, e.g., the orbitofrontal cortex, hippocampus, and temporal pole. Indeed, as MFFs and high frequency fluctuations acquire increased differentiation among brain stem and midbrain regions, they appear to lose some expected connectivity structures in cortical regions (**Figure 1**). Notwithstanding, Boubela et al. (2013) observed prototypical resting-state networks in BOLD data sampled above 0.25 Hz. Kalcher et al. (2014) confirmed the presence of long-range functional connectivity at high frequencies from rapid TR BOLD data.

At the low end of the LFF frequency range (0.01–0.024 Hz, D6P1 packet) cortical networks were similar to the wideband average. By comparison, DC frequency networks appear blurred. The blurring is likely from a noise source as DC frequency networks structures are surprisingly similar despite the presence of any higher frequency information. Birn et al. (2013) noted that longer scans increase test-retest reliability of FC studies. Methods from the present study may be adapted to investigate if and how very slow brain rhythms (< 0.01 *Hz*) coordinate unique functional networks.

The present study observed that FC networks establish the appearance of limbic MFF networks and cortical LFF networks. Hypothetically, this is an indication that slow cortical dynamics emerge from rapid information exchange among deeper brain structures. If this is the case, then the difference maps in **Figure 3** may show the accumulation of rapid ($>$0.12 Hz) limbic activity into slow (0.024 and 0.048 Hz) cortical structures. Alternatively, MFF BOLD signaling could be a kind of structured noise.

The presence of noise confounds is the chief concern limiting the interpretation of study results. The gray-matter mask of the present study included any voxel having at least a 50% probability of containing gray matter in all volunteer images. Some voxels were thereby included from outside gray matter (e.g., from cerebrospinal fluid, white matter, and extra-cerebral tissues). For instance, in **Figures 1**, **3**, voxels at the edges of gray matter regions appear to segment into their own clusters. Some anatomical locations labeled in the supplemental tables mark points in these clusters. Better segmentation of gray matter regions may remove these confounds. None-the-less, the smooth transition from limbic to cortical network types as brain rhythms slow was observed in pairwise correlations between very many gray matter voxels.

Observations of multispectral variability in brain FC are contrary to the expectation that 1/f-type systems are scale-free. There are, however, other interpretations that admit to the simultaneous presence of 1/f-type power spectral densities

alongside unique multiscale structures. Namely, unique large-scale structures may be emergent properties of multiscale granular activities. In the case of the brain, very many binary action potentials must somehow sum to become a lifetime of thoughts and feelings. Theoretically, the capacity for a system to share information across scales is a measure of the system's complexity (Wolfram, 2002). Natural complex systems like the brain must simultaneously build large-scale structures from granular processes and fine-tune multiscale functions with subband information. The unique information bearing capacity of both granular and coarse measures of natural complex systems should therefore encourage FC-fMRI studies to leverage multispectral basis transforms (Billings and Keilholz, 2018).

DATA AVAILABILITY STATEMENT

The original data supporting the results of this article are freely available from http://fcon_1000.projects.nitrc.org/indi/pro/eNKI_RS_TRT/FrontPage.html

AUTHOR CONTRIBUTIONS

All authors designed the study. JB conducted the analysis with advice from all authors, especially AM and SK. JB authored the manuscript with input and revisions provided by all authors. Each author has given final approval of the manuscript's publication and agrees to be accountable for all aspects of the work.

FUNDING

This work was supported by the Air Force Center of Excellence on Bio-Nano-Enabled Inorganic/Organic Nanostructures and Improved Cognition (BIONIC) at Georgia Institute of Technology; NIH R01NS078095-02 and R01NS078095-02S1; and by Professional Development Supports Funds provided by Laney Graduate School, Emory University.

ACKNOWLEDGMENTS

Portions of this work appeared in the dissertation entitled *Multiscale Statics and Dynamics of Cerebral Functional Connectivity*, by JB (2017). Emory University, Atlanta. SK, adviser.

SUPPLEMENTARY MATERIAL

The Supplementary Material for this article can be found online at: https://www.frontiersin.org/articles/10.3389/fnins.2018.00812/full#supplementary-material

REFERENCES

Achard, S., and Bullmore, E. (2007). Efficiency and cost of economical brain functional networks. *PLoS Comput. Biol.* 3:e17. doi: 10.1371/journal.pcbi.0030017

Alexander-Bloch, A. F., Gogtay, N., Meunier, D., Birn, R., Clasen, L., Lalonde, F., et al. (2010). Disrupted modularity and local connectivity of brain functional networks in childhood-onset schizophrenia. *Front. Syst. Neurosci.* 4:147. doi: 10.3389/fnsys.2010.00147

Bandettini, P. A. (2012). Twenty years of functional MRI: the science and the stories. *Neuroimage* 62, 575–588. doi: 10.1016/j.neuroimage.2012.04.026

Bassett, D. S., Nelson, B. G., Mueller, B. A., Camchong, J., and Lim, K. O. (2012). Altered resting state complexity in schizophrenia. *Neuroimage* 59, 2196–2207. doi: 10.1016/j.neuroimage.2011.10.002

Belliveau, J. W., Kennedy, D. N. Jr., Mckinstry, R. C., Buchbinder, B. R., Weisskoff, R. M., Cohen, M. S., et al. (1991). Functional mapping of the human visual cortex by magnetic resonance imaging. *Science* 254, 716–719. doi: 10.1126/science.1948051

Bielczyk, N. Z., Llera, A., Buitelaar, J. K., Glennon, J. C., and Beckmann, C. F. (2017). The impact of hemodynamic variability and signal mixing on the identifiability of effective connectivity structures in BOLD fMRI. *Brain Behav.* 7:e00777. doi: 10.1002/brb3.777

Billings, J. C. W. (2017). *Multiscale Statics and Dynamics of Cerebral Functional Connectivity*. Doctor of Philosophy, Emory University.

Billings, J. C. W., and Keilholz, S. D. (2018). The Not-So-Global BOLD signal. *Brain Connect.* 8, 121–128. doi: 10.1089/brain.2017.0517

Billings, J. C. W., Medda, A., Shakil, S., Shen, X., Kashyap, A., Chen, S., et al. (2017). Instantaneous brain dynamics mapped to a continuous state space. *Neuroimage* 162, 344–352. doi: 10.1016/j.neuroimage.2017.08.042

Birn, R. M., Molloy, E. K., Patriat, R., Parker, T., Meier, T. B., Kirk, G. R., et al. (2013). The effect of scan length on the reliability of resting-state fMRI connectivity estimates. *Neuroimage* 83, 550–558. doi: 10.1016/j.neuroimage.2013.05.099

Biswal, B., Deyoe, E. A., and Hyde, J. S. (1996). Reduction of physiological fluctuations in fMRI using digital filters. *Magn. Reson. Med.* 35, 107–113. doi: 10.1002/mrm.1910350114

Biswal, B., Yetkin, F. Z., Haughton, V. M., and Hyde, J. S. (1995). Functional connectivity in the motor cortex of resting human brain using echo-planar MRI. *Magn. Reson. Med.* 34, 537–541. doi: 10.1002/mrm.1910340409

Boubela, R. N., Kalcher, K., Huf, W., Kronnerwetter, C., Filzmoser, P., and Moser, E. (2013). Beyond noise: using temporal ICA to extract meaningful information from high-frequency fMRI signal fluctuations during rest. *Front. Hum. Neurosci.* 7:168. doi: 10.3389/fnhum.2013.00168

Bullmore, E., Fadili, J., Maxim, V., Sendur, L., Whitcher, B., Suckling, J., et al. (2004). Wavelets and functional magnetic resonance imaging of the human brain. *Neuroimage* 23(Suppl. 1), S234–S249. doi: 10.1016/j.neuroimage.2004.07.012

Chang, C., and Glover, G. H. (2010). Time-frequency dynamics of resting-state brain connectivity measured with fMRI. *Neuroimage* 50, 81–98. doi: 10.1016/j.neuroimage.2009.12.011

Ciuciu, P., Varoquaux, G., Abry, P., Sadaghiani, S., and Kleinschmidt, A. (2012). Scale-free and multifractal time dynamics of fMRI signals during rest and task. *Front. Physiol.* 3:186. doi: 10.3389/fphys.2012.00186

Coifman, R. R., Meyer, Y., and Wickerhauser, V. (1992). "Wavelet analysis and signal processing," in *In Wavelets and Their Applications: CiteSeerX*, ed M. B. Ruskai (Boston: Jones and Bartlett), 153–178.

Coifman, R. R., and Wickerhauser, M. V. (1992). Entropy-based algorithms for best basis selection. *Inform. Theor. IEEE Trans.* 38, 713–718. doi: 10.1109/18.119732

Daubechies, I. (1988). Orthonormal bases of compactly supported wavelets. *Commun. Pure Appl. Math.* 41, 909–996. doi: 10.1002/cpa.3160410705

Daubechies, I. (1992). *Ten Lectures on Wavelets.* Philadelphia, PA: Society for Industrial and Applied Mathematics.

Eryilmaz, H., Van De Ville, D., Schwartz, S., and Vuilleumier, P. (2011). Impact of transient emotions on functional connectivity during subsequent resting state: a wavelet correlation approach. *Neuroimage* 54, 2481–2491. doi: 10.1016/j.neuroimage.2010.10.021

Feinberg, D. A., Moeller, S., Smith, S. M., Auerbach, E., Ramanna, S., Glasser, M. et al. (2010). Multiplexed echo planar imaging for sub-second whole brain FMRI and fast diffusion imaging. *PLoS ONE* 5:e15710. doi: 10.1371/journal.pone.0015710

Fox, M. D., Snyder, A. Z., Vincent, J. L., Corbetta, M., Van Essen, D. C., and Raichle, M. E. (2005). The human brain is intrinsically organized into dynamic, anticorrelated functional networks. *Proc. Natl. Acad. Sci. U.S.A.* 102, 9673–9678. doi: 10.1073/pnas.0504136102

Friston, K. J., Ashburner, J. T., Kiebel, S. J., Nichols, T. E., and Penny, W. D. (2011). *Statistical Parametric Mapping: The Analysis of Functional Brain Images: The Analysis of Functional Brain Images*. London, UK: Academic Press.

Goldberger, A. L., Amaral, L. A., Hausdorff, J. M., Ivanov, P. C. H., Peng, C. K., and Stanley, H. E. (2002). Fractal dynamics in physiology: alterations with disease and aging. *Proc. Natl. Acad. Sci. U.S.A.* 99(Suppl. 1), 2466–2472. doi: 10.1073/pnas.012579499

Grossmann, A., and Morlet, J. (1984). Decomposition of hardy functions into square integrable wavelets of constant shape. *SIAM J. Math. Anal.* 15, 723–736. doi: 10.1137/0515056

Guo, C. C., Kurth, F., Zhou, J., Mayer, E. A., Eickhoff, S. B., Kramer, J. H., et al. (2012). One-year test-retest reliability of intrinsic connectivity network fMRI in older adults. *Neuroimage* 61, 1471–1483. doi: 10.1016/j.neuroimage.2012.03.027

He, B. J. (2011). Scale-free properties of the functional magnetic resonance imaging signal during rest and task. *J. Neurosci.* 31, 13786–13795. doi: 10.1523/JNEUROSCI.2111-11.2011

He, B. J. (2014). Scale-free brain activity: past, present, and future. *Trends Cogn. Sci.* 18, 480–487. doi: 10.1016/j.tics.2014.04.003

He, B. J., Snyder, A. Z., Zempel, J. M., Smyth, M. D., and Raichle, M. E. (2008). Electrophysiological correlates of the brain's intrinsic large-scale functional architecture. *Proc. Natl. Acad. Sci.* 105, 16039–16044. doi: 10.1073/pnas.0807010105

Herman, P., Sanganahalli, B. G., Hyder, F., and Eke, A. (2011). Fractal analysis of spontaneous fluctuations of the BOLD signal in rat brain. *Neuroimage* 58, 1060–1069. doi: 10.1016/j.neuroimage.2011.06.082

Kalcher, K., Boubela, R. N., Huf, W., Bartova, L., Kronnerwetter, C., Derntl, B., et al. (2014). The spectral diversity of resting-state fluctuations in the human brain. *PLoS ONE* 9:e93375. doi: 10.1371/journal.pone.0093375

Kronland-Martinet, R., Morlet, J., and Grossmann, A. (1987). Analysis of sound patterns through wavelet transforms. *Int. J. Pattern Recogn. Artif. Intell.* 1, 273–302. doi: 10.1142/S0218001487000205

Lam, S. C., Wang, Z., Li, Y., Franklin, T., O'brien, C., Magland, J., et al. (2013). Wavelet-transformed temporal cerebral blood flow signals during attempted inhibition of cue-induced cocaine craving distinguish prognostic phenotypes. *Drug Alcohol Depend.* 128, 140–147. doi: 10.1016/j.drugalcdep.2012.08.018

Logothetis, N. K., Pauls, J., Augath, M., Trinath, T., and Oeltermann, A. (2001). Neurophysiological investigation of the basis of the fMRI signal. *Nature* 412, 150–157. doi: 10.1038/35084005

Lu, H., Zuo, Y., Gu, H., Waltz, J. A., Zhan, W., Scholl, C. A., et al. (2007). Synchronized delta oscillations correlate with the resting-state functional MRI signal. *Proc. Natl. Acad. Sci. U.S.A.* 104, 18265–18269. doi: 10.1073/pnas.0705791104

Mallat, S. (1999). *A Wavelet Tour of Signal Processing*. Burlington, MA: Elsevier.

Mallat, S. G. (1989). A theory for multiresolution signal decomposition: the wavelet representation. *Pattern Anal. Mach. Intell. IEEE Trans.* 11, 674–693. doi: 10.1109/34.192463

Mandelbrot, B. B. (2013). *Multifractals and 1/f Noise: Wild Self-Affinity in Physics (1963–1976)*. New York, NY: Springer.

Mantini, D., Perrucci, M. G., Del Gratta, C., Romani, G. L., and Corbetta, M. (2007). Electrophysiological signatures of resting state networks in the human brain. *Proc. Natl. Acad. Sci. U.S.A.* 104, 13170–13175. doi: 10.1073/pnas.0700668104

Medda, A., Hoffmann, L., Magnuson, M., Thompson, G., Pan, W. J., and Keilholz, S. (2016). Wavelet-based clustering of resting state MRI data in the rat. *Magn. Reson. Imaging* 34, 35–43. doi: 10.1016/j.mri.2015.10.005

Meilă, M. (2007). Comparing clusterings—an information based distance. *J. Multivar. Anal.* 98, 873–895. doi: 10.1016/j.jmva.2006.11.013

Meng, C., Brandl, F., Tahmasian, M., Shao, J., Manoliu, A., Scherr, M., et al. (2013). Aberrant topology of striatum's connectivity is associated with the number of episodes in depression. *Brain* 137, 598–609. doi: 10.1093/brain/awt290

Meyer, Y. (1993). *Wavelets-Algorithms and Applications*. Ann Arbor, MI: Wavelets-Algorithms and applications Society for Industrial and Applied Mathematics Translation, 142.

Milham, M.P. (2013). *1000 Functional Connectomes Project*. Available online at: http://fcon_1000.projects.nitrc.org/: International Neuroimaging Data-Sharing Initiative (Accessed December 1, 2013).

Misiti, M., Misiti, Y., Oppenheim, G., and Poggi, J.-M. (2013). Wavelet Toolbox User's Guide. Natick, MA: The Math Works Inc.

Murphy, K., Birn, R. M., and Bandettini, P. A. (2013). Resting-state fMRI confounds and cleanup. *Neuroimage* 80, 349–359. doi: 10.1016/j.neuroimage.2013.04.001

Nathan Kline Institute for Psychiatric Research (2013). *Enhanced Rockland Sample Multiband Imaging Test-Retest Pilot Dataset*. Available online at: http://fcon_1000.projects.nitrc.org/indi/pro/eNKI_RS_TRT/FrontPage.html 1000 Functional Connectomes Project.

Nooner, K. B., Colcombe, S. J., Tobe, R. H., Mennes, M., Benedict, M. M., Moreno, A. L., et al. (2012). The NKI-rockland sample: a model for accelerating the pace of discovery science in psychiatry. *Front. Neurosci.* 6:152. doi: 10.3389/fnins.2012.00152

Ogawa, S., Lee, T. M., Kay, A. R., and Tank, D. W. (1990). Brain magnetic resonance imaging with contrast dependent on blood oxygenation. *Proc. Natl. Acad. Sci. U.S.A.* 87, 9868–9872. doi: 10.1073/pnas.87.24.9868

Raichle, M. E., and Mintun, M. A. (2006). Brain work and brain imaging. *Annu. Rev. Neurosci.* 29, 449–476. doi: 10.1146/annurev.neuro.29.051605.112819

Salomon, R. M., Cowan, R. L., Rogers, B. P., Dietrich, M. S., Bauernfeind, A. L., Kessler, R. M., et al. (2011). Time series fMRI measures detect changes in pontine raphe following acute tryptophan depletion. *Psychiatry Res.* 191, 112–121. doi: 10.1016/j.pscychresns.2010.10.007

Salomon, R. M., Karageorgiou, J., Dietrich, M. S., Mclellan, J. Y., Charboneau, E. J., Blackford, J. U., et al. (2012). MDMA (Ecstasy) association with impaired fMRI BOLD thalamic coherence and functional connectivity. *Drug Alcohol Depend.* 120, 41–47. doi: 10.1016/j.drugalcdep.2011.06.022

Sato, J. R., Fujita, A., Amaro, E. Jr., Miranda, J. M., Morettin, P. A., and Brammer, M. J. (2007). DWT-CEM: an algorithm for scale-temporal clustering in fMRI. *Biol. Cybern.* 97, 33–45. doi: 10.1007/s00422-007-0154-4

Schröter, M. S., Spoormaker, V. I., Schorer, A., Wohlschläger, A., Czisch, M., Kochs, E. F., et al. (2012). Spatiotemporal reconfiguration of large-scale brain functional networks during propofol-induced loss of consciousness. *J. Neurosci.* 32, 12832–12840. doi: 10.1523/JNEUROSCI.6046-11.2012

Shakil, S., Billings, J. C., Keilholz, S. D., and Lee, C.-H. (2017). Parametric dependencies of sliding window correlation. *IEEE Trans. Biomed. Eng.* 99, 254–263. doi: 10.1109/TBME.2017.2762763

Skidmore, F., Korenkevych, D., Liu, Y., He, G., Bullmore, E., and Pardalos, P. M. (2011). Connectivity brain networks based on wavelet correlation analysis in Parkinson fMRI data. *Neurosci. Lett.* 499, 47–51. doi: 10.1016/j.neulet.2011.05.030

Smith, S. M., Fox, P. T., Miller, K. L., Glahn, D. C., Fox, P. M., Mackay, C. E., et al. (2009). Correspondence of the brain's functional architecture during activation and rest. *Proc. Natl. Acad. Sci. U.S.A.* 106, 13040–5. doi: 10.1073/pnas.0905267106

Supekar, K., Menon, V., Rubin, D., Musen, M., and Greicius, M. D. (2008). Network analysis of intrinsic functional brain connectivity in Alzheimer's disease. *PLoS Comput. Biol.* 4:e1000100. doi: 10.1371/journal.pcbi.1000100

Thompson, W. H., and Fransson, P. (2015). The frequency dimension of fMRI dynamic connectivity: network connectivity, functional hubs and integration in the resting brain. *Neuroimage* 121, 227–242. doi: 10.1016/j.neuroimage.2015.07.022

Vincent, J. L., Kahn, I., Snyder, A. Z., Raichle, M. E., and Buckner, R. L. (2008). Evidence for a frontoparietal control system revealed by intrinsic functional connectivity. *J. Neurophysiol.* 100, 3328–3342. doi: 10.1152/jn.90355.2008

Wagner, S., and Wagner, D. (2007). *Comparing Clusterings: An Overview*. Universität Karlsruhe, Fakultät für Informatik.

Wang, J., Zuo, X., Dai, Z., Xia, M., Zhao, Z., Zhao, X., et al. (2013). Disrupted functional brain connectome in individuals at risk for Alzheimer's disease. *Biol. Psychiatry* 73, 472–481. doi: 10.1016/j.biopsych.2012.03.026

Wolfram, S. (2002). *A New Kind of Science*. Champaign, IL: Wolfram Media.

Wu, C. W., Gu, H., Lu, H., Stein, E. A., Chen, J.-H., and Yang, Y. (2008). Frequency specificity of functional connectivity in brain networks. *Neuroimage* 42, 1047–1055. doi: 10.1016/j.neuroimage.2008.05.035

Xue, S. W., Li, D., Weng, X. C., Northoff, G., and Li, D. W. (2014). Different neural manifestations of two slow frequency bands in resting fMRI: a systemic survey at regional, inter-regional, and network levels. *Brain Connect*. 4, 242–255.doi: 10.1089/brain.2013.0182

Yeo, B. T., Krienen, F. M., Sepulcre, J., Sabuncu, M. R., Lashkari, D., Hollinshead, M., et al. (2011). The organization of the human cerebral cortex estimated by intrinsic functional connectivity. *J Neurophysiol.* 106, 1125–1165. doi: 10.1152/jn.00338.2011

Zahn, C.T. (1971). Graph-theoretical methods for detecting and describing gestalt clusters. *Comput. IEEE Trans. C* 20, 68–86. doi: 10.1109/T-C.1971.223083

Zuo, X. N., Di Martino, A., Kelly, C., Shehzad, Z. E., Gee, D. G., Klein, D. F., et al. (2010). The oscillating brain: complex and reliable. *Neuroimage* 49, 1432–1445. doi: 10.1016/j.neuroimage.2009.09.037

Conflict of Interest Statement: The authors declare that the research was conducted in the absence of any commercial or financial relationships that could be construed as a potential conflict of interest.

frontiers in Neuroscience

ORIGINAL RESEARCH
published: 13 November 2018
doi: 10.3389/fnins.2018.00809

Complexity of Wake Electroencephalography Correlates With Slow Wave Activity After Sleep Onset

Fengzhen Hou[1], Zhinan Yu[1], Chung-Kang Peng[2], Albert Yang[2], Chunyong Wu[3,4]* and Yan Ma[2]*

[1] *Key Laboratory of Biomedical Functional Materials, School of Science, China Pharmaceutical University, Nanjing, China,* [2] *Division of Interdisciplinary Medicine and Biotechnology, Department of Medicine, Beth Israel Deaconess Medical Center/Harvard Medical School, Boston, MA, United States,* [3] *Key Laboratory of Drug Quality Control and Pharmacovigilance, Ministry of Education, China Pharmaceutical University, Nanjing, China,* [4] *Department of Pharmaceutical Analysis, China Pharmaceutical University, Nanjing, China*

OPEN ACCESS

Edited by:
Yaroslav O. Halchenko, Dartmouth College, United States

Reviewed by:
Ilona Kotlewska, Nicolaus Copernicus University in Torun, Poland and Dartmouth College, United States
Gilles Vandewalle, Université de Liège, Belgium

***Correspondence:**
Fengzhen Hou
houfz@cpu.edu.cn
Chunyong Wu
cywu@cpu.edu.cn

Specialty section:
This article was submitted to Brain Imaging Methods, a section of the journal Frontiers in Neuroscience

Received: *31 May 2018*
Accepted: *17 October 2018*
Published: *13 November 2018*

Citation:
Hou F, Yu Z, Peng C-K, Yang A, Wu C and Ma Y (2018) Complexity of Wake Electroencephalography Correlates With Slow Wave Activity After Sleep Onset. Front. Neurosci. 12:809. doi: 10.3389/fnins.2018.00809

Sleep electroencephalography (EEG) provides an opportunity to study sleep scientifically, whose chaotic, dynamic, complex, and dissipative nature implies that non-linear approaches could uncover some mechanism of sleep. Based on well-established complexity theories, one hypothesis in sleep medicine is that lower complexity of brain waves at pre-sleep state can facilitate sleep initiation and further improve sleep quality. However, this has never been studied with solid data. In this study, EEG collected from healthy subjects was used to investigate the association between pre-sleep EEG complexity and sleep quality. Multiscale entropy analysis (MSE) was applied to pre-sleep EEG signals recorded immediately after light-off (while subjects were awake) for measuring the complexities of brain dynamics by a proposed index, CI_{1-30}. Slow wave activity (SWA) in sleep, which is commonly used as an indicator of sleep depth or sleep intensity, was quantified based on two methods, traditional Fast Fourier transform (FFT) and ensemble empirical mode decomposition (EEMD). The associations between wake EEG complexity, sleep latency, and SWA in sleep were evaluated. Our results demonstrated that lower complexity before sleep onset is associated with decreased sleep latency, indicating a potential facilitating role of reduced pre-sleep complexity in the wake-sleep transition. In addition, the proposed EEMD-based method revealed an association between wake complexity and quantified SWA in the beginning of sleep (90 min after sleep onset). Complexity metric could thus be considered as a potential indicator for sleep interventions, and further studies are encouraged to examine the application of EEG complexity before sleep onset in populations with difficulty in sleep initiation. Further studies may also examine the mechanisms of the causal relationships between pre-sleep brain complexity and SWA, or conduct comparisons between normal and pathological conditions.

Keywords: EEG, brain activity, non-linear, sleep medicine, sleeps stages, complexity

INTRODUCTION

Sleep medicine has been increasingly recognized as an important discipline in recent decades; however, the current limitations of electroencephalography (EEG)-based sleep analysis and quantification may have led to ongoing controversy. Sleep is a complex physiological process that involves functions of every organ system at different levels. Alternative metrics have been proposed, aiming to provide insights into the dynamics of sleep. In sleep medicine, EEG is one of the most frequently recorded biological signals, but it is mainly used as the basis for scoring sleep stages in sleep laboratories and clinics, as sleep is classified as either rapid-eye-movement (REM) sleep or non-REM (NREM) sleep (including sleep stages N1, N2, and N3). Owing to the non-linear and dynamic features of EEG, non-linear approaches may lead to better understanding of the profound complexity of sleep.

Non-linear dynamics theory provides new opportunities for understanding the behavior of EEG (Acharya et al., 2005). Previously, EEG has been used to mark features of sleep (He et al., 2005; Janjarasjitt et al., 2008; Yeh et al., 2013; Abeysuriya et al., 2014), and it has been reported that nonlinearity depends on sleep stage (Shen et al., 2003). Recently, studies have increasingly used non-linear methods to investigate the nature of brain activities during sleep (Ma et al., 2018), but there are still limitations in the existing literature. The full advantages of non-linear approaches have yet to be determined (Ma et al., 2018).

According to the complexity theories, somewhat higher complexity is associated with relatively improved health conditions and greater chances of survival (Costa et al., 2002a, 2005), while a reduction in or loss of complexity is often associated with imbalance or disturbed physiological conditions, usually implying disease or aging (Goldberger et al., 2002). In many studies, complexity-based metrics of the dynamics of a physiological system have demonstrated better prognostic power (Mejaddam et al., 2013; Lin et al., 2014; Vandendriessche et al., 2014; Moshirvaziri et al., 2016; Chiu et al., 2017; Ma et al., 2017). The complexity theories also suggest that different levels of complexity can indicate whether a system is under stress or relatively relaxed (Costa et al., 2002a, 2005; Goldberger et al., 2002). In a novel application of complexity theory, Casali et al. found that measuring complexity can provide a reliable way to discriminate the level of consciousness in single individuals during wakefulness, sleep, and anesthesia, as well as in patients who had emerged from coma and recovered a minimal level of consciousness (Casali et al., 2013). When complexity is used in the evaluation of sleep, studies have shown that complexity indices (e.g., entropy) decrease as sleep gets deeper, and reach their lowest level when slow wave sleep (SWS) occurs (Ma et al., 2018). Moreover, Abásolo et al. found that activated brain states—wakefulness and REM sleep—are characterized by higher complexity compared with NREM sleep (Abásolo et al., 2015). Based on these well-established theories and previous studies, investigating the sleep-related temporal structure of brain activity based on measures such as multi-scale entropy (MSE) (Costa et al., 2002a, 2005), the perturbational complexity index (Casali et al., 2013), or Lempel-Ziv complexity (Abásolo et al., 2015) should provide insights that go beyond those obtained with conventional techniques for signal analysis.

In sleep medicine, one question that remains unsolved is whether the complexity of brain waves in the pre-sleep state or during sleep latency can determine or predict sleep quality. In fact, most people with insomnia complain of being unable to fall asleep because they cannot switch off their "racing" mind (Lichstein and Rosenthal, 1980; Espie et al., 1989; Harvey, 2000). Under high mental load, the sense of urgency about falling asleep adversely affects sleep onset latency (Ansfield et al., 1996). Since stressful brain activities always show higher complexity, we can reasonably hypothesize that lower complexity of brain waves at pre-sleep status can facilitate sleep initiation, reduce sleep latency, and further lead to a high quality of sleep characterized by sufficient deep sleep or SWS.

Slow wave sleep SWS is defined as the state in which large-amplitude, low-frequency waves are dominant and it occurs when delta rhythm is dominant in the EEG signal. Slow wave activity (SWA), which is equivalent to delta activity and encompasses components of the EEG signal in the frequency range of ∼0.5–4.5 Hz, is considered to be one of the most important functional EEG parameters during sleep (Brunner et al., 1990; Peter Achermann and Borbély, 2011). Under physiological conditions, SWA is commonly used as a quantitative measure of NREM sleep dynamics and an indicator of sleep depth or sleep intensity (Borbély and Achermann, 1999); Olivier et al. (2010). Fast Fourier transform (FFT) analysis is the most popular method for quantifying SWA. However, it has intrinsic limitations in capturing the underlying dynamics of brain oscillations (Ma et al., 2018). First, FFT analysis takes complex EEG oscillations, composed of sine waves with different frequencies (Campbell, 2009), and decomposes them into frequency component bands, such as beta, alpha, theta, and delta. However, it has long been known that brain oscillation is not a linear combination of these arbitrary frequency components, a property called "nonlinearity" (Bedard et al., 2006). Second, FFT analysis assumes that none of these frequency components changes in amplitude or shape as time evolves, which is clearly against what has been observed in complex brain oscillations, a property called "nonstationarity" (Campbell, 2009). In recent years, ensemble empirical mode decomposition (EEMD) has been adopted to solve this problem (Wu and Huang, 2005). EEMD is an adaptive and noise-assisted data analysis method that is based on local characteristics of the data, requiring no predefined basis. EEMD decomposes an original non-linear and non-stationary signal into a series of simple intrinsic mode functions (IMFs), and has the advantage that every IMF can be physically meaningful via the quantification of the instantaneous amplitude and frequency (Wang et al., 2012). EEMD has become popular for analyzing EEG signals in recent years (Chen et al., 2010, 2014; Kuo et al., 2011; Bizopoulos et al., 2013; Al-Subari et al., 2015a,b; Kanoga and Mitsukura, 2015; Bai et al., 2016; Zeng et al., 2016; Gotz et al., 2017; Hassan and Bhuiyan, 2017). Employing EEMD to quantify SWA might lead to additional findings.

Therefore, the aim of the present study was to examine whether the complexity of brain waves in the pre-sleep state

is associated with sleep quality. We hypothesized that lower complexity of brain waves before sleep may play a potential facilitating role in wake-sleep transition and improve the subsequent sleep depth. To this end, the MSE method was applied to EEG signals recorded during the first 5 min after light-off, when the participants were still awake. Sleep latency was determined by manual scoring, and sleep depth was quantified by SWA using an EEMD-based approach or traditional FFT analysis.

METHODS

Overnight Polysomnography (PSG)

Overnight polysomnography (PSG) data obtained from the Sleep Heart Health Study-1 (SHHS-1) were used in this study. The SHHS was a multi-center cohort study implemented by the National Heart Lung and Blood Institute to determine the cardiovascular and other consequences of sleep-disordered breathing, and its characteristics have been described in detail elsewhere (Quan et al., 1997; Redline et al., 1998). Unattended overnight PSG was performed with a portable PS-2 system (Compumedics, Abottsville, Australia). Sensors were placed and equipment was calibrated during an evening home visit by a certified technician. Data collection included C3/A2 and C4/A1 EEGs, sampled at 125 Hz; right and left electrooculograms; a bipolar submental electromyogram; thoracic and abdominal excursions (inductive plethysmography bands); airflow (detected by a nasal-oral thermocouple (Protec, Woodinville, WA); finger pulse oximetry (Nonin, Minneapolis, MN) sampled at 1 Hz; electrocardiogram sampled at 125 Hz; body position (mercury gauge sensor); and ambient light (on/off, by a light sensor secured to the recording garment). After equipment retrieval, the data were forwarded to a central reading center (Case Western Reserve University, Cleveland, OH) for scoring according to a standard protocol. Finally, every 30 s epoch was scored (Thomas et al., 2007). The polysomnographic methods, scoring protocol, and quality assurance procedures were as previously described (Quan et al., 1997; Redline et al., 1998; Thomas et al., 2007).

Sleep variables derived from visual scoring were calculated for each participant, including: total sleep time (TST) (time spent asleep between sleep onset and light-on); wake time after sleep onset (WASO, total amount of time awake after falling asleep); and the duration of each sleep stage, calculated as a percentage of TST. Sleep latency, defined as the period from light-off to the first three consecutive epochs of stage N1 sleep or an epoch of any other stage, was also computed.

Subjects

The study included 103 healthy subjects who met the inclusion criteria: (1) no usual daily alcohol intake; (2) no benzodiazepines or non-tricyclic antidepressants intake within 2 weeks of the SHHS-1 visit; (3) no history of diabetes; (4) no history of stroke; (5) no hypertension status based on second and third blood pressure readings or current treatment with anti-hypertensives; (6) no self-reported hypertension; (7) no self-reported sinus trouble; (8) no coronary angioplasty, heart failure, heart attack, pace maker, or stroke; (9) apnea–hypopnea index, representing the number of apnea and hypopnea events with $\geq$3% oxygen desaturation per hour of sleep, of $<$5; (10) the entire recording was scored, and scoring started before light-off and ended after light-on; (11) no more than 30 min of the sleep period had either lost or unscorable EEG, respiratory, or oximetry data; (12) the time spent on sleep was no less than 50% of the total time spent in bed; (13) at least one epoch during each sleep stage, i.e., REM, N1, N2, and N3; (14) sleep latency no less than 5 min. See the **Supplementary Material** for identifiers of the included subjects, which were created by the National Sleep Research Resource team for easier matching with file downloads.

The Theory of Multiscale Entropy (MSE)

MSE was introduced by Costa et al. (2002a,b); Costa et al. (2005) to quantify the complexity of biologic systems. Entropy-based methods characterize uncertainty about a source of information and the probability distribution of the samples drawn from it. The entropy increases with the degree of disorder and reaches its maximum in completely random systems. However, an increase in the entropy may not always be associated with an increase in dynamical complexity. For instance, a randomized time series has higher entropy than the original time series, although the process of generating surrogate data destroys correlations and degrades the information content of the original signal. This inconsistency may be related to the fact that widely used entropy measures are based on single-scale analysis and do not take into account complex temporal fluctuations. Therefore, MSE has been proposed as a method for assessing complexity by measuring the entropy inherent in a time series over multiple time scales.

The procedures involved in calculating MSE have been well reviewed (Costa et al., 2002a,b, 2005) and can be summarized in the following three steps (Yang et al., 2013): (1) construction of a coarse-grained time series according to a scale factor; (2) quantification of the sample entropy of each coarse-grained time series; and (3) examination of the sample entropy profile over a range of scales. The length of each coarse-grained time series is equal to the length of the original time series divided by the scale factor. For scale 1, the time series is simply the original time series. Sample entropy is defined by the negative natural logarithm of the conditional probability that a dataset of length N, having repeated itself within a tolerance r (similarity factor) for m points (pattern length), also repeats itself for $m + 1$ points, without allowing self-matches (Richman and Moorman, 2000).

One requirement in the calculation of sample entropy is to determine the pattern length m and similarity factor r. In this study, we set m to 2 and r to 0.15 $\times$ SD, where SD is the standard deviation of the analyzed time series. As 30 scales were considered and the entropy on each scale does not necessarily have a specific physiological meaning, a complexity index, called CI_{1-30}, was additionally employed in the current study. CI_{1-30} was defined as the mean value of the entropies from scale 1 to scale 30, as in many other published studies (Vieira et al., 2017). CI_{1-30} provides insight into the integrated complexity of the system over the time scales of interest. See the **Supplementary Material** for the MATLAB code for MSE analysis.

The Theory of EMD and EEMD

Empirical mode decomposition (EMD) is an adaptive data analysis method based on local characteristics of the data, requiring no predefined basis. The details of the method can be found in the work of Huang (2000).

In the EMD approach, the targeted data $x(t)$ is decomposed in terms of IMFs, c_j, i.e.,

$$x(t) = \sum_{j=1}^{n} c_j + r_n \quad (1)$$

where r_n is the residue of data $x(t)$ after n number of IMFs have been extracted. IMFs are simple oscillatory functions with varying amplitude and frequency. In practice, the EMD is implemented through a sifting process that uses only local extremes, and the process stops when the residue, r_n, becomes a monotonic function from which no more IMFs can be extracted (Huang, 2000).

However, mode-mixing, defined as any IMF consisting of oscillations of dramatically disparate scale, can be caused by intermittency of the driving mechanisms and obstructs the true physical interpretations (Wu and Huang, 2005). Therefore, EEMD was developed to alleviate this drawback, making use of the facts that adding noise to the data can provide a uniformly distributed reference scale, and the means of the corresponding IMFs of different white noise series are likely to cancel each other out. The detailed steps for EEMD are (Wu and Huang, 2005): (1) add a white noise series to the targeted data; (2) decompose the data with added white noise into IMFs based on EMD; (3) repeat step (1) and step (2), but with different white noise series each time; and (4) obtain the (ensemble) means of corresponding IMFs of the decompositions as the final result. The MATLAB code for EEMD was shared by RCADA (http://rcada.ncu.edu.tw/research1.htm).

A Hilbert transform can then be used to calculate the instantaneous frequency of the IMFs (Feldman and Braun, 1995). For a IMF $c(t)$, one can define its Hilbert transform $\hat{c}(t)$ and analytic signal $z(t)$ as shown in Equation (2) and (3), respectively.

$$\hat{c}(t) = \int_{-\infty}^{+\infty} c(\tau)\, h(t-\tau)\, d\tau = \frac{1}{\pi} \int_{-\infty}^{+\infty} \frac{c(\tau)}{t-\tau} d\tau \quad (2)$$

$$z(t) = c(t) + i \times \hat{c}(t) = A(t) e^{i\varnothing(t)} \quad (3)$$

Here, $\varnothing(t)$ is the instantaneous phase (IP) of $c(t)$. The instantaneous frequency $f(t)$ is the derivation of IP and t shown in Equation (4):

$$f(t) = \frac{1}{2\pi} \frac{d\varnothing(t)}{dt} \quad (4)$$

The Computation of SWA Based on EEMD

Both FFT and EEMD were used for the decomposition of the EEG signal into its constituent frequency components. Once the original EEG signal $x(t)$ was decomposed to n number of IMFs (denoted as c_i) and a residue based on EEMD, a different way to measure SWA (denoted as *EEMD-SWA*) could be proposed, as shown in Equation (5).

$$EEMD - SWA = \sum_{i=k}^{l} std(c_i) / \sum_{i=1}^{n} std(c_i) \quad (5)$$

In Equation (5), function $std(c_i)$ refers to the standard derivation of IMF c_i, and the parameters k and l are determined by the orders of the IMFs that fall into the frequency range of SWA, according to the instantaneous frequency range of each IMF. Thus, *EEMD-SWA* actually reflects the relative power of slow waves in the signal.

Framework of the Current Research

In this study, EEG signals from derivation C3/A2 was imported into MATLAB for offline analysis. For each subject, two key time points were identified, light-off and sleep onset. **Figure 1** briefly shows the analysis protocol. The first 5 min EEG immediately after light-out was analyzed by MSE.

On the other hand, SWA was calculated at the beginning of sleep episodes (90 min after sleep onset) and over the whole night's sleep after sleep onset, respectively. EEMD were applied to each 30 s EEG epoch in each time scope. As each 30 s EEG epoch is a time series with 3750 data points, the values of *EEMD-SWA* for all the epochs in each duration were calculated and averaged, resulting in two metrics, denoted as $EEMD\text{-}SWA_{90}$ and $EEMD\text{-}SWA_{\text{all}}$, for each participant. For comparison, the traditional FFT-based evaluation of SWA was applied in a similar way and resulted in another two metrics, denoted as $FFT\text{-}SWA_{90}$ and $FFT\text{-}SWA_{all}$, respectively. In the calculation of $FFT\text{-}SWA_{90}$ and $FFT\text{-}SWA_{all}$, power spectral density was estimated via the period-gram procedure with direct current filtering and Hamming windowing. SWA for each 30 s epoch was calculated by taking the power in the 0.5–4.5 Hz range as a percentage of the total signal power in the frequency range (0.5–62.5 Hz). See the **Supplementary Material** for the MATLAB code for *FFT-SWA*.

Then, the correlations between the proposed complexity index CI_{1-30} and sleep latency, $EEMD\text{-}SWA_{90}$, $EEMD\text{-}SWA_{all}$, $FFT\text{-}SWA_{90}$, and $FFT\text{-}SWA_{all}$, were evaluated to investigate the associations between EEG complexity and proposed measures during the wake-sleep transition and overall sleep. When sleep pressure accumulates, slow brain waves gradually become significant or dominant, which may be in line with a decline in EEG complexity. Inspired by this hypothesis, we investigated the association between brain wave complexity and sleep pressure during pre-sleep wakefulness. Theta activity (4–8 Hz), which is generally considered as a marker for the build-up of sleep pressure (Fattinger et al., 2017), was thus measured by averaging the FFT-based relative power (percentage of the power in the frequency range 0.5–62.5 Hz, denoted as P_{theta} in this study) for all the 30 s EEG epochs in the first 5 min after light-off, the same time course as that used for the MSE analysis.

We further analyzed whether early SWA in sleep can be predicted by the pre-sleep EEG complexity using median split subgrouping, where we divided the subjects by ranked SWA into top 50% vs. bottom 50% groups according to $EEMD\text{-}SWA_{90}$ or $FFT\text{-}SWA_{90}$. Such a strategy of median split has an enormous popularity in consumer research,

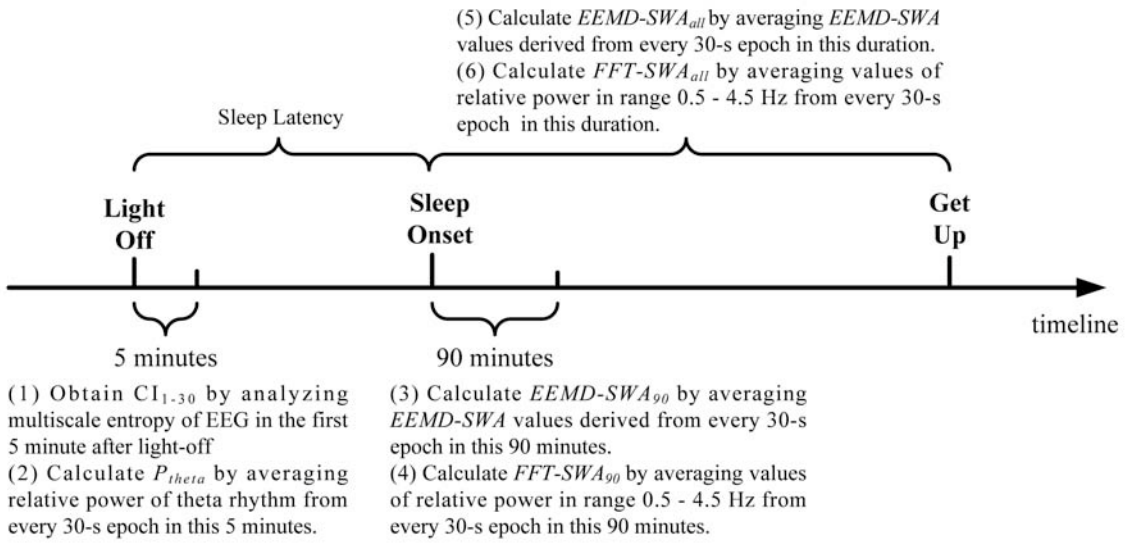

FIGURE 1 | Schematic diagram of the timeline regarding EEG analysis.

psychology, and numerous other fields (Iacobucci et al., 2015a,b). For instance, Nordström et al. investigated whether age is a suicide risk factor for each sex by median split (Nordström et al., 2010). In addition to that, the subgrouping in the current study provided us an intuitive way to investigate the statistical difference in the values of sample entropy between the two groups over multiple time scales, making a meaningful complementation to CI_{1-30} used in regressions.

Statistical Analyses

SPSS version 19.0 (IBM SPSS Statistics, NY, United States) and MATLAB (MathWorks R2014a, Inc., Natick, MA, United States) were used for the statistical analyses. The demographics and sleep variables derived from visual scoring were reported as mean with standard deviation if data were normally distributed, and as median with lower and upper quartiles otherwise. Comparisons of the demographics and sleep variables between subgroups from the median split were assessed by chi-square test for categorical variables and unpaired *t*-test or two-sided Wilcoxon rank sum test for continuous ones. A $p < 0.05$ was considered statistically significant.

Since sleep may vary with age and sex, and high body mass index (BMI) is a strong risk factor for sleep disorders (Hou et al., 2016), these three variables were included as covariates in the statistical test for correlation between pre-sleep EEG complexity and sleep latency, as well as subsequent sleep quality. General linear models (GLM) were thus employed for the statistical analyses in SPSS 19.0 between CI_{1-30} and sleep latency, *EEMD-SWA*$_{90}$, *EEMD-SWA*$_{\text{all}}$, *FFT-SWA*$_{90}$, *FFT-SWA*$_{\text{all}}$ and P_{theta}, controlling age, gender, and BMI.

For each scale in the MSE analysis, the statistical difference in the sample entropy between the *EEMD-SWA*$_{90}$ top 50% and bottom 50% groups, as well as between the *FFT-SWA*$_{90}$ top 50% and bottom 50% groups, were investigated by covariance analysis, controlling age, gender, and BMI. The false discovery rate (FDR) procedure was included for multiple testing.

RESULTS

Modes Analyses From EEMD

In practice, there are three parameters that should be determined for the application of EEMD: the ratio of the standard deviation of the noise to the target data (denoted by ε), the number of prescribed IMFs (denoted by NI), and the number of ensemble members (denoted by NE). In this study, ε was set to 0.1, NI to 7, and NE to 200. **Figure 2** shows a typical result of EEMD on a 30 s EEG epoch derived from a subject in the current study.

Further estimation of the frequency range of IMFs was performed on all epochs in the current study according to Equations (2–4). For each IMF signal, **Table 1** lists its frequency range, which uses two quartiles, the 2.5 and 97.5 centiles, and leaves 5% of normal outside the "normal range." As shown in **Table 1** and **Figure 2**, the IMF1 decomposition was mainly associated with the brain beta rhythm (13–30 Hz), while IMF2 decomposition was associated with the alpha rhythm (8–13 Hz), IMF3 decomposition with the theta rhythm (4–8 Hz), and IMF4, IMF5, IMF6, and IMF7 decompositions with the delta rhythm (<4 Hz). Therefore, in this study, we set the values of *k*, *l*, *n* in Equation (5) to be 4, 7, and 7, respectively.

Demographics and Sleep Variables Derived From Visual Scoring

As shown in **Table 2**, the sample had a median age of 57 years and mean BMI of 25.6 kg/m^2. A majority of the participants were identified as being of normal weight (BMI: 18.5–25 kg/m^2) or overweight (BMI: 25–30 kg/m^2). The standard PSG scoring

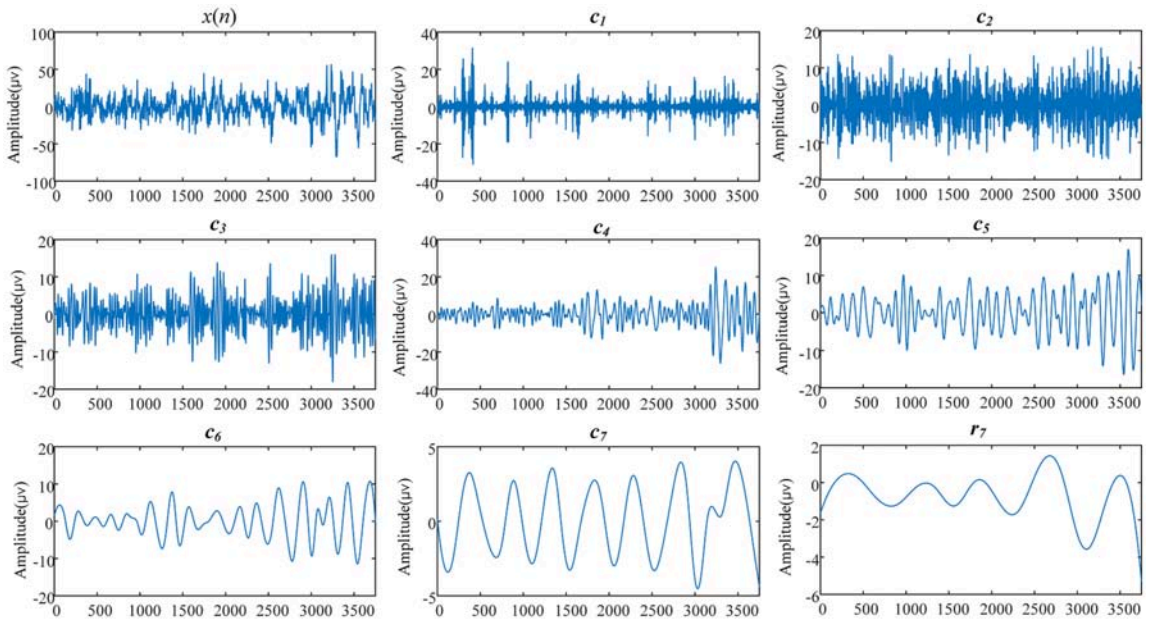

FIGURE 2 | The EEMD results of a 30 s EEG signal derived from a 69-years-old woman (subject ID in SHHS-1 is 200301). $x(n)$ is the original EEG signal, $c_i(i = 1,2,\ldots,7)$ are the IMFs, and r_7 is the residual part of data $x(n)$ after 7 IMFs were extracted.

TABLE 1 | Frequency range in seven IMFs of EEMD.

Signal	Frequency range (Hz)	Associated brain rhythm
IMF1	25.2 [20.2–38.1]	beta
IMF2	12.1 [10.3–16.9]	alpha
IMF3	6.3 [5.5–8.8]	theta
IMF4	3.5 [2.8–4.9]	delta
IMF5	2.1 [1.3–3.5]	delta
IMF6	1.5 [0.6–3.5]	delta
IMF7	1.1 [0.3–3.9]	delta

The frequency range is expressed as median [the 2.5 centile - the 97.5 centile].

results revealed that the mean TST was 371 min, while the percentages of scored sleep stages N1, N2, N3, and REM sleep were ∼ 4, 55, 20, and 21%, respectively. These results are consistent with the general sleep architecture in adults (Berry, 2012).

The demographic characteristics were balanced between the top and bottom 50% groups, with no significant differences regarding age, gender, or BMI. Sleep variables for the *EEMD-SWA*$_{90}$ top 50% and bottom 50%, as well as for the *FFT-SWA*$_{90}$ top 50% and bottom 50%, are also shown in **Table 2**. Between the groups divided by *EEMD-SWA*$_{90}$, significant differences were found between REM sleep and SWA. However, for the *FFT-SWA*$_{90}$ top 50% and bottom 50% groups, in addition to the quantified SWA, WASO, N1, N2, and N3 also showed significant between-group differences. For studied measures (**Table 2**), no significant differences were found between the two partitions when the same grouping rules (top 50% vs. bottom 50%) were applied.

Association Between EEG Complexity and Sleep Measures

As shown in **Table 3**, GLM revealed a significant positive correlation between CI_{1-30} and sleep latency ($r = 0.328$, $p = 0.001$), indicating that higher complexity level was moderately associated with prolonged sleep latency.

In the regression model, where we adjusted for age, gender, and BMI, *EEMD-SWA*$_{90}$ showed a statistical trend for a weak correlation with CI_{1-30} ($r = -0.190$, $p = 0.06$), whereas no association was found between *FFT-SWA*$_{90}$ and CI_{1-30}. However, for the whole-night data, no correlation was found between CI_{1-30} and *EEMD-SWA*$_{all}$ or *FFT-SWA*$_{all}$. Furthermore, the GLM model, controlling age, gender, and BMI, revealed a significant positive correlation ($r = 0.373$, $p = 0.0001$) between P_{theta} and CI_{1-30}.

When sample entropies on scales 1–30 were compared between the *EEMD-SWA*$_{90}$ top 50% and bottom 50% groups, significant differences (controlled by the FDR procedure) were found on all the chosen scales, except that of scale 1. As presented in **Figure 3**, the group with the higher *EEMD-SWA*$_{90}$ in sleep showed a reduced complexity of pre-sleep brain dynamics. When the *FFT-SWA*$_{90}$ top 50% and bottom 50% groups were compared, as shown in **Figure 4**, a similar negative correlation was observed, but significant differences ($p < 0.05$) between the two groups were found only on the short time scales (scales 2–9). However, after FDR controlling, no significant differences remained for any of the 30 scales, indicating that the EEMD-based method might provide a more robust way to measure SWA.

TABLE 2 | Demographics and sleep variables derived from visual scoring.

	All	*EEMD-SWA*$_{90}$		*FFT-SWA90*	
	***N* = 103**	**top 50% *N* = 52**	**bottom 50% *N* = 51**	**top 50% *N* = 52**	**bottom 50% *N* = 51**
Gender	19M/84F	6M/46F	13M/38F	7M/45F	12M/39F
Age (years)	57.3 ± 11.4	58.8 ± 11.9	55.8 ± 10.8	57.6 ± 11.9	57.0 ± 11.0
Body mass index (kg/m^2)	25.6 ± 4.1	25.8 ± 4.3	25.3 ± 4.0	25.6 ± 4.3	25.6 ± 4.0
Total sleep time (min)	370.5 ± 58.6	379.6 ± 58.2	361.1 ± 58.0	380.8 ± 61.2	360.0 ± 54.3
Wake after sleep onset (min)	[20.5,62.5]	[19.0,55.8]	[22.9,69.9]	[18.3,52.0]	[25.8,67.9]*
Stage N1 sleep (%)	[2.6,5.2]	[2.6,4.7]	[2.5,5.3]	[2.4,4.2]	[2.7,5.7]*
Stage N2 sleep (%)	54.9 ± 10.9	53.1 ± 9.3	56.8 ± 12.2	51.8 ± 9.0	58.2 ± 11.9*
Stage N3 sleep (%)	20.3 ± 11.8	21.4 ± 11.3	19.1 ± 12.2	23.3 ± 11.2	17.2 ± 11.6*
REM sleep (%)	[16.7,24.6]	[18.8,25.4]	19.4 ± 5.3*	21.2 ± 4.9	19.8 ± 5.9
Sleep latency (min)	[10.0,34.0]	[8.3,29.3]	[10.5,34.4]	[8.0,29.3]	[10.6,34.4]
Slow wave activity (%)		0.744 ± 0.046	0.635 ± 0.086*	0.752 ± 0.037	0.626 ± 0.078*

Descriptive statistics were reported as mean ± standard deviation if data are normally distributed and as median [lower quartile, upper quartile] otherwise. The symbol '' indicates significant difference ($p < 0.05$, unpaired t-test in the case of normally distributed data or two-sided Wilcoxon rank sum test in other case) between values of the bottom 50% and the corresponding top 50% group.*

TABLE 3 | Correlations between pre-sleep EEG complexity or demographics and sleep measures in GLM models.

Independent / Dependent	CI_{1-30}		Age		Gender		BMI	
	R	P	R	P	R	P	R	P
Sleep Latency	0.328	0.001	0.074	0.434	0.080	0.398	−0.059	0.541
EEMD-SWA$_{90}$	−0.190	0.060	0.024	0.805	0.065	0.513	0.009	0.931
FFT-SWA$_{90}$	−0.165	0.103	−0.035	0.729	0.029	0.771	−0.093	0.358
EEMD-SWA$_{all}$	−0.017	0.863	−0.058	0.561	0.009	0.930	0.202	0.046
FFT-SWA$_{all}$	0.063	0.529	−0.123	0.220	−0.051	0.607	0.125	0.217
P_{theta}	0.373	0.0001	−0.021	0.822	0.071	0.449	0.095	0.316

R, correlation coefficient; P, probability.

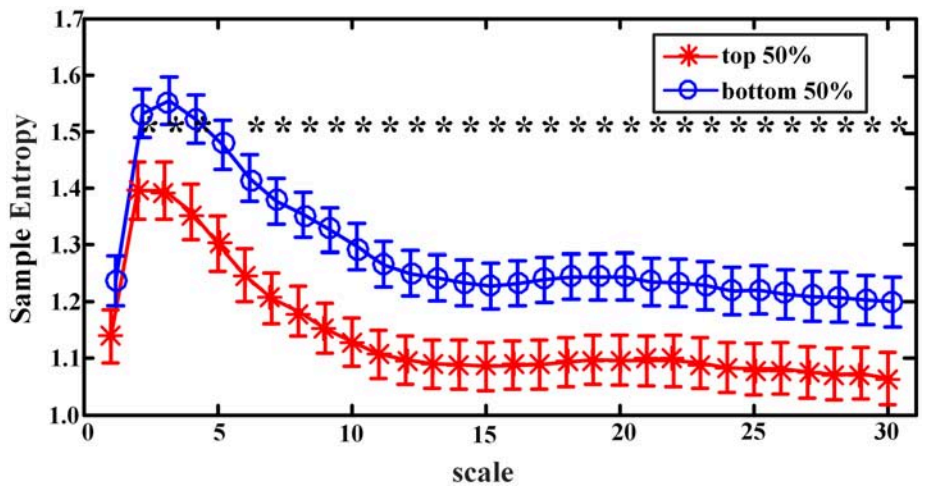

FIGURE 3 | Complexity indices (sample entropy, mean ± SD) on scale 1–30 in groups classified by the rank of *EEMD-SWA*$_{90}$ (top 50% vs. bottom 50%). The symbol '*' indicates significant difference between groups ($p < 0.05$, covariance analysis, controlling the age, gender, and BMI). After the procedure of FDR, the significant differences all remained.

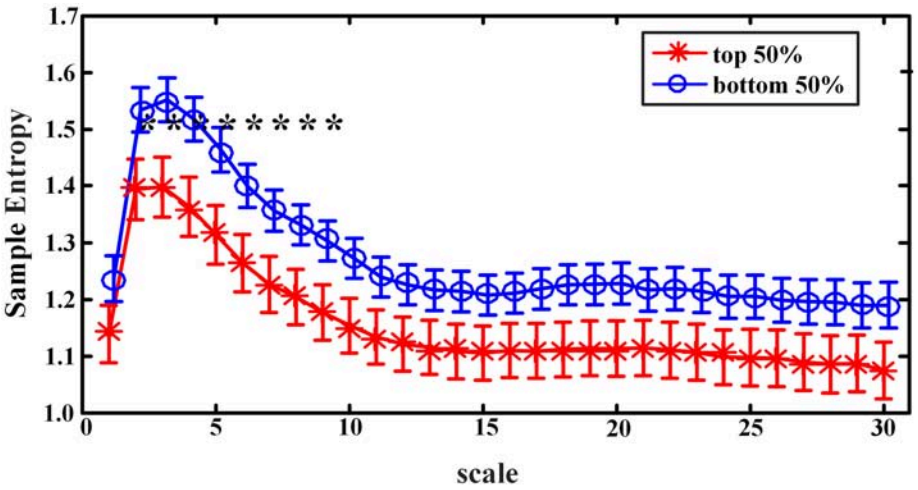

FIGURE 4 | Complexity indices (sample entropy, mean ± standard deviation) on scale 1–30 in groups classified by the rank of *FFT-SWA*$_{90}$ (top 50% vs. bottom 50%). The symbol '*' indicates significant difference between groups ($p < 0.05$, covariance analysis, controlling the age, gender and BMI). However, after the procedure of FDR, none of the significant differences remained.

DISCUSSION

In this study, we examined the associations among wake EEG complexity, sleep latency, and the subsequent SWA quantities during early sleep and over the entire night. Our results revealed a positive correlation between the complexity during the 5 min wakeful EEG and sleep latency. Such complexity also showed a statistical trend for a weak and negative correlation with EEMD-SWA at the beginning of sleep (90 min after sleep onset). Our results suggest that the lower complexity of brain waves in the pre-sleep state may facilitate sleep initiation and reduce sleep latency.

As mentioned in the Introduction, high mental load and urgency to fall asleep increase sleep onset latency (Ansfield et al., 1996) and may lead to non-restorative and unsatisfying sleep, especially in patients with mental disorders or with sleep-onset insomnia, that is, difficulty in sleep initiation. Existing evidence suggests that the manipulation of pre-sleep cognitive activity can lead to changes in sleep onset latency (Ansfield et al., 1996; Nelson and Harvey, 2003; Wuyts et al., 2012). Therefore, future studies are encouraged to examine the complexity before sleep among such populations and to investigate whether interventions that reduce brain wave complexity can assist in promoting restful sleep and improved sleep quality by increasing SWA. In addition, as previously introduced, when a system is under stress or relatively relaxed, levels of complexity can be an appropriate indicator (Costa et al., 2002a, 2005; Goldberger et al., 2002). In recent years, some studies used complexity measures to quantify or evaluate the relaxation states (Aftanas and Golocheikine, 2002; Natarajan et al., 2004). Therefore, we can assume that complexity measures may be useful to examine relaxation interventions such as meditation, slow-paced breathing, music therapy, and cognitive therapy. Effective approaches might be expected to reduce pre-sleep brain complexity and therefore improve sleep quality.

Although in adults, a pronounced increase of theta activity has often been found during the course of sleep deprivation (Aeschbach et al., 1997, 1999; Finelli et al., 2000; Strijkstra et al., 2003; Fattinger et al., 2017), we observed a counterintuitive link between EEG complexity and theta activity during wakefulness in the studied population with normal sleep rather than sleep deprivation. Owing to the counteraction of the circadian process, a linear function with a superimposed 24 h sine wave is generally fitted to theta power and time awake (Åkerstedt and Gillberg, 1990; Finelli et al., 2000). In this way, theta activity may not increase within a session until extreme sleepiness is encountered (Åkerstedt and Gillberg, 1990; Finelli et al., 2000). Aeschbach et al. investigated the influence of the circadian pacemaker and of the duration of time awake on EEG (Aeschbach et al., 1999). They found that the theta rhythm was exhibited a minimum of 1 h after the onset of melatonin secretion (the clock time of melatonin onset in Aeschbach's study ranged from 22:05 to 22:43), indicating evident dissociation, as the circadian maximum of theta activity appeared to be delayed with respect to the maximum of sleep propensity. In our study, 72 out of 103 participants reported their clock time for light-off in the range of 22:05–23:43, however, it is still lack of evidence to make clear the association between sleep pressure and EEG complexity before nocturnal sleep in normal populations. The association between complexity/MSE and sleep-wake regulation is therefore not straightforward and deserves further investigations.

We also analyzed SWA over the entire night for each subject. However, those whole-night results showed significantly weaker correlations with wake complexity compared with SWA$_{90}$. As it is well-recognized that SWA exhibits a global declining trend over the course of the night and its level in the first non-REM episode increases as a function of prior waking (Achermann et al., 1993), which may indicate the reason why the observed association only present between pre-sleep EEG complexity and

SWA in early sleep rather than the whole night. Nonetheless, it would be worth investigating the dynamic changes in pre-sleep complexity and SWA through the entire night, and examining the potential causal relationship in future work. As mentioned above, most of the previous studies of EEG complexity focused on analyses of entropy for each sleep stage, showing a trend of decreasing complexity as sleep becomes deeper (Ma et al., 2018). Non-linear features, including complexity indices, may provide assistance in automatic sleep classification, but, more importantly, studies are encouraged to break the boundaries of limitation to expand the application of non-linear approaches, so that we can better understand the sleep dynamics (Ma et al., 2018). A further step would be to study the complexity differences between normal and pathological conditions, and investigate whether abnormal sleep can be predicted by the first few minutes of pre-sleep EEG recording while a subject is still awake. It would also be of value to determine the potential mechanisms of pre-sleep EEG complexity and sleep-wake transitions and overall sleep quality. Again, we encourage broad applications of such complexity-based approaches in future studies.

Regarding the methodology, the groups defined by FFT-SWA_{90} showed significant differences regarding manually scored sleep parameters (e.g., WASO, N1, N2, N3), while the differences were not significant when groups were defined by EEMD-SWA_{90}. One possible reason is that both manual scoring and FFT spectral analysis are based on the wave morphology and feature waves. However, for revealing the underlying association between wake complexity and quantified sleep SWA, the proposed EEMD-based method had better performance than traditional FFT-based spectral analysis. GLM revealed a weak correlation between pre-sleep EEG complexity and EEMD-SWA during the first 90 min of sleep. Furthermore, when we split the participants into two groups according to the values of *EEMD-SWA_{90}*, the sample entropies at almost all time scales exhibited significant differences between the two groups, suggesting that waking EEG complexity can distinguish between lower and higher groups of SWA after sleep onset quantified by the EEMD approach. However, when SWA was measured using a traditional way such as FFT, any association between waking complexity and sleep SWA was insignificant. Owing to the non-linear and non-stationary characteristics of EEG signals during sleep, there would be a drifting of the frequency ranges of the EEG components for each individual. In this situation, as demonstrated in the current study, compared with the frequency band fixed method, a data adaptive approach such as EEMD to measure SWA would be more sensitive to the underlying dynamics of sleep and better able to uncover its mechanisms.

One strength of this study was that we used an existing database and included a reasonably large number of subjects provided by the freely available database (SHHS) to test our hypothesis. Meanwhile, limitations of this study include that associations measured at the population level may not reflect associations at the individual level, and that the study is prone to confounding by other factors. In our study, 82% of the participants were female, which may limit the generalizability of our finding, given that hormonal changes during the menstrual cycle or in peri-menopausal transition may affect sleep (Mallampalli and Carter, 2014; Jehan et al., 2015). However, no such information was provided for the participants in the database. Future studies with prospective designs are strongly encouraged. In addition, the PSG data provided in SHHS-1 were collected from two scalp-placed electrodes: C3 and C4. Since each brain region is associated with different EEG feature waves, future studies are encouraged to perform such complexity and SWA analyses using multiple EEG montages.

In conclusion, lower complexity before sleep onset is associated with a decline of sleep latency and higher SWA after sleep onset, suggesting that reduced complexity of brain waves may improve sleep quality. The application of complexity measures is important to extend our knowledge of sleep. Future studies are encouraged to explore the complexity before sleep among subjects with sleep disorders, to determine its relationship with the efficacy of interventional approaches or for developing screening tools for use with short-term pre-sleep EEG. Although the current study elucidated the association between wakeful brain complexity and nocturnal sleep quality in the healthy population, future investigations should focus on patients with sleep disorders. We would like to encourage interdisciplinary efforts to address this research question.

ETHICS STATEMENT

The study protocol of SHHS was approved by the institutional review board of each participating center, and each participant signed informed consent. All methods were carried out in accordance with relevant guidelines and regulations. The current study only analyzed de-identified data from the SHHS database, and did not involve a research protocol requiring approval by the relevant institutional review board or ethics committee.

AUTHOR CONTRIBUTIONS

FH, C-KP, CW, and YM designed this study. FH, AY and ZY analyzed data. FH and YM wrote the article.

FUNDING

This work was supported by the National Natural Science Foundation of China (61401518, 81673681, and 81473357) and the Delta Environmental and Educational Foundation.

ACKNOWLEDGMENTS

We would like to acknowledge the support team of the forum in the Sleep Heart Health Study for their detailed explanations and assistance in our use of the dataset.

SUPPLEMENTARY MATERIAL

The Supplementary Material for this article can be found online at: https://www.frontiersin.org/articles/10.3389/fnins.2018.00809/full#supplementary-material

REFERENCES

Åkerstedt, T., and Gillberg, M. (1990). Subjective and objective sleepiness in the active individual. *Int. J. Neurosci.* 52, 29–37. doi: 10.3109/00207459008994241

Abásolo, D., Simons, S., Morgado da Silva, R., Tononi, G., and Vyazovskiy, V. V. (2015). Lempel-Ziv complexity of cortical activity during sleep and waking in rats. *J. Neurophysiol.* 113, 2742–2752. doi: 10.1152/jn.00575.2014

Abeysuriya, R. G., Rennie, C. J., Robinson, P. A., and Kim, J. W. (2014). Experimental observation of a theoretically predicted nonlinear sleep spindle harmonic in human EEG. *Clin. Neurophysiol.* 125, 2016–2023. doi: 10.1016/j.clinph.2014.01.025

Acharya, U. R., Faust, O., Kannathal, N., Chua, T., and Laxminarayan, S. (2005). Non-linear analysis of EEG signals at various sleep stages. *Comput. Methods Prog. Biomed.* 80, 37–45. doi: 10.1016/j.cmpb.2005.06.011

Achermann, P., and Borbély, A. A. (2011). "Sleep homeostasis and models of sleep regulation," in *Principles and Practice of Sleep Medicine.* (Philadelphia, PA: Elsevier/Saunders, Elsevier Inc.), Chapter 37, 431–444. doi: 10.1016/C2009-0-59875-3

Achermann, P., Dijk, D. J., Brunner, D. P., and Borbély, A. A. (1993). A model of human sleep homeostasis based on EEG slow-wave activity: quantitative comparison of data and simulations. *Brain Res. Bull.* 31, 97–113. doi: 10.1016/0361-9230(93)90016-5

Aeschbach, D., Matthews, J. R., Postolache, T. T., Jackson, M. A., Giesen, H. A., and Wehr, T. A. (1997). Dynamics of the human EEG during prolonged wakefulness: evidence for frequency-specific circadian and homeostatic influences. *Neurosci. Lett.* 239, 121–124. doi: 10.1016/S0304-3940(97)00904-X

Aeschbach, D., Matthews, J. R., Postolache, T. T., Jackson, M. A., Giesen, H. A., and Wehr, T. A. (1999). Two circadian rhythms in the human electroencephalogram during wakefulness. *Am. J. Physiol.* 277, 1771–1779. doi: 10.1152/ajpregu.1999.277.6.R1771

Aftanas, L. I., and Golocheikine, S. A. (2002). Non-linear dynamic complexity of the human EEG during meditation. *Neurosci. Lett.* 330, 143–146. doi: 10.1016/S0304-3940(02)00745-0

Al-Subari, K., Al-Baddai, S., Tome, A. M., Goldhacker, M., Faltermeier, R., and Lang, E. W. (2015a). EMDLAB: a toolbox for analysis of single-trial EEG dynamics using empirical mode decomposition. *J. Neurosci. Methods* 253, 193–205. doi: 10.1016/j.jneumeth.2015.06.020

Al-Subari, K., Al-Baddai, S., Tome, A. M., Volberg, G., Hammwohner, R., and Lang, E. W. (2015b). Ensemble empirical mode decomposition analysis of EEG data collected during a contour integration task. *PLoS ONE* 10:e0119489. doi: 10.1371/journal.pone.0119489

Ansfield, M. E., Wegner, D. M., and Bowser, R. (1996). Ironic effects of sleep urgency. *Behav. Res. Ther.* 34, 523–531. doi: 10.1016/0005-7967(96)00031-9

Bai, Y., Wan, X., Zeng, K., Ni, Y., Qiu, L., and Li, X. (2016). Reduction hybrid artifacts of EMG-EOG in electroencephalography evoked by prefrontal transcranial magnetic stimulation. *J. Neural Eng.* 13:066016. doi: 10.1088/1741-2560/13/6/066016

Bedard, C., Kroger, H., and Destexhe, A. (2006). Does the 1/f frequency scaling of brain signals reflect self-organized critical states? *Phys. Rev. Lett.* 97:118102. doi: 10.1103/PhysRevLett.97.118102

Berry, R. B. (2012). *Fundamentals of Sleep Medicine*. Philadelphia, PA: Elsevier/Saunders, 1320–1321. doi: 10.1016/B978-1-4377-0326-9.00037-3

Bizopoulos, P. A., Al-Ani, T., Tsalikakis, D. G., Tzallas, A. T., Koutsouris, D. D., and Fotiadis, D. I. (2013). An automatic electroencephalography blinking artefact detection and removal method based on template matching and ensemble empirical mode decomposition. *Conf. Proc. IEEE Eng. Med. Biol. Soc.* 2013:5853–5856. doi: 10.1109/EMBC.2013.6610883

Borbély, A. A., and Achermann, P. (1999). Sleep homeostasis and models of sleep regulation. *J. Biol. Rhythms* 14, 557–568.

Brunner, D. P., Dijk, D. J., Tobler, I., and Borbély, A. A. (1990). Effect of partial sleep deprivation on sleep stages and EEG power spectra: evidence for non-REM and REM sleep homeostasis. *Electroencephalogr. Clin. Neurophysiol.* 75, 492–499. doi: 10.1016/0013-4694(90)90136-8

Campbell, I. G. (2009). EEG recording and analysis for sleep research. *Curr. Protoc. Neurosci.* 49, 10.2.1-10.2.19. doi: 10.1002/0471142301.ns1002s49

Casali, A. G., Gosseries, O., Rosanova, M., Boly, M., Sarasso, S., Casali, K. R., et al. Tononi, G. (2013). A theoretically based index of consciousness independent of sensory processing and behavior. *Sci. Transl. Med.* 5:198ra105. doi: 10.1126/scitranslmed.3006294

Chen, D., Li, D., Xiong, M., Bao, H., and Li, X. (2010). GPGPU-aided ensemble empirical-mode decomposition for EEG analysis during anesthesia. *IEEE Trans. Inf. Technol. Biomed.* 14, 1417–1427. doi: 10.1109/TITB.2010.2072963

Chen, X., Liu, A., McKeown, M. J., Poizner, H., and Wang, Z. J. (2014). An EEMD-IVA framework for concurrent multidimensional EEG and unidimensional kinematic data analysis. *IEEE Trans. Biomed. Eng.* 61, 2187–2198. doi: 10.1109/TBME.2014.2319294

Chiu, H. C., Ma, H. P., Lin, C., Lo, M. T., Lin, L. Y., Wu, C. K., et al. (2017). Serial heart rhythm complexity changes in patients with anterior wall ST segment elevation myocardial infarction. *Sci. Rep.* 7:43507. doi: 10.1038/srep43507

Costa, M., Goldberger, A. L., and Peng, C. K. (2002a). Multiscale entropy analysis of complex physiologic time series. *Phys. Rev. Lett.* 89:068102. doi: 10.1103/PhysRevLett.89.068102

Costa, M., Goldberger, A. L., and Peng, C. K. (2002b). Multiscale entropy to distinguish physiologic and synthetic RR time series. *Comput. Cardiol.* 29, 137–140. doi: 10.1109/CIC.2002.1166726

Costa, M., Goldberger, A. L., and Peng, C. K. (2005). Multiscale entropy analysis of biological signals. *Phys Rev E Stat Nonlin Soft Matter Phys.* 71(Pt 2):021906. doi: 10.1103/PhysRevE.71.021906

Espie, C. A., Brooks, D. N., and Lindsay, W. R. (1989). An evaluation of tailored psychological treatment of insomnia. *J. Behav. Ther. Exp. Psychiatry* 20, 143–153. doi: 10.1016/0005-7916(89)90047-5

Fattinger, S., Kurth, S., Ringli, M., Jenni, O. G., and Huber, R. (2017). Theta waves in children's waking electroencephalogram resemble local aspects of sleep during wakefulness. *Sci. Rep.* 7:11187. doi: 10.1038/s41598-017-11577-3

Feldman, M., and Braun, S. (1995). Identification of non-linear system parameters via the instantaneous frequency: application of the hilbert transform and Wigner-Ville techniques. *Proc. SPIE* 2460:637.

Finelli, L. A., Baumann, H., Borbély, A. A., and Achermann, P. (2000). Dual electroencephalogram markers of human sleep homeostasis: correlation between theta activity in waking and slow-wave activity in sleep. *Neuroscience* 101:523–529. doi: 10.1016/S0306-4522(00)00409-7

Goldberger, A. L., Peng, C. K., and Lipsitz, L. A. (2002). What is physiologic complexity and how does it change with aging and disease? *Neurobiol. Aging* 23, 23–26. doi: 10.1016/S0197-4580(01)00266-4

Gotz, T., Stadler, L., Fraunhofer, G., Tome, A. M., Hausner, H., and Lang, E. W. (2017). A combined cICA-EEMD analysis of EEG recordings from depressed or schizophrenic patients during olfactory stimulation. *J. Neural Eng.* 14:016011. doi: 10.1088/1741-2552/14/1/016011

Harvey, A. G. (2000). Pre-sleep cognitive activity: a comparison of sleep-onset insomniacs and good sleepers. *Br J Clin Psychol.* 39 (Pt 3), 275–286. doi: 10.1348/014466500163284

Hassan, A. R., and Bhuiyan, M. I. H. (2017). Automated identification of sleep states from EEG signals by means of ensemble empirical mode decomposition and random under sampling boosting. *Comput. Methods Prog. Biomed.* 140, 201–210. doi: 10.1016/j.cmpb.2016.12.015

He, W. X., Yan, X. G., Chen, X. P., and Liu, H. (2005). Nonlinear feature extraction of sleeping EEG signals. *Conf. Proc. IEEE Eng. Med. Biol. Soc.* 5, 4614–4617. doi: 10.1109/IEMBS.2005.1615498

Hou, F. Z., Li, F. W., Wang, J., and Yan, F. R. (2016). Visibility graph analysis of very short-term heart rate variability during sleep. *Phys. A Stat. Mech. Appl.* 458, 140–145. doi: 10.1016/j.physa.2016.03.086

Huang, N. E. (2000). New method for nonlinear and nonstationary time series analysis: empirical mode decomposition and Hilbert spectral analysis. *Proc. SPIE Int. Soc. Opt. Eng.* 4056, 197–209. doi: 10.1117/12.381681

Iacobucci, D., Posavac, S. S., Kardes, F. R., Schneider, M. J., and Popovich, D. L. (2015a). The median split: Robust, refined, and revived ?. *J. Consum. Psychol.* 25, 690–704. doi: 10.1016/j.jcps.2015.06.014

Iacobucci, D., Posavac, S. S., Kardes, F. R., Schneider, M. J., and Popovich, D. L. (2015b). Toward a more nuanced understanding of the statistical properties of a median split. *J. Consum. Psychol.* 25, 652–665. doi: 10.1016/j.jcps.2014.12.002

Janjarasjitt, S., Scher, M. S., and Loparo, K. A. (2008). Nonlinear dynamical analysis of the neonatal EEG time series: the relationship between sleep state and complexity. *Clin. Neurophysiol.* 119, 1812–1823. doi: 10.1016/j.clinph.2008.03.024

Jehan, S., Mastersisarilov, A., Salifu, I., Zizi, F., Jeanlouis, G., Pandiperumal, S. R. et al. (2015). Sleep disorders in postmenopausal women. *J. Sleep Disord. Ther.* 4:1000212.doi: 10.4172/2167-0277.1000212

Kanoga, S., and Mitsukura, Y. (2015). Eye blink artifact rejection in single-channel electroencephalographic signals by complete ensemble empirical mode decomposition and independent component analysis. *Conf. Proc. IEEE Eng. Med. Biol. Soc.* 2015, 121–124. doi: 10.1109/EMBC.2015.7318315

Kuo, C. C., Lin, W. S., Dressel, C. A., and Chiu, A. W. (2011). Classification of intended motor movement using surface EEG ensemble empirical mode decomposition. *Conf. Proc. IEEE Eng. Med. Biol. Soc.* 2011, 6281–6284. doi: 10.1109/IEMBS.2011.6091550

Lichstein, K. L., and Rosenthal, T. L. (1980). Insomniacs' perceptions of cognitive versus somatic determinants of sleep disturbance. *J. Abnorm. Psychol.* 89, 105–107. doi: 10.1037/0021-843X.89.1.105

Lin, Y. H., Huang, H. C., Chang, Y. C., Lin, C., Lo, M. T., Liu, L. Y., et al. (2014). Multi-scale symbolic entropy analysis provides prognostic prediction in patients receiving extracorporeal life support. *Crit Care* 18:548. doi: 10.1186/s13054-014-0548-3

Ma, Y., Shi, W., Peng, C. K., and Yang, A. C. (2018). Nonlinear dynamical analysis of sleep electroencephalography using fractal and entropy approaches. *Sleep Med. Rev.* 37, 85–93. doi: 10.1016/j.smrv.2017.01.003

Ma, Y., Tseng, P. H., Ahn, A., Wu, M. S., Ho, Y. L., Chen, M. F., et al. (2017). Cardiac autonomic alteration and metabolic syndrome: an ambulatory ECG-based study in a general population. *Sci. Rep.* 7:44363. doi: 10.1038/srep44363

Mallampalli, M. P., and Carter, C. L. (2014). Exploring sex and gender differences in sleep health: a society for women's health research report. *J. Womens Health* 23:553–562. doi: 10.1089/jwh.2014.4816

Mejaddam, A. Y., Birkhan, O. A., Sideris, A. C., Van der Wilden, G. M., Imam, A. M., Hwabejire, J. O., et al. (2013). Real-time heart rate entropy predicts the need for lifesaving interventions in trauma activation patients. *J. Trauma Acute Care Surg.* 75, 607–612. doi: 10.1097/TA.0b013e31829bb991

Moshirvaziri, H., Ramezan-Arab, N., and Asgari, S. (2016). Prediction of the outcome in cardiac arrest patients undergoing hypothermia using EEG wavelet entropy. *Conf. Proc. IEEE Eng. Med. Biol. Soc.* 2016, 3777–3780. doi: 10.1109/EMBC.2016.7591550

Natarajan, K., Acharya, R. U., Alias, F., Tiboleng, T., and Puthusserypady, S. K. (2004). Nonlinear analysis of EEG signals at different mental states. *BioMed. Eng. Online* 3, 7–7. doi: 10.1186/1475-925X-3-7

Nelson, J., and Harvey, A. G. (2003). An exploration of pre-sleep cognitive activity in insomnia: imagery and verbal thought. *Br J Clin Psychol.* 42(Pt 3), 271–288. doi: 10.1348/01446650360703384

Nordström, P., Samuelsson, M., and Åsberg, M. (2010). Survival analysis of suicide risk after attempted suicide. *Acta Psychiatr. Scand.* 91, 336–340. doi: 10.1111/j.1600-0447.1995.tb09791.x

Olivier, J., Mathieu, P., Julie, C., Jacques, M., and Antonio, Z. (2010). Analysis of slow-wave activity and slow-wave oscillations prior to somnambulism. *Sleep* 33, 1511–1516. doi: 10.1093/sleep/33.11.1511

Quan, S. F., Howard, B. V., Iber, C., Kiley, J. P., Nieto, F. J., O'Connor, G. T., et al. (1997). The Sleep Heart Health Study: design, rationale and methods. *Sleep* 20, 1077–1085.

Redline, S., Sanders, M. H., Lind, B. K., Quan, S. F., Iber, C., Gottlieb, D. J., et al. (1998). Methods for obtaining and analyzing unattended polysomnography data for a multicenter study.pdf. *Sleep* 21, 759–767.

Richman, J. S., and Moorman, J. R. (2000). Physiological time-series analysis using approximate entropy and sample entropy. *Am. J. Physiol. Heart Circ. Physiol.* 278, H2039–H2049. doi: 10.1152/ajpheart.2000.278.6.H2039

Shen, Y., Olbrich, E., Achermann, P., and Meier, P. F. (2003). Dimensional complexity and spectral properties of the human sleep EEG. *Electroencephal. Clin. Neurophysiol.* 114, 199–209. doi: 10.1016/S1388-2457(02)00338-3

Strijkstra, A. M., Beersma, D. G., Drayer, B., Halbesma, N., and Daan, S. (2003). Subjective sleepiness correlates negatively with global alpha (8-12 Hz) and positively with central frontal theta (4-8 Hz) frequencies in the human resting awake electroencephalogram. *Neurosci. Lett.* 340, 17–20. doi: 10.1016/S0304-3940(03)00033-8

Thomas, R. J., Mietus, J. E., Peng, C.-K., Gilmartin, G., Daly, R. W., Goldberger, A. L., et al. (2007). Differentiating obstructive from central and complex sleep apnea using an automated electrocardiogram-based method. *Sleep* 30, 1756–1769. doi: 10.1093/sleep/30.12.1756

Vandendriessche, B., Peperstraete, H., Rogge, E., Cauwels, P., Hoste, E., Stiedl, O., et al. (2014). A multiscale entropy-based tool for scoring severity of systemic inflammation. *Crit. Care Med.* 42, e560–e569. doi: 10.1097/CCM.0000000000000299

Vieira, M. F., Lemos, T. S., da Costa, P. H. L., and Andrade, A. O. (2017). "On the use of multifractal detrended fluctuation analysis and multiscale entropy to analyze postural sway data," in *Paper Presented at the XVII Congresso Brasileiro de Biomecânica*. Porto Alegre, RS.

Wang, T., Zhang, M., Yu, Q., and Zhang, H. (2012). Comparing the applications of EMD and EEMD on time–frequency analysis of seismic signal. *J. Appl. Geophys.* 83, 29–34. doi: 10.1016/j.jappgeo.2012.05.002

Wu, Z., and Huang, N. E. (2005). Ensemble empirical mode decomposition: a noise-assisted data analysis method. *Adv. Adapt. Data Anal.* 1, 1–41. doi: 10.1142/S1793536909000047

Wuyts, J., De Valck, E., Vandekerckhove, M., Pattyn, N., Bulckaert, A., Berckmans, D., et al. (2012). The influence of pre-sleep cognitive arousal on sleep onset processes. *Int. J. Psychophysiol.* 83, 8–15. doi: 10.1016/j.ijpsycho.2011.09.016

Yang, A. C., Wang, S. J., Lai, K. L., Tsai, C. F., Yang, C. H., Hwang, J. P. et al. (2013). Cognitive and neuropsychiatric correlates of EEG dynamic complexity in patients with Alzheimer's disease. *Prog. Neuropsychopharmacol. Biol. Psychiatry.* 47, 52–61. doi: 10.1016/j.pnpbp.2013.07.022

Yeh, J. R., Peng, C. K., Lo, M. T., Yeh, C. H., Chen, S. C., Wang, C. Y., et al. (2013). Investigating the interaction between heart rate variability and sleep EEG using nonlinear algorithms. *J. Neurosci. Methods* 219, 233–239. doi: 10.1016/j.jneumeth.2013.08.008

Zeng, K., Chen, D., Ouyang, G., Wang, L., Liu, X., and Li, X. (2016). An EEMD-ICA Approach to enhancing artifact rejection for noisy multivariate neural data. *IEEE Trans. Neural Syst. Rehabil. Eng.* 24, 630–638. doi: 10.1109/TNSRE.2015.2496334

Conflict of Interest Statement: The authors declare that the research was conducted in the absence of any commercial or financial relationships that could be construed as a potential conflict of interest.

The reviewer IK and handling Editor declared their shared affiliation.

frontiers in Neuroscience

ORIGINAL RESEARCH
published: 20 November 2018
doi: 10.3389/fnins.2018.00826

Interactions of *BDNF* Val66Met Polymorphism and Menstrual Pain on Brain Complexity

Intan Low[1,2], Po-Chih Kuo[3], Cheng-Lin Tsai[4], Yu-Hsiang Liu[1], Ming-Wei Lin[5], Hsiang-Tai Chao[6], Yong-Sheng Chen[7,8], Jen-Chuen Hsieh[1,2,9] and Li-Fen Chen[1,2,4,9]**

[1] Institute of Brain Science, National Yang-Ming University, Taipei, Taiwan, [2] Integrated Brain Research Unit, Department of Medical Research, Taipei Veterans General Hospital, Taipei, Taiwan, [3] Institute of Statistical Science, Academia Sinica, Taipei, Taiwan, [4] Institute of Biomedical Informatics, National Yang-Ming University, Taipei, Taiwan, [5] Institute of Public Health, National Yang-Ming University, Taipei, Taiwan, [6] Department of Obstetrics and Gynecology, Taipei Veterans General Hospital, Taipei, Taiwan, [7] Department of Computer Science, National Chiao Tung University, Hsinchu, Taiwan, [8] Center for Emergent Functional Matter Science, National Chiao Tung University, Hsinchu, Taiwan, [9] Brain Research Center, National Yang-Ming University, Taipei, Taiwan

OPEN ACCESS

Edited by:
Danny J. J. Wang, University of Southern California, United States

Reviewed by:
Ze Wang, Temple University, United States
Jie Xiang, Taiyuan University of Technology, China

***Correspondence:**
Jen-Chuen Hsieh
jchsieh@ym.edu.tw
Li-Fen Chen
lfchen@ym.edu.tw

Specialty section:
This article was submitted to Brain Imaging Methods, a section of the journal Frontiers in Neuroscience

Received: *09 June 2018*
Accepted: *23 October 2018*
Published: *20 November 2018*

Citation:
Low I, Kuo P-C, Tsai C-L, Liu Y-H, Lin M-W, Chao H-T, Chen Y-S, Hsieh J-C and Chen L-F (2018) Interactions of BDNF Val66Met Polymorphism and Menstrual Pain on Brain Complexity. Front. Neurosci. 12:826. doi: 10.3389/fnins.2018.00826

The irregularity and uncertainty of neurophysiologic signals across different time scales can be regarded as neural complexity, which is related to the adaptability of the nervous system and the information processing between neurons. We recently reported general loss of brain complexity, as measured by multiscale sample entropy (MSE), at pain-related regions in females with primary dysmenorrhea (PDM). However, it is unclear whether this loss of brain complexity is associated with inter-subject genetic variations. Brain-derived neurotrophic factor (BDNF) is a widely expressed neurotrophin in the brain and is crucial to neural plasticity. The *BDNF* Val66Met single-nucleotide polymorphism (SNP) is associated with mood, stress, and pain conditions. Therefore, we aimed to examine the interactions of *BDNF* Val66Met polymorphism and long-term menstrual pain experience on brain complexity. We genotyped *BDNF* Val66Met SNP in 80 PDM females (20 Val/Val, 31 Val/Met, 29 Met/Met) and 76 healthy female controls (25 Val/Val, 36 Val/Met, 15 Met/Met). MSE analysis was applied to neural source activity estimated from resting-state magnetoencephalography (MEG) signals during pain-free state. We found that brain complexity alterations were associated with the interactions of *BDNF* Val66Met polymorphism and menstrual pain experience. In healthy female controls, Met carriers (Val/Met and Met/Met) demonstrated lower brain complexity than Val/Val homozygotes in extensive brain regions, suggesting a possible protective role of Val/Val homozygosity in brain complexity. However, after experiencing long-term menstrual pain, the complexity differences between different genotypes in healthy controls were greatly diminished in PDM females, especially in the limbic system, including the hippocampus and amygdala. Our results suggest that pain experience preponderantly affects the effect of *BDNF* Val66Met polymorphism on brain complexity. The results of the present study also highlight the potential utilization of resting-state brain complexity for the development of new therapeutic strategies in patients with chronic pain.

Keywords: *BDNF* Val66Met polymorphism, primary dysmenorrhea, brain complexity, multiscale entropy, magnetoencephalography, chronic pain

INTRODUCTION

Chronic pain can be considered as "pain that persists for a given length of time," where the length of time is determined by common medical experience (Merskey and Bogduk, 2002), and have pronounced female predominance (Mogil, 2012). Primary dysmenorrhea (PDM) indicates "pain with menstruation not associated with a well-defined pathology"[1] and is classified as chronic pelvic pain syndrome (IASP, 2011). It has a prevalence of 45–95% among reproductive age females (Berkley, 2013; Iacovides et al., 2015). Most importantly, dysmenorrhea early in life often co-occurs with many chronic pain syndromes later in life, linking its susceptibility to the development of chronic pain conditions (Berkley, 2013) and marking the assaults of central sensitization on dysfunctional pain modulatory system (Nijs et al., 2015).

Long-term PDM serves as a genuine model to study clinical pain with its natural cyclic painful (menstruation) and pain-free (periovulatory) states (Wei et al., 2016a). Structural and functional brain alterations are reported in PDM females (PDMs), including hypotrophic and hypertrophic changes in gray matter volume (Tu et al., 2010, 2013; Liu et al., 2016), white matter microstructural alterations (Liu J. et al., 2017), maladaptive descending pain modulatory system (Wei et al., 2016a), shift of functional connectivity between resting-state networks (Wu et al., 2016; Liu P. et al., 2017), increased theta activity (Lee et al., 2017), and loss of brain complexity (Low et al., 2017) in brain regions related to sensory, affective, and cognitive dimensions of pain. Notably, genetic polymorphisms have been implicated to contribute to inter-subject variations in susceptibility to menstrual pain (Lee et al., 2014; Wei et al., 2016b, 2017), inviting more studies of neuroimaging genetics in PDM.

Brain-derived neurotrophic factor (BDNF) is the most expressed neurotrophin in the brain, especially in the cerebral cortex and hippocampus (Binder and Scharfman, 2004; Tapia-Arancibia et al., 2004). BDNF has pleiotropic roles in the central nervous system, including neurogenesis, neuronal growth, maturation, survival, synaptic plasticity, and microarchitectural integrity (Park and Poo, 2013; Bathina and Das, 2015). It is a driving force behind neural plasticity and protects neuronal cells upon adverse circumstances (Bathina and Das, 2015), such as stress or pain. BDNF is considered as a pain modulator given its participation in activity-dependent synaptic plasticity within the pain modulatory circuitry (Merighi et al., 2008; Haas et al., 2010; Caumo et al., 2016; Generaal et al., 2016).

Human *BDNF* gene at chromosome 11p14.1 displays a variety of polymorphisms. The replacement of Valine (Val) by Methionine (Met) at codon 66, namely *BDNF* Val66Met single-nucleotide polymorphism (rs6265), is considered to disrupt normal trafficking of BDNF and consequently reduces activity-dependent secretion of BDNF and BDNF activity in Met carriers (Egan et al., 2003). Animal studies reported that spike-timing-dependent plasticity in the pyramidal neurons of the infralimbic medial prefrontal cortex was absent in *BDNF* Met/Met mice, suggesting that *BDNF* Val66Met polymorphism strongly affect synaptic transmission (Pattwell et al., 2012). The *BDNF* Met allele has been reported to associate with deleterious effects on brain, such as smaller regional brain volumes (Pezawas et al., 2004), higher vulnerability in white matter structural connectivity (Park et al., 2017), and potentially greater susceptibility to various neurological and mood disorders (Notaras et al., 2015). Studies of the effects of *BDNF* Val66Met polymorphism on pain also predominantly report impaired pain modulation or augmented pain responses in Met carriers, including migraine (Cai et al., 2017), chronic musculoskeletal pain (Generaal et al., 2016), chronic abdominal pain (Reddy et al., 2014), electrical stimulation for trigeminal pain (Di Lorenzo et al., 2012), intracutaneous pain in chronic low back pain patients (Vossen et al., 2010), and esophageal visceral pain (Vasant et al., 2011). However, our understanding of the role of *BDNF* genetic variants in recurrent menstrual pain is still limited.

Previous *BDNF* Val66Met polymorphism studies in PDM observed a significant main effect of *BDNF* genotype on anxiety level in PDM group, in which Met/Met PDMs scored higher in anxiety compared with Val-carrier PDMs during menstrual phase (Lee et al., 2014). The authors suggested that *BDNF* Val66Met polymorphism is modestly associated with the supraspinal modulation of menstrual pain-laden emotional processing. On the other hand, resting-state functional connectivity study in PDM (Wei et al., 2016b) revealed that Val/Val PDMs engaged functional connectivity between pain modulatory region and sensory regions, suggesting adaptive pain modulation, while Met/Met PDMs rigidly engaged functional connectivity between pain modulatory region and limbic structures, implying maladaptive pain modulation underlying pain chronicity. Together, *BDNF* Val66Met polymorphism might affect spontaneous low-frequency BOLD signal oscillations differently in individuals with or without long-term menstrual pain experience.

The irregularity and unpredictability (uncertainty) of a system's output signal across varying temporal scales can be regarded as the system's complexity (Costa et al., 2002). Neural complexity, the complexity of the nervous system, could represent the capacity or dynamical range of information processing in the brain, the richness of information available in the nervous system, or adaptability or resilience of the nervous system (Tononi et al., 1994; Nakagawa et al., 2013; McDonough and Nashiro, 2014; Wang et al., 2018). Neural complexity might reflect the brain's tendency to wander (itinerancy) among all alternative states of neuronal transients, and as a characterization of the "flexibility of rapid transitions" (Friston, 2000, 2001; Friston et al., 2012; Wang et al., 2018). Loss of complexity is often reported in neuropsychiatric diseased and aged groups; increased complexity has been seen in recovery conditions and healthy groups (Yang and Tsai, 2013; Hager et al., 2017).

Complexity is non-linear and complex to define but is often computationally quantified with entropy measurements. Sample entropy, proposed by Richman and Moorman (Richman and Moorman, 2000), is a well-defined index of complexity and has been applied to brain activity (Yao et al., 2013; Wang et al., 2014,

[1]This statement has been reproduced with permission of the International Association for the Study of Pain® (IASP). The statement may not be reproduced for any other purpose without permission.

2017; Lebedev et al., 2016; Li et al., 2016; Zhou et al., 2016; Jia et al., 2017; Nelson et al., 2017; Chang et al., 2018; Song et al., 2018). It is noteworthy that multiscale entropy (MSE) analysis (Costa et al., 2002, 2005; Yang and Tsai, 2013; Courtiol et al., 2016) calculates a series of sample entropy over multiple time scales, which captures the temporal complexity characteristcs of time-series neural signals from microscopic to macroscopic aspects. Recently, MSE analysis has also been applied to brain signals (Heisz and McIntosh, 2013; Yang et al., 2013; Courtiol et al., 2016), pain (Sitges et al., 2010; Valencia et al., 2016; Liu Q. et al., 2017), and PDM studies (Kuo et al., 2017; Low et al., 2017). By applying MSE analysis on resting-state magnetoencephalography (MEG) signals acquired from PDMs during pain-free state, we observed a general loss of regional complexity in PDMs at brain regions related to chronic pain, including the limbic circuitry, default mode network, sensorimotor network, and salience network (Low et al., 2017). Our findings implicated the assaults of long-term menstrual pain on brain complexity and adaptability. However, it is unclear whether this loss of brain complexity in PDMs is associated with genetic variations.

Long-term menstrual pain is a chronic stressor to PDMs that might affect the secretion levels of BDNF and subsequent BDNF functions in an activity-dependent manner. Given the loss of brain complexity in PDMs and the effects of *BDNF* Val66Met polymorphism on mood and resting-state functional connectivity in PDMs, we aimed to examine the interactions of *BDNF* Val66Met polymorphism and long-term menstrual pain experience on brain complexity. We hypothesized that there might be genotype-specific complexity differences in healthy controls, and such complexity differences might be affected by long-term menstrual pain especially in pain- and emotion-related brain circuits.

METHODS

Participants

The participants were a subset of the participants from our multimodal imaging genetics (magnetic resonance imaging and magnetoencephalography) and behavioral studies of PDM at Taipei Veterans General Hospital in Taiwan (Lee et al., 2014; Wei et al., 2016a; Wu et al., 2016; Low et al., 2017) who were eligible for neuroimaging studies. Written informed consent form and psychological inventories were approved by the ethics committee of Institutional Review Board of Taipei Veterans General Hospital, Taiwan. Before the study, all participants who were assessed for eligibility signed the written informed consent form. Studies were conducted in accordance with the Declaration of Helsinki.

The inclusion criteria for PDMs were (1) 20 to 30 years old Taiwanese (Asian) females; (2) 27 to 32 days of regular menstrual cycle; (3) right-handedness assessed by the Edinburgh Handedness Inventory; (4) menstrual pain history longer than half year; (5) averaged menstrual pain rating within the last 6 months of experiment was higher than four out of ten using verbal numerical rating scale (0 = no pain, 10 = worst imaginable pain); (6) no pelvic pathologies examined using pelvic ultrasonography and diagnosed as PDM by gynecologist. We excluded volunteers with (1) organic pelvic diseases; (2) pituitary gland pathologies; (3) history of neurological or psychiatric disorders; (4) history of brain surgery or trauma; (5) history or immediate plans for pregnancy or childbirth; (6) history of using medications or supplements of hormonal therapy including oral contraceptives, central-acting medication, or Chinese herbal medicine within the last 6 months of experiment; (7) claustrophobia; (8) contraindications to magnetic resonance imaging. Also, no painkillers were used 24 h before the experiment. Healthy female controls (CONs) had the same inclusion and exclusion criteria except they had no lower abdominal pain during the menstrual period.

Genotyping

Whole blood was collected during the inception stage and stored in 4 mL EDTA tubes at 4°C refrigerator. DNA was extracted using the Puregene kit following the manufacturer's guidelines (Gentra Systems, Inc., Minneapolis, MN, USA). Genotyping was conducted using commercial TaqMan single-nucleotide polymorphism assays (Applied Biosystems, Inc., Foster City, CA, USA). The polymerase chain reaction amplification protocol was as follows: 10 μL; 50°C (2 min), 95°C (10 min), 40 cycles of 92°C (15 s), and 60°C (1 min). Fluorescence measurements were done using the ABI HT7900 (Applied Biosystems, Inc.). Allele calling was performed by the SDS 2.2 software package (Applied Biosystems, Inc.). Two independent technicians blinded to the participants' personal information assigned the genotypes.

Demographic Data, Pain Experiences, and Psychological Characteristics

Demographic data included age, body mass index (BMI), and handedness. Menstrual features included age at menarche, years of menstruating, and averaged menstrual cycle length. All participants completed the Chinese version of Basic Personality Inventory (BPI; Wu et al., 1999) to assess their personality traits. There are several scale clusters in the BPI, including the personal emotional adjustment scale cluster (depression, anxiety, and hypochondriasis scales), which is of particular interest of this study. The IQOLA SF-36 Taiwan Standard Version 1.0 (SF-36; Tseng et al., 2003) was used to assess long-term physical and mental quality of life. Since emotional perception and pain chronification can be exacerbated by anxiety and depression and both have been linked to PDM, anxious and depressive moods were investigated using Chinese versions of Spielberger State-trait Anxiety Inventory (STAI; Ma et al., 2013), Beck Depression Inventory (BDI-IA; Beck et al., 1979), and Beck Anxiety Inventory (BAI; Lin, 2000). We also studied pain catastrophizing cognitive style, which is the negative appraisal style of pain, using the Chinese version of Pain Catastrophizing Scale (PCS; Yap et al., 2008).

Menstrual pain experiences were evaluated only in PDMs using the Chinese version of McGill Pain Questionnaire (MPQ; Melzack, 1975, 1983) and verbal numerical rating scale (VNRS). MPQ classifies four categories of qualities of pain, including sensory, affective, evaluative, and miscellaneous. MPQ scores are calculated as the sum of the rank values of the words chosen, summing up to a pain rating index (PRI) for each category. The

MPQ present pain index (PPI), based on a 0-to-5 intensity scale (0 = no pain, 1 = mild, 2 = discomforting, 3 = distressing, 4 = horrible, 5 = excruciating), was used as the indicator of menstrual pain intensity. VNRS is a verbal report of menstrual pain intensity rated from 0 to 10 (0 = not at all, 10 = the worst imaginable pain). PDMs recalled different aspects of their overall menstrual pain experiences over the last 6 months, yielding recalled MPQ scores and recalled pain scores.

Data Acquisition

Resting-State MEG Signals Acquisition

Three-minute eye-closed resting-state MEG signals were recorded using a whole-head 306-channel neuromagnetometer (Vectorview, Elekta Neuromag, Helsinki, Finland) comprising 102 triple sensors (two orthogonal planar gradiometers and one magnetometer at each triple-set) at Taipei General Veterans Hospital, Taiwan. Electrooculography (EOG) was recorded using two vertical and two horizontal electrodes to be used for rejection of epochs coinciding with blinks and excessive eye movements with an amplitude cut-off of 600 μV. Locations of three anatomical landmarks (nasion and two bilateral pre-auricular points) were identified with a three-dimensional digitizer (Isotrak 3S10002, Polhemus Navigation Sciences, Colchester, Vermont USA) to align MEG coordinate system with MRI coordinate system. Four head position indicator (HPI) coils were used to trace the position of subject's head in the MEG system. The online sampling rate was 1,000 Hz, and online bandpass filter was between 0.03 and 330 Hz with a 60 Hz notch filter. Signals exceeding 6,000 fT/cm were rejected. MEG signals recorded from 204 planar gradiometers were further analyzed; MEG signals recorded from 102 magnetometers were excluded from further analyses due to their susceptibility to distant noises. Participants sat comfortably in a magnetically shielded room (Euroshield, Eura, Finland) with heads covered by the helmet and were instructed to relax, eliminate eye movements, and focus only on their breathing (Low et al., 2017).

Structural MRI Images Acquisition

T1-weighted brain images were acquired using a 3 Tesla magnetic resonance imaging (MRI) scanner (Magnetom Trio Tim, Siemens, Erlangen, Germany) at National Yang-Ming University, Taiwan with 12-channel head coil and standard three-dimensional magnetization-prepared rapid gradient-echo (3D MP-RAGE) sequence. The parameters were as follows (Low et al., 2017): TR = 2530 ms, TE = 3.03 ms, TI = 1,100 ms, flip angle = 7°, field-of-view (FOV) = 224 × 256 mm^2, number of slices = 192, matrix size = 224 × 256, thickness = 1 mm.

Brain Region Parcellation

A total of 90 cortical regions (45 regions in each hemisphere) were defined using the automated anatomical labeling (AAL) template (Tzourio-Mazoyer et al., 2002) with a spatial resolution of 1 × 1 × 1 mm provided in MRIcro freeware (Rorden and Brett, 2000). We first normalized the Montreal Neurological Institute (MNI) template to individual's MRI images using IBASPM (Individual Brain Atlases using Statistical Parametric Mapping; Alemán-Gómez et al., 2006). The AAL template was subsequently transformed into individual space using the estimated deformation field. Hence, parcellation of 90 brain regions in the individual brain was obtained, and voxel-wise source analyses (section Source Analyses) and MSE calculations (section Multiscale Sample Entropy) were carried out in each brain region. The purpose of this procedure was to avoid interpolation of functional activity and thus preserved the precision of MSE statistical analysis in individual space. Finally, eight resting-state networks based on literature were discussed, including the limbic, default mode, salience, sensorimotor, executive control, attention, visual processing, and auditory processing networks (Low et al., 2017).

Source Analyses

MEG signals from each participant were preprocessed before voxel-wise source reconstruction. The signals were segmented into non-overlapping epochs of 8 s (Low et al., 2017). Artifact rejection threshold was set to 2,000 fT/cm, and EOG rejection threshold was set to 250 μV. Any epoch with amplitude larger than these thresholds was excluded, resulting in around 14 eight-second epochs remained. Signal space projected MEG signals were subsequently band-pass filtered within 0.5–90 Hz (Low et al., 2017) and with a notch filter of 55–65 Hz. Zero-mean adjustment was also applied.

After co-registering the coordinate systems between individual's MRI volume and MEG device, the source activity was estimated with an isotropic resolution of 4 mm. Maximum contrast beamformer (MCB) was used for brain source calculation (Chen Y. S. et al., 2006). To estimate source activity $y_v(t)$ at each location v, a spatial filter $\mathbf{w}_v$ was applied to the MEG recordings $\mathbf{m}(t)$:

$$y_v(t) = \mathbf{w}_v^{\mathrm{T}}\mathbf{m}(t). \tag{1}$$

For each location, $\mathbf{w}_v$ was obtained by minimizing variance in the output signal $y_v(t)$ with the unit-gain constraint $\mathbf{w}_v^{\mathrm{T}}\,\mathbf{l}_v = 1$, where $\mathbf{l}_v$ is the lead field vector. The details of the calculation can be found in our recent report (Kuo et al., 2017). Source activity of all voxels in every brain region was used in the following analysis.

Multiscale Sample Entropy

Multiscale sample entropy (MSE) was proposed to measure the complexity with multiple time scales (Costa et al., 2002) by applying the sample entropy (SE) method (Richman and Moorman, 2000) to different time scales. First, the coarse-grained time series $\mathbf{z}_v{}^{\tau} = [z_v{}^{\tau}(1), z_v{}^{\tau}(2), \ldots, z_v{}^{\tau}(N/\tau)]$ of the original time series $\mathbf{y}_v = [y_v(1), y_v(2), \ldots, y_v(N)]$ with N sample points was obtained for each scale factor τ (τ was set from 1 to 100 in this study; Low et al., 2017):

$$z_v{}^{\tau}(k) = \frac{1}{\tau}\sum_{i=(k-1)\tau+1}^{k\times\tau} y_v(i),\ 1 \le k \le \frac{N}{\tau}. \tag{2}$$

Then the SE method was applied to each $\mathbf{z}_v{}^{\tau}$. In the SE algorithm, a set of vector $\mathbf{g}_i$ with m elements can be defined as follows (m = 2 in this study; Low et al., 2017):

$$\mathbf{g}_i = [z_v{}^{\tau}(i), z_v{}^{\tau}(i+1)], \textit{where } i = 1, \ldots, N-2. \tag{3}$$

For each i, the absolute difference between $\mathbf{g}_i$ and $\mathbf{g}_j$ ($1 \leq j \leq N-2$ and $j \neq i$) was calculated, and c_τ^g, the number of the difference smaller than r, was determined. Here, the value r was set as 0.25×standard deviation of the signal $y_v(t)$ (Low et al., 2017). Then, the extended vectors with $m+1$ elements were defined as follows:

$$\mathbf{h}_i = [\, z_v{}^\tau(i)\,,\, z_v{}^\tau(i+1)\,,\, z_v{}^\tau(i+2)], \quad where\ i = 1, \ldots, N-3, \tag{4}$$

and c_τ^h was determined by the same means. Finally, MSE for time scale τ can be calculated as:

$$MSE_\tau = -\ln \frac{c_\tau^h}{c_\tau^g}. \tag{5}$$

The MSE value of each voxel was calculated and then averaged within each region. **Figure 1** illustrates examples of MEG signals at different representative time scale factors (τ) in one region (the left amygdala) from one representative subject in each group.

Statistical Analyses

There were two between-group factors in this study: group (PDM and CON) and *BDNF* Val66Met genotype (Val/Val, Val/Met, and Met/Met). Statistical analyses of genotypes, demographic data, psychological characteristics, and correlation analyses were performed in IBM SPSS Statistics. Statistical analyses of multiscale sample entropy were performed in Matlab.

BDNF Genotype Distributions and Allele Frequency

The Hardy-Weinberg equilibrium of the *BDNF* Val66Met genotype distributions and allele frequency were tested using *chi*-square tests of goodness-of-fit ($p < 0.05$). The associations between *BDNF* genotype and PDM were tested using *chi*-square tests of independence ($p < 0.05$) under SPSS binary logistic regression test, in which PDM (group) was treated as the dependent (outcome) variable, genotype as the categorical predictor variable, and Val/Val, Val/Met, or Val carriers as the reference groups.

Demographic Data, Pain Experiences, and Psychological Characteristics

Descriptive and normality tests (Shapiro-Wilk test, $p < 0.05$, two-tailed) were first examined by group before any inferential statistical tests (Ghasemi and Zahediasl, 2012). As many of the demographic and psychological scores were not normally distributed, we used non-parametric inferential statistical tests. Group difference of each genotype was tested using Mann-Whitney U tests ($p < 0.01$, two-tailed). Genotype differences in each group were tested using Kruskal-Wallis H tests ($p < 0.01$, two-tailed) for continuous data and *chi*-square tests ($p < 0.01$) for categorical data. As there is no corresponding nonparametric two-way ANOVA test, significant group and genotype main effects and group × genotype interactions were tested using two-way ANOVAs ($p < 0.01$, two-tailed). *Post-hoc* pairwise comparisons were performed using Dunn-Bonferroni adjusted $p < 0.01$ (two-tailed).

Multiscale Sample Entropy

For the averaged MSE value in each brain region, the main effects and interactions of group and genotype were tested using two-way ANOVA (Bonferroni-adjusted $p < 0.05$, two-tailed). Due to possible errors induced by the above-mentioned normalization procedure (section Brain Region Parcellation), we excluded the brain regions that contained <10 voxels. We focused on testing the *post-hoc* planned pairwise comparisons between groups for each genotype and comparisons between genotypes for each group using permutation tests (iterations = 5000, $p < 0.005$, two-tailed). We also tested *post-hoc* planned comparisons using the more conservative Bonferroni-correction (Bonferroni-adjusted $p < 0.05$, two-tailed).

MSE of the brain regions that showed significant group differences in the same genotype group (Val/Val: PDM vs. CON; Val/Met: PDM vs. CON; Met/Met: PDM vs. CON) were termed as "pain-associated regional MSE." MSE of the brain regions that showed significant genotype differences (Val/Val vs. Val/Met, Val/Val vs. Met/Met, Val/Met vs. Met/Met) in the same group were termed as "*BDNF*-associated regional MSE." To examine the effect sizes of pain-associated regional MSE and *BDNF*-associated regional MSE, standardized effect sizes were calculated using Cohen's d (Cohen, 1988) with an online effect size calculator (Wilson and Lipsey, 2001).

Correlations Between Regional MSE and Psychological Characteristics

Correlations between PDMs' menstrual pain experiences/psychological characteristics and pain-associated or *BDNF*-associated regional MSE were examined using Spearman correlation analysis ($p < 0.01$, two-tailed).

RESULTS

BDNF Val66Met Genotype Distributions and Allele Frequency

Genotype distributions of *BDNF* Val66Met (rs6265) in the CON group, PDM group, and all participants were in Hardy-Weinberg equilibrium ($p > 0.05$; **Table S1**). The number of participants in each genotype subgroup were as follows (**Table 1**): Val/Val CONs = 25, Val/Met CONs = 36, Met/Met CONs = 15, Val/Val PDMs = 20, Val/Met PDMs = 31, Met/Met PDMs = 29. PDMs differed sub-significantly from CONs in *BDNF* Val66Met genotype distributions ($p = 0.071$) and allele frequency ($p = 0.066$); there was a trend of excessive Met allele in PDMs than in CONs (**Table 1**).

Table 2 shows the odds ratios of PDM. Treating Val carriers (Val/Val and Val/Met) as the reference group, the odds ratio for Met/Met was statistically significant [(Met/Met PDMs x Val-carrier CONs)/(Val-carrier PDMs x Met/Met CONs)]. Treating Val/Val or Val/Met individually as the reference group, the odds ratios for Met/Met were also statistically significant. In contrast, when treating Met carriers (combining Met/Met and Val/Met as one group) or Val/Met as case (exposed group) with Val/Val as reference group, the odds ratios for Met carriers or Val/Met were not significant. These results implied that the odds of PDM

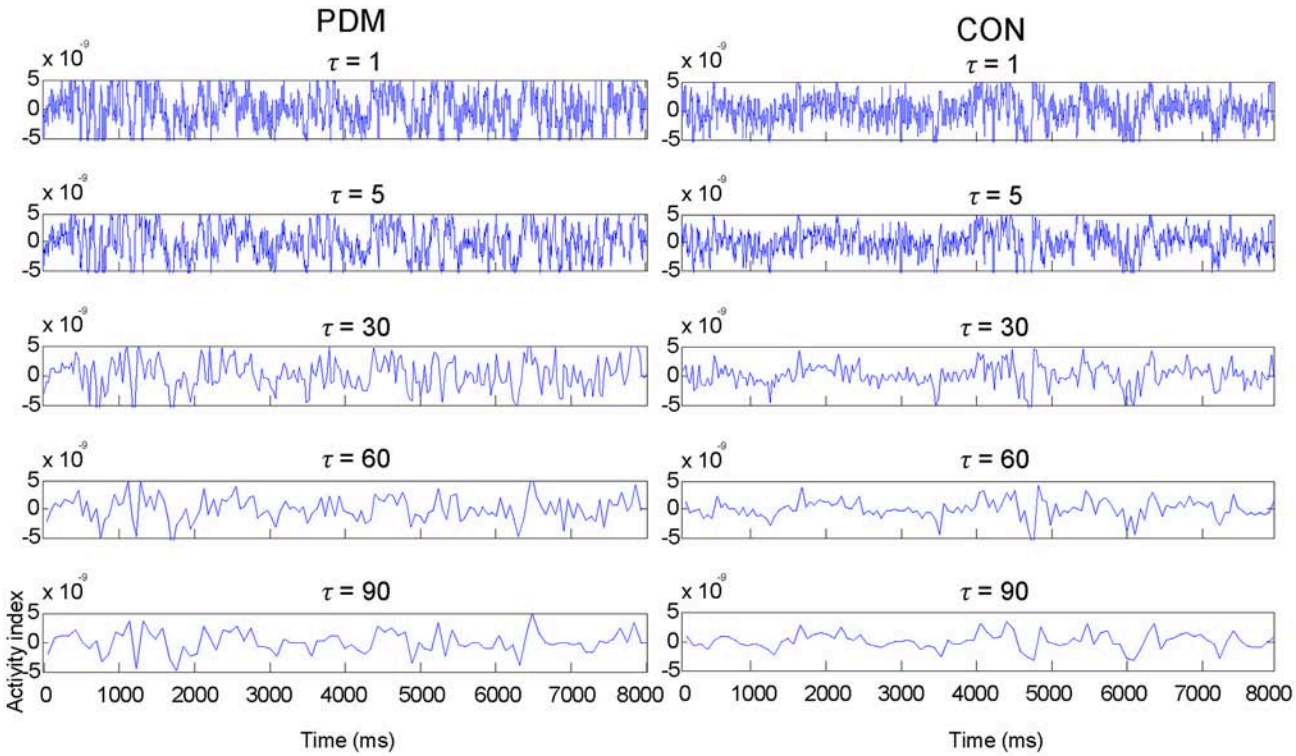

FIGURE 1 | Examples of MEG signals at different representative time scale factors (τ) in one region (the left amygdala) from one representative subject in each group.

TABLE 1 | *BDNF* Val66Met (rs6265) genotype distributions and allele frequency.

	Genotype (*n*, %)			χ^2	*p*	Allele frequency		χ^2	*p*
	Val/Val	Val/Met	Met/Met			Val allele	Met allele		
PDM (*n* = 80)	20 (35.0%)	31 (38.8%)	29 (36.6%)	5.28	0.071	44.40%	55.60%	3.38	0.066
CON (*n* = 76)	25 (32.9%)	36 (47.4%)	15 (19.7%)			56.60%	43.40%		

Significant differences were tested using chi-square tests ($p < 0.05$). PDM, primary dysmenorrhea patients; CON, healthy female controls; BDNF, brain-derived neurotrophic factor; Val/Val, Valine/Valine; Val/Met, Valine/Methionine; Met/Met, Methionine/Methionine.

were at least 2.25 higher in Met/Met homozygous females than in Val-carrier females.

Demographic, Pain Experiences, and Psychological Characteristics

For demographic data and menstrual features, no significant main effects of group and genotype, and no interactions of group and genotype were found (**Table S2**). Thus, *post-hoc* pairwise comparisons were not performed on demographic information. Among the three genotypes in PDMs, there were overall no differences in their menstrual pain experiences except the menstrual pain history ($p = 0.006$; **Table S3**), though *post-hoc* pairwise comparison revealed no significant difference in menstrual pain history between genotypes.

For psychological characteristics, there were consistently significant main effects of group but no main effects of genotype and no group × genotype interactions. PDMs reported significantly lower quality of life and higher personal emotional adjustment problems than those in CONs (**Table S4**). PDMs also scored higher in negative mood (depression and anxiety) and negative cognitive style to pain (pain catastrophizing) compared to CONs (**Table 3**).

Multiscale Sample Entropy

In this study, we focused on the interactions of *BDNF* Val66Met polymorphism and long-term menstrual pain. Significant group by genotype interactions were found in brain regions including the hippocampus, amygdala, insula, thalamus, putamen, superior temporal pole, supramarginal

TABLE 2 | Associations of different *BDNF* Val66Met genotypes with PDM.

Reference	Case	Odds ratio	95% CI	χ^2	*p*-value
Val/Val	Met/Met	2.42	1.03–5.69	4.142	0.042*
Val/Met	Met/Met	2.25	1.02–4.93	4.125	0.042*
Val carrier	Met/Met	2.31	1.12–4.78	5.248	0.022*
Val/Val	Met carrier	1.47	0.73–2.95	1.183	0.277
Val/Val	Val/Met	1.08	0.50–2.30	0.036	0.849

**Significant odds ratios were tested using chi-square tests ($p < 0.05$). PDM, primary dysmenorrhea patients; CI, confidence interval; Val/Val, Valine/Valine; Val/Met, Valine/Methionine; Met/Met, Methionine/Methionine; Val carrier, Val/Val and Val/Met; Met carrier, Met/Met and Val/Met.*

gyrus, superior temporal gyrus, and others (**Table 4** and **Figure 2**).

Specifically, we tested planned comparisons of *BDNF* Val66Met genotypes and groups (**Figure 3**). For *BDNF*-associated regional MSE differences (between-genotype differences in each group) in CONs (**Figure 3A** and **Table S5**), MSE values were all larger in Val/Val CONs than in Val/Met CONs and Met/Met CONs. In PDMs (**Figure 3A** and **Table S6**), MSE values were also mostly larger in Val/Val PDMs than in Val/Met PDMs and Met/Met PDMs, except in the left amygdala. Val/Val PDMs manifested significant larger regional MSE in the left posterior cingulate gyrus (PCC) than in Val/Met PDMs and Met/Met PDMs, a phenomenon which was not found in the CON group. We also noticed that in both PDM and CON groups, regional MSE values in the left Heschl's gyrus were all larger in Val/Val than in Val/Met and Met/Met groups.

For pain-associated regional MSE (between-group differences of the same genotype; **Figure 3B** and **Table 5**) in Val/Val individuals, MSE values were found to be lower in the right hippocampus and left amygdala in Val/Val PDMs than in Val/Val CONs. On the other hand, in Met/Met individuals, pain-associated regional MSE values were found to be larger in the left amygdala, left superior temporal pole, and right calcarine sulcus in Met/Met PDMs than in Met/Met CONs.

MSE profiles of six subgroups (Val/Val, Val/Met, and Met/Met in PDMs and CONs) in the right hippocampus (**Figure 4**), one of the most interested regions in our studies, were depicted from time scale factors $\tau = 1$ to 100 for visual comparisons. Overall, Val/Met and Met/Met genotype groups had lower regional MSE than Val/Val group in both PDM and CON groups. At coarse time scales, the differences between Val/Val and Met carriers (Val/Met and Met/Met) were large in CONs, but such differences were diminished in PDMs. Same observations held for those in the left amygdala.

Correlations Between *BDNF*-Associated or Pain-Associated Regional MSE and Psychological Characteristics

Correlation results were summarized into different resting-state networks and different categories of psychological characteristics (**Figure 5** and **Table S7**). We found that significant correlations in Met/Met group and PDM group mainly emerged in the subcortical regions (such as amygdala, hippocampus) and sensorimotor regions (such as thalamus), whereas significant correlations in Val/Val group and CON group emerged largely in the cortical regions (such as middle temporal gyrus, superior temporal gyrus, fusiform gyrus) and some of the subcortical regions (such as hippocampus). Also, after long-term menstrual pain, the correlations found in CONs were reversed or diminished in PDMs. MSE values in the amygdala showed trends towards negative correlations with both depression and anxiety scores in Met/Met CONs but were positively correlated to those in Met/Met PDMs (**Figure 5A**). On the other hand, MSE values in the hippocampus were also negatively correlated to depression scores in Met/Met CONs but positively correlated to those in Met/Met PDMs (**Figure 5B**), and were negatively correlated to anxiety scores in Met/Met CONs but positively correlated to those in Val/Val PDMs.

In PDMs, correlations between pain experiences and regional MSE mainly emerged in the Val/Val group but absent in the Val/Met or Met/Met groups. In Val/Val PDMs, pain chronification (menstrual pain history, PDM onset, menstrual pain duration) experiences were negatively correlated with MSE values. The younger the PDM onset age, or the longer the PDM history/duration, the lower the MSE in the limbic regions including the amygdala (**Figure 5C**), thalamus, and posterior cingulate gyrus. In contrast, pain intensity experiences (pain score, pain rating indexes) were mostly positively correlated with MSE in the thalamus (**Figure 5D**) and Heschl's gyrus.

DISCUSSION

In this study, we used multiscale sample entropy analysis, a powerful tool that quantifies non-linear dynamics in time-varying signals, to investigate whether inter-subject genetic variation interacts with long-term menstrual pain experience to affect brain complexity. First, we found that *BDNF* Val66Met polymorphism (Met/Met homozygosity) is a potential genetic risk factor associated with primary dysmenorrhea, which is in line with previous studies (Lee et al., 2014; Wei et al., 2016b). Second, our findings indicate that long-term menstrual pain experience alters the effects of *BDNF* Val66Met polymorphism on brain complexity. By comparing brain complexity in females of different genotypes with or without menstrual pain, we revealed a characteristic tendency. There was considerable genotype-specific complexity differences in CONs, where Met-carrier (Val/Met and Met/Met) CONs showed extensive lower brain complexity compared to Val/Val CONs. However, the complexity differences were remarkably diminished in PDMs, implying the assaults of chronic recurrent pain on brain complexity. Third, we observed pain-associated brain complexity alterations in the limbic regions, especially the hippocampus and amygdala, in females with same *BDNF* Val66Met genotype.

In our recent study (Low et al., 2017), we categorized female participants according to menstrual pain experience to have a general understanding of brain complexity alterations in PDM. In this study, we further categorized all participants according to *BDNF* Val66Met genotypes together with menstrual

TABLE 3 | Results of negative mood (anxiety and depression) and negative cognitive style to pain (pain catastrophizing) stratified by group and *BDNF* Val66Met genotype.

	PDM ($n = 80$)	CON ($n = 76$)	Group main effect (F)	Genotype main effect (F)	Group x Genotype interaction (F)	Between-group (p)
ANXIETY						
BAI (0–63)						
Val/Val	7.25 (7.3)	3.04 (3.0)	$F_{(1,150)} = 17.23^{**}$	$F_{(2,150)} = 0.85$	$F_{(2,150)} = 0.29$	0.082
Val/Met	5.94 (5.6)	2.94 (2.5)				0.008*
Met/Met	7.07 (5.6)	4.27 (3.7)				0.101
Genotype (p)	0.659	0.511				
STAI total score (40–160)						
Val/Val	82.16 (17.3)	66.16 (9.90)	$F_{(1,143)} = 23.14^{**}$	$F_{(2,143)} = 1.37$	$F_{(2,143)} = 0.74$	< 0.0005*
Val/Met	81.23 (16.0)	71.62 (12.6)				0.012
Met/Met	84.31 (15.8)	74.60 (14.6)				0.049
Genotype (p)	0.732	0.123				
State anxiety (20–80)						
Val/Val	37.55 (9.1)	30.88 (5.8)	$F_{(1,149)} = 13.27^{**}$	$F_{(2,149)} = 1.43$	$F_{(2,149)} = 0.36$	0.003*
Val/Met	37.65 (8.5)	33.08 (9.1)				0.063
Met/Met	39.14 (8.2)	35.33 (7.7)				0.164
Genotype (p)	0.571	0.199				
Trait anxiety (20–80)						
Val/Val	45.05 (8.7)	35.28 (5.1)	$F_{(1,143)} = 27.82^{**}$	$F_{(2,143)} = 0.57$	$F_{(2,143)} = 1.08$	< 0.0005*
Val/Met	43.43 (8.7)	37.50 (6.8)				0.003*
Met/Met	44.50 (9.2)	39.27 (7.9)				0.056
Genotype (p)	0.772	0.244				
DEPRESSION						
BDI (0–63)						
Val/Val	7.80 (8.1)	3.52 (3.4)	$F_{(1,150)} = 4.65$	$F_{(2,150)} = 2.12$	$F_{(2,150)} = 1.40$	0.078
Val/Met	5.48 (5.6)	3.56 (5.3)				0.044
Met/Met	6.93 (6.3)	6.87 (6.2)				0.950
Genotype (p)	0.614	0.084				
PAIN CATASTROPHIZING						
PCS total score (0–52)						
Val/Val	16.80 (9.1)	4.88 (6.8)	$F_{(1,146)} = 44.47^{**}$	$F_{(2,146)} = 0.65$	$F_{(2,146)} = 0.50$	< 0.0005*
Val/Met	16.94 (13.3)	8.03 (9.0)				0.003*
Met/Met	19.04 (9.4)	5.20 (7.8)				< 0.0005*
Genotype (p)	0.570	0.271				
Helplessness (0–16)						
Val/Val	7.30 (4.2)	2.12 (2.8)	$F_{(1,146)} = 44.47^{**}$	$F_{(2,146)} = 0.65$	$F_{(2,146)} = 0.50$	< 0.0005*
Val/Met	7.87 (6.0)	3.61 (4.6)				0.001*
Met/Met	8.46 (4.8)	2.33 (3.8)				< 0.0005*
Genotype (p)	0.711	0.422				
Magnification (0–24)						
Val/Val	2.65 (2.1)	1.24 (1.9)	$F_{(1,146)} = 21.03^{**}$	$F_{(2,146)} = 0.41$	$F_{(2,146)} = 0.29$	0.011
Val/Met	3.10 (3.1)	1.48 (1.8)				0.031
Met/Met	3.39 (2.1)	1.27 (1.9)				0.001*
Genotype (p)	0.460	0.602				
Rumination (0–12)						
Val/Val	6.85 (4.0)	1.52 (2.6)	$F_{(1,146)} = 56.14^{**}$	$F_{(2,146)} = 0.07$	$F_{(2,146)} = 1.96$	< 0.0005*
Val/Met	5.97 (4.7)	2.94 (3.3)				0.006*
Met/Met	7.18 (3.9)	1.60 (2.4)				< 0.0005*
Genotype (p)	0.454	0.145				

*Significance main effects of group, genotype, and group x genotype interactions were tested using two-way ANOVAs ($p < 0.01$, two-tailed). *$p < 0.005$, **$p < 0.00001$. Significant between-group within-genotype planned comparisons were tested using Mann-Whitney U-tests ($p < 0.01$, two-tailed). Significant between-genotype differences in each group ("Genotype") were tested using Kruskal-Wallis H tests ($p < 0.01$, two-tailed). Score ranges are bracketed after each item name. Data are presented as mean (SD). PDM, primary dysmenorrhea patients; CON, healthy female controls; Val/Val, Valine/Valine; Val/Met, Valine/Methionine; Met/Met, Methionine/Methionine; STAI, Spielberger state-trait anxiety inventory; BAI, Beck anxiety inventory; BDI, Beck depression inventory; PCS, pain catastrophizing scale.*

TABLE 4 | Significant interactions of *BDNF* Val66Met genotype and group.

Brain region	L/R	τ	Group x Genotype interaction (*F*)	Bonferroni-adjusted (*p*)
Limbic regions				
Hippocampus	R	79,91	3.32, 3.45	0.034, 0.039
Amygdala	L	78,84,88,91	3.62∼5.75	0.004∼0.029
	R	85	3.97	0.021
Putamen	L	79	3.50	0.033
Superior temporal pole	L	94	3.24	0.042
Middle temporal pole	L	78,98	3.30, 3.95	0.021, 0.040
Salience network				
Insula	L	88	3.50	0.033
Sensorimotor network				
Thalamus	L	73	3.16	0.045
Supramarginal g	L	79,80	3.48, 3.59	0.030, 0.033
	R	65,66,76,82,88,89	3.07∼3.79	0.025∼0.049
Auditory network				
Superior temporal g	L	92	3.17	0.045
Visual network				
Calcarine	L	83	3.30	0.040
Fusiform g	L	87,94	3.21, 3.30	0.040, 0.043
SOG	R	96	3.84	0.024
MOG	L	86,92,98	3.15∼3.41	0.026∼0.046
IOG	L	74,77,80,87,90,92	3.12∼4.97	0.008∼0.047

Significant differences were tested using two-way ANOVAs (Bonferroni-corrected $p < 0.05$, two-tailed). L, left hemisphere; R, right hemisphere; g, gyrus; SOG, superior occipital gyrus; MOG, middle occipital gyrus; IOG, inferior occipital gyrus.

pain experience. It is noted that Met allele frequencies of *BDNF* Val66Met polymorphism vary markedly across global populations, ranging from 0 to 72% (Petryshen et al., 2010) with higher frequency in Asian populations (more than 40%) and lower frequency in European populations (around 20%). Hence, the population genetic distribution of *BDNF* Val66Met in Asians allows us to recruit adequate Met-carrier participants to delineate genuine inter-subject genetic variation, as seen in our between-genotype MSE differences. We advise that combining Met carriers (Val/Met and Met/Met) or Val carriers (Val/Met and Val/Val) as one single genotype group, due to the paucity of Met/Met or Val/Val homozygotes, could overlook subtle yet informative genotype-specific changes at the brain level.

Our results demonstrated that the alterations of MSE in PDMs were majorly clustered on large time scales (τ = 50–100), including interactions above scales 73 (**Table 4**), pain-associated differences above scale 78 (**Table 5**), *BDNF*-associated differences above scale 50 (**Tables S5**, **S6**), and correlations above scale 50 (**Table S7**). Time scales in MSE are reported to have some correspondences with signal frequencies (Mizuno et al., 2010; Courtiol et al., 2016). Coarse-graining procedure in MSE analysis resembles applying low-pass filtering or down-sampling procedure to the original time-series signal. According to Nyquist-Shannon's sampling theorem, sample entropy value at scale factor τ could reveal the irregularity of the signal under the frequency of $(f_s/\tau)/2$ Hz (Courtiol et al., 2016), where f_s is the sampling frequency of the original signal. Given a sampling rate around 1000 Hz in the current study, SE values at time scales 20/50/75/100 might reveal the irregularity of the signal under 25/10/6.7/5 Hz. Our findings of large-scale MSE alterations in PDMs implicate that the resting-state neural complexity altered by the interactions of long-term menstrual pain and *BDNF* Val66Met polymorphism emerged approximately below theta and alpha frequency bands. Moreover, different brain regions exhibited different patterns of alterations, such as the limbic regions (<theta band), the sensorimotor regions (<alpha band), and the default mode network regions (<beta band). These are in line with previous studies, which reported alterations of theta oscillations at limbic regions in PDMs (Lee et al., 2017) and spectral alterations in low frequencies (theta and alpha bands) in chronic pain patients (Pinheiro et al., 2016; Ploner et al., 2017). Thus, MSE could be an important method to explore brain complexity and neural adaptability alterations.

The findings of MSE differences between *BDNF* Val66Met genotypes in healthy female controls support our hypothesis of genotype-specific complexity differences. Regional MSE values in Met-carrier CONs (Val/Met and Met/Met) were extensively lower at different brain regions compared with those in Val/Val individuals (**Figure 3A**). In healthy conditions, *BDNF* Val/Val homozygotes might serve a protective role on neural complexity, whereas Met allele(s) (Val/Met or Met/Met) might lead to lower neural complexity, implying a defective role of Met allele on the overall brain complexity in healthy females. One common explanation is the "neurotrophic model" that the replacement of Val by Met variant disrupts intracellular trafficking, distribution, and activity-dependent BDNF secretion at synapses in Met

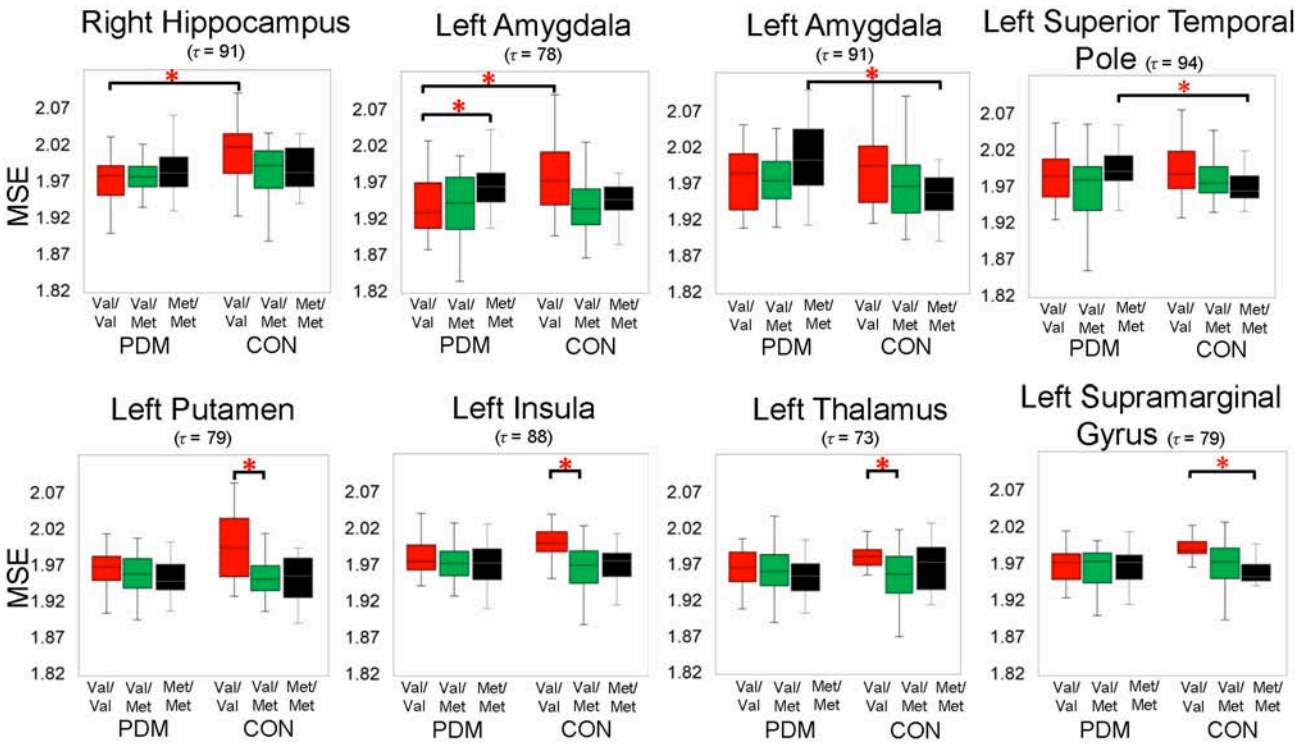

FIGURE 2 | Significant group by genotype interactions on brain complexity in regions, including the left amygdala and right hippocampus. Significant planned comparisons labeled in the figure (*) were tested using permutation tests (iterations = 5000, $p < 0.005$, two-tailed). Box plots with 25th (Q1), 50th (median), 75th (Q3) percentiles are demonstrated; the largest and smallest values within 1.5 times the interquartile range (IQR) are plotted as whiskers. Colors: *BDNF* Val/Val (red), Val/Met (green), and Met/Met (black). PDM, primary dysmenorrhea patients; CON, healthy female controls; Val/Val, Valine/Valine; Val/Met, Valine/Methionine; Met/Met, Methionine/Methionine; τ, time scale factors.

carriers (Egan et al., 2003; Chen et al., 2004). As neural complexity might reflect neuronal transients or flexible rapid transitions between neuronal microstates (Friston, 2000; Wang et al., 2018), we reason that Met carriers displayed a general loss of brain complexity compared with Val/Val homozygotes. This result is in line with previous resting-state fMRI study (Wei et al., 2016b) that healthy females with different *BDNF* Val66Met genotypes engaged larger variations in functional connectivity within the descending pain modulatory system. Without the influence of long-term pain experience, healthy individuals might preserve more substantial viability and flexibility in neural dynamics.

However, in PDMs, the between-genotype complexity differences in healthy females was greatly diminished (**Figure 3A**). This finding suggests that three genotype groups in PDMs demonstrated a less resilient brain system after the experience of long-term menstrual pain. BDNF contributes to the sensitizing capacity of the pain pathways from peripheral nociceptors, spinal level, to brain level, and is cardinally involved in central sensitization of pain (Nijs et al., 2015). Individuals with a single Val allele might "preserve," at least to some extent, the neural complexity compared to Met carriers. In Val/Val PDMs but not in Met-carrier PDMs, the shorter the PDM history or duration was, the higher the neural complexity was preserved (close to those in Val/Val CONs) in pain-related regions (including the amygdala, thalamus, and posterior cingulate gyrus). These results suggest that the protective role of Val/Val homozygosity with respect to pain chronification is preserved in PDMs and only substitution of both alleles (as in Met/Met PDMs) might lead to loss of complexity in relatively more regions, which might reflect maladaptive neural plasticity upon long-term pain insults.

On the other hand, between-group comparisons of the same genotype (**Figure 3B**) revealed that neural complexity in the limbic regions (hippocampus, amygdala) was affected by long-term menstrual pain experience in a genotype-specific manner. From our recent study (Low et al., 2017), we learned that the complexity of the hippocampus and amygdala was generally lower in PDMs than in CONs. In the current study, in the hippocampus, Val/Val CONs (the reference group) had the highest regional MSE values and there was no difference among the three genotype subgroups in PDMs. This result suggests that complexity in the hippocampus might be vulnerable to long-term menstrual pain regardless of genotype. Moreover, the hippocampal MSE values were negatively correlated to anxiety and depressive scores in Met/Met CONs but positively correlated in Met/Met PDMs and Val/Val PDMs (**Figure 5B**), implying

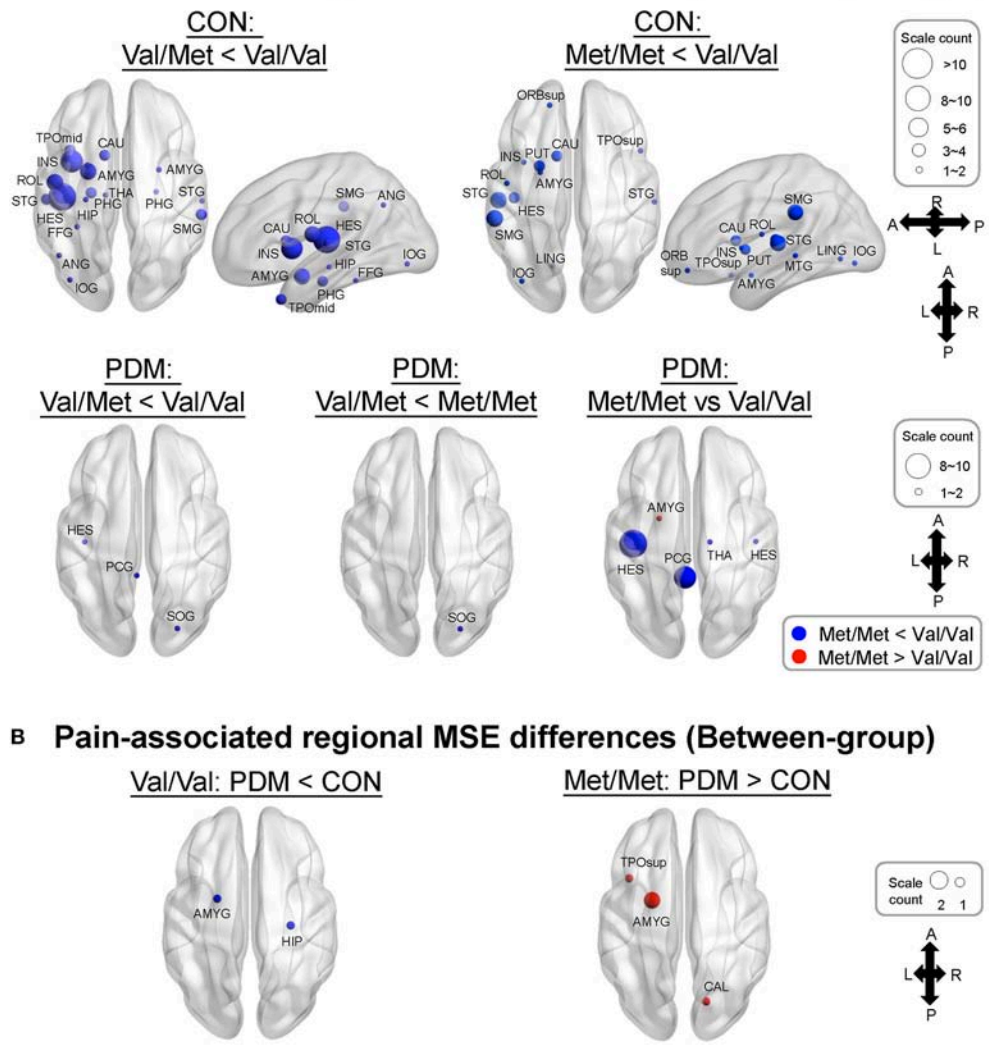

FIGURE 3 | MSE differences between *BDNF* Val66Met genotypes and between groups. **(A)** *BDNF*-associated regional MSE differences in each group ("Between-genotype"). Complexity differences between different genotypes in CONs was greatly diminished in PDMs. Regional MSE values were mostly lower in Val/Met and Met/Met than in Val/Val genotype except in the left amygdala in PDMs. Colors of sphere: Val/Met < Val/Val (blue), Met/Met < Val/Val (blue), Val/Met < Met//Met (blue), Met/Met > Val/Val (red). Size of sphere represents count of scale factors that showed significant MSE differences. **(B)** Pain-associated regional MSE differences in females with the same genotype ("Between-group"). Colors of sphere: PDM < CON (blue), PDM > CON (red). Val/Val, Valine/Valine; Val/Met, Valine/Methionine; Met/Met, Methionine/Methionine.

possible maladaptive neuroplasticity after the experience of long-term menstrual pain. This speculation is in accordance with the findings in animal study, in which stressful environment leads to increased anxiety-related behaviors in *BDNF* Met/Met mice but not in wild-type mice (Chen et al., 2004). In other words, the effect of chronic pain experience (environmental stress) might preponderantly affect the effect of *BDNF* Val66Met polymorphism on brain complexity.

Interestingly, in the amygdala, Met/Met PDMs showed higher regional MSE values compared with Val/Val PDMs and Met/Met CONs, suggesting that the complexity in the amygdala might be modulated differently by long-term menstrual pain in specific genotype. From the patterns of altered neural complexity observed in the amygdala and hippocampus in PDMs, we speculate the relationships lie between the amygdala, hippocampus, hypothalamus–pituitary–adrenal axis (HPA axis) system, and BDNF. Evidence from cellular to human studies indicates that pain and stress activate the HPA axis. The amygdala and hippocampus may play important yet distinct roles in the HPA axis (Smith and Vale, 2006; Weidenfeld and Ovadia, 2017). BDNF also substantially participates in the regulation of HPA axis activity (Naert et al., 2011). Under stressful environment, hippocampal atrophy and decreased BDNF secretion were found in mice (Chen Z. Y. et al., 2006). In depressive individuals,

TABLE 5 | Pain-associated (between-group) regional MSE differences.

Brain region	L/R	Count	τ	*p*-value	*t*-score	Cohen's *d*
Val/Val: PDM < CON (Count = 2)						
Limbic regions						
Hippocampus*	R	1	91	0.0016	−3.41	−1.024
Amygdala*	L	1	78	0.0026	−2.98	−0.894
Met/Met: PDM > CON (Count = 4)						
Limbic regions						
Amygdala	L	2	84,91	0.0007, 0.001	3.34, 3.75	1.063, 1.193
Superior temporal pole	L	1	94	0.0036	3.00	0.953
Visual network						
Calcarine s	R	1	83	0.0046	2.83	0.899

*Significant planned comparisons tested for whole brain using permutation tests (iterations = 5000, $p < 0.005$, two-tailed). * represents significant brain regions that also survived under stricter correction (Bonferroni-adjusted $p < 0.05$, two-tailed). PDM, primary dysmenorrhea patients; CON, healthy female controls; Val/Val, Valine/Valine; Met/Met, Methionine/Methionine; L, left hemisphere; R, right hemisphere; s, sulcus.*

decreased level of BDNF leads to hippocampal atrophy and prefrontal cortex atrophy (Duman and Monteggia, 2006). Neuronal morphology studies in rats reveal that exposure to chronic stress leads to hippocampus atrophy but amygdala hypertrophy (Vyas et al., 2002). Both acute and chronic stress trigger opposite effects and different temporal profiles on BDNF levels in the amygdala (BLA) vs. hippocampus (CA3) in rats (Lakshminarasimhan and Chattarji, 2012). Thus, chronic stress leads to contrasting patterns of neuronal dendritic remodeling in the hippocampus and amygdala that results in dysregulation of HPA axis (Vyas et al., 2002), which are consistent with our results. Atrophy of the hippocampus causes a loss of hippocampal inhibitory control over the HPA axis, whereas hypertrophy of the amygdala causes a gain in excitatory control over the HPA axis. Our results indicate that the hippocampus might be vulnerable to long-term menstrual pain regardless of *BDNF* Val66Met genotypes, whereas amygdala might be affected by different *BDNF* Val66Met genotypes, implicating a genetic mechanism of variation in brain complexity related to chronic pain. Alternatively, we speculate that the dissociation pattern between the hippocampus and amygdala could be a manifestation of system damping; an adaptive and coping mechanism to relieve the brain from overloaded limbic information while maintaining the pain salience and harmful signal detection. These findings suggest that MSE-brain complexity could be a more sensitive measurement of neurodynamics in comparison to conventional functional connectivity observed in fMRI to reflect the central responses to brain stress (i.e., painful insults).

There is a lack of direct evidence of the association between BDNF or *BDNF* Val66Met polymorphism and neural complexity (as measured by MSE). A clinical case study of a single autism spectrum disorder patient reported electroconvulsive therapy-induced changes of EEG complexity and increased serum BDNF concentrations during and after therapy (Okazaki et al., 2015); yet, the authors did not offer an adequate explanation for the underlying association between BDNF level and EEG complexity. Nevertheless, we speculate a possible link between BDNF and complexity from several points based on the neurobiological functioning of BDNF (Sasi et al., 2017). First, BDNF may be a key mediator and modulator of functional synaptic plasticity, such as activity-induced long-term potentiation and long-term depression (Park and Poo, 2013; Benarroch, 2015). Second, BDNF is also reported to increase the morphology or complexity of dendritic arbors, spines, and microarchitectural integrity, thereby influences structural plasticity (Tolwani et al., 2002; Cohen-Cory et al., 2010; Park and Poo, 2013). Third, both functional and structural plasticity reflect changes in synaptic strength that change in short and long terms. These changes are non-linear and non-stationary and are embedded in time-varying activities of neuronal populations. Therefore, quantifying the irregularity or unpredictability of these activities or synaptic dynamics might shed light on the complexity of the neural system.

From our resting-state regional MSE findings, the effects of *BDNF* Val or Met alleles might be far beyond simple deleterious or protective. We recognized that *BDNF* genetic polymorphism and BDNF protein have complex actions/regulations in the brain that could not be simplified to a single or unifying explanation based on our resting-state brain complexity study at this stage. Other confounding factors, such as age, gender (Stefani et al., 2012), environmental factors, sample size, ethnicity, and phenotype assessment, might also result in controversial findings in *BDNF* genetic studies (Hong et al., 2011; Notaras et al., 2015; Tsai, 2018). Moreover, it is still an ongoing debate whether the Met allele of *BDNF* Val66Met might serve as a deleterious role on brain structures, performances, or health (Autry and Monteggia, 2012; Tingting et al., 2014; Benarroch, 2015; Notaras et al., 2015). Part of these studies was carried out in healthy individuals to avoid possible confounding factors such as illness, medication, or genetic risk factors associated with certain diseases (Harrisberger et al., 2014). For example, a study from healthy Chinese population reported larger gray matter volume in Met/Met homozygotes (Liu et al., 2014), although the underlying mechanism remains elusive. Therefore, for individuals who experience chronic recurrent pain or long-term illnesses, the pain or stress might lead to maladaptive neural plasticity or adaptive coping strategy in different *BDNF* Val66Met carriers due to the activity-dependent manner of *BDNF*, and might come to different conclusions.

Associating genetic variation and chronic recurrent pain with brain complexity may assist in the understanding of individual neural resilience/susceptibility to pain chronification. Moreover, from the polygenic etiology view, it is implausible that *BDNF* is the single gene mediating menstrual pain while gene-gene interactions and epigenetic modulations have their profound contributions on chronic pain development (Denk and McMahon, 2012; Bai et al., 2017). We speculate that epigenetic modulations of long-term menstrual pain on *BDNF* genotypes might better explain our findings. However, to investigate the epigenetic modulations of genetic polymorphism, relevant technologies and tools are required (Weinhold, 2006), and further investigations are needed to fully comprehend the contribution of epigenetic processes to chronic pain states.

There are several limitations in this brain complexity genetic study. First, we only focused on *BDNF* Val66Met genetic

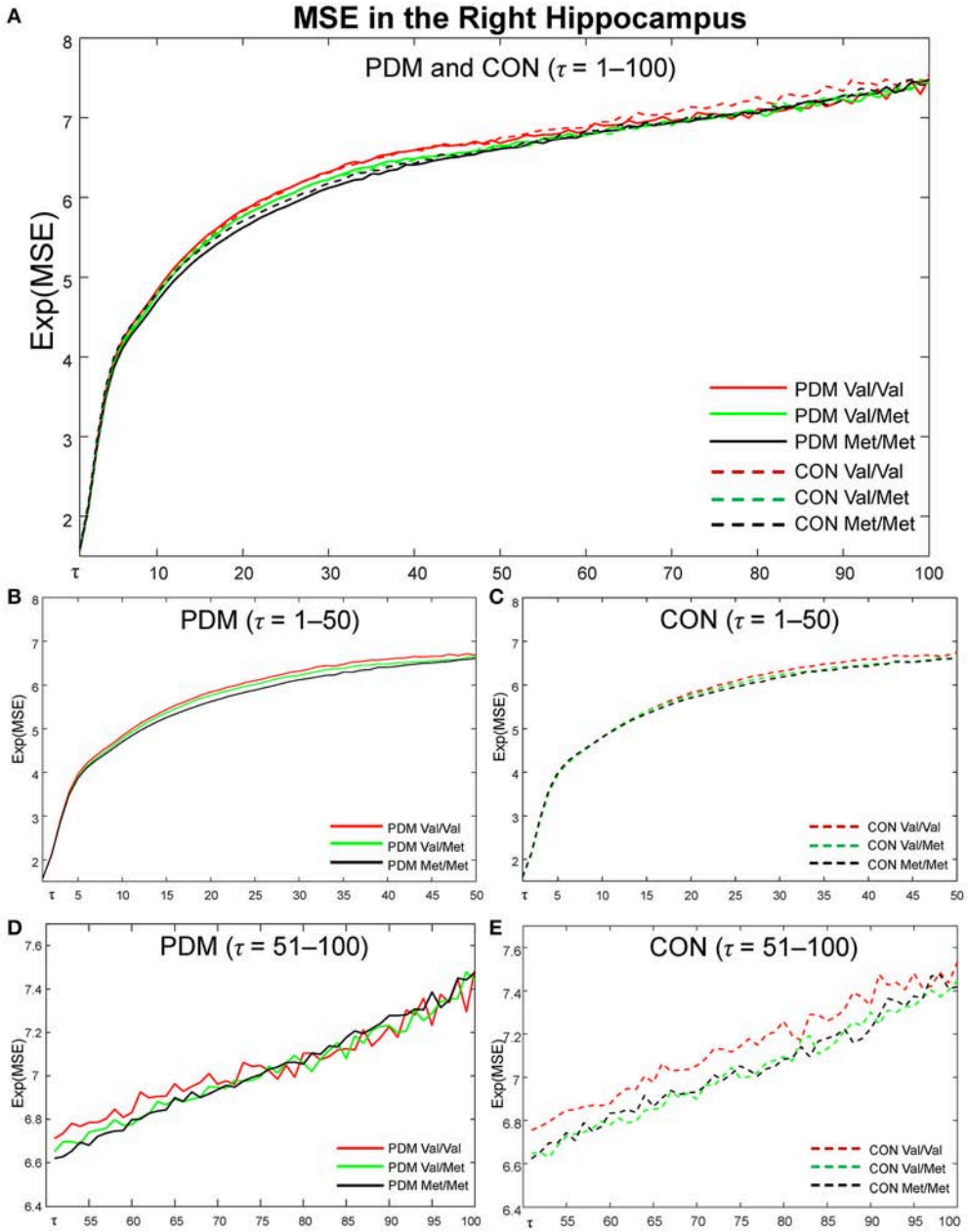

FIGURE 4 | MSE profiles in the right hippocampus. Colors: *BDNF* Val/Val (red), Val/Met (green), Met/Met (black). Lines: PDMs (solid), CONs (dashed). **(A)** MSE profiles of six subgroups from fine to coarse scales across $\tau = 1$ to 100. **(B)** MSE profiles from $\tau = 1$ to 50 in PDM group. **(C)** MSE profiles from $\tau = 1$ to 50 in CON group. **(D)** MSE profiles from $\tau = 51$ to 100 in PDM group. **(E)** MSE profiles from $\tau = 51$ to 100 in CON group. PDM group is illustrated on the left and CON group on the right. Val/Val, Valine/Valine; Val/Met, Valine/Methionine; Met/Met, Methionine/Methionine; τ, time scale factors.

polymorphism; there was no information of *BDNF* gene expression, BDNF protein levels, or cortisol levels to test for their associations with brain complexity. Second, other pain-related genetic polymorphisms, such as *BDNF* rs2049046 and G-712A reported in migraine studies (Azimova et al., 2013; Sutherland et al., 2014) or *OPRM1* A118G reported in PDM study (Wei et al., 2017), might also be potential candidates of genetic modulators of chronic pain-sculpted brain complexity. Finally, most neuroimaging genetic studies encounter the problem of small sample sizes compared to traditional genetic studies. Our PDM study samples were particularly limited by challenges of data acquisition of different neuroimaging modalities on the same day, rigorous inclusion/exclusion criteria, and a high exclusion rate. Nevertheless, 156 participants (80 PDMs and 76 CONs) were recruited in the present study, which was relatively large in neuroimaging studies. Future studies are invited to test the neuroimaging genetic results in brain complexity.

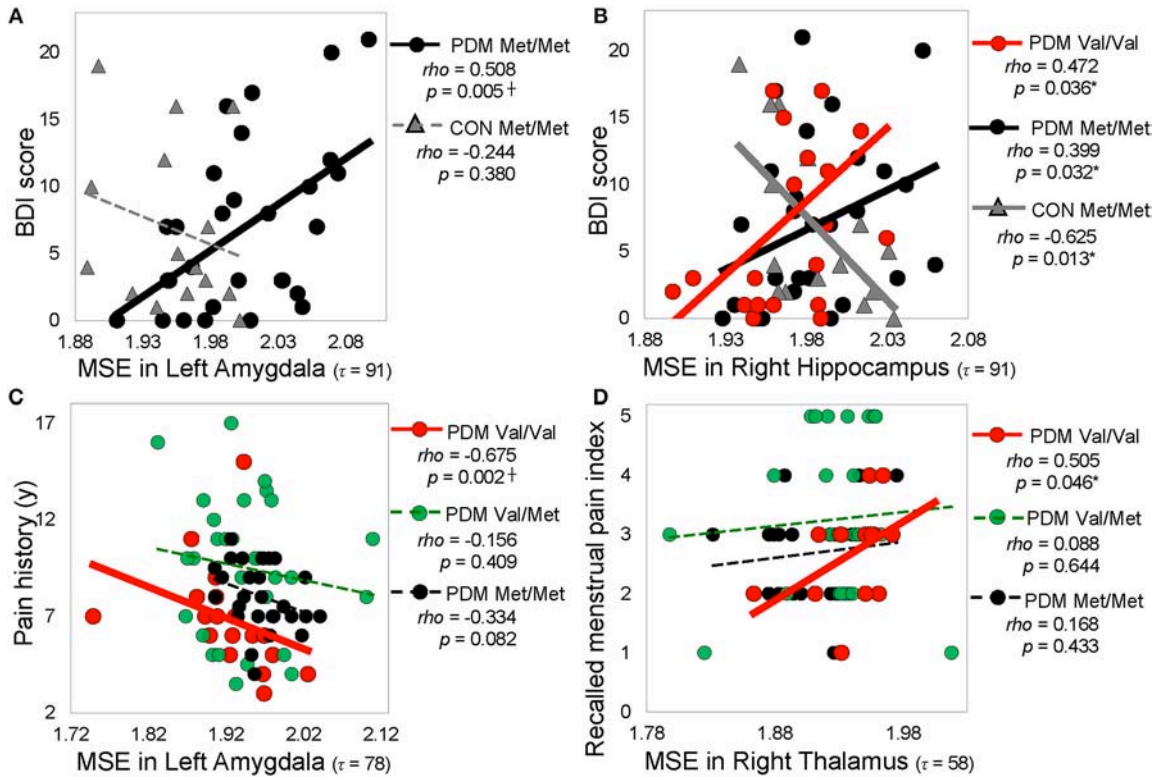

FIGURE 5 | Significant correlations between regional MSE and pain-related psychological characteristics. **(A)** Correlations between MSE in the left amygdala ($\tau = 91$) and depression (BDI score). **(B)** Correlations between MSE in the right hippocampus ($\tau = 91$) and depression score (BDI score). **(C)** Correlations between MSE in the left amygdala ($\tau = 78$) and pain history. **(D)** Correlations between MSE in the right thalamus ($\tau = = 58$) and recalled menstrual pain index. Spearman rho ($p < 0.05$, two-tailed). Significant correlations are plotted as solid lines; correlations that are not significant are plotted as dashed lines. Colors: *BDNF* Val/Val (red), Val/Met (green), and Met/Met (black). Shapes: PDMs (circle), CONs (triangle). MSE, multiscale sample entropy; Val/Val, Valine/Valine; Val/Met, Valine/Methionine; Met/Met, Methionine/Methionine; PDM, primary dysmenorrhea patients; CON, healthy female controls; BDI, Beck depression inventor; McGill pain questionnaire; PPI, present pain index; y, year; τ, time scale factors.

CONCLUSIONS

Applying MSE analysis to time-varying MEG signals provides valuable information about neural complexity. We found that PDMs exhibited a general loss of brain complexity in pain-related regions and *BDNF* Val66Met polymorphism is involved in the complexity differences in a genotype-specific manner. Overall, the *BDNF* Val/Val homozygosity might serve as a protective role that preserves the brain complexity. Our results suggest that pain experience preponderantly affects the effect of *BDNF* Val66Met polymorphism on brain complexity, particularly those in the limbic circuits (hippocampus and amygdala), implicating gene-environment interaction on brain complexity.

AUTHOR CONTRIBUTIONS

L-FC and J-CH conceived and designed the experiments. IL and Y-HL performed the experiments. H-TC performed the clinical assessment. M-WL performed the genotyping. P-CK and Y-SC developed the methodology. IL, C-LT, Y-HL, and M-WL analyzed the data. J-CH provided substantial intellectual input for the work. IL, P-CK, Y-SC, L-FC, and J-CH wrote the manuscript. All authors had reviewed the paper. L-FC and J-CH approved the final submission.

FUNDING

This study was supported in part by grants from Ministry of Science Technology (NSC-102-2629-B-010-001, MOST-105-2221-E-009-057, MOST-105-2321-B-010-002, MOST-106-2218-E-010-004-MY3, MOST-106-2410-H-010-003, MOST-106-2420-H-009-001, MOST-106-2629-B-010-001-MY3, MOST-107-2811-E-010-002), Taipei Veterans General Hospital (V100D-001, V104C-127, V106C-082), TVGH-NTUH joint research program (VN105-03), Integrated Brain Research Unit, Department of Medical Research, Taipei Veterans General Hospital, and the Brain Research Center, National Yang-Ming University from The Featured Areas Research Center Program within the framework of the Higher Education Sprout Project by the Ministry of Education (MOE) in Taiwan.

ACKNOWLEDGMENTS

All participants are thanked for their support and contribution to this study. We appreciate the assistance of Cheng-Hao Tu, Wei-Chi Li, Ian-Ting Chu, Ching-Ju Yang, Tzu-Ling Tzeng, Chih-Ying Chuang, Chih-Cher Chou, Lin-Chien Lee, Yu-Mei Chang, Chiu-Jung Huang, Ruei-Jyun Hung, Yi-Jun Liu, and Li-Kai Cheng with participant recruitment and MEG/MRI experiments. We thank Dr. Albert C Yang, Dr. Bai-Chuang Shyu, and Dr. Chia-Shu Lin for providing valuable comments and constructive suggestions to improve the quality of this paper.

SUPPLEMENTARY MATERIAL

The Supplementary Material for this article can be found online at: https://www.frontiersin.org/articles/10.3389/fnins.2018.00826/full#supplementary-material

REFERENCES

Alemán-Gómez, Y., Melie-García, L., and Valdés-Hernandez, P. (2006). "IBASPM: Toolbox for automatic parcellation of brain structures," in *12th Annual Meeting of the Organization for Human Brain Mapping*. Florence.

Autry, A. E., and Monteggia, L. M. (2012). Brain-derived neurotrophic factor and neuropsychiatric disorders. *Pharmacol. Rev.* 64, 238–258. doi: 10.1124/pr.111.005108

Azimova, Y., Sergeev, A., and Skorobogatykh, K. (2013). BDNF gene polymorphysm RS2049046 in episodic and chronic migraine. *J. Headache Pain* 14:P16. doi: 10.1186/1129-2377-14-S1-P16

Bai, G., Ren, K., and Dubner, R. (2017). "Chapter 8 - Epigenetics in chronic pain" in *Translating Epigenetics to the Clinic,* ed. M. V. Beusekom. (Boston, MA: Academic Press), 185–226.

Bathina, S., and Das, U. N. (2015). Brain-derived neurotrophic factor and its clinical implications. *Arch. Med. Sci.* 11, 1164–1178. doi: 10.5114/aoms.2015.56342

Beck, A. T., Rush, A. J., Shaw, B. F., and Emery, G. (1979). *Cognitive Therapy of Depression*. New York, NY: The Guilford Press.

Benarroch, E. E. (2015). Brain-derived neurotrophic factor - regulation, effects, and potential clinical relevance. *Neurology* 84, 1693–1704. doi: 10.1212/wnl.0000000000001507

Berkley, K. J. (2013). Primary dysmenorrhea: an urgent mandate. *Pain: Clinical Updates* 21, 1–8. Available online at: http://www.iasp-pain.org/PublicationsNews/NewsletterIssue.aspx?ItemNumber=2062

Binder, D. K., and Scharfman, H. E. (2004). Brain-derived Neurotrophic Factor. *Growth Factors* 22, 123–131. doi: 10.1080/08977190410001723308

Cai, X., Shi, X., Zhang, X., Zhang, A., Zheng, M., and Fang, Y. (2017). The association between brain-derived neurotrophic factor gene polymorphism and migraine: a meta-analysis. *J. Headache Pain* 18:13. doi: 10.1186/s10194-017-0725-2

Caumo, W., Deitos, A., Carvalho, S., Leite, J., Carvalho, F., Dussan-Sarria, J. A., et al. (2016). Motor cortex excitability and BDNF levels in chronic musculoskeletal pain according to structural pathology. *Front. Hum. Neurosci.* 10:357. doi: 10.3389/fnhum.2016.00357

Chang, D., Song, D., Zhang, J., Shang, Y., Ge, Q., and Wang, Z. (2018). Caffeine caused a widespread increase of resting brain entropy. *Sci. Rep.* 8:2700. doi: 10.1038/s41598-018-21008-6

Chen, Y. S., Cheng, C. Y., Hsieh, J. C., and Chen, L. F. (2006). Maximum contrast beamformer for electromagnetic mapping of brain activity. *IEEE Trans. Biomed. Eng.* 53, 1765–1774. doi: 10.1109/TBME.2006.878115

Chen, Z. Y., Jing, D., Bath, K. G., Ieraci, A., Khan, T., Siao, C. J., et al. (2006). Genetic variant BDNF (Val66Met) polymorphism alters anxiety-related behavior. *Science* 314, 140–143. doi: 10.1126/science.1129663

Chen, Z. Y., Patel, P. D., Sant, G., Meng, C. X., Teng, K. K., Hempstead, B. L., et al. (2004). Variant brain-derived neurotrophic factor (BDNF) (Met66) alters the intracellular trafficking and activity-dependent secretion of wild-type BDNF in neurosecretory cells and cortical neurons. *J. Neurosci.* 24, 4401–4411. doi: 10.1523/JNEUROSCI.0348-04.2004

Cohen, J. (1988). *Statistical Power Analysis for the Behavioral Sciences.* Hillsdale, NJ: L. Erlbaum Associates.

Cohen-Cory, S., Kidane, A. H., Shirkey, N. J., and Marshak, S. (2010). Brain-derived neurotrophic factor and the development of structural neuronal connectivity. *Dev. Neurobiol.* 70, 271–288. doi: 10.1002/dneu.20774

Costa, M., Goldberger, A. L., and Peng, C. K. (2002). Multiscale entropy analysis of complex physiologic time series. *Phys. Rev. Lett.* 89:068102. doi: 10.1103/PhysRevLett.89.068102

Costa, M., Goldberger, A. L., and Peng, C. K. (2005). Multiscale entropy analysis of biological signals. *Phys. Rev. E Stat. Nonlin. Soft Matter. Phys.* 71(2 Pt 1):021906. doi: 10.1103/PhysRevE.71.021906

Courtiol, J., Perdikis, D., Petkoski, S., Muller, V., Huys, R., Sleimen-Malkoun, R., et al. (2016). The multiscale entropy: guidelines for use and interpretation in brain signal analysis. *J. Neurosci. Methods* 273, 175–190. doi: 10.1016/j.jneumeth.2016.09.004

Denk, F., and McMahon, S. B. (2012). Chronic pain: emerging evidence for the involvement of epigenetics. *Neuron* 73, 435–444. doi: 10.1016/j.neuron.2012.01.012

Di Lorenzo, C., Di Lorenzo, G., Daverio, A., Pasqualetti, P., Coppola, G., Giannoudas, I., et al. (2012). The Val66Met polymorphism of the BDNF gene influences trigeminal pain-related evoked responses. *J. Pain* 13, 866–873. doi: 10.1016/j.jpain.2012.05.014

Duman, R. S., and Monteggia, L. M. (2006). A neurotrophic model for stress-related mood disorders. *Biol. Psychiatry* 59, 1116–1127. doi: 10.1016/j.biopsych.2006.02.013

Egan, M. F., Kojima, M., Callicott, J. H., Goldberg, T. E., Kolachana, B. S., Bertolino, A., et al. (2003). The BDNF val66met polymorphism affects activity-dependent secretion of BDNF and human memory and hippocampal function. *Cell* 112, 257–269. doi: 10.1016/S0092-8674(03)00035-7

Friston, K., Breakspear, M., and Deco, G. (2012). Perception and self-organized instability. *Front. Comput. Neurosci.* 6:44. doi: 10.3389/fncom.2012.00044

Friston, K. J. (2000). The labile brain. II. transients, complexity and selection. *Philos. Trans. R. Soc. Lond. B Biol. Sci.* 355, 237–252. doi: 10.1098/rstb.2000.0561

Friston, K. J. (2001). Brain function, nonlinear coupling, and neuronal transients. *Neuroscientist* 7, 406–418. doi: 10.1177/107385840100700510

Generaal, E., Milaneschi, Y., Jansen, R., Elzinga, B. M., Dekker, J., and Penninx, B. W. (2016). The brain-derived neurotrophic factor pathway, life stress, and chronic multi-site musculoskeletal pain. *Mol. Pain* 12:174480691664678. doi: 10.1177/1744806916646783

Ghasemi, A., and Zahediasl, S. (2012). Normality tests for statistical analysis: a guide for non-statisticians. *Int. J. Endocrinol. Metab.* 10, 486–489. doi: 10.5812/ijem.3505

Haas, L., Portela, L. V., Bohmer, A. E., Oses, J. P., and Lara, D. R. (2010). Increased plasma levels of brain derived neurotrophic factor (BDNF) in patients with fibromyalgia. *Neurochem. Res.* 35, 830–834. doi: 10.1007/s11064-010-0129-z

Hager, B., Yang, A. C., Brady, R., Meda, S., Clementz, B., Pearlson, G. D., et al. (2017). Neural complexity as a potential translational biomarker for psychosis. *J. Affect. Disord.* 216, 89–99. doi: 10.1016/j.jad.2016.10.016

Harrisberger, F., Spalek, K., Smieskova, R., Schmidt, A., Coynel, D., Milnik, A., et al. (2014). The association of the BDNF Val66Met polymorphism and the hippocampal volumes in healthy humans: a joint meta-analysis of published and new data. *Neurosci. Biobehav. Rev.* 42, 267–278. doi: 10.1016/j.neubiorev.2014.03.011

Heisz, J. J., and McIntosh, A. R. (2013). Applications of EEG neuroimaging data: event-related potentials, spectral power, and multiscale entropy. *J. Vis. Exp.* 76:50131. doi: 10.3791/50131

Hong, C. J., Liou, Y. J., and Tsai, S. J. (2011). Effects of BDNF polymorphisms on brain function and behavior in health and disease. *Brain Res. Bull.* 86, 287–297. doi: 10.1016/j.brainresbull.2011.08.019

Iacovides, S., Avidon, I., and Baker, F. C. (2015). What we know about primary dysmenorrhea today: a critical review. *Hum. Reprod. Update* 21, 762–778. doi: 10.1093/humupd/dmv039

IASP (2011). "Visceral and Other Syndromes of the Trunk Apart From Spinal and Radicular Pain," in *Classification of Chronic Pain: Descriptions of Chronic Pain Syndromes and Definitions of Pain Terms, 2nd Edn (revised)* (Seattle, WA: IASP Press). Available online at: http://www.iasp-pain.org/PublicationsNews/Content.aspx?ItemNumber=1673&navItemNumber=677

Jia, Y., Gu, H., and Luo, Q. (2017). Sample entropy reveals an age-related reduction in the complexity of dynamic brain. *Sci. Rep.* 7:7990. doi: 10.1038/s41598-017-08565-y

Kuo, P. C., Chen, Y. T., Chen, Y. S., and Chen, L. F. (2017). Decoding the perception of endogenous pain from resting-state MEG. *Neuroimage* 144(Pt A), 1–11. doi: 10.1016/j.neuroimage.2016.09.040

Lakshminarasimhan, H., and Chattarji, S. (2012). Stress leads to contrasting effects on the levels of brain derived neurotrophic factor in the hippocampus and amygdala. *PLoS ONE* 7:e30481. doi: 10.1371/journal.pone.0030481

Lebedev, A. V., Kaelen, M., Lovden, M., Nilsson, J., Feilding, A., Nutt, D. J., et al. (2016). LSD-induced entropic brain activity predicts subsequent personality change. *Hum. Brain Mapp.* 37, 3203–3213. doi: 10.1002/hbm.23234

Lee, L. C., Tu, C. H., Chen, L. F., Shen, H. D., Chao, H. T., Lin, M. W., et al. (2014). Association of brain-derived neurotrophic factor gene Val66Met polymorphism with primary dysmenorrhea. *PLoS ONE* 9:e112766. doi: 10.1371/journal.pone.0112766

Lee, P. S., Low, I., Chen, Y. S., Tu, C. H., Chao, H. T., Hsieh, J. C., et al. (2017). Encoding of menstrual pain experience with theta oscillations in women with primary dysmenorrhea. *Sci. Rep.* 7:15977. doi: 10.1038/s41598-017-16039-4

Li, Z., Fang, Z., Hager, N., Rao, H., and Wang, Z. (2016). Hyper-resting brain entropy within chronic smokers and its moderation by Sex. *Sci. Rep.* 6:29435. doi: 10.1038/srep29435

Lin, Y. J. (2000). *Chinese Beck Anxiety Inventory*. Taipei: Chinese Behavioral Science Corporation.

Liu, J., Liu, H., Mu, J., Xu, Q., Chen, T., Dun, W., et al. (2017). Altered white matter microarchitecture in the cingulum bundle in women with primary dysmenorrhea: a tract-based analysis study. *Hum. Brain Mapp.* 38, 4430–4443. doi: 10.1002/hbm.23670

Liu, M. E., Huang, C. C., Chen, M. H., Yang, A. C., Tu, P. C., Yeh, H. L., et al. (2014). Effect of the BDNF Val66Met polymorphism on regional gray matter volumes and cognitive function in the Chinese population. *Neuromol. Med.* 16, 127–136. doi: 10.1007/s12017-013-8265-7

Liu, P., Liu, Y., Wang, G., Li, R., Wei, Y., Fan, Y., et al. (2017). Changes of functional connectivity of the anterior cingulate cortex in women with primary dysmenorrhea. *Brain Imaging Behav.* 12, 710–717. doi: 10.1007/s11682-017-9730-y

Liu, P., Yang, J., Wang, G., Liu, Y., Liu, X., Jin, L., et al. (2016). Altered regional cortical thickness and subcortical volume in women with primary dysmenorrhoea. *Eur. J. Pain* 20, 512–520. doi: 10.1002/ejp.753

Liu, Q., Chen, Y. F., Fan, S. Z., Abbod, M. F., and Shieh, J. S. (2017). EEG artifacts reduction by multivariate empirical mode decomposition and multiscale entropy for monitoring depth of anaesthesia during surgery. *Med. Biol. Eng. Comput.* 55, 1435–1450. doi: 10.1007/s11517-016-1598-2

Low, I., Kuo, P.-C., Liu, Y.-H., Tsai, C.-L., Chao, H.-T., Hsieh, J.-C., et al. (2017). Altered brain complexity in women with primary dysmenorrhea: a resting-state magneto-encephalography study using multiscale entropy analysis. *Entropy* 19:12. doi: 10.3390/e19120680

Ma, W. F., Liu, Y. C., Chen, Y. F., Lane, H. Y., Lai, T. J., and Huang, L. C. (2013). Evaluation of psychometric properties of the Chinese Mandarin version State-Trait Anxiety Inventory Y form in Taiwanese outpatients with anxiety disorders. *J. Psychiatr. Ment. Health Nurs.* 20, 499–507. doi: 10.1111/j.1365-2850.2012.01945.x

McDonough, I. M., and Nashiro, K. (2014). Network complexity as a measure of information processing across resting-state networks: evidence from the Human Connectome Project. *Front. Hum. Neurosci.* 8:409. doi: 10.3389/fnhum.2014.00409

Melzack, R. (1975). The McGill pain questionnaire: major properties and scoring methods. *Pain* 1, 277–299.

Melzack, R. (1983). *Pain Measurement and Assessment*. New York, NY: Raven Press.

Merighi, A., Salio, C., Ghirri, A., Lossi, L., Ferrini, F., Betelli, C., et al. (2008). BDNF as a pain modulator. *Prog. Neurobiol.* 85, 297–317. doi: 10.1016/j.pneurobio.2008.04.004

Merskey, H., and Bogduk, N. (2002). *Classification of Chronic Pain : Descriptions of Chronic Pain Syndromes and Definitions of Pain Terms, 2nd Edn (revised)*. Seattle, WA: IASP Press.

Mizuno, T., Takahashi, T., Cho, R. Y., Kikuchi, M., Murata, T., Takahashi, K., et al. (2010). Assessment of EEG dynamical complexity in Alzheimer's disease using multiscale entropy. *Clin. Neurophysiol.* 121, 1438–1446. doi: 10.1016/j.clinph.2010.03.025

Mogil, J. S. (2012). Sex differences in pain and pain inhibition: multiple explanations of a controversial phenomenon. *Nat. Rev. Neurosci.* 13:859–866. doi: 10.1038/nrn3360

Naert, G., Ixart, G., Maurice, T., Tapia-Arancibia, L., and Givalois, L. (2011). Brain-derived neurotrophic factor and hypothalamic-pituitary-adrenal axis adaptation processes in a depressive-like state induced by chronic restraint stress. *Mol. Cell. Neurosci.* 46, 55–66. doi: 10.1016/j.mcn.2010.08.006

Nakagawa, T. T., Jirsa, V. K., Spiegler, A., McIntosh, A. R., and Deco, G. (2013). Bottom up modeling of the connectome: linking structure and function in the resting brain and their changes in aging. *Neuroimage* 80, 318–329. doi: 10.1016/j.neuroimage.2013.04.055

Nelson, M., Dehaene, S., Pallier, C., and Hale, J. (2017). "Entropy Reduction correlates with temporal lobe activity," in *The Workshop on Cognitive Modeling & Computational Linguistics* (Valencia).

Nijs, J., Meeus, M., Versijpt, J., Moens, M., Bos, I., Knaepen, K., et al. (2015). Brain-derived neurotrophic factor as a driving force behind neuroplasticity in neuropathic and central sensitization pain: a new therapeutic target? *Expert Opin. Ther. Targets* 19, 565–576. doi: 10.1517/14728222.2014.994506

Notaras, M., Hill, R., and van den Buuse, M. (2015). The BDNF gene Val66Met polymorphism as a modifier of psychiatric disorder susceptibility: progress and controversy. *Mol. Psychiatry* 20:916. doi: 10.1038/mp.2015.27

Okazaki, R., Takahashi, T., Ueno, K., Takahashi, K., Ishitobi, M., Kikuchi, M., et al. (2015). Changes in EEG complexity with electroconvulsive therapy in a patient with autism spectrum disorders: a multiscale entropy approach. *Front. Hum. Neurosci.* 9:106. doi: 10.3389/fnhum.2015.00106

Park, C. H., Kim, J., Namgung, E., Lee, D. W., Kim, G. H., Kim, M., et al. (2017). The BDNF Val66Met polymorphism affects the vulnerability of the brain structural network. *Front. Hum. Neurosci.* 11:400. doi: 10.3389/fnhum.2017.00400

Park, H., and Poo, M.- M. (2013). Neurotrophin regulation of neural circuit development and function. *Nat. Rev. Neurosci.* 14, 7–23. doi: 10.1038/nrn3379

Pattwell, S. S., Bath, K. G., Perez-Castro, R., Lee, F. S., Chao, M. V., and Ninan, I. (2012). The BDNF Val66Met polymorphism impairs synaptic transmission and plasticity in the infralimbic medial prefrontal cortex. *J. Neurosci.* 32, 2410–2421. doi: 10.1523/JNEUROSCI.5205-11.2012

Petryshen, T. L., Sabeti, P. C., Aldinger, K. A., Fry, B., Fan, J. B., Schaffner, S. F., et al. (2010). Population genetic study of the brain-derived neurotrophic factor (BDNF) gene. *Mol. Psychiatry* 15, 810–815. doi: 10.1038/mp.2009.24

Pezawas, L., Verchinski, B. A., Mattay, V. S., Callicott, J. H., Kolachana, B. S., Straub, R. E., et al. (2004). The brain-derived neurotrophic factor val66met polymorphism and variation in human cortical morphology. *J. Neurosci.* 24, 10099–10102. doi: 10.1523/JNEUROSCI.2680-04.2004

Pinheiro, E. S., de Queiros, F. C., Montoya, P., Santos, C. L., do Nascimento, M. A., Ito, C. H., et al. (2016). Electroencephalographic patterns in chronic pain: a systematic review of the literature. *PLoS ONE* 11:e0149085. doi: 10.1371/journal.pone.0149085

Ploner, M., Sorg, C., and Gross, J. (2017). Brain rhythms of pain. *Trends Cogn. Sci.* 21, 100–110. doi: 10.1016/j.tics.2016.12.001

Reddy, S. Y., Rasmussen, N. A., Fourie, N. H., Berger, R. S., Martino, A. C., Gill, J., et al. (2014). Sleep quality, BDNF genotype and gene expression

in individuals with chronic abdominal pain. *BMC Med. Genomics* 7:61. doi: 10.1186/s12920-014-0061-1

Richman, J. S., and Moorman, J. R. (2000). Physiological time-series analysis using approximate entropy and sample entropy. *Am. J. Physiol. Heart Circ. Physiol.* 278, H2039–2049. doi: 10.1152/ajpheart.2000.278.6.H2039

Rorden, C., and Brett, M. (2000). Stereotaxic display of brain lesions. *Behav. Neurol.* 12, 191–200. doi: 10.1155/2000/421719

Sasi, M., Vignoli, B., Canossa, M., and Blum, R. (2017). Neurobiology of local and intercellular BDNF signaling. *Pflügers Archi. Eur. J. Physiol.* 469, 593–610. doi: 10.1007/s00424-017-1964-4

Sitges, C., Bornas, X., Llabres, J., Noguera, M., and Montoya, P. (2010). Linear and nonlinear analyses of EEG dynamics during non-painful somatosensory processing in chronic pain patients. *Int. J. Psychophysiol.* 77, 176–183. doi: 10.1016/j.ijpsycho.2010.05.010

Smith, S. M., and Vale, W. W. (2006). The role of the hypothalamic-pituitary-adrenal axis in neuroendocrine responses to stress. *Dialogues Clin. Neurosci.* 8, 383–395.

Song, D., Chang, D., Zhang, J., Peng, W., Shang, Y., Gao, X., et al. (2018). Reduced brain entropy by repetitive transcranial magnetic stimulation on the left dorsolateral prefrontal cortex in healthy young adults. *Brain Imaging Behav.* doi: 10.1007/s11682-018-9866-4. [Epub ahead of print].

Stefani, L. C., Torres, I. L., de Souza, I. C., Rozisky, J. R., Fregni, F., and Caumo, W. (2012). BDNF as an effect modifier for gender effects on pain thresholds in healthy subjects. *Neurosci. Lett.* 514, 62–66. doi: 10.1016/j.neulet.2012.02.057

Sutherland, H. G., Maher, B. H., Rodriguez-Acevedo, A. J., Haupt, L. M., and Griffiths, L. R. (2014). Investigation of brain-derived neurotrophic factor (BDNF) gene variants in migraine. *Headache* 54, 1184–1193. doi: 10.1111/head.12351

Tapia-Arancibia, L., Rage, F., Givalois, L., and Arancibia, S. (2004). Physiology of BDNF: focus on hypothalamic function. *Front. Neuroendocrinol.* 25, 77–107. doi: 10.1016/j.yfrne.2004.04.001

Tingting, Y., Lijuan, W., Weihong, K., Jiajun, X., Suping, L., Jie, C., et al. (2014). Brain-derived neurotrophic factor Val66Met polymorphism association with antidepressant efficacy: a systematic review and meta-analysis. *Asia-Pacific Psychiatry* 6, 241–251. doi: 10.1111/appy.12148

Tolwani, R. J., Buckmaster, P. S., Varma, S., Cosgaya, J. M., Wu, Y., Suri, C., et al. (2002). BDNF overexpression increases dendrite complexity in hippocampal dentate gyrus. *Neuroscience* 114, 795–805. doi: 10.1016/S0306-4522(02)00301-9

Tononi, G., Sporns, O., and Edelman, G. M. (1994). A measure for brain complexity: relating functional segregation and integration in the nervous system. *Proc. Natl. Acad. Sci. U.S.A.* 91, 5033–5037. doi: 10.1073/pnas.91.11.5033

Tsai, S.-J. (2018). Critical issues in BDNF Val66Met genetic studies of neuropsychiatric disorders. *Front. Mol. Neurosci.* 11:156. doi: 10.3389/fnmol.2018.00156

Tseng, H. M., Lu, J. F., and Gandek, B. (2003). Cultural issues in using the SF-36 Health Survey in Asia: results from Taiwan. *Health Qual. Life Outcomes* 1:72. doi: 10.1186/1477-7525-1-72

Tu, C. H., Niddam, D. M., Chao, H. T., Chen, L. F., Chen, Y. S., Wu, Y. T., et al. (2010). Brain morphological changes associated with cyclic menstrual pain. *Pain* 150, 462–468. doi: 10.1016/j.pain.2010.05.026

Tu, C. H., Niddam, D. M., Yeh, T. C., Lirng, J. F., Cheng, C. M., Chou, C. C., et al. (2013). Menstrual pain is associated with rapid structural alterations in the brain. *Pain* 154, 1718–1724. doi: 10.1016/j.pain.2013.05.022

Tzourio-Mazoyer, N., Landeau, B., Papathanassiou, D., Crivello, F., Etard, O., Delcroix, N., et al. (2002). Automated anatomical labeling of activations in SPM using a macroscopic anatomical parcellation of the MNI MRI single-subject brain. *Neuroimage* 15, 273–289. doi: 10.1006/nimg.2001.0978

Valencia, J., Melia, U., Vallverd,ú, M., Borrat, X., Jospin, M., Jensen, E., et al. (2016). Assessment of nociceptive responsiveness levels during sedation-analgesia by entropy analysis of EEG. *Entropy* 18:103. doi: 10.3390/e18030103

Vasant, D. H., Payton, A., Algladi, T., Mistry, S., and Hamdy, S. (2011). Early evidence implicating the brain derived neurotrophic factor (BDNF) val66met polymorphism in the pathogenesis of oesophageal visceral sensitivity. *Gut* 60(Suppl. 1), A166–A166. doi: 10.1136/gut.2011.239301.353

Vossen, H., Kenis, G., Rutten, B., van Os, J., Hermens, H., and Lousberg, R. (2010). The Genetic Influence on the Cortical Processing of Experimental Pain and the Moderating Effect of Pain Status. *PLOS ONE* 5:e13641. doi: 10.1371/journal.pone.0013641

Vyas, A., Mitra, R., Shankaranarayana Rao, B. S., and Chattarji, S. (2002). Chronic stress induces contrasting patterns of dendritic remodeling in hippocampal and amygdaloid neurons. *J. Neurosci.* 22, 6810–6818. doi: 10.1523/JNEUROSCI.22-15-06810.2002

Wang, B., Niu, Y., Miao, L., Cao, R., Yan, P., Guo, H., et al. (2017). Decreased complexity in Alzheimer's disease: resting-state fMRI evidence of brain entropy mapping. *Front. Aging Neurosci.* 9:378. doi: 10.3389/fnagi.2017.00378

Wang, D. J. J., Jann, K., Fan, C., Qiao, Y., Zang, Y.-F., Lu, H., et al. (2018). Neurophysiological basis of multi-scale entropy of brain complexity and its relationship with functional connectivity. *Front. Neurosci.* 12:352. doi: 10.3389/fnins.2018.00352

Wang, Z., Li, Y., Childress, A. R., and Detre, J. A. (2014). Brain entropy mapping using fMRI. *PLOS ONE* 9:e89948. doi: 10.1371/journal.pone.0089948

Wei, S. Y., Chao, H. T., Tu, C. H., Li, W. C., Low, I., Chuang, C. Y., et al. (2016a). Changes in functional connectivity of pain modulatory systems in women with primary dysmenorrhea. *Pain* 157, 92–102. doi: 10.1097/j.pain.0000000000000340

Wei, S. Y., Chao, H. T., Tu, C. H., Lin, M. W., Li, W. C., Low, I., et al. (2016b). The BDNF Val66Met polymorphism is associated with the functional connectivity dynamics of pain modulatory systems in primary dysmenorrhea. *Sci. Rep.* 6:23639. doi: 10.1038/srep23639

Wei, S. Y., Chen, L. F., Lin, M. W., Li, W. C., Low, I., Yang, C. J., et al. (2017). The OPRM1 A118G polymorphism modulates the descending pain modulatory system for individual pain experience in young women with primary dysmenorrhea. *Sci. Rep.* 7:39906. doi: 10.1038/srep 39906

Weidenfeld, J., and Ovadia, H. (2017). "The role of the amygdala in regulating the hypothalamic-pituitary-adrenal axis," in *The Amygdala: Where Emotions Shape Perception, Learning and Memories*, ed B. Ferry (London: IntechOpen), 173–186. doi: 10.5772/67828

Weinhold, B. (2006). Epigenetics: the science of change. *Environ. Health Perspect.* 114, A160–167. doi: 10.1289/ehp.114-a160

Wilson, D., and Lipsey, M. (2001). *Practical Meta-Analysisi Effect Size Calculator [Online]*. Available online at: https://www.campbellcollaboration.org/escalc/html/EffectSizeCalculator-SMD2.php

Wu, T. H., Tu, C. H., Chao, H. T., Li, W. C., Low, I., Chuang, C. Y., et al. (2016). Dynamic changes of functional pain connectome in women with primary dysmenorrhea. *Sci. Rep.* 6:24543. doi: 10.1038/srep24543

Wu, W.-T., Lin, H.-T., Wang, J.-D., and Kuo, C.-C. (1999). *Basic Personality Inventory*. Taipei: Psychological Publishing Co., Ltd.

Yang, A. C., and Tsai, S. J. (2013). Is mental illness complex? From behavior to brain. *Prog. Neuropsychopharmacol. Biol. Psychiatry* 45, 253–257. doi: 10.1016/j.pnpbp.2012.09.015

Yang, A. C., Wang, S. J., Lai, K. L., Tsai, C. F., Yang, C. H., Hwang, J. P., et al. (2013). Cognitive and neuropsychiatric correlates of EEG dynamic complexity in patients with Alzheimer's disease. *Prog. Neuropsychopharmacol. Biol. Psychiatry* 47, 52–61. doi: 10.1016/j.pnpbp.2013.07.022

Yao, Y., Lu, W. L., Xu, B., Li, C. B., Lin, C. P., Waxman, D., et al. (2013). The increase of the functional entropy of the human brain with age. *Sci. Rep.* 3:2853. doi: 10.1038/srep02853

Yap, J. C., Lau, J., Chen, P. P., Gin, T., Wong, T., Chan, I., et al. (2008). Validation of the Chinese pain catastrophizing scale (HK-PCS) in patients with chronic pain. *Pain Med.* 9, 186–195. doi: 10.1111/j.1526-4637.2007.00307.x

Zhou, F., Zhuang, Y., Gong, H., Zhan, J., Grossman, M., and Wang, Z. (2016). Resting state brain entropy alterations in relapsing remitting multiple sclerosis. *PLoS ONE* 11:e0146080. doi: 10.1371/journal.pone.0146080

Conflict of Interest Statement: The authors declare that the research was conducted in the absence of any commercial or financial relationships that could be construed as a potential conflict of interest.

frontiers in Neuroscience

ORIGINAL RESEARCH
published: 27 November 2018
doi: 10.3389/fnins.2018.00869

Imbalance of Functional Connectivity and Temporal Entropy in Resting-State Networks in Autism Spectrum Disorder: A Machine Learning Approach

Robert X. Smith[1]*, *Kay Jann*[2], *Mirella Dapretto*[3] and *Danny J. J. Wang*[2]

[1] NeuroImaging Laboratories (NIL) at Washington University School of Medicine, Washington University in Saint Louis, Saint Louis, MO, United States, [2] Keck School of Medicine of USC, University of Southern California, Los Angeles, CA, United States, [3] Department of Psychiatry and Biobehavioral Sciences, University of California Los Angeles, Los Angeles, CA, United States

OPEN ACCESS

Edited by:
Bradley J. MacIntosh, Sunnybrook Research Institute (SRI), Canada

Reviewed by:
Seok Jun Hong, Child Mind Institute, United States
Casey Paquola, Montreal Neurological Institute and Hospital, McGill University, Canada
Sarah Atwi, Sunnybrook Research Institute (SRI), Canada

***Correspondence:**
Robert X. Smith
smith.x.robert@gmail.com

Specialty section:
This article was submitted to Brain Imaging Methods, a section of the journal Frontiers in Neuroscience

Received: *01 June 2018*
Accepted: *07 November 2018*
Published: *27 November 2018*

Citation:
Smith RX, Jann K, Dapretto M and Wang DJJ (2018) Imbalance of Functional Connectivity and Temporal Entropy in Resting-State Networks in Autism Spectrum Disorder: A Machine Learning Approach. Front. Neurosci. 12:869. doi: 10.3389/fnins.2018.00869

Background: Two approaches to understanding the etiology of neurodevelopmental disorders such as Autism Spectrum Disorder (ASD) involve network level functional connectivity (FC) and the dynamics of neuronal signaling. The former approach has revealed both increased and decreased FC in individuals with ASD. The latter approach has found high frequency EEG oscillations and higher levels of epilepsy in children with ASD. Together, these findings have led to the hypothesis that atypical excitatory-inhibitory neural signaling may lead to imbalanced association pathways. However, simultaneously reconciling local temporal dynamics with network scale spatial connectivity remains a difficult task and thus empirical support for this hypothesis is lacking.

Methods: We seek to fill this gap by combining two powerful resting-state functional MRI (rs-fMRI) methods—functional connectivity (FC) and wavelet-based regularity analysis. Wavelet-based regularity analysis is an entropy measure of the local rs-fMRI time series signal. We examined the relationship between the RSN entropy and integrity in individuals with ASD and controls from the Autism Brain Imaging Data Exchange (ABIDE) cohort using a putative set of 264 functional brain regions-of-interest (ROI).

Results: We observed that an imbalance in intra- and inter-network FC across 11 RSNs in ASD individuals ($p = 0.002$) corresponds to a weakened relationship with RSN temporal entropy ($p = 0.02$). Further, we observed that an estimated RSN entropy model significantly distinguished ASD from controls ($p = 0.01$) and was associated with level of ASD symptom severity ($p = 0.003$).

Conclusions: Imbalanced brain connectivity and dynamics at the network level coincides with their decoupling in ASD. The association with ASD symptom severity presents entropy as a potential biomarker.

Keywords: complexity, resting-state, fMRI, connectivity, dynamics, Autism Spectrum Disorders

INTRODUCTION

Autism spectrum disorder (ASD) impacts the neurodevelopment of networks underlying social function and communication as well as sensorimotor abilities (APA, 1994). ASD has been linked to imbalanced functional connectivity (FC) in the brain (Jeste, 2011). FC measures synchronous neuronal signaling and has been used to identify several resting-state networks (RSNs) (Greicius et al., 2004; Seeley et al., 2009). Studies have reported intra- and inter-network FC among several RSNs to be either reduced (Villalobos et al., 2005; Welchew et al., 2005; Kana et al., 2006, 2007; Kleinhans et al., 2008; Uddin et al., 2013) or increased (Anderson et al., 2011; Supekar et al., 2013; Uddin et al., 2013) in ASD. Most work has focused on intra-network FC for specific RSNs. Notably, several studies have reported that the Default Mode Network (DMN), a set of brain regions that exhibit increased activity in the absence of an external stimuli (Raichle and MacLeod, 2001), exhibits both increased and decreased FC in ASD (Jann et al., 2015). However, research focused on a specific network is inherently limited at delineating the mechanisms of brain disruption at the global level. A growing number of reports have also shown that inter-network FC is also strongly impacted in ASD (Belmonte et al., 2004; Courchesne et al., 2007; Rudie et al., 2013; Cerliani et al., 2015).

Imbalance of excitation and inhibition within neural microcircuitry may impair the formation of intra- and inter-network connections that typify the segregation of RSNs during typical neurodevelopment. Hyper-excitability (elevated excitation/inhibition balance) has been hypothesized (E/I hypothesis) as an underlying mechanism for behavioral deficits in ASD (Rubenstein and Merzenich, 2003; Chao et al., 2010; Vattikuti and Chow, 2010; Yizhar et al., 2011). However, reconciling cortical dynamics with spatial network connectivity remains a difficult task. Resting-state functional MRI (rs-fMRI) is a widely used method offering a balance between temporal and spatial resolution. The rs-fMRI time series signal represents intrinsic blood oxygen level dependent (BOLD) activity that is correlated with neuronal activation (Logothetis et al., 2001). Evidence of spontaneous BOLD fluctuations suggests that stochastic processes govern neuronal activity (He et al., 2010). However, most studies investigate brain connectivity using FC analysis (e.g., mean intra- and inter-network correlations) which carries little information about the dynamic structure typifying neuronal activity. The relationship between FC and brain dynamics in ASD is not well-understood.

Recently, non-linear statistical measures based on approximate entropy (Pincus, 1991) and sample entropy (Richman and Moorman, 2000; Costa et al., 2002) have been used to investigate the dynamic structure and complexity of the brain by characterizing the recurring patterns of temporal fluctuations (Smith et al., 2014). A time series containing many repetitive patterns has relatively small entropy. Conversely, a time series containing few repetitive patterns has a higher entropy. Entropy studies have shown changes in dynamics in aging (Liu et al., 2012; Yang et al., 2013a), Alzheimer's disease (Yang et al., 2013b), schizophrenia (Takahashi et al., 2010), and depression (Pei-Shan Ho et al., 2018). Here we investigate the relationship between FC and brain dynamics at the network level using a recently developed wavelet-based regularity analysis (Smith et al., 2015). This approach to assess network dynamics is based on noise estimation capabilities of the wavelet transform to measure recurrent temporal pattern stability within the rs-fMRI signal across multiple temporal scales. The method consists of performing a stationary wavelet transform (SWT) to preserve signal structure, followed by construction of "lagged" subsequences to adjust for correlated features, and finally the calculation of sample entropy across wavelet scales based on an "objective" estimate of noise level at each scale.

Previous applications of wavelet-based regularity analysis showed the DMN, the most 'active' areas of the brain at rest (De Luca et al., 2006), exhibited higher rs-fMRI signal entropy than rest of the brain (Smith et al., 2015). This suggested increased rs-fMRI signal activity is characterized by not only increased amplitudes, but also more complex trajectories through a diverse array of temporal patterns. Further investigation of wavelet-based regularity suggested it may be sensitive to neurobiological changes that underscore cognitive dysfunction. Specifically, widespread entropy differences in the DMN and executive control networks were detected between individuals with mild cognitive impairment and healthy controls. Taken together, these observations suggest wavelet-based regularity analysis is a promising measure of the rs-fMRI signal's dynamic structure.

Leveraging the spatial resolution of rs-MRI, we use machine learning to model the FC-entropy relationship across cortical and subcortical RSNs. We hypothesized that FC measures would be associated with RSN entropy in both ASD and TD participants. However, per the E/I hypothesis, we expected the FC-entropy relationship to be significantly weaker in ASD participants.

METHODS

Participants

Resting-state fMRI (rs-fMRI) and structural imaging data of 85 individuals with ASD and 163 matched controls from multiple sites of the ABIDE data set (Di Martino et al., 2014) were included in this study for a total of $N = 248$ individuals. Inclusion criteria were: (A) a T1-weighted structural MRI image, (B) a resting-state functional MRI (rs-fMRI) with full cortical coverage, (C) a full-scale IQ > 100, and (D) a mean framewise displacement (FD)(Power et al., 2012) of >0.10 mm. Additionally, individuals for a site were included if a total of at least 7 ASD and 7 control participants met the above inclusion criteria. Demographic information is summarized in **Table 1**. Details of acquisition, informed consent, site-specific protocols, specific diagnostic criteria for each data set can be found at the ABIDE website http://fcon_1000.projects.nitrc.org/indi/abide/index.html. Institutional Review Board approval was provided by each site.

MRI Data Analysis

Structural MRI

T1-weighted structural images were transformed to standard Montreal Neurological Institute (MNI) 2 mm space using the

TABLE 1 | Eighty-five individuals with ASD (18.0 yrs, 76 male, IQ = 117, FD = 0.065) and 163 TD children (17.4 yrs, 132 male, IQ = 115.8, FD = 0.064).

Demographics (Mean ± SD)	Controls ($n = 163$)	ASD ($n = 85$)	*P*-value
Age (years)	17.4 ± 8.0	18.0 ± 10.2	0.84
Sex (% male)	81	89	
IQ	115.8 ± 9.0	117 ± 11.3	0.76
Motion (mm)	0.064 ± 0.02	0.065 ± 0.02	0.70
ADOS-G (score)	NA	10.1 ± 5.4	

suite of tools available in the FMRIB software library (FSL) 5.0.9 (http://www.fmrib.ox.ac.uk/fsl/). First, skull stripping was performed using the brain extraction tool [BET (Smith, 2002)]. Second, a 12 degrees-of-freedom affine transform from the brain extracted structural image to the MNI 2 mm reference image using FMRIB's linear image registration tool (FLIRT) (Jenkinson et al., 2002). The computed affine transform was applied to the original (non-brain extracted) structural image. Finally, non-linear warping was applied to the linearly registered original structural image using the FMRIB's non-linear image registration tool (FNIRT) (Andersson et al., 2007). Tissue segmentation was performed using FMRIB's automated segmentation tool (FAST) (Zhang et al., 2001). White matter and ventricle masks were created for later use in rs-fMRI nuisance regression. Visual inspection was performed at each stage for each individual to ensure successful brain extraction, tissue segmentation, and normalization.

Resting-State Functional MRI (rs-fMRI)

The rs-fMRI data were pre-processed as follows. First, correction for rigid body head motion was conducted using motion correction FLIRT (MCFLIRT) (Jenkinson et al., 2002) (default parameters, with final sinc interpolation). Second, an individual's mean rs-fMRI image was aligned with their structural image via a 7 degree-of-freedom affine registration using FLIRT, and the transformation was applied to all volumes in the time series. Frames with excessive motion were identified and scrubbed (Power et al., 2012) if the framewise displacement exceeded 0.3 mm. Individuals with >10% of their frames flagged for scrubbing were excluded. The mean framewise displacement of controls (FD = 0.064) was not significantly different ($W = 7{,}135$, $p = 0.74$; **Table 1**) compared to ASD participants (FD = 0.065) as determined by the Wilcoxon rank-sum test. The time series was band-pass filtered removing >0.1 and <0.01 Hz. Lastly, voxel times series were linear detrended, and reduction of spurious variance was implemented by linear regression of nuisance waveforms derived from head motion (including motion derivatives) and ROI extracted time series in white matter, cerebrospinal fluid (CSF), and global signal. White matter and CSF time series were obtained similar to Chang and Glover (2009) by reverse-normalizing 6 mm spheres at MNI coordinates (26, −12, 35) and (19, −33, 18), respectively, to the native space of each individual. Individual specific white matter and ventricle masks were used to ensure no signal of interest in gray matter was included. Spatially smoothing was performed at the end with a 7 mm FWHM Gaussian filter.

Functional Connectivity Principal Components Analysis

An intra- and inter-network-wise method for analyzing distributed connectivity patterns was employed. Our analyses focused on a putative set of 264 functional regions-of-interest (ROIs) previously organized into 11 RSNs (Power et al., 2011). ROIs were defined as 10 mm diameter spheres whose center coordinates are given in MNI atlas space (Power et al., 2011). For each individual, we computed a 264 × 264 FC matrix by: (i) MNI atlas transformation of the pre-processed functional data, (ii) computation of the mean voxel time series within each ROI, (iii) and computation of the pairwise correlation between all ROI time series.

Data reduction was performed in two steps to isolate a metric of distributed FC changes. First, using each ROI's RSN designation (Power et al., 2011), we computed the average intra- and inter-network correlation for each RSN yielding a reduced 11 × 11 matrix for each individual. The 11 intra-network and $\frac{11\times(11-1)}{2} = 55$ inter-network averages (total of 11 + 55 = 66) were compiled for all $N = 248$ individuals into a single 248 × 66 matrix M. Second, a principal component analysis (PCA) of the matrix M was performed by singular value decomposition (SVD):

$$\mathrm{M} = \mathrm{UAV}^{\mathrm{T}}. \tag{1}$$

PCA is a simple eigenvector-based multivariate analysis that reveals the internal data structure in a way that best explains its variance. A single PCA including both control and ASD individuals provides a set of components common to both groups. This avoids the latent root and vector problem (Krzanowski, 1979) that occurs when separate PCAs are performed for each group. The principal components $c_n = UA$ were obtained by projection of the RSN averages onto the principal vectors V. The primary component, c_1, was selected. c_1-values vary along the primary vector V_1. Variation along this vector explained 29% of the inter-individual RSN variance.

Wavelet-Based Regularity Analysis

We computed the entropy, H, of the mean rs-fMRI time series for the same 264 ROIs used in the FC analysis using a previously developed wavelet-based regularity analysis (Smith et al., 2015). This approach is sensitive to, in addition to any non-linear structure, the presence of intrinsic non-stationary processes (i.e., how variable the moments of the signal distribution are over time) within the rs-fMRI signal (Chang and Glover, 2009). Non-stationary structure is preserved with high fidelity across multiple scales using the SWT using the WaveLab850 toolbox (Buckheit et al., 2005). The time series noise level is estimated from the highest frequency subband using wavelet-based de-noising schemes (Donoho and Johnstone, 1994; Donoho, 1995; Chang et al., 2000) and used to tune sensitivity to the entropy of the intrinsic signal. The regularity with which rs-fMRI signal patterns

recur is measured with Sample Entropy (Pincus, 1991):

$$H(m, r, N_m) = -\log\left(\frac{C^{m+1}(r)}{C^{m}(r)}\right), \quad (2)$$

where recurrence probability of m-length subsequences within a tolerance distance r is given by:

$$C^{m}(r) = \frac{1}{2}\sum_{q,p\neq q}^{N_m}\frac{\Theta(r)}{N_m(N_m-1)}. \quad (3)$$

N_m is the number of subsequences, Θ is the Heaviside function, and $r = r_0\sigma + t$ is the distance threshold for pattern similarity that depends on a scaling r_0 of the time series standard deviation σ and a scale-dependent threshold t based on the BayesShrink approach (Chang et al., 2000). Patterns were constructed from time-delayed points to account for the serial correlations present in rs-fMRI data. Pattern lengths were kept small to increase the total number of patterns and improve the statistical power. In this study, patterns of length m(+1) = 1(2) were compared using a distance threshold of $r_0 = 0.2$. The distance threshold, r_0, was selected using a procedure described previously (Smith et al., 2015). The entropy was computed for a range of thresholds, 0.1–0.3 with 0.05 increments. The r_0-value the maximized the range of observed entropy values across all individuals was selected. The mean entropy across two scales (0.031–0.063 and 0.063–0.13 Hz) for each of the 11 RSNs was obtained for each individual. The dyadic wavelet scales are based on the number of time points. Here, the scales most sensitive to the 0.01–0.10 Hz frequency band, where most slow-wave neuronal activity occurs, were selected.

Patterns containing one or more flagged frames were removed from consideration. Specifically, a binary time series for each individual equal in length to the rs-fMRI frames. Time points equaled one if a frame was flagged for excessive motion. A SWT was applied to this binary series. For each scale, m-length patterns were formed using the same parameters to form patterns for the rs-fMRI series. If any value in these patterns equal one, then the corresponding rs-fMRI pattern is removed from the wavelet-base regularity analysis.

Multilinear Regression Model

ASD and controls were pooled together and a multilinear regression model was used to evaluate the relationship between c_1 (FC PCA scores) and RSN entropies, H. Specifically, we modeled c_1 as:

$$c_1 = X_H\beta + \varepsilon, \quad (4)$$

where X_H is the 248 × 11 matrix of network entropies for the 11 RSNs for all 248 individuals (both ASD and control), β are the model coefficients to be estimated, and ε are the residuals to be minimized. Importantly, no information about group membership (i.e., ASD or control) has been explicitly passed to the model.

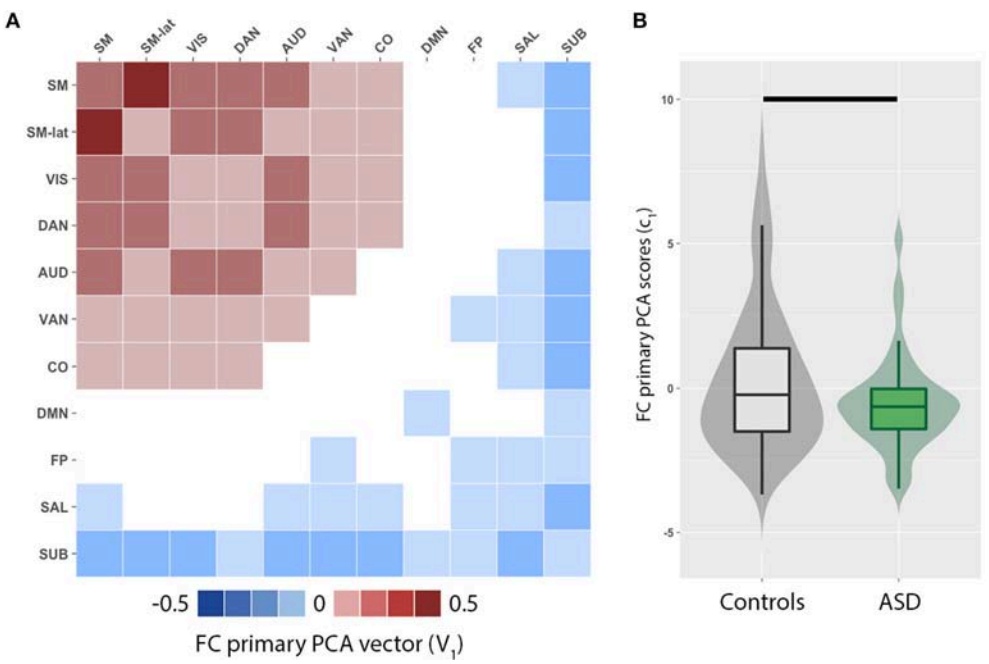

FIGURE 1 | Principal component analysis (PCA) reveals imbalance in functional connectivity (FC) across cortical and subcortical resting-state networks (RSN). **(A)** Primary PCA vector, V_1, is positively weighted by the intra- and inter-network FC among several RSNs including the sensorimotor (SM, SM-lat), visual (VIS), auditory (AUD), dorsal attention (DAN), ventral attention (VAN), and cingulo-opercular (CO). Conversely, the intra- and inter-network FC of the default mode (DMN), salience (SAL), fronto-parietal (FP), and subcortical (SUB) RSNs are negatively weighted. **(B)** Violin and box plots of the primary PCA component score distributions for controls (gray) and individuals with autism spectrum disorders (ASD; green). Horizontal black line denotes significant difference ($p = 0.002$).

Elastic net regularization was performed to avoid overfitting using the "glmnet" package (Friedman et al., 2010) within the R statistical computing language (R Core Team, 2017). Elastic net regularization is a common machine learning approach to building linear models that combines L1 (lasso; Tibshirani, 1996) and L2 (ridge; Tikhonov et al., 1995) regularization. L1 regularization tends to produce sparse solutions by selecting predictors strongly correlated with the outcome and zeroing out the remaining. L2 regularization is suited to deal with high collinearity among predictors. Estimated coefficients, $\hat{\beta}$, from elastic net regularization are formulated as:

$$\hat{\beta} = \min_{\beta} \left(\|c_1 - X_H\beta\|^2 + \frac{\lambda}{2}\left[(1-\alpha)\,\|\beta\|_2^2 + 2\alpha\,\|\beta\|_1\right]\right) \quad (5)$$

where λ is a model complexity parameter, and α is a tradeoff between L1 ($\alpha = 1$) and L2 ($\alpha = 0$) regularization. $\hat{\beta}$values represent the importance of certain RSN entropies over others. Model validation was performed using 10-fold cross validation. A grid search for the minimum mean squared error (MSE) was performed across λ and αvalues.

Statistical Analyses

FC PCA score and entropy model distributions for ASD and control individuals were compared using the Wilcoxon rank-sum test. A *post-hoc* linear regression analysis was used to test for an interaction of entropy model estimates, $c_{1H} = X_H\hat{\beta}$, by group (i.e., ASD vs. controls) in predicting c_1: $c_1 = \gamma_0 + \gamma_1 G + \gamma_2 c_{1H} + \gamma_3 G c_{1H} + \varepsilon_r$. Here γ_i are the regression coefficients, G is a binary variable representing ASD individuals or controls, and ε_r are the regression residuals. The regression coefficient γ_3 measures the entropy model by group interaction and characterizes the relative model performance between groups. The associations between c_1 and c_{1H} with the individuals' ADOS-G severity scores (Lord et al., 2000) (for individuals with available scores) were computed using a Pearson correlation. The mean age difference between ASD and controls was 0.6 years, and not statistically significant ($W = 6{,}816$, $p = 0.66$; **Table 1**). As such, age was not included as a regressor to avoid loss of statistical power in detecting entropy related group differences.

RESULTS

Imbalance in Functional Connectivity

We observed a distributed set of intra- and inter-network FC. The brain networks that exhibit the most inter-individual variation were evaluated by principal component analysis of functional connectivity matrices for ASD and control groups. The primary PCA vector V_1 (**Figure 1A**) is positively weighted by the intra- and inter-network FC among several RSNs including the sensorimotor (SM, SM-lat), visual (VIS), auditory (AUD), dorsal attention (DAN), ventral attention (VAN), and cingulo-opercular (CO). Conversely, the intra- and inter-network FC of the default mode (DMN), salience (SAL), fronto-parietal (FP),

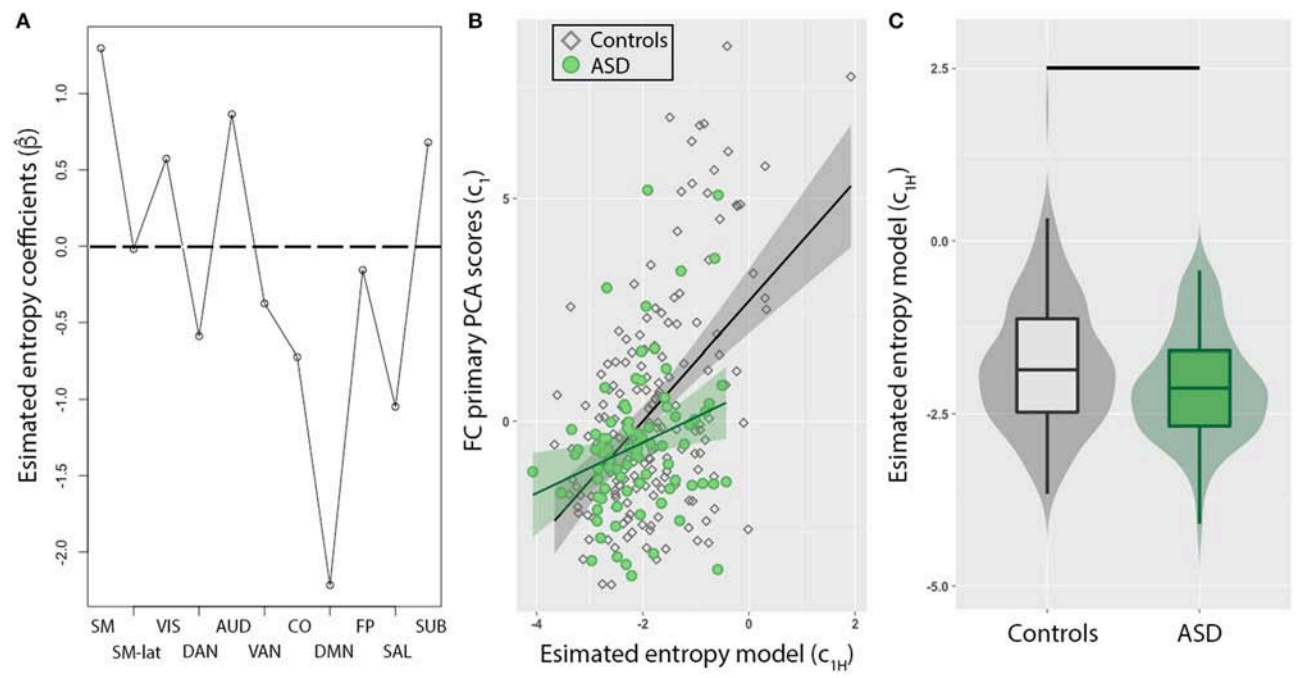

FIGURE 2 | Resting-state network (RSN) entropy is a stronger predictor of functional connectivity (FC) for TD compared to ASD. **(A)** Model coefficients determined from elastic net method show sensory networks (SM, SM-lat, VIS, AUD, SUB) are positively weighted, while higher order cognitive networks (DMN, SAL, CO, DAN, VAN, FP) are negatively weighted. **(B)** Scatter plot showing the relationship between FC (PCA primary component projections) and entropy model for control (diamonds) and ASD (circles) individuals. The model was significantly weaker in predicting FC in ASD compared to controls ($p = 0.02$). **(C)** Box plot of entropy model distributions for control (gray) and ASD (green) groups. Horizontal black line denotes significant difference ($p = 0.01$).

and subcortical (SUB) RSNs were negatively weighted. FC PCA scores, c_1, significantly differed between ASD and control groups (**Figure 1B**; $W = 5{,}846$, $p = 0.04$).

Imbalance in Brain Entropy

To evaluate whether this imbalance in intra- and inter-network FC in ASD individuals corresponds to dynamical changes, the mean entropy for each of the 11 RSNs were included as predictors to model FC PCA scores (c_1) of all individuals. First, we observed that a combination of most RSNs (**Figure 2A**) reliably predicted c_1. The minimum MSE computed from a 10-fold cross validation was $11.4 \pm 7.2\%$ of c_1 variance, and was observed for $\alpha = 0.15$. The DMN exhibited the strongest weighting, but interestingly, estimated model coefficients ($\hat{\beta}$), for sensory networks (SM, SM-lat, VIS, AUD, SUB) were positively weighted, while higher order cognitive networks (DMN, SAL, CO, DAN, VAN, FP) were negatively weighted. Second, in a *post-hoc* linear regression analysis that included binary variable representing group (i.e., ASD vs. controls), we observed an interaction of group with c_{1H} in predicting c_1 (**Figure 2B**; $\gamma_3 = 0.82$, $t = 2.3$, standard error $= 0.35$, $p = 0.02$). Lastly, we observed c_{1H} were significantly different for ASD compared to controls (**Figure 2C**; $W = 5{,}628$, $p = 0.02$).

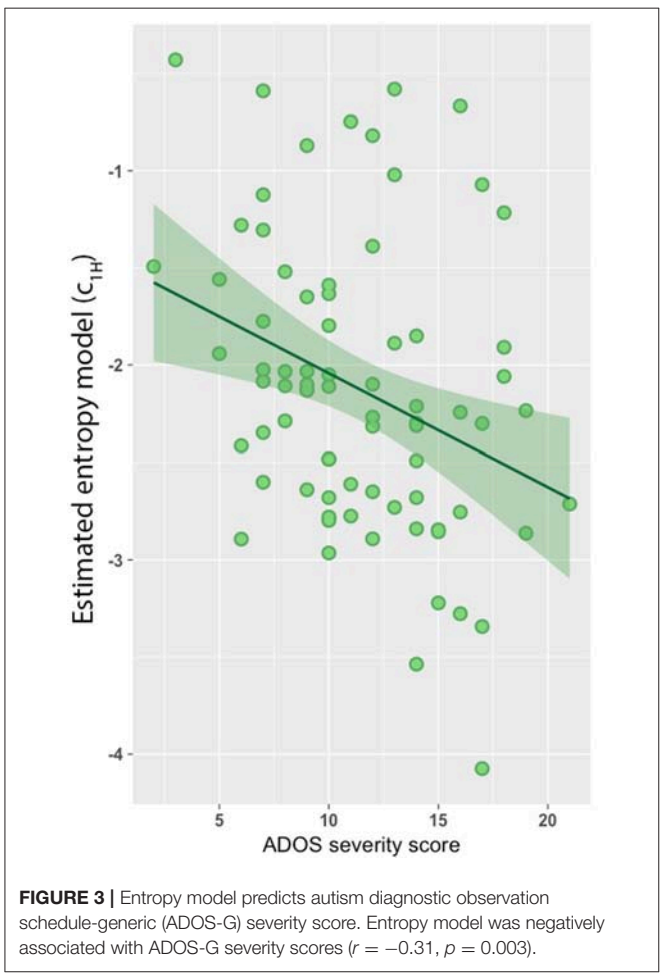

FIGURE 3 | Entropy model predicts autism diagnostic observation schedule-generic (ADOS-G) severity score. Entropy model was negatively associated with ADOS-G severity scores ($r = -0.31$, $p = 0.003$).

Severity Score Association

Lastly, we found a significant negative association between the estimated model predictors (c_{1H}) and severity scores based on the Autism Diagnostic Observation Schedule-Generic (ADOS-G; **Figure 3**; $r = -0.31$, $p = 0.003$). However, no association was observed between c_1 and ADOS-G severity scores.

DISCUSSION

Our findings revealed distributed alterations in FC across multiple RSNs in ASD individuals. Alterations in FC were characterized by negatively weighted sensory and positively weighted cognitive RSNs, suggesting an imbalance of intra- and inter-network FC in ASD. Linear modeling of these alterations in FC revealed a significant association with alterations in brain dynamics, as measured by the time series entropy of multiple RSNs. We observed the observed FC imbalance in ASD individuals was mirrored by a similar imbalance in brain dynamics. Specifically, alterations in brain dynamics were characterized by positively weighted sensory and negatively weighted cognitive RSNs. Alterations in the brain dynamics were further associated with level of symptom severity in individuals with ASD.

Our results provide insight into the impact that ASD has on the intra- and inter-network FC balance among several RSNs. Previous studies have reported hypo-connectivity in the VIS (Villalobos et al., 2005), SM (Mostofsky et al., 2009), and DAN/VAN (Belmonte et al., 2010) networks. Conversely, hyper-connectivity of the salience (Uddin et al., 2013) and subcortical (Padmanabhan et al., 2013; Jann et al., 2015) networks have also been reported. Consistent with these reports, we find imbalanced FC may be a whole-brain phenomenon distributed across multiple RSNs. Further, the imbalanced FC largely discriminated sensory from cognitive networks. Sensory networks primarily develop early during childhood while cognitive networks continue to develop into early adulthood (Somerville et al., 2010; Petanjek et al., 2011). Altered segregation of cognitive networks (as indexed by stronger inter-network connectivity) may reflect the atypical developmental trajectories (e.g., delayed or incomplete pruning process) seen in ASD (Penzes et al., 2011).

There is rapidly growing literature on the relationship between FC and brain dynamics (Hutchison et al., 2013a,b; Allen et al., 2014; Laumann et al., 2017). Here we found that, when taken together, the dynamics of 11 RSNs reliably predicted their engagement of distributed pattern of FC. The strongest contributors to the entropy model were the DMN, SM, and SAL networks. We note, the SM and SAL contributions to both the primary PCA vector and the entropy model were strong, and in both cases opposing each other. This suggests that changes in network dynamics largely follow local FC changes. This is consistent with histological studies reporting disorganized pyramidal cells, consistent with focal cortical dysplasia, extend across many cortical columns in such a fashion that impedes coordinated signaling to other regions in ASD (Casanova, 2007; Schmitz and Rezaie, 2008; Mosconi et al., 2009; Casanova et al.,

2013). Conversely, the DMN was a small contributor to the primary PCA vector, but was the largest contributor to the entropy model. This may reflect the tremendous heterogeneity that characterizes ASD (Courchesne et al., 2011). Specifically, both hypo- and hyper-connectivity have been reported within the DMN in individuals with ASD (Raichle and MacLeod, 2001), suggesting these opposing effects may have averaged each other out.

Overall, our results indicate FC and entropy provide complementary information regarding the spatiotemporal organization of the brain. Similar to FC, the entropy model discriminated sensory from cognitive networks. Interestingly our entropy model—rather than FC—was significantly associated with ASD symptom severity. Specifically, the time series signals in the negatively weighted cognitive networks (e.g., DMN, SAL) become less repetitive with increasing symptom severity, suggesting increased excitatory behavior. Conversely, the time series signals in the positively weighted sensory networks (e.g., SM, SUB) become more repetitive with increasing symptom severity. This may suggest increased inhibitory signaling associated with repetitive behaviors in ASD (Lombardo et al., 2016). Taken together, these findings point to entropy as a sensitive measure of the hypothesized excitation and inhibition imbalance underlying ASD behavioral deficits (Rubenstein and Merzenich, 2003; Chao et al., 2010; Vattikuti and Chow, 2010; Yizhar et al., 2011) and may serve as a potential biomarker.

ETHICS STATEMENT

This study was carried out in accordance with the recommendations of each sites Institutional Review Board. The protocol was approved by each sites Institutional Review Board. All subjects gave written informed consent in accordance with the Declaration of Helsinki.

AUTHOR CONTRIBUTIONS

RS, KJ, MD, and DW contributed to the conceptualization of this paper. RS contributed data analysis. RS, KJ, MD, and DW contributed to the drafting of the manuscript.

REFERENCES

Allen, E. A., Damaraju, E., Plis, S. M., Erhardt, E. B., Eichele, T., and Calhoun, V. D. (2014). Tracking whole-brain connectivity dynamics in the resting state. *Cereb. Cortex* 24, 663–676. doi: 10.1093/cercor/bhs352

Anderson, J. S., Nielsen, J. A., Froehlich, A. L., DuBray, M. B., Druzgal, T. J., Cariello, A. N., et al. (2011). Functional connectivity magnetic resonance imaging classification of Autism. *Brain* 134, 3742–3754. doi: 10.1093/brain/awr263

Andersson, J., Jenkinson, M., and Smith, S. (2007). *Non-linear Registration aka Spatial Normalisation.* Internal Technical Report TR07JA2. Oxford: Oxford Centre for Functional Magnetic Resonance Imaging of the Brain, Department of Clinical Neurology, Oxford University. Available online at: www.fmrib.ox.ac.uk/analysis/techrep for downloading

APA (1994). *Diagnostic, and Statistical Manual of Mental Disorders*. Washington, DC: American Psychiatric Association.

Belmonte, M. K., Allen, G., Beckel-Mitchener, A. B., Boulanger, L. M., Carper, R. A., and Webb, S. J. (2004). Autism and abnormal development of brain connectivity. *J. Neurosci.* 24, 9228–9231. doi: 10.1523/JNEUROSCI.3340-04.2004

Belmonte, M. K., Gomot, M., and Baron-Cohen, S. (2010). Visual attention in Autism families: 'unaffected' sibs share atypical frontal activation. *J. Child Psychol. Psychiatry* 51, 259–276. doi: 10.1111/j.1469-7610.2009.02153.x

Buckheit, J., Chen, S., Donoho, D., and Johnstone, I. (2005). Available online at: www.stat.stanford.edu:80/wavelab/

Casanova, M. F. (2007). The neuropathology of Autism. *Brain Pathol.* 17, 422–433. doi: 10.1111/j.1750-3639.2007.00100.x

Casanova, M. F., El-Baz, A. S., Kamat, S. S., Dombroski, B. A., Khalifa, F., Elnakib, A., et al. (2013). Focal cortical dysplasias in Autism spectrum disorders. *Acta Neuropathol. Commun.* 1:67. doi: 10.1186/2051-5960-1-67

Cerliani, L., Mennes, M., Thomas, R. M., Di Martino, A., Thioux, M., and Keysers, C. (2015). Increased functional connectivity between subcortical and cortical resting-state networks in Autism Spectrum Disorder. *JAMA Psychiatry* 72, 767–777. doi: 10.1001/jamapsychiatry.2015.0101

Chang, C., and Glover, G. (2009). Effects of model-based physiological noise correction on default mode network anti-correlations and correlations. *Neuroimage* 47, 1448–1459. doi: 10.1016/j.neuroimage.2009.05.012

Chang, S., Yu, B., and Vetterli, M. (2000). Adaptive wavelet thresholding for image denoising and compression. *IEEE Trans. Image Process.* 9, 1532–1546. doi: 10.1109/83.862633

Chao, H. T., Chen, H., Samaco, R. C., Xue, M., Chahrour, M., Yoo, J., et al. (2010). Dysfunction in GABA signalling mediates Autism-like stereotypies and Rett syndrome phenotypes. *Nature* 468, 263–269. doi: 10.1038/nature09582

Costa, M., Goldberger, A., and Peng, C. K. (2002). Multiscale entropy analysis of complex physiologic time series. *Phys. Rev. Lett.* 89: 068102. doi: 10.1103/PhysRevLett.89.068102

Courchesne, E., Mouton, P. R., Calhoun, M. E., Semendeferi, K., Ahrens-Barbeau, C., Hallet, M. J., et al. (2011). Neuron number and size in prefrontal cortex of children with Autism. *JAMA* 306, 2001–2010. doi: 10.1001/jama.2011.1638

Courchesne, E., Pierce, K., Schumann, C. M., Redcay, E., Buckwalter, J. A., Kennedy, D. P., et al. (2007). Mapping early brain development in Autism. *Neuron* 56, 399–413. doi: 10.1016/j.neuron.2007.10.016

De Luca, M., Beckmann, C. F., Stefano, N., Matthews, P. M., and Smith, S. M. (2006). fMRI resting state networks define distinct modes of long-distance interactions in the human brain. *Neuroimage* 29, 1359–1367. doi: 10.1016/j.neuroimage.2005.08.035

Di Martino, A., Yan, C. G., Li, Q., Denio, E., Castellanos, F. X., Alaerts, K., et al. (2014). The Autism brain imaging data exchange: towards a large-scale evaluation of the intrinsic brain architecture in Autism. *Mol. Psychiatry* 19, 659–667. doi: 10.1038/mp.2013.78

Donoho, D. (1995). De-noising by soft-thresholding. *IEEE Trans. Inform. Theor.* 41, 613–627. doi: 10.1109/18.382009

Donoho, D., and Johnstone, I. (1994). Ideal spatial adaptation via wavelet shrinkage. *Biometrika* 81, 425–455. doi: 10.1093/biomet/81.3.425

Friedman, J., Hastie, T., and Tibshirani, R. (2010). Regularization paths for generalized linear models via coordinate descent. *J. Stat. Softw.* 33, 1–22. doi: 10.18637/jss.v033.i01

Greicius, M., Srivastava, G., Reiss, A., and Menon, V. (2004). Default-mode network activity distinguishes Alzheimers disease from healthy aging: evidence from functional MRI. *Proc. Natl. Acad. Sci. U.S.A.* 101, 4637–4642. doi: 10.1073/pnas.0308627101

He, B. J., Zempel, J. M., Snyder, A. Z., and Raichle, M. E. (2010). The temporal structures and functional significance of scale-free brain activity. *Neuron* 66, 353–369. doi: 10.1016/j.neuron.2010.04.020

Hutchison, R. M., Womelsdorf, T., Allen, E. A., Bandettini, P. A., Calhoun, V. D., Corbetta, M., et al. (2013a). Dynamic functional connectivity: promise, issues, and interpretations. *Neuroimage* 80, 360–378. doi: 10.1016/j.neuroimage.2013.05.079

Hutchison, R. M., Womelsdorf, T., Gati, J. S., Everling, S., and Menon, R. S. (2013b). Resting-state networks show dynamic functional connectivity in

awake humans and anesthetized macaques. *Hum. Brain Mapp*. 34, 2154–2177. doi: 10.1002/hbm.22058

Jann, K., Hernandez, L. M., Beck-Pancer, D., McCarron, R., Smith, R. X., Dapretto, M., et al. (2015). Altered resting perfusion and functional connectivity of default mode network in youth with Autism Spectrum Disorder. *Brain Behav.* 5:e00358. doi: 10.1002/brb3.358

Jenkinson, M., Bannister, P. R., Brady, J. M., and Smith, S. M. (2002). Improved optimisation for the robust and accurate linear registration and motion correction of brain images. *Neuroimage* 17, 825–841. doi: 10.1006/nimg.2002.1132

Jeste, S. S. (2011). The neurology of Autism Spectrum Disorders. *Curr. Opin. Neurol.* 24, 132–139. doi: 10.1097/WCO.0b013e3283446450

Kana, R. K., Keller, T. A., Cherkassky, V. L., Minshew, N. J., and Just, M. A. (2006). Sentence comprehension in Autism: thinking in pictures with decreased functional connectivity. *Brain* 129, 2484–2493. doi: 10.1093/brain/awl164

Kana, R. K., Keller, T. A., Minshew, N. J., and Just, M. A. (2007). Inhibitory control in high-functioning Autism: decreased activation and underconnectivity in inhibition networks. *Biol. Psychiatry* 62, 198–206. doi: 10.1016/j.biopsych.2006.08.004

Kleinhans, N. M., Richards, T., Sterling, L., Stegbauer, K. C., Mahurin, R., Johnson, L. C., et al. (2008). Abnormal functional connectivity in Autism spectrum disorders during face processing. *Brain* 131, 1000–1012. doi: 10.1093/brain/awm334

Krzanowski, W. J. (1979). Between-groups comparison of principal components. *J. Am. Stat. Assoc.* 74, 703–707. doi: 10.1080/01621459.1979.10481674

Laumann, T. O., Snyder, A. Z., Mitra, A., Gordon, E. M., Gratton, C., Adeyemo, B., et al. (2017). On the stability of BOLD fMRI correlations. *Cereb. Cortex* 27, 4719–4732.

Liu, C. Y., Krishnan, A. P., Yan, L., Smith, R. X., Kilroy, E., Alger, J. R., et al. (2012). Complexity and synchronicity of resting state blood oxygenation level-dependent (bold) functional MRI in normal aging and cognitive decline. *J. Magn. Reson. Imaging* 38, 36–45. doi: 10.1002/jmri.23961

Logothetis, N. K., Pauls, J., Augath, M., Trinath, T., and Oeltermann, A. (2001). Neurophysiological investigation of the basis of the fMRI signal. *Nature* 412, 150–157. doi: 10.1038/35084005

Lombardo, M. V., Lai, M.-C., Auyeung, B., Holt, R. J., Allison, C., Smith, P., et al. (2016). Unsupervised data-driven stratification of mentalizing heterogeneity in Autism. *Sci. Rep.* 6:35333. doi: 10.1038/srep35333

Lord, C., Risi, S., Lambrecht, L., Cook, E. H. Jr., Leventhal, B. L., DiLavore, P. C., et al. (2000). The Autism diagnostic observation schedule-generic: a standard measure of social and communication deficits associated with the spectrum of Autism. *J. Autism Dev. Disord.* 30, 205–223. doi: 10.1023/A:1005592401947

Mosconi, M. W., Kay, M., D'Cruz, A.-M., Seidenfeld, A., Guter, S., Stanford, L. D., et al. (2009). Impaired inhibitory control is associated with higher-order repetitive behaviors in Autism Spectrum Disorders. *Psychol. Med.* 39, 1559–1566.

Mostofsky, S. H., Powell, S. K., Simmonds, D. J., Goldberg, M. C., Caffo, B., and Pekar, J. (2009). Decreased connectivity and cerebellar activity in Autism during motor task performance. *Brain* 132, 2413–2425. doi: 10.1093/brain/awp088

Padmanabhan, A., Lynn, A., Foran, W., Luna, B., and O'Hearn, K. (2013). Age related changes in striatal resting state functional connectivity in Autism. *Front. Hum. Neurosci.* 7:814. doi: 10.3389/fnhum.2013.00814

Pei-Shan Ho, S., Chemin L., Guan-Yen c., Ho-Ling, L., Chih-Mao, H., Tatia Mei-Chun L., et al. (2018). "Complexity analysis of resting state fMRI signals in depressive patients," in *2017 39th Annual International Conference of the IEEE Engineering in Medicine and Biology Society (EMBC)* (Jeju Island), 3190–3193.

Penzes, P., Cahill, M. E., Jones, K. A., VanLeeuwen, J. E., and Woolfrey, K. M. (2011). Dendritic spine pathology in neuropsychiatric disorders. *Nat. Neuro* 14, 285–293. doi: 10.1038/nn.2741

Petanjek, Z., Judaš, M., Šimic, G., Rasin, M. R., Uylings, H. B., Rakic, P., et al. (2011). Extraordinary neoteny of synaptic spines in the human prefrontal cortex. *Proc. Natl. Acad. Sci. U.S.A.* 108, 13281–13286. doi: 10.1073/pnas.1105108108

Pincus, S. (1991). Approximate entropy as a measure of system complexity. *Proc. Natl. Acad. Sci. U.S.A.* 88, 2297–2301. doi: 10.1073/pnas.88.6.2297

Power, J. D., Barnes, K. A., Snyder, A. Z., Schlaggar, B. L., and Petersen, S. E. (2012). Spurious but systematic correlations in functional connectivity MRI networks arise from subject motion. *Neuroimage* 59, 2142–2154. doi: 10.1016/j.neuroimage.2011.10.018

Power, J. D., Cohen, A. L., Nelson, S. M., Wig, G. S., Barnes, K. A., Church, J. A., et al. (2011). Functional network organization of the human brain. *Neuron* 72, 665–678. doi: 10.1016/j.neuron.2011.09.006

R Core Team (2017). *R: A Language and Environment for Statistical Computing*. Vienna: R Foundation for Statistical Computing. Available online at: https://www.R-project.org/

Raichle, M. E., and MacLeod, A. M. (2001). A default mode of brain function. *Proc. Natl. Acad. Sci. U.S.A.* 98, 676–682. doi: 10.1073/pnas.98.2.676

Richman, J. S., and Moorman, J. (2000). Physiological time-series analysis using approximate entropy and sample entropy. *Am. J. Physiol. Heart Circ. Physiol.* 278, 2039–2049. doi: 10.1152/ajpheart.2000.278.6.H2039

Rubenstein, J. L., and Merzenich, M. M. (2003). Model of Autism: increased ratio of excitation/inhibition in key neural systems. *Genes Brain Behav.* 2, 255–267. doi: 10.1034/j.1601-183X.2003.00037.x

Rudie, J. D., Brown, J. A., Beck-Pancer, D., Hernandez, L., Dennis, E. L., Thompson, P. M., et al. (2013). Altered functional and structural brain network organization in Autism. *Neuroimage Clin.* 2, 79–94. doi: 10.1016/j.nicl.2012.11.006

Schmitz, C., and Rezaie, P. (2008). The neuropathology of Autism: where do we stand? *Neuropathol. Appl. Neurobiol.* 34, 4–11. doi: 10.1111/j.1365-2990.2007.00872.x

Seeley, W. W., Crawford, R., Zhou, J., Miller, B., and Greicius, M. (2009). Neurodegenerative diseases target large-scale human brain networks. *Neuron* 62, 42–52. doi: 10.1016/j.neuron.2009.03.024

Smith, R. X., Jann, K., Ances, B., and Wang, D. J. J. (2015). Wavelet-based regularity analysis reveals recurrent spatiotemporal behavior in resting-state fMRI. *Hum. Brain Mapp.* 36, 3603–3620. doi: 10.1002/hbm.22865

Smith, R. X., Yan, L., and Wang, D. (2014). Multiple time scale complexity analysis of resting state fMRI. *Brain Imaging Behav.* 8, 284–291. doi: 10.1007/s11682-013-9276-6

Smith, S. M. (2002). Fast robust automated brain extraction. *Hum. Brain Mapp.* 17, 143–155. doi: 10.1002/hbm.10062

Somerville, L. H., Jones, R. M., and Casey, B. J. (2010). A time of change: behavioral and neural correlates of adolescent sensitivity to appetitive and aversive environmental cues. *Brain Cogn.* 72, 124–133. doi: 10.1016/j.bandc.2009.07.003

Supekar, K., Uddin, L. Q., Khouzam, A., Phillips, J., Gaillard, W. D., Kenworthy, L. E., et al. (2013). Brain hyperconnectivity in children with Autism and its links to social deficits. *Cell Rep.* 5, 738–747. doi: 10.1016/j.celrep.2013.10.001

Takahashi, T., Cho, R., Mizuno, T., Kikuchic, M., Takahashi, T. M. K., and Wada, Y. (2010). Antipsychotics reverse abnormal EEG complexity in drug-naive schizophrenia: a multiscale entropy analysis. *Neuroimage* 51, 173–182. doi: 10.1016/j.neuroimage.2010.02.009

Tibshirani, R. (1996). Regression shrinkage and selection via the lasso. *J. R. Stat. Soc. B* 58, 267–288.

Tikhonov, A. N., Goncharsky, A. V., Stepanov, V. V., and Yagola, A. G. (1995). *Numerical Methods for the Solution of Ill-Posed Problems*. Boston, MA: Kluwer Academic Publishers. doi: 10.1007/978-94-015-8480-7

Uddin, L. Q., Supekar, K., Lynch, C. J., Khouzam, A., Phillips, J., Feinstein, C., et al. (2013). Salience network-based classification and prediction of symptom severity in children with Autism. *JAMA Psychiatry* 70, 869–879. doi: 10.1001/jamapsychiatry.2013.104

Vattikuti, S., and Chow, C. C. (2010). A computational model for cerebral cortical dysfunction in Autism Spectrum Disorders. *Biological Biol. Psychiatry* 67, 672–678. doi: 10.1016/j.biopsych.2009.09.008

Villalobos, M. E., Mizuno, A., Dahl, B. C., Kemmotsu, N., and Müller, R.-A. (2005). Reduced functional connectivity between V1 and inferior frontal cortex associated with visuomotor performance in Autism. *Neuroimage* 25, 916–925. doi: 10.1016/j.neuroimage.2004.12.022

Welchew, D. E., Ashwin, C., Berkouk, K., Salvador, R., Suckling, J., Baron-Cohen, S., et al. (2005). Functional disconnectivity of the medial

temporal lobe in Asperger's syndrome. *Biol. Psychiatry* 57, 991–998. doi: 10.1016/j.biopsych.2005.01.028

Yang, A. C., Huang, C. C., Yeh, H. L., Liu, M. E., Hong, C. J., Tu, P. C., et al. (2013a). Complexity of spontaneous BOLD activity in default mode network is correlated to cognitive Function in normal male elderly: a multiscale entropy analysis. *Neurobiol. Aging* 34, 428–438. doi: 10.1016/j.neurobiolaging.2012.05.004

Yang, A. C., Wang, S.-J., Lai, K.-L., Tsai, C. F., Yang, C. H., Hwang, J. P., et al. (2013b). Cognitive and neuropsychiatric correlates of EEG dynamic complexity in patients with Alzheimer's disease. *Prog. Neuropsychopharmacol. Biol. Psychiatry* 47, 52–61. doi: 10.1016/j.pnpbp.2013.07.022

Yizhar, O., Fenno, L. E., Prigge, M., Schneider, F., Davidson, T. J., O'Shea, D. J., et al. (2011). Neocortical excitation/inhibition balance in information processing and social dysfunction. *Nature* 477, 171–178. doi: 10.1038/nature10360

Zhang, Y., Brady, M., and Smith, S. M. (2001). Segmentation of brain MR images through a hidden Markov random field model and the expectation-maximization algorithm. *IEEE Trans. Med. Imaging* 20, 45–57. doi: 10.1109/42.906424

Conflict of Interest Statement: The authors declare that the research was conducted in the absence of any commercial or financial relationships that could be construed as a potential conflict of interest.

The reviewer SA and handling editor declared their shared affiliation at time of review.

Advantages of publishing in Frontiers

OPEN ACCESS
Articles are free to read for greatest visibility and readership

FAST PUBLICATION
Around 90 days from submission to decision

HIGH QUALITY PEER-REVIEW
Rigorous, collaborative, and constructive peer-review

TRANSPARENT PEER-REVIEW
Editors and reviewers acknowledged by name on published articles

Frontiers
Avenue du Tribunal-Fédéral 34
1005 Lausanne | Switzerland

Visit us: www.frontiersin.org
Contact us: info@frontiersin.org | +41 21 510 17 00

REPRODUCIBILITY OF RESEARCH
Support open data and methods to enhance research reproducibility

DIGITAL PUBLISHING
Articles designed for optimal readership across devices

FOLLOW US
@frontiersin

IMPACT METRICS
Advanced article metrics track visibility across digital media

EXTENSIVE PROMOTION
Marketing and promotion of impactful research

LOOP RESEARCH NETWORK
Our network increases your article's readership